PhD THESIS

Self-organization in biology: From quasispecies to ecosystems

José Ángel Capitán Gómez

UNIVERSIDAD CARLOS III DE MADRID

PhD THESIS

Self-organization in biology: From quasispecies to ecosystems

Author

José Ángel Capitán Gómez

Supervisor

José Antonio Cuesta Ruiz

DEPARTMENT OF MATHEMATICS

Leganés, October 2010

a mi tía Isabel

Agradecimientos

El tiempo pasa más rápido de lo que uno piensa. Parece que fue ayer cuando empecé, de la mano de José Cuesta, mi carrera científica. Hay muchas razones para estarle agradecido. En la parte científica me quedo con su gran intuición y su facilidad para abordar problemas desde distintas perspectivas. Gracias por todo lo que he aprendido. En la parte personal hay que destacar su generosidad, cercanía y buen humor. Gracias por dedicarme este tiempo.

Esta tesis no habría visto la luz si no hubiera sido por la colaboración con otros grupos. A Susanna C. Manrubia y Jacobo Aguirre, del Centro de Astrobiología, les agradezco su generosidad al abrirme la puerta al campo de la evolución viral. A Richard Law y Gustav W. Delius, de la Universidad de York, no puedo sino darles las gracias por su cálida acogida y su hospitalidad durante mis dos estancias, y el haberme enseñado lo poco que sé de ecosistemas marinos. Y a Jordi Bascompte le estoy agradecido por su orientación y colaboración en nuestros trabajos sobre redes ecológicas. A todos ellos, mi gratitud más sincera.

La gente que he ido conociendo durante este tiempo merece también ser recordada. Aunque es un "viejo conocido", a Saúl le debo el ponerme en contacto con el GISC, que no es poco. A toda la gente del GISC mi reconocimiento, pero entre ellos obligatoriamente debo destacar a Anxo y Yuri. Por otra parte, no puedo dejar de recordar a los miembros del grupo de Ecología Teórica de la Universidad de York, en especial a Mariella. Y, por supuesto, a mis amigos de la Complu: Ángel, Luis Sánchez y sobre todo Javi Corrales.

A Manuel Fontán, uno de mis profesores de enseñanza media, le agradezco que me abriera la ventana al mundo de la física.

Por supuesto, mi familia merece un lugar destacado. A mis padres les agradezco que siempre hayan estado apoyándome en todo lo que he hecho, y tantas otras cosas que sería largo enumerar. A mi hermano, gracias por soportarme y por los buenos ratos que hemos pasado. A Conchi mi agradecimento porque probablemente ella despertó, durante mi infancia, el interés por la ciencia.

Y por último, *but not the least*, está Sara. Gracias, Sara, por estos diez años que decidiste compartir conmigo. No podrían haber sido mejores.

José A. Capitán
Leganés, Octubre de 2010

This work has been possible thanks to finantial support from projects MOSAICO (Ministerio de Educación y Ciencia), MOSSNOHO and MODELICO-CM (Comunidad de Madrid), COST Action MP0801 (European Science Foundation) and a contract from Comunidad de Madrid and Fondo Social Europeo.

Contents

1

Introduction

1

Statistical mechanics and complex systems

No gluing together of partial studies of a complex nonlinear system
can give a good idea of the behavior of the whole.
—Murray Gell-Mann.

Traditionally, physics has been regarded as a search for fundamental laws. It was assumed that once these laws were discovered, the behavior of any physical system would follow from them and, in some sense, physical sciences would come to their end[1]. Physical systems were dissected again and again, and the resulting fragments were studied separately. Once the components were well described, physicists hoped that systems could be reassembled to derive all its relevant properties (Anderson 1973). Admittedly, this reductionist approach has yielded remarkable theories ranging from quantum to celestial mechanics.

For a long time the idea prevailed that the perception of complex behavior arises from incomplete information, related to the presence of a huge number of variables and parameters hiding the underlying regularities (Nicolis and Prigogine 1989). Over the years new theoretical progress has challenged this reductionist viewpoint, showing that *complexity* is closely linked to the fundamental laws of physics. For example, the discovery of chaos (Lorenz 1963) showed us that simple rules can produce intrinsically complicated behavior and small changes can lead to large effects (Waldrop 1993). As of today, *complexity science* constitutes a highly interdisciplinary, fast growing branch

[1]Probably this is the kind of thinking that led C. Anderson to declare, after discovering the positron in 1932, *"The rest is chemistry!"*

of science, that uses concepts and tools coming from nonlinear dynamics, statistical physics, probability theory, data analysis and numerical simulation.

1.1 Complexity and emergence

The concept of complexity is well synthesized by the title of the renowned paper by P. Anderson *"More is different"* (Anderson 1973). To find a less concise definition is almost impossible. Some technical definitions of "complex systems" can be found in the special edition of Science **284**, No. 5411 (1999) devoted to complexity. The interdisciplinary character of complexity science and its broad scope obviously complicate the task of finding an all-encompassing definition. We start analyzing some misleading conceptions about complex systems:

Simple systems have simple behavior. There is a wide family of simple models exhibiting complex features. For example, the nonlinear dynamics of a forced pendulum or a double pendulum are chaotic (Baker and Gollub 1990).

A complex behavior is due to complex causes. This misconception, related to the previous one, lies on the basis of physical systems modeling. A simple, paradigmatic model can capture the essential mechanisms underlying physical processes, even quantitatively, leading to complex behavior itself. The Ising model (Huang 1987) constitutes a good example of this fact (it represents an idealization of real ferromagnetic materials, but importantly, it captures their global phemonenology). Although paradigms are more fundamental in their conception, subsequent refinements can help to understand quantitatively the fine detail of observations. We will discuss further on this point in Section 1.2.

In order to obtain a more precise idea of what complexity means, it is useful to think of the similarities between systems of very different nature. Traffic jams, dessert dunes, water properties, cell metabolism, ecosystems.... All these phenomena share a common feature: the collective behavior of a large number of "agents" (be them cars, sand grains, water molecules, proteins, species...) that interact with one another causes the *emergence* of the phenomenon itself. Such systems cannot be simply described from the "microscopic" interactions involved. It is their combined effect what yields complex patterns and behavior. Therefore, to predict these phenomena, individual effects need to be "integrated" into collective magnitudes. An emergent collective behavior and the hierarchical organization in different levels of complexity are footprints of these kind of systems. Each organization level has its own properties emergent from the previous level. For instance, at the microscopic level a fluid is just an assemblage of molecules; at a mesoscopic level such molecules self-organize themselves to form, say, vortices; interactions between vortices give raise to macroscopic turbulence patterns. This way, turbulence is an emergent phenomenon that cannot be observed at a microscopic level.

Complexity science has been an emergent phenomenon itself, resulting from the interplay of many scientific disciplines aimed at understanding collective phenomena.

Complexity science is characterized by its interdisciplinary nature, which is a consequence of complex systems being unfit in any single discipline. On the one hand, microscopic constituents and their emergent phenomena typically lie in different scientific branches. On the other hand, complex systems usually require of different methodologies —always with a strong statistical background— to approach their behavior. It is precisely the statistical approach which allows the typical, bottom-up description of complex systems (i.e., microscopic collective behavior is grouped into elements belonging to a higher level of description).

Understanding complex systems is of major importance to society, because many of these systems have a strong social and economic component (this is the case of traffic jams or stock prices, for example) and others have key technological applications (disciplines like material science, laser technology, communications, biotechnology, etc., benefit from complex systems research). For these reasons, complexity science has undergone a fast development over the last decades. However, in spite of this recent explosion, this new science has an old root: its origin can be traced back more than a century, to the appearance of statistical mechanics.

1.2 Statistical mechanics and complexity

Statistical mechanics was founded as an attempt to explain thermodynamics from interactions between atoms and molecules, the basic constituents of matter. The success of this branch of physics was to provide strong support to the atomic hypothesis of matter; however, nowadays statistical mechanics has become a stand-alone methodology to deal with any physical system in which the interplay of a large number of particles produces macroscopic collective phenomena. Originally, the name of this new discipline alluded to its using probabilistic and statistical reasoning to simplify what a priori turned out to be far too complex problems to be dealt with by standard methods. Its predictive abilities has been exploited all along the past century in many fields of physics.

One of the most remarkable achievements of statistical mechanics has been the creation of paradigms for a wide range of systems. They are minimalistic models, based on elements sometimes far from the real objects that motivated them, which nevertheless capture the phenomenology of the modeled system. The usefulness of creating paradigms has been two-fold: on the one hand, they simplify the original systems so as to make them amenable to study, and on the other hand, they have revealed that many apparently different phenomena are but different faces of the same collective phenomenon, because they all fit in a common paradigm. For instance, the celebrated Ising model, originally devised to understand the para-ferromagnetic transition in magnetic materials, can also describe demixing in colloidal fluids or alloys, or vapor-liquid condensation in ordinary fluids. In the same spirit, in the second and third part of this thesis we have devised simplified models, built on a minimal number of ingredients, to describe quasispecies and ecosystems with the aim of reproducing the global behavior of the described phenomena.

The fact that the same paradigms describing many different physical systems are also able to explain phenomena occurring in fields so far from physics is what transformed statistical mechanics into the science of complex systems. In sociology, for example, the model by Schelling (1971), aimed at explaining racial segregation in cities of the United States, is but —once more— the diluted Ising model at zero temperature with a magnetization-preserving (Kawasaki) dynamics. Realization of this ability inherent to statistical mechanics has motivated its entering the fields of sociology, economics, biology, etc. As of today, statistical physics is interdisciplinary by construction, not only because it translates models between different disciplines, but also because it formulates scientific problems which lie at the border between disciplines and which give rise to utterly new science.

1.3 Self-organization, universality and scaling

Complex systems usually lie in an intermediate situation between order and disorder at the edge of chaos (Kauffman 1995). They exhibit fine-tuned processes and structures apparently arising simply from "randomness" (Stanley 2000). Actually, this balance between order and disorder could be intuitively identified with "complexity".

If complex systems are found in between of order and disorder is because their evolution is not ruled by an external mechanism, but they *self-organize*. Globally coherent patterns in complex systems arise from the local interaction of their constituents, in such a way that the organization is achieved with all the elements acting simultaneously and with no element acting as "coordinator". Self-organization in fields other than physics is very easy to find. Here are some examples.

In chemistry: Molecular self-assembly, autocatalytic networks, liquid crystals, colloids, micelles.

In biology: Protein folding, formation of lipid bilayer membranes, homeostasis, morphogenesis and embryology, the creation of structures by social animals (such as social insects and many mammals), ecosystems assembly.

In mathematics and computer science: Cellular automata, random graphs, artificial life, multi-agent systems, Internet.

In social sciences: Examples such as the emergence of cooperation, the organization of stock markets, bank lending networks and others abound in sociology, economics, and anthropology.

In linguistics: The generation of semantic conventions in populations of agents, or the emergence of syntactic structures.

Interestingly, this self-organization is very common in critical phenomena and phase transitions (Stanley 1971). In some sense, phase transitions arise from a trade-off between opposing forces. The Ising model, where spin-spin interaction and thermal fluctuations oppose each other, remains again a good example of this. The same competition between forces acting in regime shifts has been observed in other branches

of science (Waldrop 1993; Scheffer et al. 2001). Therefore, a theoretical framework like statistical mechanics, that allows a systematic description of phase transitions, is crucial to understand self-organization. In this context, the study of phase transitions has impelled the development of two key concepts in the science of complex systems, closely interrelated: *universality* and *scaling*.

As we have mentioned before, very often common global behaviors are observed in systems of substantially different nature. This is the so-called *universality*. These systems follow universal laws that are independent of the constituents. Consequently, the existence of "universality classes" implies that a common, usually simple mechanism is at work. We will exploit the connection between systems belonging to a common universality class to describe the critical behavior of the model of spatial viral infection presented in the second part of this thesis.

The presence of *scaling laws* in a self-organized system implies that its functionality is not affected by changes in its size, i.e., the system does not have a characteristic, optimal size. For example, as for height, we humans have a well-defined "scale". In fact, a person taller than, say, 4 meters is beyond any physiological possibility of the human body. However, a city with thousands of inhabitants and no physical constraints can grow up several orders of magnitude in population since it self-organizes to cope with that increase (Watts 2003). Since a city can be functional for very different sizes, we say that is *scale-invariant*. We will apply the principle of scale invariance in the derivation of the model of marine size spectra introduced in the fourth part of this thesis.

1.4 Population dynamics

Many tools commonly used in the analysis of complex systems come from the framework of population dynamics. The aim of population dynamics is to describe a given ensemble of elements (be them molecules, genes, species, opinions...) as stochastic processes in time. In population dynamics three factors come into play: *replication,* the mechanism by which entities can create copies of themselves; *mutation,* the mechanism that produces small variations within those copies; and *selection,* the mechanism by which the "fittest" copies are able to displace other species over the generations.

Obviously, this terminology comes directly from biology. On the one hand, living organisms reproduce themselves by producing offspring. On the other hand, at some rate new offspring can undergo a "mutation" which transforms them from the original species into a different one. Finally, the interaction with the environment affects the chances of a given species to produce descendants and change its adaptation conditions, resulting in what is known as selection. Usually selection arises as a consequence of the existence of limited resources, but the competition with other species can also produce selection.

It is worth remarking that any system that can be described with these three ingredients falls within the framework of population dynamics. Opinion formation is a good example of this: replication occurs through the propagation of opinions from one

individual to another, mutation takes place when an individual changes its mind spontaneously, and selection occurs as a result of the different ability of ideas to propagate.

It is also interesting to note that the environment associated to the population can be structured. For instance, plant species are spread over lands, which produces a direct competition for resources between adjacent individuals. Propagation of epidemics or opinions are very dependent of the structure of the "infected" population, in many cases dominated by the social network (especially in opinion propagation). These structures determine different selection factors and are crucial to understand the time evolution of the system. This effect will be illustrated clearly in the second part of this thesis, where we will see the crucial impact that spatial structures have in the propagation of viral infections.

Throughout this thesis we have studied different complex biological systems (such as ensembles of viruses, food-webs, or marine ecological communities) within the framework of population dynamics, and we have characterized their emergent behavior and self-organization using tools provided by statistical mechanics and stochastic processes theory. Apart from the systems that we have analyzed in this thesis, there are many more examples of complex biological systems exhibiting self-organization. Let us describe some of them at a minimal level of detail.

1.5 Self-organization in biology

Complex behavior arises recurrently in biological systems. We have listed some examples of self-organizing biological systems in Section 1.3. In this section we will discuss in some detail several biological systems exhibiting self-organization. We do not pretend this description to be exhaustive —which would certainly be a rather complicated task. On the contrary, our aim is simply to describe particular examples of complex biological systems, for which the interactions between their components leads to collective behavior and emergence of global patterns. We will concern ourselves in some selected examples extracted from different levels of organization, ranging from morphogenesis and biochemical networks to ecosystems.

Morphogenesis and cell segmentation

The major emphasis in developmental biology studies has traditionally been focused on the hierarchical regulatory relationships among genes. Recently, however, research efforts have tried to address the roles played by the physical and dynamical properties of cells and tissues in producing biological traits along *morphogenesis* (i.e., during the formation of individuals). Interactions among genes, ions, metabolites, etc., lead to multistable, oscillatory, and pattern forming dynamics. These interactions can predict most of the structures of animal bodies, such as cell differentiation, tissue multilayering, or segmentation. It has been pointed out that these effects have played an important role in the origin of ancestral multicellular organisms, more than for modern organisms, which are dominated by a hierarchical genetic control (Newman and Forgacs 2005).

Complex biochemical networks

Complex biochemical systems are hard to study as a whole due to their overwhelming number of elements and interactions. However, a simple approach to these systems focuses on the networks of interactions between these constituents. Many examples, such as the contact network in a folded protein, protein-protein interaction networks and gene regulatory networks, show that some properties of biochemical systems can be predicted through the study of their corresponding networks (Fernández and Solé 2005).

The folded protein structure constitutes a first example of complex biochemical network. The linear chain of aminoacids is folded and its final shape induces contact interactions among the aminoacid residues. A network analysis reveals a small-world structure (Watts and Strogatz 1998) with a high degree of modularity for contact networks. Other example comes from gene regulatory networks, which determine the functioning of cells. These networks can be analyzed as Kauffman's boolean networks (Kauffman 1969) and exhibit a number of dynamic and collective properties such as robustness and phase transitions. Available data of several genetic regulatory networks (for example, those of the bacteria *Escherichia coli* and the yeast *Saccharomyces cerevisiae*) have confirmed their scale-free character. Describing complex biochemical systems under the framework of network analysis is especially relevant for providing well-defined quantitative properties, which in turn can be reproduced by dynamical models of network evolution.

Vesicles and membranes

A micelle in aqueous solution is an aggregate of molecules composed by an hydrophilic "head" in contact with the solvent, and hydrophobic tails that remain in the micelle center. This phase arises by the insufficient packing of single tailed lipids in a bilayer. When all the interior volume of a double layer can be filled, the resulting aggregate that forms is known as vesicle.

Adsorption of vesicles on surfaces (Nollert et al. 1995) and flow of vesicles in capillaries (Kraus et al. 1996) are very important processes in a variety of biological contexts. Despite the increasing experimental interest in these problems, available models often neglect relevant features, such as the structure and flexibility of the double layer, the presence of local interactions with the substrate, etc. These features ultimately change the collective behavior of vesicles and even induce phase transitions.

Heterogeneous ensembles of viral populations

Studies on evolution of populations have traditionally focused on the description of homogeneous populations, where all individuals are identical. However, such an approach fails when the mutation rate or the population size increase beyond some thresholds. Populations formed by a large number of rapidly mutating individuals are genotypically and phenotypically heterogeneous (Eigen and Schuster 1977). RNA viruses

constitute the simplest instance of heterogeneous population where many different individual (pheno)types can coexist. Such populations, known as *quasispecies*, exhibit features different from those of homogeneous populations (Tarazona 1992), some of which are: (i) quasispecies tend to maximize their robustness, (ii) they can quickly react to selective pressures or fluctuating environments, (iii) beneficial mutations which recover the viability of a quasispecies are frequent, and (iv) viral infectivity can vanish due to slight increases in the mutation rate. This latter result has led to identify a new path to extinction due to the existence of a parasitic class in the quasispecies.

Current theories show disagreements with observations in natural systems such as RNA viruses, which allow us to witness real-time evolution. These experimental results have urged the design of new phenomenological models in better agreement with experiments. These models include genomic diversity (sequences), secondary structure diversity [through RNA folding algorithms (Stich et al. 2007)], and phenotypic diversity [replicative and infective ability, defective vs. altruistic strategies in viruses (Iranzo and Manrubia 2009), and competition between species (Aguirre and Manrubia 2008)].

Ecosystem assembly

Ecosystems are the outcome of a cumulative series of processes. These processes involve, on short time scales, the sequential arrival of newcomers defining ecological succession. On larger scales, species can evolve and co-evolution arises. Successional processes are nicely illustrated by the progressive colonization of abandoned lands, eventually ending up in the building of a forest.

Since succession is historical, contingency plays a role and different invasion pathways can lead to different communities. But the impact of path dependence on the overall ecosystem structure is not as important as it might seem. The analysis of evolved communities shows that many of their features are universal. Some examples of these regularities are the observed patterns of food-webs or the spatial distribution of species. Such universality emphasizes the importance of fundamental patterns (Kauffman 1993; Solé and Goodwin 2001). There are basic, universal laws that shape the large-scale architecture of ecological systems. Some of these basic patterns result from a limited variety of dynamical behaviors, the presence of multiplicative processes (e.g., a high-populated species is more likely to reproduce), and conflicts arising from competitive forces. For example, competition is responsible of the different levels of diversity allowed in a given habitat. The compensation of forces increasing diversity (immigration and speciation) and those reducing it (such as predation events) can explain the emergence of universal patterns of organization, in the same fashion that a phase transition arises from the competition between opposite forces. As it occurs in many physical systems, conflicting trade-offs often produce a small repertoire of patterns, which we recognize as universals.

1.6 Outline

In this thesis we have applied techniques and tools provided by statistical mechanics and stochastic processes theory to study and analyze several models motivated by complex biological systems of interest. We introduce these models trying to follow the conceptual approach of statistical mechanics, with the aim of devising oversimplified models that predict, at least qualitatively, the biological phenomena that we try to describe. In particular, we have focused on two kinds of systems: (i) heterogeneous ensembles of viruses and (ii) ecological communities. For the latter we have tackled two different viewpoints for modeling: we have studied ecosystems as feeding networks or food-webs, and we have also described ecological communities disregarding trophic interactions and considering body size as the dominant trait that determines the observed weight distribution in marine ecosystems. As complex systems, all of them exhibit self-organization and phase transitions, and are amenable to a theoretical description in the framework of statistical mechanics. All the effects that we have reviewed in a general way along this introductory chapter will show up in each one of these systems. But let us be a little bit more specific.

This thesis has a clear division into three parts. In the first one (Chapter 2), we introduce and analyze a spatial model of viral infection propagation. The replication at high mutation rates and the production of a large number of copies is a common strategy of virus survival. Frequent mutation rates boost viral adaptation to changing environments, which forces host cells to develop mechanisms to fight against the infection. The lack of knowledge of the mechanisms causing the extinction of viruses makes specially difficult the design of therapies and protocols to hinder their propagation. One of the traditional explanations of viral extinction comes from the theory of quasispecies (Eigen 1971). This theory predicts an error threshold in the mutation rate, and under increased mutagenesis the inhomogeneous population of viruses looses its entity. However, accumulating empirical evidence has led to more realistic models of viral propagation, which in turn has allowed a deeper understanding of the mechanisms leading to extinction.

Our model of viral infection propagation (Cuesta et al. 2010) is based on a new mechanism causing extinction due to competition to infect susceptible cells. The model describes the dynamics of a phenotypically heterogeneous ensemble of viruses subject to beneficial, deleterious, and lethal mutations. Besides, the host cell is allowed to develop defenses against each attempt of infection. When the number of cells available is unlimited, the virus population can grow unboundedly to overcome its extinction. In contrast, when physical space is made explicit, the advantage that the virus can obtain by increasing its progeny is limited by the ability to infect neighboring cells, and extinction may result from an increase in host defenses beyond a finite, critical threshold. Our results might be relevant to better understand propagation of infections in crops or in tissues with mobility constraints, as plant leaves, and the implications that environments with different geometrical properties might have in the design of effective control therapies.

In the second part (Chapters 3–5) we focus on the mathematical modeling of ecosystems as trophic networks. The process by which ecosystems built up is a clear example of self-organization. As we have mentioned before, global patterns can be extracted although the state of ecosystems is a direct consequence of its history. Our work (Capitán et al. 2009; Capitán and Cuesta 2010b; Capitán et al. 2010) is but a manifestation of this fact. We introduce a toy model of ecosystem assembly for which we are able to map out all assembly pathways generated by successional colonizations. The model allows us to display the whole configuration space in the form of a directed graph whose nodes are model communities and whose links are transitions between them induced by invasions. The process of building up these model communities is characterized as a finite Markov chain, for which we are able to prove that it exhibits a unique set of recurrent states. This set is therefore the end state of the process, which is resistant to subsequent invasions. In spite of its simplicity, the model shares most of the features with standard assembly models reported in the literature, such as increasing biodiversity along the assembly, or a trend to increase (but not necessarily optimize) the overall population level, with the advantage that all observables can be computed in an exact manner. Hence the full assembly process is displayed.

In Chapter 3 we provide an exhaustive analysis of the features of the model. The analysis of the assembly graph allows us to classify communities as either transient or recurrent, the latter being either a single community or a closed set of them connected through invasions. This also shows that the end state is independent of the assembly history. The chain provides an asymptotic probability distribution for recurrent states, which can be used to obtain averages of observables as well as the time dependence of these magnitudes during succession. Since the times of absorption into the recurrent set are found to be small compared to the size of the system, the end state is quickly reached (in units of the mean invasion time) and the ecosystem can be regarded as a fluctuating complex system where species get continually replaced by newcomers without ever leaving the set of recurrent patterns. The model also allows to ascertain the robustness of its results against variations of the parameters (direct competition, resource saturation, consumption rate, etc.)

In Chapter 4 we obtain analytical results and introduce some approximations which allow us to reconstruct our previous results. In particular, we prove that communities found as end states of the assembly process are pyramidal and we find that the equilibrium abundance of any species at any trophic level is approximately inversely proportional to the number of species in that level. We also find that the per capita growth rate of a top predator invading a resident community is key to understand the appearance of complex end states reported in Chapter 3. The sign of these rates allows us to separate regions in the space of parameters where the end state is either a single community or a complex set containing more than one community. We have also obtained analytical approximations to the time evolution of species abundances that help us to determine, with high accuracy, the sequence of extinctions that an invasion may cause. Finally we apply this analysis to obtain the communities in the end states. The agreement of averages calculated according to this analytical procedure with those derived by numerical integration of the population dynamics is excellent.

Our model of ecosystem assembly is minimalistic and, as such, amenable to modifications that can reveal an entirely new phenomenology. In Chapter 5 we discuss the effect that background extinctions have in our model communities, which undergo a phase transition between a species-rich and a species-poor attractor as a result. This phenomenon is not new. Real ecosystems are observed to undergo abrupt regime shifts in response to gradual external changes. These shifts are theoretically explained as a regime switch between alternative stable states of the ecosystem dynamical response to smooth changes in external conditions. Usual models introduce nonlinearities in the macroscopic dynamics that lead to different stable attractors among which the shift takes place. Our assembly model, however, provides an alternative explanation of catastrophic regime shifts. The model pictures ecological communities as systems in continuous fluctuation, according to certain transition probabilities, between different *microstates* in the configuration space of the Markov chain. An spontaneous extinction rate, that encompass different gradual changes in external conditions, serves as a control parameter. Upon increases on the extinction rate the system undergoes a regime shift. Under our microscopic viewpoint we recover the main results obtained in previous theoretical and empirical work, such as anomalous variance, hysteresis cycles, trophic cascades, etc. But more importantly, a spectral analysis of the transition probability matrix associated to the Markov chain allows us to *rigorously* establish that we are observing the fingerprints, in a finite size system, of a true phase transition driven by background extinctions (Capitán and Cuesta 2010a).

Finally, in the third part (Chapter 6) we introduce and discuss a model for population dynamics in size-structured food-webs. Marine ecological communities are better described ignoring the exact feeding relationships between species. Under this assumption, a striking regularity in the size spectrum of the marine ecosystem is observed: the abundance of organisms as a function of their weight approximately follows a power law over several orders of magnitude. We can interpret this fact as evidence that the population dynamics in the ocean is approximately scale-invariant. In Chapter 6 we use this invariance in the construction and analysis of a size-structured dynamical population model. Starting from a Markov process including predation, reproduction, maintenance respiration and intrinsic mortality as elementary events, we derive a partial differential equation describing the dependence of abundance on weight and time. Our model represents an extension of earlier models based on the McKendrick-von Foerster equation (Silvert and Platt 1978). The exponent of the steady-state power-law solution is determined by the relative scaling between the rates of the density-dependent processes (predation) and the rates of the density-independent processes (reproduction, maintenance, and mortality). We study the stability of the steady-state against small perturbations and find that inclusion of maintenance respiration and reproduction in the model has a strong stabilizing effect (Capitán and Delius 2010).

In Chapter 7 we analyze the overall implications and interpretations of our work and discuss some open problems and future research.

II

Statistical mechanics of viral infection

2

A spatially extended model of quasispecies

Nothing in biology makes sense except in the light of evolution.
—Theodosius Dobzhansky.

2.1 Adaptive landscapes

Perhaps the most remarkable contribution of S. Wright to evolutionary theory is his metaphor of *adaptive landscape* (Gavrilets 2004). This concept arises as a theoretical attempt to describe the evolutionary dynamics of species and has been applied to biological sequences (be them sequences of genes, DNA or RNA chains, proteins, etc.) We will restrict ourselves to the latter case. From a mathematical viewpoint, an adaptive landscape is a mapping $f : \mathcal{X} \to \mathbb{R}$, where $\mathcal{X}$ stands for the *configuration space* (i.e., the set of all possible configurations of the biological sequence) equipped with some notion of adjacency or distance, and whose image is the *replicative ability*[1] associated to any sequence in $\mathcal{X}$. Although we speak of replicative ability in clear reference to the constant process of replication undergone by biological sequences, in a more gen-

[1] In a broader context, the term *fitness* is used to define the adaptability degree of any biological "agent". We prefer to use here the concept of *replicative ability* since the adaptability of biological sequences is usually quantified by the number of copies per generation that they are able to produce, and therefore depends on many other effects (competition with other species, environmental parameters, the very topology of the configuration space $\mathcal{X}\ldots$).

eral context this quantity can refer to some evolutionary adaptability associated to any element in a generic configuration space.

When dealing with sequences we generically use the term *locus* to refer to a particular genetic trait, whereas *allele* stands for the different variants of that trait. Depending on the context, allele may refer to bases (DNA or RNA), amino acids (proteins) or genes (chromosomes). For example, for a DNA chain of length $L_{\rm s}$, the configuration space is $\mathcal{X} = \{\text{A, T, C, G}\}^{L_{\rm s}}$ (letters represent adenine (A), thymine (T), guanine (G) and cytosine (C), the four bases that form DNA sequences). As a measure of proximity in $\mathcal{X}$ we use the number of different loci between two sequences $x, y \in \mathcal{X}$, which defines the so-called Hamming distance $d_{\rm H}(x, y)$ on $\mathcal{X}$.

Sequences within $\mathcal{X}$ are connected through transitions, which are known as *mutations*. Point mutations refer to changes at a given locus of the sequence, i.e., substitutions of a base pair in a DNA chain, an amino acid in a protein or a different allele in a chromosome. In case that all mutations are pointwise we can build up the graph $\mathcal{G} = \{\mathcal{X}, \mathcal{L}\}$, where the set of links $\mathcal{L}$ is made of all pairs of sequences $x, y \in \mathcal{X}$ with $d_{\rm H}(x, y) = 1$.

The evolution of a given sequence is generally described as a random walk across the configuration space. A transition probability matrix $\mathsf{Q} = (Q_{xy})$ can be introduced, whose element Q_{xy} is the probability to mutate from one sequence $x \in \mathcal{X}$ to another $y \in \mathcal{X}$. Thus the dynamics of the sequence across $\mathcal{X}$ is determined by the Markov process associated to Q (see Appendix A.1).

2.1.1 Quasispecies and the replicator-mutator equation

R. A. Fisher conceived species in a situation of optimal adaptability to their environment, hence they should be placed at one of the maxima of the adaptive landscape (Gavrilets 2004). According to this picture, a particular sequence would be maximally adapted and as sequences move away from it in Hamming distance, their replicative ability should progressively decrease. Molecular biology was in its early stages when Fisher elaborated his metaphor, so he did not apply these ideas to genetic sequences. It was Eigen (1971) who used it to elaborate his theory of *quasispecies*. If the Markov process defined on the set of sequences $\mathcal{X}$ is ergodic, it will lead to an asymptotic probability distribution (see Appendix B.1). For a single-peak landscape shape, the distribution will be localized around the optimally adapted (or *master*) sequence. In spite of that being the most probable sequence, close to it (i.e. a few mutations away) there will be a "cloud" of less adapted sequences (*mutants*) coexisting with the master sequence. Eigen termed this heterogeneous ensemble of sequences as quasispecies.[2]

Quasispecies are realized in practice as RNA viruses, for instance. RNA viruses are characterized by a production of large amounts of progeny and a very high mutation

[2]Originally Eigen proposed this concept under the framework of prebiotic evolution (i.e., evolution in the beginning stage of biotic systems). The study of Eigen concerned evolutionary dynamics of replicators. After Eigen's seminal paper in 1971, the application of his theory to biological sequences (understood as replicators) was just a matter of time.

rate compared, for example, with DNA viruses. In particular, this implies that a given sample of the virus will not contain a single, well-defined sequence but a distribution of sequences which will differ from each other in several mutations. Measurements of multiple sequence alignment in samples of viruses leads to the definition of the so-called *consensus sequence*, which is formed by the most abundant residues in the alignment at each position. It is precisely the high mutation rate affecting these viruses that leads to a heterogeneous ensemble that we recognize as a quasispecies.

In order to study the behavior of a quasispecies more closely we will resort to the so-called *replicator-mutator equation* (Nowak 2006). We shall derive here its discrete-time version although a continuous description can be obtained as easy. Suppose that the population is made up of M different species with replicative abilities $\{r_i\}_{i=1}^{M}$. These parameters account for the mean number of offspring produced by each species every generation. Let $\mathbf{X}^{(t)} = (X_1^{(t)}, \ldots, X_M^{(t)})$ be the stochastic process representing the populations of each species at discrete time t. Species will replicate, but replication is not error-free. In general, replication errors lead to non-viable individuals that cannot survive. These errors can be accounted for by adjusting the replication rate. Occasionally, however, a mutation can produce an offspring of a different and viable type. Thus mutation can be regarded as a stochastic process by which individuals of species i produce individuals of species j with a probability $q_{ij} (\ll 1)$. This mechanism introduces variability in an otherwise homogeneous population. We define $q_{ii} = 1 - \sum_{j \neq i} q_{ij} (\geq 0)$ and introduce the stochastic matrix $\mathsf{Q} = (q_{ij})$ (which we will refer to as the *mutation matrix*) for the later convenience. The stochastic character of Q can be expressed in matrix form as $\mathsf{Q}\mathbf{1}^{\mathsf{T}} = \mathbf{1}^{\mathsf{T}}$, where $\mathbf{1} = (1, \ldots, 1)$.

The conditional probability that a single individual of species i at time t will produce a distribution $\mathbf{k}$ of individuals at the next generation, assuming time independence, is denoted by

$$\Pr\{\mathbf{X}^{(t+1)} = \mathbf{k} | \mathbf{X}^{(t)} = \boldsymbol{\delta}_i\} = p_i(\mathbf{k}), \tag{2.1}$$

where $\boldsymbol{\delta}_i = (\delta_{ij})$ (the Kronecker symbol) for all $j = 1, \ldots, M$. Obviously the general process starting with an arbitrary distribution —not a single individual— at time t is a multitype branching process generated by the replication and mutation of all individuals at each generation (Kimmel and Axelrod 2002).

After a time step, species i will produce on average r_i copies and, with probability q_{ij}, some offspring will have mutated to species j. Although the probability distribution $p_i(\mathbf{k})$ is not specified, the mutation matrix and the replication abilities allow for the calculation of expected values. In fact, the average number of individuals w_{ij} of species j that species i produces at each time step is given by

$$w_{ij} \equiv \mathrm{E}\{X_j^{(t+1)} | \mathbf{X}^{(t)} = \boldsymbol{\delta}_i\} = r_i q_{ij}. \tag{2.2}$$

In matrix form, $\mathsf{W} = (w_{ij}) = \mathsf{RQ}$, where $\mathsf{R} = \mathrm{diag}(r_1, \ldots, r_M)$. W is known as the mutation-replication matrix, which in turn determines the time evolution of the average number of individuals of each species under these assumptions. The expected number

of individuals at time t, $\mathbf{N}^{(t)} = \mathrm{E}\{\mathbf{X}^{(t)}\}$, will therefore satisfy the (discrete-time) replicator-mutator equation,

$$\mathbf{N}^{(t+1)} = \mathbf{N}^{(t)}\mathsf{W}. \tag{2.3}$$

Some consequences can be directly extracted from it. Since W is a non-negative matrix, Perron-Frobenius theory (Seneta (2006); see Appendix B.1.4 for a brief summary) tells us that the asymptotic populations determined by (2.3) are given by the left-eigenvectors (all of whose components are non-negative) of matrix W corresponding to its largest eigenvalue in modulus, which is real. Furthermore, if Q is irreducible (see Appendix B.1.3 for a definition) then there is only one such eigenvector. Hence the population behaves asymptotically as

$$\mathbf{N}^{(t)} \approx \lambda_{\max}^{t}\mathbf{u}_{\max}, \tag{2.4}$$

$\mathbf{u}_{\max}$ being the left-eigenvector corresponding to the largest eigenvalue $\lambda_{\max}$. Therefore, in the absence of additional constraints, the growth of the population is exponential.

Secondly, we can envisage from (2.3) the principle of "survival of the fittest". Let i be the species with maximal replicative ability. In the absence of mutations, $\mathsf{W} = \mathsf{R}$, the eigenvector $\boldsymbol{\delta}_i$ corresponding to that species rules asymptotically the growth. Thus, as $t \to \infty$, individuals of the best adapted species dominate the population.

The dynamics of the population can be better described in terms of the population densities $\mathbf{x}^{(t)} = \mathbf{N}^{(t)}/(\mathbf{N}^{(t)}\mathbf{1}^{\mathsf{T}})$. The replicator-mutator equation turns out to be

$$\mathbf{x}^{(t+1)} = \frac{\mathbf{x}^{(t)}\mathsf{W}}{\mathbf{x}^{(t)}\mathsf{W}\mathbf{1}^{\mathsf{T}}}. \tag{2.5}$$

Multiplying both sides by $\mathbf{1}^{\mathsf{T}}$, it follows immediately that $\mathbf{x}^{(t)}\mathbf{1}^{\mathsf{T}} = 1$ is a constraint that equation (2.5) preserves. The equilibrium density vector $\mathbf{x}$ satisfies the eigenvalue equation

$$\mathbf{x}\mathsf{W} = \langle r\rangle\mathbf{x}, \tag{2.6}$$

where $\langle r\rangle \equiv \mathbf{x}\mathsf{W}\mathbf{1}^{\mathsf{T}}$. Since Q is stochastic,

$$\langle r\rangle = \mathbf{x}\mathsf{R}\mathbf{1}^{\mathsf{T}} = \sum_{i=1}^{M} r_i x_i, \tag{2.7}$$

so the eigenvalue $\langle r\rangle$ is precisely the average replicative ability of the population.

The fact that mutations maintain the variability of the population can be put into mathematical terms. It can be shown that every irreducible matrix has at least one non-diagonal element in each row, so the equilibrium vector necessarily has more than one non-zero component. This means that when all species can mutate, the equilibrium population cannot be homogeneous.

2.1.2 The error catastrophe

We are now ready to study the behavior of a quasispecies more closely using the replicator-mutator equation. For simplicity we shall assume that sequences have finite length $L_\mathrm{s} \gg 1$, that the master sequence has replicative ability $r_1 = r > 1$ and that all other sequences have replicative ability $r_2 = \cdots = r_M = 1$. We shall also assume that the probability per locus that a point mutation occurs is $p \ll 1$, independent of the sequence. Let $x_1 = x$ denote the population density of the master sequence; thus $x_2 + \cdots + x_M = 1 - x$ and the average replicative ability is $\langle r \rangle = rx + 1 - x$. Then equation (2.5) becomes

$$\sum_{j=1}^{M} x_j r_j q_{ji} = x_i[1 + (r-1)x]. \tag{2.8}$$

Setting $i = 1$, we get

$$x\left[r(1-p)^{L_\mathrm{s}} + \mathcal{O}(p)\right] = x\left[1 + (r-1)x\right]. \tag{2.9}$$

The term $\mathcal{O}(p)$ accounts for the transitions from the L_s nearest neighbor sequences of the master sequence that revert to the master sequence. Neglecting these terms and approximating $(1-p)^{L_\mathrm{s}} \approx 1 - pL_\mathrm{s}$ we can see that if $pL_\mathrm{s} < 1 - 1/r$, then x asymptotically approaches to $x^* = 1 - rpL_\mathrm{s}/(r-1)$, whereas if $pL_\mathrm{s} > 1 - 1/r$ the equilibrium density is $x^* = \mathcal{O}(p)$. The threshold

$$p_\mathrm{err} = \left(1 - \frac{1}{r}\right)\frac{1}{L_\mathrm{s}} \tag{2.10}$$

in the mutation rate defines the *error catastrophe*. When $p < p_\mathrm{err}$ the quasispecies is well defined because the master sequence is the most probable one. However, when $p > p_\mathrm{err}$ the identity of this master sequence gets lost in the cloud of mutants and the quasispecies disappears as such.

Experimental studies performed in the 90s seem to confirm (Nowak 2006) that indeed the length of the genome of different species —ranging from virus to Homo sapiens— and the mutation rate per base are related as $pL_\mathrm{s} \leq \mathcal{O}(p)$. Hence an increase in the mutation rate is a mechanism that this theory puts forward to fight viral infections (this process is called *mutagenesis*, whereby increasing mutation rates are attained by means of certain chemicals known as *mutagens*).

However, Eigen's theory has serious drawbacks. Quasispecies theory is based on the assumption of a single-peak adaptive landscape, which in turn leads to the existence of a master sequence (whose replicative ability *decreases* with any mutation, hence beneficial mutations are neglected) and an error threshold in the mutation rate. What would happen if the hypothesis of a single-peak adaptive landscape is not reliable?

2.1.3 The effect of neutral and beneficial mutations

At the end of the 60s it was already known that most genome mutations were neutral. Kimura proposed a good argument supporting their existence (Kimura 1968). It goes

as follows. Comparative studies of some proteins lead to the conclusion that chains 100 amino acids long undergo one substitution every 28 million years. The length of DNA chains in the two chromosome sets of mammals is about 4×10^9 base pairs. Every three base pairs code for one amino acid and, due to redundancy effects (a 20% of nucleotide substitutions are estimated as synonymous), only an 80% of base pair substitutions leads to an amino acid substitution. Hence there are about 16 million substitutions in the whole genome every 28 million years. This amounts to almost one substitution every 2 years! Kimura's conclusion is that organisms can only afford such a high mutational load provided the great majority of mutations are *neutral*, i.e., they have no effect on the adaptability of the mutated sequence.

Recent studies on RNA molecules reach similar conclusions (Fontana 2002). RNA molecules fold as a result of the interaction between the bases forming their sequences. This folding can be regarded as the molecule *phenotype*[3] because it essentially determines the function of the molecule. Thus natural selection acts directly on phenotypes, being blind to the actual sequences (Kun et al. 2005). The number of different sequences folding into the same structure is very large,[4] so there is a high redundancy in the genotype-phenotype map. This implies, once more, that a large number of mutations in the chain leave the phenotype intact (i.e. are neutral, in line with Kimura's estimation), thus avoiding selection.

The metaphor of a single-peak landscape becomes utterly inappropriate to describe the dominance of neutral mutations. A more appropriate picture would be that of a flat landscape with holes. Evolution moves sequences across this flat landscape,[5] transforming them into completely different sequences without ever changing their phenotype nor decreasing their adaptability. Undoubtedly, this mechanism speeds up not only adaptation of species to the environment but even speciation.

The fact that adaptability depends on phenotype and not on genotype favors the appearance of neutral regions in adaptive landscapes. This is what is observed in RNA (Fontana 2002). Remarkably, this new picture of adaptive landscapes implies that the main assumption of Eigen's model, namely that locally the landscape has a maximum, is incorrect. There is no such a thing as a master sequence. Instead there is a *master phenotype* that contains a large number of sequences. Correspondingly, the probability that a mutation recovers the optimal replicative ability (i.e. a non-zero *beneficial* mutation) can not be neglected (Huynen et al. 1996), as Eigen's theory assumes, because adaptability can be recovered by hitting any of the sequences corresponding to that phenotype, not necessarily the initial one. When this probability is not negligible the error catastrophe goes away (Manrubia et al. 2010). Let us, by way of conclusion, illustrate this fact with a toy example.

[3] Phenotypes are observable characteristics or traits of an organism, which result from the expression of its genes (*genotype*) as well as from the influence of environmental factors.

[4] The mean number of RNA sequences of length L_s folding into the same structure can be approximated by $0.6735 L_\mathrm{s}^{3/2} (2.1653)^{L_\mathrm{s}}$ (Schuster et al. 1994). In particular, for sequences of $L_\mathrm{s} = 100$ nucleotides, there are $\sim 10^{34}$ sequences leading to the same structure on average.

[5] Also known as *neutral network* of genotypes (Maynard Smith 1970; Gavrilets 2004).

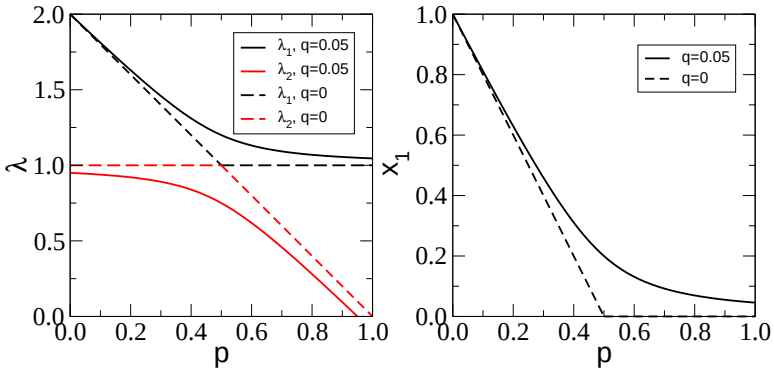

Figure 2.1: *Effect of beneficial mutations in Eigen's model.* Left panel shows the eigenvalues of matrix (2.11), the largest one in black. Right panel depicts the equilibrium density of the master class. In both cases, $q = 0$ is represented with dashed lines and $q = 0.05$ with full lines. The replicative ability of the master class is $r = 2$. In the absence of beneficial mutations, the crossing of eigenvalues at $p = 1/2$ represents the error threshold predicted by the theory: for $p > 1/2$, the density x_1 of the master class vanishes. When $q > 0$ the population fraction of the master class is always positive, even for large mutation rates, and the error catastrophe disappears.

The effect of a non-zero probability of beneficial mutation can be showed up easily (Bull et al. 2005). Consider a system composed by $M = 2$ phenotypes with replicative abilities $r_1 = r > 1$ and $r_2 = 1$. When beneficial mutations are not neglected, the mutator-replicator matrix is given by

$$\mathsf{W} = \begin{pmatrix} r(1-p) & rp \\ q & 1-q \end{pmatrix}, \tag{2.11}$$

since class 1 undergoes deleterious mutations (with probability p) to the second class, but there are beneficial mutations (with probability $q \ll 1$) that increase the replicative ability of the less-fitted class. Figure 2.1 left shows the two eigenvalues of W for $q > 0$ (full lines) and $q = 0$ (dashed lines). When $q = 0$, both eigenvalues meet at $p = 1 - 1/r$. This causes a non-analyticity of the leading eigenvalue, which corresponds to the error threshold.[6] Correspondingly, the density of the master class vanishes above the error threshold. However, for $q > 0$ there can not be a crossing of eigenvalues because W is then irreducible. The presence of non-negligible beneficial mutations renders the density of the master class strictly positive, as the right panel of Figure 2.1 shows.

[6] We will see in Chapter 5 that such a crossing of eigenvalues provides a signal that the system undergoes a phase transition, in the sense defined by statistical mechanics.

2.2 Spatial competition conditions infection spreading

Cellular parasites are an ineluctable outcome of evolutionary processes (Koonin et al. 2006). A great variety of viruses, usually with a high degree of specificity, targets animal and plant cells. Viruses commonly attain host infection thanks to the steady production of mutants and of enormous amounts of offspring. Success depends, among others, on host's ability to fight infection, on its capacity to struggle the parasite through the immune system, and on the features of the environment where infection takes place.

The design of therapies able to cause viral extinction is a challenging subject. A clear knowledge of the mechanisms that render an infection extinct seems prior to the design of successful strategies to eradicate the pathogen. According to Eigen's model, increased mutagenesis has been successfully used *in vitro* to remove infections, though there is no general agreement on the pathways that induce extinction (Wilke 2005; Bull et al. 2005; Takeuchi and Hogeweg 2007; Manrubia et al. 2010). Most likely, strong increases in the mutation rate lead to extinction though *mutational meltdown*[7] (Gabriel et al. 1993), a process different from the error threshold predicted by classical quasispecies theory. On the other hand, mild increases in the mutation rate might cause stochastic extinction due to an increased production of defective phenotypes (Grande-Pérez et al. 2005; Iranzo and Manrubia 2009). The interference of subpopulations close to extinction or the precise effect of chemical inhibitors together with mutagens (Perales et al. 2009) are two mechanisms under investigation. An improved understanding of the mechanisms causing viral extinction is required before they can be applied *in vivo*.

Actual viral behavior often deviates substantially from the predictions of simple models like the one presented in Section 2.1 (Eigen 2002). Quasispecies models are realistic since they assume that mutations are frequent enough as to maintain heterogeneous populations —a property of most viruses infecting plants (García-Arenal et al. 2001) and many *in vitro* systems of viral evolution on cellular monolayers (Manrubia and Lázaro 2006). However, one of its most remarkable drawbacks is the assumption that all new mutations have a deleterious effect, thus neglecting neutral and beneficial mutations, which is in disagreement with the fact that adaptation (thus improvement) occurs frequently even at low population numbers. Further, as we have mentioned, classical quasispecies models are based on a single-peak adaptive landscape, so they assume the existence of a unique master sequence of maximal replicative ability. As of today, due to the extreme redundancy of the genotype-phenotype map, we know that there is a huge amount of different sequences yielding phenotypes that perform equally well. The inclusion of beneficial and compensatory mutations in models of viral evolution leads to a new class of collective behavior where no error threshold is to be found, and where extinction occurs through other mechanisms (Manrubia et al. 2010).

The progress of an infection is further conditioned by the geometry of the space where it occurs (Petermann and de los Ríos 2004; Barrat et al. 2008). Infection spread-

[7] Mutational meltdown refers to the process by which a small population accumulates deleterious mutations, which leads to loss of adaptability and decline of the population size, which in turn may lead to further accumulation of deleterious mutations due to the breeding of related individuals.

ing in cells suspended in a well stirred media (three-dimensional media) or on a lawn (two-dimensional media), for example, can be dramatically different. Plant leaves, in particular, are well described as two-dimensional tissues. Plant-to-plant propagation in crops is another example with the same geometry. Experiments with the *bacteriophage* $Q\beta$ under increased mutagenesis have shown that the number of mutations fixed in liquid medium or in bacterial monolayers is substantially different (Cases-González et al. 2008). Spatial constraints cause a strict clustering of the propagation in crops (Coutts et al. 2004) and even of subpopulations of clonal viruses. Mutant phenotypes that remain clustered in a lawn of cells have also been identified in experiments with the *bacteriophage T7* (Lee and Yin 1996).

The outcome yielded by different models of viral infection depend on whether physical space is explicitly considered or not (Rand et al. 1995). In quasispecies models, cell-to-cell transmission or local diffusion of viruses unavoidably produces a lower value of the error threshold (Altmeyer and McCaskill 2001; Toyabe and Sano 2005). Clusterization of viral types is responsible for the latter effect, as well as for enhancing heterogeneity in the coexisting types of the quasispecies (Pastor-Satorras and Solé 2001; Aguirre and Manrubia 2008).

In the remaining of the chapter we will introduce and analyze a model for viral infection spreading on two-dimensional arrays of cells. The model incorporates two realistic features of infection propagation: there is a non-negligible fraction of beneficial mutations and the host is allowed to develop resistance against the pathogen. When there are no limits in the number of cells susceptible to be infected, we prove that the virus can overcome host resistance by increasing the number of offspring per replication cycle. However, this strategy fails with the incorporation of physical space. When types compete for the same cell, it turns out that propagation comes to a halt at a finite value of the host's resistance to infection, regardless of the progeny production of the virus. Using standard techniques of statistical mechanics, we can prove that the (phase) transition to extinction belongs to the universality class of directed percolation. These results can be extended to any situation where there is a limited number of susceptible cells per generation, irrespective of their geometrical configuration.

2.3 Dynamical model

In this model viral populations are described as quasispecies, i.e., as ensembles of (pheno)types characterized by the number of offspring produced by each type under replication which are able to infect healthy cells.[8] Thus species are defined according to their replicative ability $r = 0, \ldots, M$. Without loss of generality, we speak of viruses as the pathogenic agent and of individual cells as hosts. An offspring of a viral strain is affected by deleterious (decreasing its progeny production in one unit with probability p) or beneficial mutations (increasing its replicative ability in one unit with

[8]The actual number of offspring can be orders of magnitude larger than the number of their effective infections. For instance, in vesicular stomatitis virus only a single viral particle in ten-thousand is able to infect on its own.

probability q). Lethal mutations can hit the lowest class $r = 1$ with probability p.[9] Susceptible cells develop a resistance against infection quantified through probability π, that is to say, a viral particle can infect a host with probability $1 - \pi$.

As we have mentioned in Section 2.1.3, when beneficial mutations are present, phenotypes of high r can be recovered from mutants of low r, even if mutations accumulate steadily in a genome. On the other hand, most known viral resistance mechanisms in plants target either viral replication or mobility (Knipe and Howley 2007). The former mechanism can be subsumed under parameter p; the latter is explicitly represented by host resistance π. These two ingredients, i.e. the inclusion of mutations with positive effect on adaptability and of host resistance to infection, are major differences with respect to quasispecies models studied so far. We assume that time updates occur in discrete generations (although the model can be extended to continuous time with similar results).

We have tackled two different situations. In the first one, there is an unlimited abundance of cells and every viral particle can *a priori* infect a susceptible cell. In the second one, the number of cells is limited due to geometric constraints and thus viral particles must compete to enter a cell.

2.3.1 Unlimited number of cells

Let us first assume that the availability of susceptible cells is large enough for every infective viral particle (with $r > 0$) to actually meet a cell to infect, irrespectively of its replicative ability r. This situation with excess of resources corresponds to a mean-field approximation to the dynamics, where infection occurs with probability $1 - \pi$. Under these assumptions, if $N_r(t)$ denotes the number of viral particles of type r at generation t, the population dynamics follows the iterative equation

$$N_r(t+1) = (1-\pi)\left[r(1-p-q)N_r(t) + (r+1)pN_{r+1}(t) + (r-1)qN_{r-1}(t)\right] \tag{2.12}$$

for classes $r = 1, \ldots, M-1$ and

$$N_M(t+1) = (1-\pi)\left[M(1-p)N_M(t) + (M-1)qN_{M-1}(t)\right]. \tag{2.13}$$

The total number of individuals in class r at generation $t+1$ receives contributions from the replication without changes of individuals of the same class plus adjacent classes $r \pm 1$ which mutate to r. Besides, there is a class $r = 0$ which has lost its replicative ability, whose population is maintained by the class $r = 1$ through deleterious mutations, i.e. $N_0(t+1) = (1-\pi)pN_1(t)$. As initial condition we take $N_r(0) = \delta_{rM}$.

This set of equations cannot be fully solved for arbitrary values of the parameters.[10] However, for $q = 0$ an exact analytical solution exists, which allows for the calculation

[9] The effect of microscopic (genotypic) mutations on the phenotype of RNA molecules during their adaptation has been recently investigated computationally (Stich et al. 2010). The probability distribution of the distance to a target secondary structure allows for the definition of *phenotypic* fractions of beneficial and deleterious changes q and p, respectively.

[10] A generating function can be calculated for the sequence $\{N_r(t)\}_{t=0}^{\infty}$, but the series expansion that eventually yields the sequence is difficult to perform (Cuesta 2010).

of lower bounds for the extinction thresholds. In this case beneficial mutations are absent, so it represents the worst possible situation for the survival of the virus (if extinction does not occur for $q = 0$, it will not occur for any positive q either).

In the asymptotic limit $t \to \infty$, the population of every class grows at a fixed rate, $N_r(t+1) = \lambda N_r(t)$. System (2.12)–(2.13) becomes a spectral problem, λ being the largest eigenvalue. In this regime, λ stands for the growth rate of the population. For $q = 0$ it can be easily checked [by substitution into (2.12)–(2.13)] that the fraction of viral particles of type r is

$$x_r \equiv \lim_{t\to\infty} \frac{N_r(t)}{\sum_{r=0}^{M} N_r(t)} = \binom{M}{r} p^{M-r}(1-p)^r \,, \tag{2.14}$$

and that the asymptotic growth rate $\lambda = (1-\pi)(1-p)M$. From this expression the average replicative ability of the infective classes (excluding type $r = 0$) turns out to be

$$\langle r \rangle = \frac{\sum_{r=1}^{M} r x_r}{\sum_{r=1}^{M} x_r} = \frac{Mp}{1-(1-p)^M}. \tag{2.15}$$

Extinction occurs when $\lambda \leq 1$, a condition fulfilled by all viral populations with maximal progeny production $M \leq M_c = (1-\pi)^{-1}(1-p)^{-1}$. The larger the resistance to infection of the cell, the most demanding is the condition on replicative ability. This notwithstanding, there is no limitation in the increase of M. There is always a value of M such that the asymptotic growth rate of the population is above one.[11] Therefore, irrespectively of the defenses developed by the host, the virus can in principle increase the production of progeny so as to keep an on-going infection. Hence if the number of susceptible cells is unlimited, a runaway co-evolution between the virus and the host is to be expected.

2.3.2 Limited number of cells

Restrictions in the number of susceptible cells available change qualitatively the mean-field dynamics discussed previously. One of these situations occurs when cells have a spatial distribution and the mobility of viruses is limited. To assess the consequences of this constraint, we have to specify how the infection spreads in a space-explicit environment. Our model is inspired by an often applied protocol in which the infection spreading occurs on cellular monolayers (Manrubia and Lázaro 2006). The process is started when the offsprings of a viral particle infecting a cell are released to the medium after cell death. A fraction of that progeny infects adjacent, susceptible cells. The process repeats and the size of the (lytic) plaque formed by dead cells grows. After a transient period, all activity occurs at the perimeter of the plaque. If the population does not tend to extinction, in the asymptotic limit the number of cells killed per infective cycle reaches a constant value. Even if infection starts off from a single infected cell, it

[11] In the case $q > 0$ it can be shown that the population growth is asymptotically *super-exponential* (Cuesta 2010).

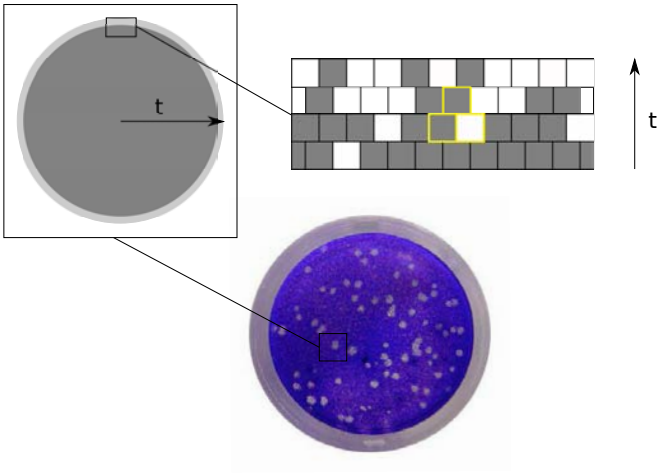

Figure 2.2: *A two-dimensional set-up for viral spreading.* In the limit $t \to \infty$ the growth of a lytic plaque in a two-dimensional mololayer is approximated by an array of length L_a representing the propagation front. Shaded cells are those infected by viral particles. At generation t, the infective classes occupying two adjacent sites compete with each other to enter a cell and produce an offspring at generation $t+1$ (cells involved are shown with yellow borders).

proceeds like the propagation of a front, and asymptotically this front will become practically flat (Aguirre and Manrubia 2008). Hence we consider a flat propagating front from the beginning. Note that, although the propagation is two-dimensional, the radial growth can be assimilated to time. Cells thus form arrays in one spatial dimension, and the front propagates perpendicularly and advances one row of cells per generation (see Figure 2.2). Our model is basically a (1+1)-dimensional, probabilistic cellular automaton evolving in discrete time (see Appendix A for a discussion on probabilistic cellular automata).

Thus, without loss of generality, we assume that the dynamics of the model proceeds in discrete generations on a triangular lattice with periodic boundary conditions (see Figure 2.3 for a typical configuration close to extinction). Let $r_i(t)$ be the replicative ability of the individual occupying site i at generation t. Cells are labeled by their position $i = 1, \ldots, L_\mathrm{a}$ in the row (L_a being the length of the array) and the generation $t = 0, 1, \ldots$ at which the front reaches them.

Initially we take $r_i(0) = M$ for all $i = 1, \ldots, L_\mathrm{a}$. To account for the limited mobility of viral particles, these were constrained to infect only neighboring cells. Hence, at generation $t+1$ site i will be occupied by one of the offspring of the individuals at sites i or $i+1$ at the parental generation t. Then the conditional probability that $r_i(t+1) = r$, given that the replicative abilities of these individuals are $r_i(t) = r_1$ and

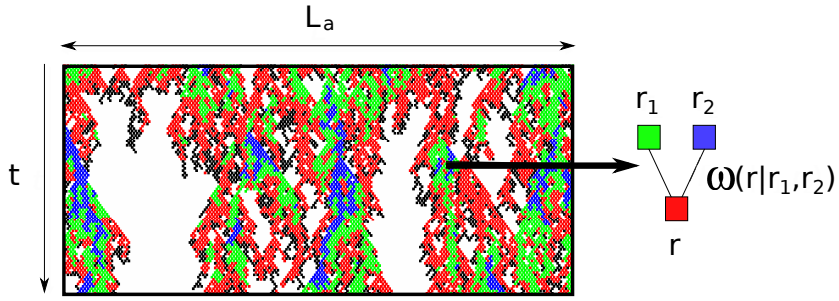

Figure 2.3: *Dynamics of the model of infection propagation close to the extinction threshold.* A linear array of infected cells represents the propagation front and produces offspring to infect the next infective cycle. For this example, $M = 4$. Individuals of each class form clusters (black: $r = 1$, red: $r = 2$, green: $r = 3$, blue: $r = 4$). Failure to infect leaves an empty site; success means occupation according to the probabilistic rules given by (2.17).

$r_{i+1}(t) = r_2$, denoted

$$\omega(r|r_1, r_2) \equiv \Pr\{r_i(t+1) = r | r_i(t) = r_1, r_{i+1}(t) = r_2\}, \tag{2.16}$$

is independent of the site and given by

$$\omega(r|r_1, r_2) = \pi^{r_1+r_2}\delta_{r0} + \left(1 - \pi^{r_1+r_2}\right) \frac{r_1 p_{r_1,r} + r_2 p_{r_2,r}}{r_1 + r_2}, \tag{2.17}$$

where

$$p_{r_1,r_2} = p\delta_{r_1,r_2+1} + (1-p-q)\delta_{r_1 r_2} + q\delta_{r_1,r_2-1} \tag{2.18}$$

for $r_1, r_2 < M$ and $p_{M,r} = p\delta_{M,r+1} + (1-p)\delta_{Mr}$. According to (2.17), the probability that the cell resists the viral attack is given by $\pi^{r_1+r_2}$, i.e. the probability that infection fails after $r_1 + r_2$ independent trials. With the complementary probability infection occurs, and subsequently one randomly chosen individual among the $r_1 + r_2$ offspring enters the cell. Its replicative ability may change due to mutations according to the specified probabilities p and q. The limit case $\pi \to 1$ represents an immune host, whereas in the limit $\pi \to 0$ the host plays no role in the progress of infection. Note also that the probability of infection tends to zero as the number of viral particles trying to infect a particular cell increases, and tends to one as the cell resistance improves. Since the entry of more than one viral particle is not allowed, the model implicitly assumes that different genotypes rarely infect the same cell (Takahashi et al. 2007). This is a "winner takes all" rule that could be easily relaxed to account for different processes, including a multiplicity of infection larger than one or superinfection of a cell.

Two relevant quantities that define the dynamical state of the system are the spatial density of active sites (those occupied by viruses with $r \geq 1$) at time t,

$$\rho(t) = 1 - \frac{1}{L_\mathrm{a}} \sum_{i=1}^{L_\mathrm{a}} \delta_{0 r_i(t)}, \tag{2.19}$$

and the average replicative ability of the population $\langle r(t) \rangle = (\rho(t) L_\mathrm{a})^{-1} \sum_{i=1}^{L_\mathrm{a}} r_i(t)$. A systematic study of these two magnitudes in the limit $t \to \infty$ as a function of p, q and π portrays the asymptotic behavior of the model.

Extinction without beneficial mutations: Error thresholds

When beneficial mutations are absent ($q = 0$), the class with the highest r present disappears when p or π increase beyond a threshold value (white curves of the phase space represented in Figure 2.4) . These transitions are analogous to the error threshold described for simple models of quasispecies (Eigen 1971), where the master sequence disappears and the population turns into a cloud of less-adapted replicating mutants. In our case, it is the "master phenotype" that disappears, the population turning into an organized ensemble of types with lower replicative ability. When the resistance to infection π is kept constant, there is a hierarchy of domains in the phase space where high-r classes are sequentially lost as p increases. For p positive but close enough to zero, all types are still present. As p increases, high-r classes begin to disappear, first class M, then class $M-1$, and so on, until only individuals with $r = 1$ are left, and they also become eventually extinct. The cascade of extinctions as p increases depends on the value of π. For increasingly large values of π, complete extinction of the population occurs with types of increasingly larger replicative ability present.

There are two features of Figure 2.4 for $q = 0$ which are amenable to further analysis. The first one is the last error threshold, when class $r = 1$ disappears. There is a mapping of this transition to the *Domany-Kinzel* (DK) probabilistic cellular automaton (Hinrichsen 2000). This automaton evolves in a spatial set-up similar to the present one, where sites can be either occupied or empty (Appendix A summarizes the main features of DK model). The elementary probabilities that define the automaton are $\omega(1|0,0) = 0$, $p_1 \equiv \omega(1|1,0) = \omega(1|0,1)$, $p_2 \equiv \omega(1|1,1)$ [and of course $\omega(0|x,y) = 1 - \omega(1|x,y)$]. In the (p_1, p_2) plane, a transition line separates an active phase from a phase consisting of an array of empty sites [see Figure A.1; that phase diagram has been reproduced from Hinrichsen (2000)].

In our case, and when only classes $r = 1$ and $r = 0$ are present, sites can either be replicative (occupied) or non-replicative (empty). According to (2.17), the corresponding DK automaton has probabilities $\omega(1|0,0) = 0$, $p_1 = \omega(1|1,0) = \omega(1|0,1) = (1-\pi)(1-p)$, and $p_2 = \omega(1|1,1) = (1-\pi^2)(1-p)$. This defines a mapping between the (π, p) plane and the (p_1, p_2) plane. Therefore the transition line obtained by numerical simulation for the DK automaton can be represented in Figure 2.4 as the C curve (orange dashed). The top white curve of that figure coincides with the DK transition cast in the variables (π, p) describing our model. Two special cases of the DK

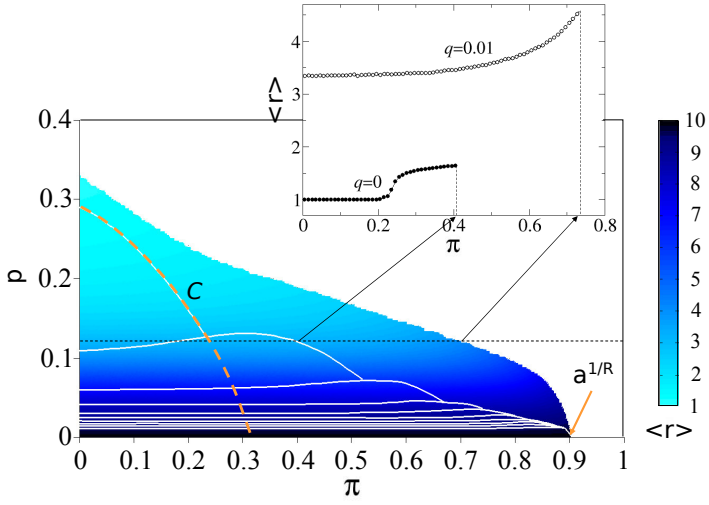

Figure 2.4: *Phase space of the model.* Two choices for the probability of a beneficial mutation q are shown: $q = 0$, where high-r classes are sequentially lost as the probability of a deleterious mutation p increases, and $q = 0.01$, where only the global extinction of the population is possible. In these examples, the top class has replicative ability $M = 10$. White lines correspond to the thresholds for the successive loss of the highest replicative class present (r decreasing from bottom to top) when $q = 0$. Colors code for the average replicative ability $\langle r \rangle$ as a function of p and the host resistance π when $q = 0.01$. In the inactive phase (white domain), infection is cleared in finite time. Inset shows $\langle r \rangle$ as a function of π for $p = 0.11$ and two values of q. Data have been obtained simulating a system of size $L_a = 10^4$ sites and averaging over 5×10^3 time steps after a transient of 2×10^4 generations.

automaton are calculated with high precision (see Appendix A): site percolation, which corresponds here to $\pi = 0$, and bond percolation, which maps to the limit $p = 0$. The latter is irrelevant for any $M > 1$ because it is preempted by the extinction transitions of higher r classes. However, using the simulation critical point for site percolation (see Table A.2), we obtain the meeting point with the vertical axis at $p_c = 0.294510(6)$.

The second feature that can be obtained again from a mapping with the DK model is the extinction threshold of the highest class $r = M$ at $p = 0$. Given that the initial condition only contains individuals of the master type, no other classes will ever appear in the evolution because of the lack of deleterious mutations. Hence sites can either be occupied by an $r = M$ individual or empty, just as in the DK model. Probabilities are $\omega(M|0,0) = 0$, $p_1 = \omega(M|M,0) = \omega(M|0,M) = 1 - \pi^M$, and $p_2 = \omega(M|M,M) = 1 - \pi^{2M}$. These probabilities correspond to the bond per-

colation case, from which it follows that the threshold occurs at $\pi_c = a^{1/M}$, with $a = 0.3552998(9)$. Only in the limit $p = 0$ and $M \to \infty$ would $\pi_c \to 1$, taking a finite value for any other combination of parameters.

Extinction with beneficial mutations: Struggle for space

For $p \neq 0$ and $q > 0$, no matter how small, all error thresholds disappear, as Figure 2.4 illustrates. The population again becomes extinct beyond a critical line in the (π, p) plane, which is different for each value of q. Now, however, all replicative types are present in the infective phase and the infective population is cleared as a whole. From that figure we deduce that, for a fixed value of the resistance to infection π, low-r classes get more populated upon increasing p, and hence the average replicative ability decreases. At the threshold line, $\langle r \rangle$ drops abruptly to zero.

The behavior as π increases at constant p is of a different nature, though, as we observe from the inset of Figure 2.4. To understand this effect one has to consider the changes produced in the structure of the population as it approaches extinction. In particular, the average replicative ability increases with π, at the same time that infected cells become sparser. In the absence of neighbors, the probability that a cell at generation $t + 1$ is infected by offspring of an individual of class r at generation t is proportional to $1 - \pi^r$. This quantity penalizes more severely low-r classes as π increases, such that high-r classes receive a relative advantage as π_c is approached. At the critical value π_c the quasispecies eventually collapses because propagation is prevented by host defenses, and again $\langle r \rangle$ drops abruptly to zero from the highest value it has been able to reach. The inset of Figure 2.4 shows a cross-section at constant p, where the internal and final extinction thresholds for $q = 0$ and $q = 0.01$ are clearly visible.

More importantly, there is another difference between the two models. Increasing the maximal progeny production M when cells are in excess is a mechanism to circumvent the host resistance to infection, because there is a lower bound M_c for each π such that increasing the replicative ability above that bound helps to avoid infection clearance. In contrast, when viral classes have to compete for susceptible cells, there is a critical value of π above which the propagation of the viral infection comes to a halt. In Figure 2.4, we were using a finite value of $M = 10$ as an example. However, the struggle for infecting a limited number of cells makes that an increase in progeny production is no longer a useful strategy. Increasing M above a critical value does not endow the virus with any additional advantage. To illustrate this statement, we have analyzed the dependence with M of the average replicative ability at the value of π where extinction supervenes. Our results are summarized in Figure 2.5. Initially the average replicative ability increases with M. However, $\langle r \rangle$ quickly saturates to a constant value. In order to show that this effect results from the limitation in the number of cells available, we have modified the model to consider an additional situation. Up to now, only two cells were available to each parental cell. We have also studied a case where viral mobility is larger, and four cells are available for each infection event. This amounts to increasing the competition between types, such that low-r classes are at a

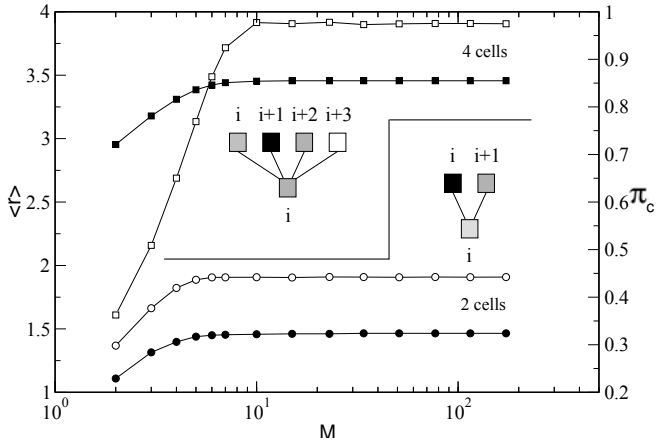

Figure 2.5: *An increase in progeny production does not imply an improvement in virus survival.* When the number of available cells is finite, the average replicative ability $\langle r \rangle$ (open symbols, left vertical axis) and the critical value of the resistance to infection $\pi_{\rm c}$ (solid symbols, right vertical axis) saturate to finite values as the maximal progeny production M increases. Small increases in M provide the virus with an advantage, but this regime crosses-over to saturation at a value of M that depends on the number of new susceptible cells available per cell and generation. In these curves, $p = 0.2$, $q = 0.01$, and averages over 50 independent realizations for each value of $\pi_{\rm c}$ have been performed. Mean-square deviations are smaller than symbol size.

disadvantage with respect to the previous situation, and the average replicative ability of the population should thus increase (Aguirre and Manrubia 2008). This is what is observed and represented in Figure 2.5. Note that, irrespectively of M, the number of actual offspring is bounded by the number of susceptible cells available. As a consequence, $\langle r \rangle$ is bounded even for types with a high replication rate, as we indeed observe in the saturation curves. As a side effect, the critical value of host resistance, $\pi_{\rm c}$, at which extinction occurs also saturates to a value below 1 as $M \to \infty$. The possibility of a runaway co-evolution is therefore excluded in this case: if the host cell is able to increase its defenses beyond $\pi_{\rm c}$, infection will not progress.

Critical behavior of spatial extinctions

When the number of susceptible cells is limited, the extinction transitions, both of the whole population ($q > 0$) and the class with the highest replicative ability present ($q = 0$), belong to the universality class of *directed percolation* (DP). This has been rigorously proven in the latter ($q = 0$) case for the extinction of the $r = 1$ class (for the range of p where it is the only remaining class, see Figure 2.4) as well as when $p \to 0$, by mapping the model to a DK cellular automaton, whose belonging to the DP class is

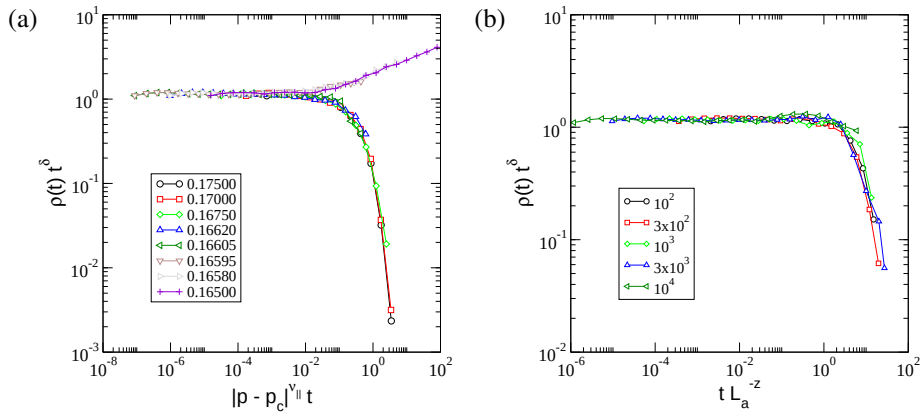

Figure 2.6: *The extinction transition belongs to the universality class of directed percolation.* Data collapse of curves $\rho(t)$ according to the critical exponents known to characterize (1+1) directed percolation. These exponents are $\delta = 0.159464(6)$, $\nu_{\|} = 1.733847(6)$, and $z = 1.580745(10)$ (Hinrichsen 2000). Parameters in these simulations are $M = 2$, $q = 0.01$, $\pi = 0.3$. Data have been averaged over 50 independent realizations and up to 10^8 generations for each curve. (a) The system size is $L_{\mathrm{a}} = 10^4$ for this plot, and the legend shows the values of p for each curve. For this choice the transition occurs at $p_{\mathrm{c}} = 0.16600(3)$. (b) Scaling with the system size L_{a} (the legend provides the corresponding values of L_{a}).

a well established fact (Hinrichsen 2000). Besides, the DP conjecture (see Hinrichsen (2000) and Appendix A.2), so far neither proven nor disproven, implies that our model should belong to the DP universality class: our model is defined on a set of local rules, has no special symmetries or disorder, and exhibits a continuous transition to a unique absorbing state (total extinction), characterized by the behavior of the density of infected sites $\rho(t)$, which acts as an order parameter.

An empirical proof of this fact is provided by the results represented in Figure 2.6a, where $\rho(t)$ is appropriately rescaled according to the known exponents of DP. At the transition point, the density of infected sites should decay algorithmically with the number of generations as $\rho(t) \propto t^{-\delta}$, with $\delta = 0.159464(6)$. A second critical exponent, $\nu_{\|}$, characterizes the behavior of the correlation length in the temporal direction: as the critical point is approached, the correlation length diverges as $|p - p_{\mathrm{c}}|^{-\nu_{\|}}$, with $\nu_{\|} = 1.733847(6)$ for DP. Hence, a representation of $\rho(t)t^{\delta}$ as a function of the rescaled variable $|p - p_{\mathrm{c}}|^{-\nu_{\|}}$ leads to a collapse of all curves $\rho(t)$ for values of p close to p_{c}. The transition point p_{c} is numerically determined as the value of p yielding the best collapse. A third exponent is enough to determine the universality class of the transition, since all remaining exponents can be obtained as a function of just three (Grassberger and de la Torre 1979; Mendes et al. 1994). In our case, we have

studied the variation of $\rho(t)$ at $p_{\rm c}$ with the system size $L_{\rm a}$, which is characterized by the dynamic exponent $z = 1.580745(10)$. As shown in Figure 2.6b, the critical curves corresponding to different system sizes all collapse under appropriate rescaling. This numerical study has been repeated for the transition where $r = 2$ disappears at $q = 0$, with analogous results.

2.4 Analytical approximations to the transition line

To gain more insight into the mechanisms leading to extinction in situations where competition for susceptible cells is dominant, it is useful to make analytical approximations to the density of active sites and the transition line. Standard techniques have been applied in the past to probabilistic cellular automata (Tomé 1994; Atman and Dickman 2002). This methodology can be extended to our model.

Such simple approximations, applied to the DK cellular automaton, have been illustrated in Appendix A.3. These approximations exploit the fact that probabilistic cellular automata are discrete-time Markov processes and therefore they satisfy a dynamical equation [analogous to Eq. (A.7)] for the probability $p_t(\mathbf{r})$ of a given configuration of replicative abilities $\mathbf{r} = \{r_i\}_{i=1}^{L_{\rm a}}$ occupying the lattice at time t. This way, we can write down a hierarchy of equations for the one-, two-, ..., m-site marginal probabilities. Such a hierarchy is obviously infinite, but can be closed at a certain level using an approximate closure relation between marginal probabilities.

Let $\rho_i = \lim_{t\to\infty} p_t(i)$ be the asymptotic density of cells occupied by a virus of class i, where

$$p_t(i) \equiv \Pr\{r_j(t) = i\} \tag{2.20}$$

is the marginal probability that a given cell (j) is infected by a viral particle of replicative ability i (remember that $r_j \in \{0, 1, \ldots, M\}$). The one-site (or "mean-field") approximation factors the two-site marginal probability out as a product of one-site probabilities. The set of equations (A.11) satisfied by the one-site probability of cell j and the closure (A.13) yield the following nonlinear system for the asymptotic densities of each viral class,

$$\rho_i = \sum_{j=0}^{M}\sum_{k=0}^{M} \omega(i|j,k)\rho_j\rho_k, \quad i = 0, 1, \ldots, M, \tag{2.21}$$

together with the normalization condition $\sum_{i=0}^{M} \rho_i = 1$.

Two-site (pair) approximations express two-site marginal probabilities,

$$p_t(i,j) \equiv \Pr\{r_k(t) = i, r_{k+1}(t) = j\}, \tag{2.22}$$

the next in the hierarchy [Eqs. (A.11) and (A.12)]. It can be closed at this level by approximating three-site probabilities according to (A.16). The system to solve in this

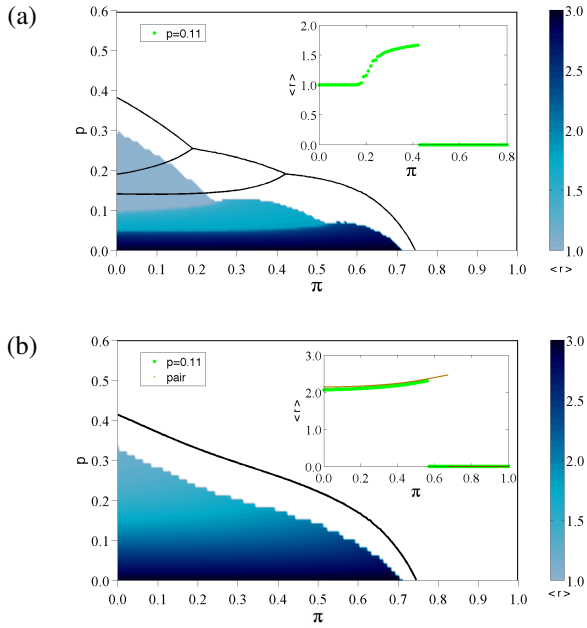

Figure 2.7: *Phase diagrams for* $M = 3$. (a) Contour plot of $\langle r \rangle$ as a function of (π, p) in the absence of beneficial mutations ($q = 0$). (b) $\langle r \rangle$ in the (π, p) plane when beneficial mutations are considered ($q = 0.01$). Pair approximations to the critical thresholds are shown as black curves, whereas simulation results appear in a color scale coding for the average replicative ability $\langle r \rangle$. Insets correspond to cross-sections of the surface at $p = 0.11$. For $q = 0.01$ we also show the dependence of $\langle r \rangle$ with π under the two-site approximation regime at fixed p.

regime is

$$\begin{aligned} \rho_i &= \sum_{j=0}^{M} \omega(i|j,j) c_{jj} + 2 \sum_{j=0}^{M} \sum_{k>j}^{M} \omega(i|j,k) c_{jk}, \\ c_{ij} &= \sum_{k=0}^{M} \frac{1}{\rho_k} \left[\sum_{l=0}^{M} \omega(i|l,k) c_{lk} \right] \left[\sum_{m=0}^{M} \omega(j|m,k) c_{mk} \right], \end{aligned} \tag{2.23}$$

for $i, j = 0, 1, \ldots, M$, where $c_{ij} = \lim_{t \to \infty} p_t(i,j)$ denote two-site correlations. Thanks to the symmetry $p_t(i,j) = p_t(j,i)$, the number of independent correlations reduces to those which satisfy the constraint $j \geq i$. The consistency condition $\rho_i = \sum_{j=0}^{M} c_{ij}$ as well as the normalization condition $\sum_{i=0}^{M} \rho_i = 1$ must be satisfied. Approximations involving higher order correlations are too cumbersome for this automaton, although

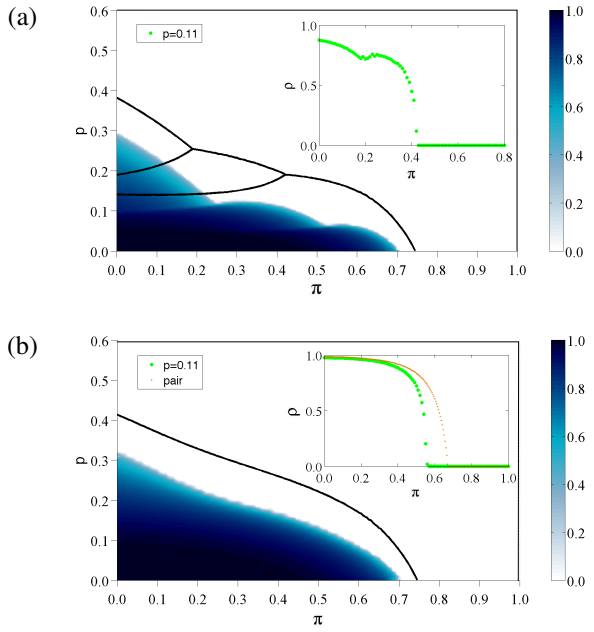

Figure 2.8: *Phase diagrams for* $M = 3$. Both panels show the variation of the density ρ of infective particles for $q = 0$ (a) and $q = 0.01$ (b). Pair approximations to the critical thresholds are shown as black curves, whereas simulation results appear in a color scale coding for density of active sites. Insets are cross-sections of the surface at $p = 0.11$. For $q = 0.01$ we also show the dependence of ρ as a function of π under the two-site approximation scheme at fixed p.

for the DK cellular automaton it is feasible to include up to three-site correlations (see Appendix A.3).

We have checked the accuracy of the two-site approximation for a maximal replicative ability $M = 3$, both in the presence ($q = 0.01$) and the absence ($q = 0$) of beneficial mutations. Results for the average replicative ability are summarized in Figure 2.7. For $q = 0$, the two-site approximation recovers qualitatively the sequence of error thresholds observed in simulation. Although the comparison with the transition line is not satisfactory, far away from the transition the surface of $\langle r \rangle$ as a function of (π, p) (at constant q) is well predicted, as we observe from the inset of Figure 2.7b. Therefore, these approximations capture the global dependence of the average replicative ability, although the approximation of the critical threshold is poor.

In Figure 2.8 the density of infected sites [Eq. (2.19)] is plotted in the (π, p) plane. Similarly, the pair approximation produces accurate results away from the transition, although the prediction of the critical line is not accurate.

These kind of approximations, when combined together for the DK cellular automaton, yield an extrapolation for the critical point (see discussion in Appendix A.3). In that case we observe a linear dependence of p_1 (at fixed p_2) with $1/m$, m being the number of sites involved in each level of approximation (see Figure A.3). This observation allows us to improve the accuracy of the transition threshold of the automaton. Our model of spatial infection propagation might be amenable to a similar extrapolation that, in turn, might improve the precision of the predicted transition line.

2.4.1 The case $M = 2$

The simplest case $M = 2$ of our model allows for analytical solutions of the transition lines in the one- and two-site regimes of approximation.

Under the one-site approximation, the densities $\boldsymbol{\rho} = (\rho_1, \rho_2)$ of infective classes are the roots of the quadratic system

$$\mathbf{a}_j \boldsymbol{\rho}^{\mathsf{T}} - (1-\pi)^2 \boldsymbol{\rho} \mathsf{M}_j \boldsymbol{\rho}^{\mathsf{T}} = 0, \qquad j = 1, 2, \tag{2.24}$$

where $\mathbf{a}_1 = (2(1-\pi)(1-p-q)-1, 2(1-\pi^2)p)$, $\mathbf{a}_2 = (2(1-\pi)q, 2(1-\pi^2)(1-p)-1)$, and matrices $\mathsf{M}_{1,2}$ are given by

$$\mathsf{M}_1 = \begin{pmatrix} 1-p-q & \frac{1}{3}[(1-q)(2+\pi) - p(1-\pi)] \\ \frac{1}{3}[(1-q)(2+\pi) - p(1-\pi)] & (1+\pi)^2 p \end{pmatrix} \tag{2.25}$$

and

$$\mathsf{M}_2 = \begin{pmatrix} q & \frac{1}{3}[q(2+\pi) + (1-p)(1+2\pi)] \\ \frac{1}{3}[q(2+\pi) + (1-p)(1+2\pi)] & (1+\pi)^2(1-p) \end{pmatrix}, \tag{2.26}$$

respectively.

In the absence of beneficial mutations, besides the absorbent state solution we find two non-trivial analytical solutions of (2.24). One of them refers to the phase for which $\rho_2 = 0$ and

$$\rho_1 = \frac{2(1-\pi)(1-p) - 1}{(1-\pi)^2(1-p)}, \tag{2.27}$$

which we immediately associate to the phase where the master type $r = 2$ has disappeared. Solving the condition $\rho = \rho_1 + \rho_2 = 0$ we find the corresponding error threshold,

$$p_{\mathrm{MF}}^{(1)}(\pi) = 1 - \frac{1}{2(1-\pi)}, \tag{2.28}$$

at this approximation level. The second solution has non-zero values for both ρ_1 and ρ_2, but the total density of infective sites is too cumbersome to be reproduced here. This notwithstanding, the corresponding error threshold can be calculated and it becomes

$$p_{\mathrm{MF}}^{(2)}(\pi) = \frac{1-2\pi^2}{2(1-\pi^2)}. \tag{2.29}$$

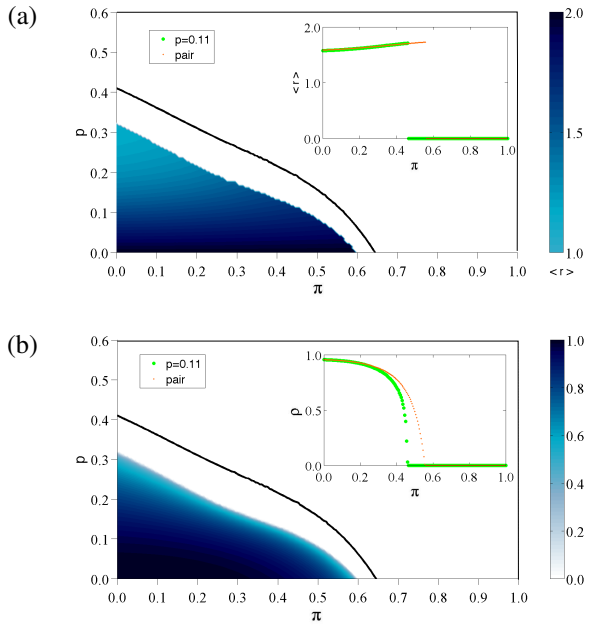

Figure 2.9: *Phase diagrams for* $M = 2$. (a) Average replicative ability, and (b) density of active sites. Pair approximations to the critical thresholds are shown in black, whereas simulation results appear in a color scale coding for $\langle r \rangle$ (a) and ρ (b). Insets show the dependence with π at fixed $p = 0.11$.

The system (2.24) is difficult to solve in general for $q > 0$. However, we can build up heuristic approximations in the following way. Near the critical line, the densities $\rho_{1,2}$ are close to zero, so terms involving ρ_1^2 and ρ_2^2 can be neglected, thus simplifying the system considerably. The resulting system can be solved and yields the transition line

$$p_{\mathrm{MF}}(\pi, q) = \frac{2 - \pi - 4\pi^2 + \sqrt{\pi^2 + 8q(1 - 3\pi^2 + 2\pi^4)}}{4(1 - \pi^2)}. \tag{2.30}$$

In particular, this threshold leads to (2.29) when $q = 0$.

We conclude this section with a similar analysis for two-site approximations. Analytical results can also be obtained at this level. For $q = 0$ we have analyzed the transition line in the regime $\pi \ll 1$, for values of p where the active phase consist only of viral particles of the lowest type. Hence the system (2.23) can be readily solved since $\rho_2 = 0$ and pair correlations involving class $r = 2$ vanish. The system reduces to (A.17), so the critical line is given by (A.19) with the substitutions

$$\begin{aligned} p_1 &= (1 - \pi)(1 - p), \\ p_2 &= (1 - \pi^2)(1 - p), \end{aligned} \tag{2.31}$$

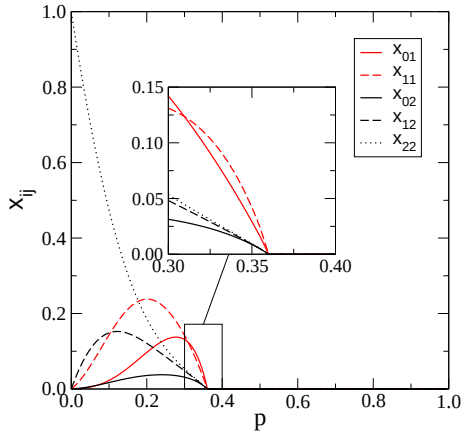

Figure 2.10: *Heuristic approximation to the transition line in the pair approximation.* The dependence, as functions of p, of the two-site correlations for $M = 2$ is depicted. Remaining parameters are $q = 0.02$ and $\pi = 0.15$.

that map the lowest-r error threshold to the DK cellular automaton. Thus,

$$p_{\mathrm{P}}(\pi) = \frac{3 - 2\pi - 2\pi^2 - \sqrt{5 - 4\pi}}{2(1 - \pi^2)} \qquad (\pi \ll 1) \tag{2.32}$$

is the two-site approximation for the error threshold of the lowest replicative ability class. Note that this approximate curve is independent of how large is the maximal replicative ability M, because in this region only types with $r = 0$ and $r = 1$ survive, so the mapping with the DK model is exact, as pointed out in Section 2.3.2.

For $q > 0$ the nonlinear system (2.23) is too complicated to be solved analytically. A numerical resolution of that system for $M = 2$ yields the phase diagrams of Figure 2.9 for $\langle r \rangle$ and ρ. This nonetheless, we can provide a heuristic, analytical approximation to the whole line under the two-site approximation scheme.

Figure 2.10 shows a typical dependence of pair correlations as functions of p. In the inset we observe that, close to the critical threshold, $x_{01} \approx x_{11}$ and $x_{02} \approx x_{12} \approx x_{22}$. By imposing that $x_{01} = x_{11}$ and $x_{02} = x_{12} = x_{22}$, Eq. (2.23) reduces to a linear, homogeneous system in variables (x_{01}, x_{02}). The approximate critical line is obtained by equating to zero the determinant of the system matrix, and takes the form

$$p_{\mathrm{P}}(\pi, q) = \frac{B_1(\pi) + \sqrt{B_2(\pi, q)}}{B_3(\pi)}, \tag{2.33}$$

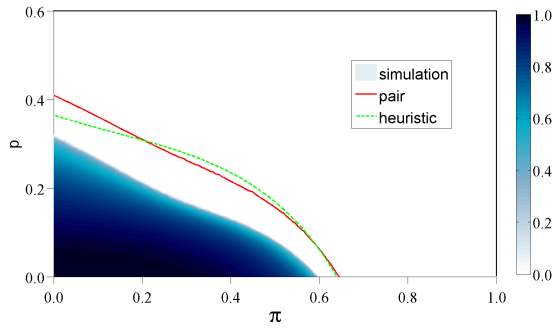

Figure 2.11: *Heuristic approximation to the transition line in the pair approximation.* The analytical curve (2.33) is compared with simulation results for $M = 2$ and $q = 0.01$.

with the polynomials

$$\begin{aligned} B_1(\pi) &= -25 + 9\pi + 50\pi^2 + 42\pi^3 + 26\pi^4 + 6\pi^5, \\ B_2(\pi, q) &= (-1 + 17\pi + 14\pi^2 + 6\pi^3)^2 \\ &\quad - 2qB_3(\pi)(-7 - 5\pi + 14\pi^2 + 18\pi^3 + 13\pi^4 + 3\pi^5), \\ B_3(\pi) &= 2(1 - \pi)(3 + \pi)(13 + 13\pi + 7\pi^2 + 3\pi^3). \end{aligned} \tag{2.34}$$

For $q = 0$ we obtain an approximation for the error threshold where both classes get extinct at the same time. This branch is

$$p_{\mathrm{P}}(\pi) = \frac{-4 + 6\pi^2 + 4\pi^3 + 3\pi^4}{-13 + 6\pi^2 + 4\pi^3 + 3\pi^4}. \tag{2.35}$$

We compare, in Figure 2.11, the threshold curve (2.33) with simulation results. As we can see, this formula fairly reproduces the transition line at the pair level. An extrapolation technique, analogous to the one applied to the DK cellular automaton in Appendix A.3, could be used to improve the performance of these analytical approximations. In contrast to what happens for the DK model, it is not obvious *a priori* how to implement such an extrapolation for our model, since there is no unique correspondence between the critical points $(\pi_{\mathrm{c}}, p_{\mathrm{c}})$ obtained either with one- and two-site approximations. Further study will be needed in order to apply these kind of improvements to our cellular automata.

2.5 Discussion

The production of large amounts of progeny is usually regarded as an adaptive strategy of viral populations. It is broadly accepted that the high mutation rates of RNA

viruses, particularly, are combined with a huge offspring production in order to enhance the diversity of the population, thus maximizing the chances of successful infection. Other relevant effects arise, however, when physical space is explicitly considered. Earlier studies have identified over-production of viral progeny in spatial infection propagations as a by-product of competition within the quasispecies (Aguirre and Manrubia 2008). Our model shows how, taking host defenses into account, progeny over-production becomes an adaptive strategy to overcome host resistance to infection. Large replicative abilities become particularly significant close to the transition to extinction, at low population densities. In simple scenarios where the availability of susceptible cells is unlimited, hosts defenses are unable to neutralize a sufficiently large progeny production increase, resulting in a run-away co-evolution between virus and host. This nonetheless, spatial constraints limiting the number of available cells give chances to host-resistance mechanisms, because infection clearance might occur if the host is able to increase its defenses beyond a finite critical threshold.

All transitions occurring when physical space is made explicit belong to the DP universality class, be they the loss of the highest-r type present when advantageous mutations are absent or the overall extinction of the population when beneficial mutations are considered. To the best of our knowledge, this mechanism is different from all other extinction transitions described in models of evolving populations so far.

When there is a competition for cells, the transition line between the infective and the non-infective phases has been calculated by numerical simulation upon variations on p, the probability of undergoing a deleterious mutation, and π, the parameter accounting for the host resistance to infection. We have performed analytical approximations to the transition line under the one- and two-site approximation regimes. The correct exponents of the DP transition can not be recovered under this approximation scheme, since it is but a mean-field approximation to the dynamics. This notwithstanding, our approximations lead to fairly good analytical results when the maximal replicative ability M is not too large. As a matter of fact, we have checked that any approximation based on two-site correlations decrease its accuracy as M increases. The reason is simple: when multiple viral types of different replicative abilities coexist, the range of correlations between sites becomes wider and an approximation based in just two sites is not enough to reproduce correctly the behavior near the transition line.

This model is relatively simple when it comes to the actual mechanisms that plants have developed to fight pathogens. However, it could be extended to account for more realistic situations. For example, many plant species present genetic polymorphism for susceptibility to a particular virus (Kang et al. 2005), i.e., different individuals might have variable degrees of resistance to viral infection and spread. Our model can be extended to account for infection propagation in crops or in tissues formed by non-identical cells by defining π as a host-dependent variable. This would introduce a form of quenched spatial disorder that may lead to universality classes for the extinction transition different from DP (Hinrichsen 2000). Spatially quenched disorder could change the properties of viral extinction to those of dynamic percolation (Grassberger 1983). Similar effects would be introduced by temporally quenched disorder, a situation holding, for instance, when age-dependence of susceptibility to infection is

considered. An example of the latter case is systemic acquired resistance, a durable form of immunization observed in plants (Durrant and Dong 2004). The scenario we have studied is a first step towards tackling new situations where different factors like individual variations in host resistance, co-evolution of the relevant parameters, or host superinfection could be made explicitly. Current knowledge on the phenomenology of percolation phenomena might inspire new strategies to stop viral propagation in different environments.

Our results suggest that pathogens benefit in practice from a larger average replicative ability when the propagation takes place in geometries that grant access to a large number of susceptible hosts per generation. In other words, it is to be expected that a virus propagating in a medium with excess of susceptible cells would be in trouble when the availability of the latter is reduced. This effect is purely ascribed to a change in the geometry where the virus spreads, and would take place irrespectively of the mutation rate of the virus or in the resistance to infection of the host. There is actually some empirical support for this prediction. While all plant viruses infect the phloem of the plant (where the number of susceptible cells is relatively large and mobility is high), not all viruses are able to infect leaves, where mobility is limited to cell-to-cell transmission and fewer fresh cells are available per generation. Actually, all plant viruses encode specific proteins used in cell-to-cell movement, this revealing how critical is this step for infection propagation. Specifically, luteoviruses and some geminiviruses (begomoviruses)[12] are restricted to the plant phloem (Knipe and Howley 2007) and do not infect leaves. The reverse situation is as yet unknown.

[12]Luteoviruses are RNA viruses whose primary hosts are plants. The name 'luteovirus' arises from the Latin *luteus*, which is translated as 'yellow'. Luteovirus was given this name due to the symptomatic yellowing of the plant that occurs as a result of infection. Geminiviruses are plant viruses which have single-stranded DNA genomes. In the case of some begomoviruses, there are two similar-sized components of DNA genomes. The nomenclature 'geminivirus' comes from their capsid shape.

III

Statistical mechanics of ecosystem assembly

3

Species assembly in model ecosystems

In short, there is no comfortable theorem assuring that increasing diversity and complexity beget enhanced community stability; rather, as a mathematical generality the opposite is true.
—Robert M. May.

3.1 Stability and complexity of natural communities

A piece of common wisdom in ecology is that biodiversity enhances the stability of ecosystems. This has traditionally been a well established observational fact since the works of Odum (1953), MacArthur (1955) and Elton (1958) who observed that simple ecosystems (e.g. man-cultivated lands) undergo very large fluctuations in population and are vulnerable to invasion, an effect that gets reduced upon increasing the number of predators and prey in the system. Vulnerability to external invasions and plagues is observed, for instance, in outbreaks of phytophagous insects, which are frequent in boreal forests but not in tropical ones. The argument supporting that complexity gives rise to stability in ecological communities was stated by MacArthur (1955), who hypothesized that "a large number of paths through each species is necessary to reduce the effects of overpopulation of one species." He concluded that "stability increases as the number of links increases" and that the more diverse is the assemblage of species the more stable it is.

This fact was commonly accepted until a renowned paper by May (1972), which challenged the up-to-date knowledge about coexistence of species. May conducted local stability analyses of randomly assembled communities and proved that their stability decreases with complexity. He analyzed simple model communities of S interacting species following Lotka-Volterra (LV) population dynamics (Lotka (1920) introduced this dynamics for two species in the context of chemical kinetics, and Volterra (1931) applied it to sets of interacting species). Let n_i be the abundance of species i, regarded as number of individuals or as a population density, where $1 \leq i \leq S$, S being the total number of species. The dynamics is determined by the ODE system

$$\frac{\dot{n}_i}{n_i} = \alpha_i + \sum_{j=1}^{S} \gamma_{ij} n_j, \qquad i = 1, \ldots, S. \tag{3.1}$$

Vector $\boldsymbol{\alpha} = (\alpha_i)$ accounts for the growth or mortality rates of species in the absence of predation (depending on whether species are producers or consumers, the sign of the rate is positive or negative, respectively). Ecological interactions are arranged in the so-called *interaction matrix* $\Gamma = (\gamma_{ij})$.

In spite of its simplicity the LV model accounts for the three main types of interaction observed between species: (i) if $\gamma_{ij} > 0$ and $\gamma_{ji} < 0$, species i benefits from the presence of species j, thus corresponding to a *predator-prey* relation where i is predator and j prey;[1] (ii) if $\gamma_{ij} < 0$ and $\gamma_{ji} < 0$ there is a *competitive* interaction between species, that can be intra-specific (i.e. within the same species; it is usually accounted for by setting $\gamma_{ii} < 0$) or inter-specific;[2] and (iii) if $\gamma_{ij} > 0$ and $\gamma_{ji} > 0$ the presence of both species is beneficial to each other, so there is a *mutualistic* (also known as cooperative or symbiotic) interaction. Obviously the detailed population dynamics of species in actual ecological communities is more complex than the simple picture provided by LV equations. However, they can be considered as a "first-order" approximation when modeling time variation in species abundances.

May took advantage of the simplicity of this model, since the linear stability of LV communities is very easy to assess. First, the *equilibrium points*[3] of system (3.1) can be calculated by solving linear systems of equations. The most interesting one is the so-called *interior* equilibrium point, given by $\mathbf{p} = -\Gamma^{-1}\boldsymbol{\alpha}$ when all the equilibrium densities p_i are strictly positive. The remaining (boundary) equilibria are obtained by setting to zero any subset of the populations and solving the linear system resulting from eliminating those variables. Second, the local behavior of any rest point is easy to sketch for LV systems. Under the assumption of small perturbations around the equilibrium point, a linear analysis shows that the local behavior of the system is ruled by the *Jacobian matrix*, which in our case reduces to the so-called *community matrix*

[1] When $\gamma_{ij} > 0$ and $\gamma_{ji} = 0$ we speak about *host-parasite* relations.

[2] Normally these competition coefficients are referred to as *direct competition* interactions, which account for competitive effects like mutual aggressions, territorial competition, etc. Note that there is a second kind of competition caused by predator-prey interactions, the so-called *indirect competition*, that arises from the indirect effect of sharing common resources.

[3] Also known as rest points, fixed points or stationary points.

$\Lambda = (\lambda_{ij})$, where $\lambda_{ij} = p_i\gamma_{ij}$. A spectral analysis of this matrix portrays the local stability of an equilibrium point, which is *stable*[4] if all the real parts of the eigenvalues of Λ are negative, so that perturbations get damped in the long-term dynamics. As measures of stability, in the ecological literature it is defined the *resilience* (Dunne 2006) of a stable rest point as

$$\lambda_{\max} = -\max_{\lambda\in\sigma(\Lambda)} \mathrm{Re}(\lambda), \tag{3.2}$$

provided that $\max \mathrm{Re}(\lambda) < 0$, and the *return time* to equilibrium as $T_{\mathrm{r}} = \lambda_{\max}^{-1}$.

May showed that randomly generated LV models for the populations of a community exhibit features opposite to those observed empirically: the larger the diversity the smaller its linear stability (May 1972; May 1973). May found that random LV communities will undergo a sharp transition from stable to unstable behavior as the complexity of the system increases. He obtained the criterion that LV model communities near equilibrium will be stable if

$$\langle\gamma\rangle\sqrt{SC} < 1, \tag{3.3}$$

in particular, as the number of species S, the average interaction strength $\langle\gamma\rangle$ or the network connectance C increase beyond critical values.

The term "connectance" refers to the fraction of non-zero elements in an interaction matrix. Considering the community as a network of feeding interactions or *food-web*, to each interaction matrix one can associate a directed graph $\mathcal{G} = \{\mathcal{S}, \mathcal{L}\}$ whose set of nodes $\mathcal{S}$ is formed by interacting species and whose directed links point from prey to predator. If the number of links is $N_{\mathcal{L}}$, the connectance of the food-web is defined in this context as $C = N_{\mathcal{L}}/S^2$. The number of nodes S in the food-web is directly related to the *diversity* of the community, and its *complexity* is measured by the connectance.

Assuming that the average interaction strength is constant, May's criterion suggest that communities can be stable for increasing diversity as long as connectance decreases. In particular, a dependence like $C \propto S^{-1}$ would guarantee that the product SC remains constant, and the upper bound (3.3) may be preserved. Unfortunately, this is far from being true. Improved data and its exhaustive analysis highlights problems with the assumption of a hyperbolic decline of C with S. Several aggregation of data and sampling analyses suggest that C is relatively robust to changes in S (Warren 1989; Martinez 1991). In agreement with former studies, the hypothesis of "constant connectance" seems to be correct (Martinez 1992). The interpretation of approximately constant connectance is that consumers are likely to exploit a constant fraction of available resources, so as diversity increases, the number of links per species increases as well. But the assumption of constant connectance leads to the conclusion that diverse communities are less stable, according to May's criterion. Once again, empirical data seem to contradict theoretical results.

[4]Mathematically, a rest point $\mathbf{p}$ is said to be stable if for any neighborhood U of the point there exists another neighborhood W such that any orbit initiating in W remains in U for all $t \geq 0$. It is said to be *asymptotically stable* if it is stable and the orbit converges to $\mathbf{p}$.

Thanks to this controversy we have gained very much insight into the nature of ecosystems (McCann 2000). Apart from the introduction of more refined concepts of ecosystem stability (Pimm 1982), one of the main conclusions arising from the comparison of empirical data with May's predictions on the bounds for community stability is that real ecosystems are within the tiny set of stable ones, no matter how large they are; in other words, ecosystems are far from being just random gatherings of species (Dunne 2006). But this debate raised also the question of giving some theoretical support to the observed positive correlation between complexity and stability. This question remained without a satisfying answer until the appearance of assembly models.

3.2 The approach of assembly models

Classical theoretical studies of ecological communities have developed the framework of community dynamics (Pimm 1982), although this theory misses an important ingredient: the arrival and disappearance of species as communities are assembled. In fact, natural communities carry out a selection mechanism that induces colonizers adaptation. There has been a lot of theoretical work in the past devoted to study the assembly of communities through successional invasions (Post and Pimm 1983; Drake 1990; Case 1990; Drake 1991; Law and Blackford 1992; Law and Morton 1993; Law and Morton 1996; Morton and Law 1997). Overall, standard assembly models have provided a theoretical framework to understand how communities are built up (Law 1999). The elementary process on which these models are based is the sequential arrival of rare species (invaders) to which natural communities are subject. Newcomers may colonize the ecosystem and get established, possibly causing a global reconfiguration of the community in the long term driving several species to extinction. Obviously, these models are but idealizations of the complex processes taking place in real community assembly, but simple mechanisms acting in these models could be expected to be the ones responsible for the formation of real ecosystems (Law 1999). Even if we leave out the inherent complexity of ecological interactions, we can still address some of the fundamental issues with simple models. This approach of devising theoretical paradigms for real situations has been successfully applied over and over in the field of statistical mechanics —where, for instance, using such an idealization as the Ising model provides the clues to understanding ferromagnetism in real materials (Huang 1987).

Previous assembly models tend all to rely on LV dynamics [but see the recent work by Lewis and Law (2007)], although differ in the criterion to accept an invasion. While Post and Pimm (1983) assumed that new species were created *ad hoc,* according to certain stochastic rules, at each invasion attempt, subsequent approaches (Drake 1990; Case 1990; Law and Morton 1993; Law and Morton 1996) introduced the concept of *species pool*. The structure that emerges locally at the community level depends as much on which species are available in geographically nearby communities. This set of potential invaders close to the community conforms the so-called regional species

pool.[5] It constitutes a (finite) set of species whose trophic interactions have been determined in advance. Pools are usually defined by labeling species according to some niche variable (usually a species trait like body size) and then drawing randomly their interactions from predetermined probability distributions (Law and Morton 1996). Sequential invaders of any given resident community are selected from the pool at each invasion attempt, and the resulting community after the invasion can be determined according to some population dynamics.

The most remarkable results of previous assembly models are: (i) a final end state is eventually reached, which can be either a single community or a cycle involving several communities (Morton and Law 1997), (ii) pools constructed from simple empirical rules using size as niche variable to model predator-prey interactions (Cohen et al. 1993) do sometimes contain more than one end state, but the number is small (Law and Morton 1996; Morton and Law 1997) (iii) average species richness (complexity) increases along the assembly (Post and Pimm 1983; Drake 1990; Law and Morton 1996), and (iv) stability, understood as the average resistance against invasions, also increases with time (Case 1990; Law and Morton 1996; Morton and Law 1997). Thus assembly models conform a well-founded theoretical framework that provides a positive relationship between stability and complexity in model communities.

The assembly of ecological communities depends on whether an invader is accepted or not in a resident community. Then assembly models rely on certain criteria for species coexistence, that are used to determine the resulting community after an invasion.

3.2.1 Criteria for coexistence

The first assumption of assembly models is a separation of the time-scale on which community dynamics takes place, from the longer time-scale of subsequent invasions. This assumption is introduced because the behavior of invaders along all possible transient paths of the resident community is too difficult to deal with. Instead, a time-scale separation ensures that the community is close to an attractor when newcomers arrive, and their behavior can be determined on the basis of what they do close to this attractor (Law 1999). Therefore the criteria for species coexistence will be focused on the equilibrium points of the community dynamics.

Whether a set of species coexist together is a matter of how their densities are coupled through deterministic population equations (Law 1999). The criterion for coexistence most widely used in theoretical ecology is the existence of an interior, *asymptotically stable* rest point. This was precisely the coexistence criterion used in the assembly models of Post and Pimm (1983) and Drake (1990). However, the local character of this measure of stability is a serious drawback of its being a good criterion for coexistence. Moreover, issues of coexistence appear when at least one density is

[5] From an empirical point of view, regional species pools are simply the union of the sets of species present in communities in some neighborhood. The origins of the concept of species pool go back to the equilibrium theory of island biogeography (MacArthur and Wilson 1967).

close to zero, i.e. close to the boundary of the space of positive species abundances, not close to any interior equilibrium point.

Global asymptotic stability would be a more powerful criterion. If the rest point is globally stable, then no orbit can hit the boundary from the interior, and species will certainly coexist. Let $\mathbf{n}(t) = (n_i(t))$ the vector of species densities as a function of time. To establish global stability, one has to find a *Lyapunov function* $\mathcal{V}(\mathbf{n})$, valid over the whole interior of the configuration space (Hofbauer and Sigmund 1998). Such a function satisfies that $\dot{\mathcal{V}}(\mathbf{n}(t))$ is negative definite[6] for any orbit $\mathbf{n}(t)$ starting from an interior initial condition. Although global stability is a good criterion, it is limited to equilibrium points. For a general dynamical system the assumption that the asymptotic state is an equilibrium point can be no longer true: there are other sort of *attractors*, such as periodic and chaotic attractors, on which all species may coexist even if the rest point is unstable. However, if the interior equilibrium exists and is globally stable any orbit with initial positive condition will converge asymptotically to the rest point.

A way to overcome these problems is to use a criterion for coexistence independent on what kind of attractor is involved. The notion of *permanence* is a good alternative (Hofbauer and Sigmund 1998). A dynamical system is said to be permanent if all orbits not initially in the boundary of the configuration space remain at least at a distance $\delta > 0$ from the boundary, i.e. the boundary is a repellor to all orbits that start in the interior space. In principle, the permanence of an arbitrary system is difficult to assess, since it amounts to find a "time-averaged" Lyapunov function.[7] For a thorough discussion on the concept of permanence and its implications we refer the reader to the book by Hofbauer and Sigmund (1998).

3.2.2 Experimental assembly of protist communities

The assembly of ecological communities has been carried out experimentally. Warren et al. (2003) conducted laboratory experiments to investigate the potential assembly pathways in a small pool of 6 protist species: *Amoeba proteus, Blepharisma japonicum, Euplotes patella, Paramecium caudatum, Colpidium estriatum,* and *Tetrahymena pyriformis.* Some of them prey on a resource of *bacterial flora.* The potential feeding interactions of such a pool have been depicted in Figure 3.1. Mapping the assembly pathways in the experiment involved two steps: testing the ability of every possible species combination to persist in time —they prepared 6 replicates of each species combination to establish their persistence—, and testing each persistent community for its capacity to be invaded and changed by every other species from the pool.

In that experiment it was found that the number of persistent communities and assembly pathways was much smaller than theoretically possible, but the system nonetheless had quite a complex range of assembly behaviors. There were many alternative paths to most communities, but overall, the species pool had just one final end state to which the process eventually led. This end state involved the oscillation between

[6] A continuously differentiable function $f : D \subset \mathbb{R}^k \to \mathbb{R}$ is negative definite if $f(x) < 0$ for every non-zero $x \in D$.

[7] In LV systems the permanence of the system is easier to characterize, see Law (1999) for details.

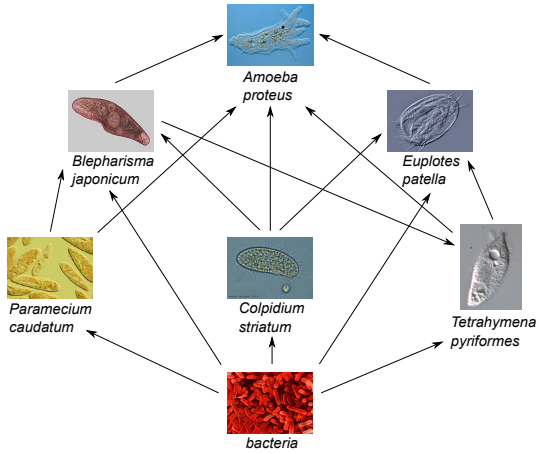

Figure 3.1: *Feeding interactions* among the species in the pool of the experiment by Warren et al. (2003). Arrows represent known, or expected, feeding interactions between species, with the arrow pointing from resource to consumer.

two communities, driven by a catalytic species[8] that could persist in neither of them. Besides, several communities capable of long-term persistence were unreachable by sequential assembly.

The main outcome of this work is the assembly graph reproduced in Figure 3.2. As to our knowledge, this was the first time that a complete assembly graph was constructed for a given pool. This graph shows the transitions that gave consistent results, where the majority of replicates (if not all) went to the same persistent community. The whole assembly process is displayed in this graph, which eventually leads —in the long term behavior— to a end cycle between two communities. Even in a six species pool, the diversity of pathways of the resulting graph is enough to produce many of the behaviors observed in models of assembly. A rich phenomenology arises from this experiment, such as the aforementioned existence of catalytic species, or the existence of certain combinations of species that are persistent in the long term when species are assembled together but are not reachable though successional invasions (such as the combination $\{A, P, T\}$, see Figure 3.2).

However, stochasticity plays a role. In some cases the replicates did not produce entirely consistent outcomes. To examine the effect of unresolved outcomes on the assembly graph, a graph containing the transitions of all replicates was also constructed by Warren et al. (2003). If these minority transitions are included, then the graph shows no entirely unreachable communities, for example. But, in any case, regardless of whether unresolved outcomes are included or not, the resulting assembly graph is complex enough to make it difficult to predict paths of community development and

[8]Catalytic species have the property of invasion, changing the resident community, and then going extinct.

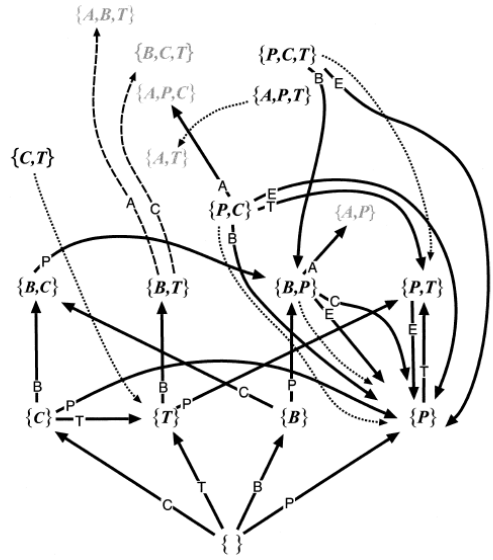

Figure 3.2: *Experimental assembly graph* reproduced from Warren et al. (2003). Letters represent abbreviations of the six protist species conforming the pool. Authors first studied the *a priori* persistence of each combination of species (among the set of $2^6 - 1 = 63$ possibilities) and those found to be persistent are shown as letters in brackets; arrows represent transitions between persistent communities following an invasion (the invader label is shown in each link). Dashed arrows indicate transitions whose designation as such is only tentative. The communities shown in gray are those which appeared to persist following invasions, but had not been identified as persistent a priori. The dotted arrows indicate uninvaded sets that did not persist for the full period of the experiment, and the states to which they collapsed. Although the graph is incomplete, from what is mapped out we can observe that a final end cycle between communities $\{P\}$ and $\{P, T\}$ can be reached by sequential assembly.

make inferences about community history just from observation of one or more communities at a given time.

3.2.3 Toward a complete characterization of the assembly process

Although assembly models provide a well-founded framework that recovers a positive correlation between diversity and stability, they are not free from criticism. One must bear in mind that not all assembly pathways have been explored in these models. The conclusions reached so far rely on averages of quantities under study over a finite set of realizations of the underlying stochastic process, that is ultimately based on a *finite*

pool of possible invaders. This has raised several questions that remained without a definitive answer. For example, there was no clear-cut answer regarding history dependence (i.e., the dependence on the invasions sequence). Morton and Law (1997) found a small number of final end states resistant to invasions by the remaining species in the pool at the end of the process, and this end state could be either a single ecosystem or a set involving more than one community connected by invasions with one another. However, Fukami and Morin's (2003) experiments seem to support the contingency of assembly pathways. In any case, we should not forget that the number of species in the pools employed is always relatively small, so the question remains as to whether larger pools lead to qualitatively different results. In this respect, it has been pointed out (Case 1991; Levine and D'Antonio 1999) that the exhaustion of good invaders in the early assembly might lie behind both, the increasing resistance to invasion as assembly proceed, and the dependence of the end states on the precise assembly history.

Trying to overcome the drawbacks of previous models, in this chapter we will introduce a minimalistic model of ecosystem assembly. Its main virtue is being sufficiently simple so as to allow mapping out all assembly pathways, thus providing a global picture of the assembly process. In spite of its simplicity, the model exhibits the same features found in earlier models. The basic idea is to provide a picture of the assembly process of an ecosystem as a Markov chain evolving in a certain configuration space (Karlin and Taylor (1975); see Appendix B for a brief summary on Markov chains). This space is made of all viable communities for a given set of parameters. Under the assumptions of the model, such a space is a finite set. The invasion process by a new species induces transitions as a result of the perturbations created in the community by the newcomer. This allows to define an *assembly graph* —similar to that of Warren et al. (2003) shown in Figure 3.2— whose nodes are viable communities and links are transitions between communities driven by species invasions. By assigning transition probabilities to links the assembly process is mapped to a Markov chain, which is tantamount to saying that we define a statistical mechanics on the set of viable communities (microstates). In other words, our model gives the probability distribution over all these microstates at any time instant.

Connecting the assembly process with a Markov chain allows for a full description of the process. For example, thanks to this mapping we are able to characterize both transient and recurrent states (see Appendix B.1.2 for the classification of states in a Markov chain), as well as to compute the time evolution of any observable along the assembly in an exact manner. But more importantly, as our model provides a complete and exact —albeit numeric— characterization of the configuration space, we can positively state that, under the assumptions of the model, the process drives the community to a *unique* end state resistant to invasions. For some parameter values this end state is just a single uninvadable community. For the remaining values, the end state is formed by a closed set of communities which transform into each other as a result of new invasions. In this set, communities can always be invaded but they never abandon the set. This way, the ecosystem is pictured as a fluctuating community that changes its composition through successional invasions. Our complex end states generalize the end cycles found in previous assembly models (Morton and Law 1997), and the fact

that they had not been observed so far is probably due to limitations in the pool of invaders.

Despite recovering the aforementioned results of increasing diversity and robustness, there are important differences between our work and previous models. First, the niche variable in our model will be the trophic level, which renders our species pool infinite —in contrast to most previous models; but see Post and Pimm (1983) for an exception. However, interactions strengths are averaged over each trophic level under a species symmetry assumption (see Section 3.4), which decreases substantially the number of different assembly pathways. Second, in our model the permanence of the final community is guaranteed because we are able to show that equilibrium communities are globally stable (Hofbauer and Sigmund 1998) within each trophic level. And third, in standard assembly models magnitudes are averaged over a set of stochastic realizations of the process of sequential invasions, where invaders are randomly chosen from the species in the pool not yet present in the community. Since we are able to map out all the invasion pathways for this model, we do not need to resort to average magnitudes over realizations but we can calculate them exactly. Even for our simple model, the number of possible pathways is too high to be accounted for through simulations. This is one of the main advantages of our model with respect to former ones, and in turn it allows us to establish the independence of the end state on history. The uniqueness of the end state for these kind of models had never been proven nor disproven so far.

In this chapter we will provide a complete description of our model and a full account of its results. Its computational and algorithmic methods will be described in Appendix C.

3.3 Trophic-level structured food-webs

How species are arranged in a network to conform a food-web is a question difficult to answer. The specific topology of the network where feeding interactions take place is very complex and several complicated models have been proposed for both the structure and the dynamics of food-webs (Dunne 2006). In contrast, our aim is to construct a minimalistic model, so we consider the traditional picture of trophic pyramids of interacting species in different trophic levels. Although trophic levels can be roughly described in real webs (Martinez et al. 2006), we will assume that feeding interactions take place strictly between species belonging to contiguous, well-defined trophic levels. This is a standard (and accurate) assumption, as the models of tri-trophic food chains show (Bascompte and Melián 2005). This notwithstanding, it is acknowledged that *omnivory*, i.e. predation from several levels, exists although is still an open question how common it is. For example, work on food-web motifs has found that omnivory is sometimes under-represented and sometimes over-represented in real networks (Bascompte and Melián 2005). However, the impact of including omnivory in the model could lead to non trivial results. Since the trophic level is normally related to species size, feeding from lower levels will provide less energy to predators, so proper allo-

$$\Gamma^3 = \begin{pmatrix} 0 & 1 & 1 \end{pmatrix}$$

$$\Gamma^2 = \begin{pmatrix} 1 & 0 & 1 & 0 \\ 1 & 1 & 1 & 0 \\ 0 & 0 & 0 & 1 \end{pmatrix}$$

$$\Gamma^1 = \begin{pmatrix} 1 \\ 1 \\ 1 \\ 1 \end{pmatrix}$$

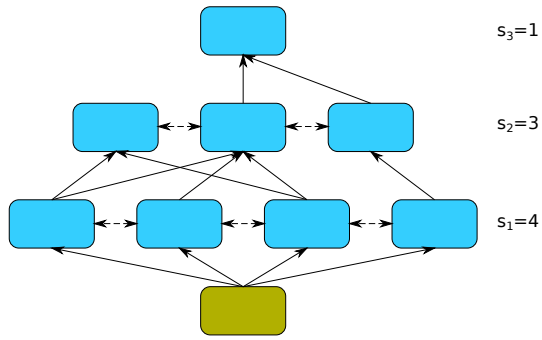

Figure 3.3: *Example of trophic-level structured food-web.* Predation links are shown by full arrows, whereas competition within trophic levels is represented by dashed double arrows. The set $\{\Gamma^\ell\}_{\ell=1}^3$ of interaction matrices for this food-web are explicitly given in the figure. For each matrix Γ^ℓ, rows represent predators at level ℓ, whereas columns account for prey at level $\ell - 1$. All species at the first level feed on a single resource.

metric relations[9] should be included in the model to fix the interaction strengths. For the sake of simplicity, we will not divert ourselves from the standard assumption of disregarding omnivory.

Therefore a basic assumption of the model is that any species at level ℓ will feed only on species at level $\ell - 1$ and will be consumed only by species at level $\ell + 1$ (see Figure 3.3). Let s_ℓ be the number of species in the ℓ-th level. Thus for an ecological community with L trophic levels the total number of species is $S = \sum_{\ell=1}^{L} s_\ell$. In order to determine which species are consumed at each level, we define the set of interaction matrices $\{\Gamma^\ell\}_{\ell=1}^{L}$, with dimensions $s_\ell \times s_{\ell-1}$, such that the element $\Gamma_{ij}^\ell = 1$ when species j in level $\ell - 1$ is a prey of species i in level ℓ, and is zero otherwise. Any particular choice of this set of matrices determines the food-web in our model.

In the aim of developing a simplified model, we propose a simple population dynamics with the purpose of capturing on average the main behavior of species abundances. It is inspired in a model previously employed to study coexistence in competing communities (Lässig et al. 2001; Bastolla et al. 2005a; Bastolla et al. 2005b). Population dynamics is modeled by LV equations, including both predator-prey interactions as well as intra- and interspecific competition. Thus, in order to keep the model minimalistic we have chosen not to include other interaction types such as mutualism.

[9] Allometric relations describe (empirically) the dependence of any interaction strength or rate on body weight usually as scaling laws. For example, it is a well-established fact that metabolic rates depend on body size approximately as $w^{-3/4}$, w being the size of the individual.

Let $\mathbf{n}^\ell = (n_i^\ell)$ be a column vector with the population densities of all species at trophic level ℓ. Following Bastolla et al. (2005a) we propose the dynamics

$$\frac{\dot{n}_i^\ell}{n_i^\ell} = \left(-\boldsymbol{\alpha} + \gamma_+^\ell \mathsf{\Gamma}^{(\ell)}\mathbf{n}^{\ell-1} - \mathsf{B}^\ell\mathbf{n}^\ell - \gamma_-^\ell(\mathsf{\Gamma}^{\ell+1})^\mathsf{T}\mathbf{n}^{\ell+1}\right)_i \tag{3.4}$$

for all $\ell = 1, \ldots, L$. The strength of the feeding interactions between contiguous levels is assumed fixed and determined by the constants γ_+^ℓ, which control the amount of energy available to reproduction for each predation event for species at level ℓ, and γ_-^ℓ ($> \gamma_+^\ell$), which take into account the mean damage caused by predation over level ℓ. The ratio $\gamma_+^\ell/\gamma_-^\ell$ measures the efficiency of conversion of prey biomass into predator biomass.

Interspecific competition in a trophic level is measured by the off-diagonal elements of the $s_\ell \times s_\ell$ matrix B^ℓ, while intraspecific competition (diagonal elements) is normalized to unity (this just amounts to fixing a time scale for the dynamics). A natural way of representing this matrix is

$$\mathsf{B}^\ell = (1-\rho^\ell)\mathsf{I} + \rho^\ell\mathsf{K}^\ell, \tag{3.5}$$

where $\rho^\ell \leq 1$ measures the relative magnitude between intra- and interspecific competition, and I is the identity matrix. Diagonal elements of $\mathsf{K}^\ell = (K_{ij}^\ell)$ are equal to 1 due to the normalization of intraspecific competition. We will assume (the reasons will become clear later) that the competition matrix is symmetric and positive definite.

Indirect competition due to sharing common prey is implicitly represented by predation terms. There is however a direct competition due to other effects, such as territorial competition, mutual aggressions, etc. We will assume [as in Bastolla et al. (2005b)] that species sharing more prey are closely related ecologically [this fact might have support from a evolutionary viewpoint as shown in Rezende et al. (2007)], so their requirements are similar. It is then reasonable to take the elements of K^ℓ proportional to the ecological overlapping between species (Lässig et al. 2001; Bastolla et al. 2005b). Let π_{ij}^ℓ represent the number of common prey for species i and j belonging to level ℓ. The species overlapping due to common prey is $K_{ij}^\ell = \pi_{ij}^\ell/\sqrt{\pi_{ii}^\ell\pi_{jj}^\ell}$. Under our matrix notation, $\pi_{ij}^\ell = (\mathsf{\Gamma}^\ell\mathsf{\Gamma}^{\ell\,\mathsf{T}})_{ij}$, so that

$$\mathsf{B}^\ell = (1-\rho^\ell)\mathsf{I} + \rho^\ell\mathsf{D}^\ell\mathsf{\Gamma}^\ell(\mathsf{D}^\ell\mathsf{\Gamma}^\ell)^\mathsf{T}, \tag{3.6}$$

D^ℓ being a diagonal matrix with elements $(\mathsf{\Gamma}^\ell\mathsf{\Gamma}^{\ell\,\mathsf{T}})_{ii}^{-1/2}$. Expressed as (3.6), it becomes apparent that B^ℓ is symmetric and positive definite. It is worth mentioning that this system does not fulfill the hypotheses leading to Gause's competitive exclusion principle (Hofbauer and Sigmund 1998; Bastolla et al. 2005a), even when there is a single level. Among other things, this is due to the fact that competition coefficients between different species are not all the same. This point will be discussed in more detail in Section 3.6.3.

We regard all species as consumers, and so they have a death rate, α_i^ℓ, which is the i-th component of vector $\boldsymbol{\alpha}^\ell$. Note that in a real food-web the interaction coefficients will not be uniform within a trophic level. In this sense, we represent interactions averaged in each level but we allow variation in interaction strengths between different trophic levels. Finally, all species at the first level prey on a single resource, whose time evolution is given by

$$\frac{\dot{n}^0}{n^0} = R - n^0 - \gamma_-^1 (\mathsf{\Gamma}^1)^\mathsf{T} \mathbf{n}^1. \tag{3.7}$$

The constant R is the maximum amount of resource in the absence of its consumers. The abundance n^0 has to be understood as the amount of a primary abiotic resource, like sunlight, water, nitrogen, etc. It has to be considered as an energetic input for the maintenance of the remaining species in the community. The amount of resource is limited, hence the saturation of n^0 at a value R in the absence of predation.

The model is supplemented by an extinction threshold, $n_\mathrm{c} > 0$, uniform for all species. If a population falls below this value it is considered extinct (real populations can not be arbitrarily small). A community will be referred to as *viable* if all its populations are above the extinction threshold. This viability condition has been previously used in similar models (Kokkoris et al. 1999; Borrvall et al. 2000; Lässig et al. 2001; Eklöf and Ebenman 2006), and accounts for the vulnerability of low density communities against external environmental variations or adverse mutations (Pimm 1991). The technical need for this extinction threshold in our model will become clear in Chapter 4, where we describe the variation of the population densities in terms of the number of species in each level.

3.3.1 Dynamic stability of the interior equilibrium point

Equations (3.4), (3.7) have several equilibria. Among them, the main one is obtained by equating the right-hand side of these equations to zero. If all the equilibrium densities are positive, this fixed point is the interior equilibrium. Populations $\mathbf{p}^\ell = (p_i^\ell)$ at equilibrium are obtained as the solution of the linear system of $S+1$ equations

$$\begin{aligned} &\gamma_+^\ell \mathsf{\Gamma}^\ell \mathbf{p}^{\ell-1} - \mathsf{B}^\ell \mathbf{p}^\ell - \gamma_-^{\ell+1} (\mathsf{\Gamma}^{\ell+1})^\mathsf{T} \mathbf{p}^{\ell+1} = \boldsymbol{\alpha}^\ell, \\ &p^0 + \gamma_-^1 (\mathsf{\Gamma}^1)^\mathsf{T} \mathbf{p}^1 = R. \end{aligned} \tag{3.8}$$

for $\ell = 1, \ldots, L$. The remaining (boundary) equilibria are obtained by setting to zero any subset of the populations and solving the resulting linear system which coincides with (3.8) but if species i at level ℓ has zero equilibrium abundance, then the i-th column in the corresponding matrix $\mathsf{\Gamma}^\ell$ has to be eliminated. Therefore one only needs the solutions of linear systems like (3.8) for a given choice of the set of matrices $\{\mathsf{\Gamma}^\ell\}_{\ell=1}^L$ in order to fully determine all the equilibrium densities.

Since feeding relations are established among contiguous levels, (3.8) acquires a block-tridiagonal structure. Due to this form, the interior equilibrium can be formally

obtained by applying Gaussian elimination. We write the equilibrium abundances in the form

$$\mathbf{p}^{\ell-1} = \mathsf{M}^{\ell}\mathbf{p}^{\ell} + \mathbf{c}^{\ell} \tag{3.9}$$

for certain $s_{\ell-1} \times s_{\ell}$ matrices M^{ℓ} and $s_{\ell-1} \times 1$ vectors $\mathbf{c}^{\ell}$ to be determined ($\ell = 1, \ldots, L+1$). Substitution into (3.8) gives the following recurrences for M^{ℓ} and $\mathbf{c}^{\ell}$,

$$\begin{aligned} \mathsf{M}^{\ell+1} &= \gamma_{-}^{\ell+1}\left(\gamma_{+}^{\ell}\mathsf{\Gamma}^{\ell}\mathsf{M}^{\ell} - \mathsf{B}^{\ell}\right)^{-1}(\mathsf{\Gamma}^{\ell+1})^{\mathsf{T}}, \\ \mathbf{c}^{\ell+1} &= \left(\gamma_{+}^{\ell}\mathsf{\Gamma}^{\ell}\mathsf{M}^{\ell} - \mathsf{B}^{\ell}\right)^{-1}\left(\boldsymbol{\alpha}^{\ell} - \gamma_{+}^{\ell}\mathsf{\Gamma}^{\ell}\mathbf{c}^{\ell}\right). \end{aligned} \tag{3.10}$$

Since the resource can only be consumed and there is no competition, we set $\mathsf{\Gamma}^0 = 0$ and $\rho^0 = 0$. This leads to the initial conditions $\mathsf{M}^1 = -\gamma_{-}^1(\mathsf{\Gamma}^1)^{\mathsf{T}}$ and $c^1 = -R$ according to (3.7). Thus, given a particular set of matrices $\{\mathsf{\Gamma}^{\ell}\}_{\ell=1}^{L}$, (3.10) fully determines M^{ℓ} and $\mathbf{c}^{\ell}$. After that, starting from the boundary condition $\mathbf{p}^{L+1} = 0$ (the community has exactly L trophic levels), we backsubstitute in (3.9) to get the equilibrium densities.

The block-tridiagonal structure of the dynamical system (3.4) can be further exploited to ascertain its dynamic stability. Let us show that any interior equilibrium $\{\mathbf{p}^{\ell}\}_{\ell=0}^{L}$ is globally stable. Thus, we can ignore species coexistence along periodic as well as chaotic orbits. This result is based on the existence a Lyapunov function, which guarantees that any positive initial condition evolves towards the interior equilibrium. The Lyapunov function for this system is

$$\mathcal{V}(\{\mathbf{n}^{\ell}\}) = \sum_{\ell=0}^{L} A_{\ell} \sum_{j=1}^{s_{\ell}} \left(n_j^{\ell} - p_j^{\ell}\log n_j^{\ell}\right) \tag{3.11}$$

where $A_k = \prod_{\ell=1}^{k} \frac{\gamma_{-}^{\ell}}{\gamma_{+}^{\ell}}$ for $k = 1, \ldots, L$ and $A_0 = 1$.

For (3.11) to be a Lyapunov function, we just need to check that $\dot{\mathcal{V}}(\{\mathbf{n}^{\ell}\}) \leq 0$ along any orbit $\{\mathbf{n}^{\ell}(t)\}_{\ell=0}^{L}$ starting with positive initial abundances (Hofbauer and Sigmund 1998). Let us calculate its time derivative. If we consider the displaced variables

$$y_j^{\ell} = n_j^{\ell} - p_j^{\ell}, \tag{3.12}$$

we can write (3.4) as $\dot{n}_i^{\ell} = n_i^{\ell} q_i^{\ell}$, where

$$\mathbf{q}^{\ell} = \gamma_{+}^{\ell}\mathsf{\Gamma}^{\ell}\mathbf{y}^{\ell-1} - \mathsf{B}^{\ell}\mathbf{y}^{\ell} - \gamma_{-}^{\ell}\left(\mathsf{\Gamma}^{\ell+1}\right)^{\mathsf{T}}\mathbf{y}^{\ell+1}, \tag{3.13}$$

hence the time derivative is simply $\dot{\mathcal{V}}(\{\mathbf{n}^{\ell}\}) = \sum_{\ell=0}^{L} A_{\ell} \sum_{j=1}^{s_{\ell}} y_j^{\ell}\, q_j^{\ell}$. After substituting (3.13), we arrive at

$$\dot{\mathcal{V}}(\{\mathbf{n}^{\ell}\}) = -\sum_{\ell=0}^{L} A_{\ell}(\mathbf{y}^{\ell})^{\mathsf{T}}\mathsf{B}^{\ell}\mathbf{y}^{\ell} + \sum_{\ell=0}^{L-1}\left(A_{\ell+1}\gamma_{+}^{\ell+1} - A_{\ell}\gamma_{-}^{\ell+1}\right)(\mathbf{y}^{\ell+1})^{\mathsf{T}}\mathsf{\Gamma}^{\ell+1}\mathbf{y}^{\ell}. \tag{3.14}$$

Thus our previous choice of A_k cancels the second sum. Since B^ℓ is positive definite, it follows that the time derivative of the Lyapunov function is negative along any orbit, and therefore Lyapunov's theorem (Hofbauer and Sigmund 1998) ensures the global stability of the non-trivial rest point $\{\mathbf{p}^\ell\}_{\ell=0}^L$. Note that the existence of this Lyapunov function is a direct consequence of the block-tridiagonal structure of the dynamical system (3.4)–(3.7), hence the assumption of predation only between contiguous levels ensures global stability.

3.4 Species symmetry assumption

In what follows, we will restrict ourselves to the dynamical system (3.4) with the particular choice of interaction matrices $\Gamma_{ij}^\ell = 1$ for any i, j, ℓ. This assumption implies that the model can now be regarded as a mean-field-like picture of real communities, since all species in contiguous levels interact with each other. We will assume as well that interaction coefficients are independent of the trophic level, and we will simply denote them as γ_+, γ_-, ρ and α. These parameters should now be understood as average strengths of the processes involved in the population dynamics. These kind of models, which do not make any explicit difference among species, are referred to as *neutral* (Hubbell 2001; Etienne and Alonso 2007). From the point of view of the trophic interactions there is no difference between species —neither the rates nor the set of prey they feed on make any distinction among species. We introduce this symmetric scenario because it will allow a simpler description of the community, and will reduce considerably the number of possible assembly pathways.

Pure neutral models do not make any distinction whatsoever between species. This is not our case, because species can be distinguished by their different balance between intra- and interspecific competition. Neutrality in our model has to be understood as a species symmetry assumption (Alonso et al. 2008) for the strength of the interactions. We will discuss the case $\rho = 1$, when the model turns to be fully symmetric (i.e. strictly neutral), in Section 3.6.3.

Under this symmetry assumption, the population dynamics (3.4) with the competition matrix (3.6) transforms into $\dot{n}_i^\ell = q_i^\ell n_i^\ell$, where

$$\begin{aligned} q_i^\ell &= -\alpha + \gamma_+ N^{\ell-1} - (1-\rho) n_i^\ell - \rho N^\ell - \gamma_- N^{\ell+1}, \\ q^0 &= R - n^0 - \gamma_- N^1, \end{aligned} \tag{3.15}$$

$N^\ell \equiv \sum_{i=1}^{s_\ell} n_i^\ell$ being the total population density of level ℓ. The set of equations (3.8) for the interior rest point imply that the equilibrium abundances are equal for any two species i and j of the same level. Hence the equilibrium abundances $\{p^\ell\}_{\ell=1}^L$ are the solution to the linear system

$$\begin{aligned} \alpha &= \gamma_+ s_{\ell-1} p^{\ell-1} - [1 + \rho(s_\ell - 1)] p^\ell - \gamma_- s_{\ell+1} p^{\ell+1}, \\ R &= p^0 + \gamma_- s_1 p^1, \end{aligned} \tag{3.16}$$

for $\ell = 1, \ldots, L$. Note that the global stability result holds only for this equilibrium point.

3.4.1 Reduced dynamical system

As in previous assembly models, equilibrium communities shall undergo invasions. Thus we are interested in the time dynamics of an invaded community initially at equilibrium. Note that the per capita growth rates (3.15) satisfy the equality

$$q_i^\ell(\dots, n_i^\ell, \dots, n_j^\ell, \dots) = q_j^\ell(\dots, n_j^\ell, \dots, n_i^\ell, \dots) \tag{3.17}$$

under the interchange of two species abundances at the same level. This symmetry, together with an initial condition where $n_i^\ell(0) = n_j^\ell(0)$, is enough to show that the time evolution of both species is identical.

To prove it, let us consider, for the sake of simplicity, a general two-dimensional autonomous system

$$\begin{aligned} \dot{x} &= f(x, y), \\ \dot{y} &= g(x, y), \end{aligned} \tag{3.18}$$

with the initial condition $x(0) = y(0)$ and which satisfies $f(x, y) = g(y, x)$. We shall prove that the Taylor expansions centered at $t = 0$ of $x(t)$ and $y(t)$ coincide. In principle, both expansions will have different radii of convergence. Let t be smaller than the minimum of these radii. Then we just need to show that all the derivatives at $t = 0$ coincide. But this follows by induction.

For the first derivatives this is straightforward because $f(0, 0) = g(0, 0)$. Let us assume that $x^{(j)}(0) = y^{(j)}(0)$ for all $j = 1, \dots, k$. Then the $(k + 1)$-th derivative will be

$$x^{(k+1)}(0) = \sum_{j=0}^{k} \left(\begin{array}{c} k \\ j \end{array} \right) \left. \frac{\partial^k f}{\partial x^j \partial y^{k-j}} \right|_{t=0} x^{(j)}(0) y^{(k-j)}(0). \tag{3.19}$$

But, since $f(x, y) = g(y, x)$, this is equivalent to

$$x^{(k+1)}(0) = \sum_{j=0}^{k} \left(\begin{array}{c} k \\ j \end{array} \right) \left. \frac{\partial^k g}{\partial y^j \partial x^{k-j}} \right|_{t=0} y^{(j)}(0) x^{(k-j)}(0), \tag{3.20}$$

and relabeling the sum index,

$$x^{(k+1)}(0) = \sum_{j=0}^{k} \left(\begin{array}{c} k \\ k-j \end{array} \right) \left. \frac{\partial^k g}{\partial x^j \partial y^{k-j}} \right|_{t=0} x^{(j)}(0) y^{(k-j)}(0) = y^{(k+1)}(0). \tag{3.21}$$

Therefore we have shown that the Taylor expansions of $x(t)$ and $y(t)$ coincide. This means that $x(t) = y(t)$ within the radius of convergence of the series. For larger times, we can apply the same argument by analytic continuation (we choose some t_0 in the interval of convergence as the centering point for a new Taylor expansion, and repeat the argument). Hence we conclude that $x(t) = y(t)$ for all t.

Note that the same considerations hold for (3.15), so we can reduce our dynamical system to a set of $L+1$ differential equations,

$$\begin{aligned}\frac{\dot{n}^{\ell}}{n^{\ell}} &= -\alpha + \gamma_{+} s_{\ell-1} n^{\ell-1} - [1+\rho(s_{\ell}-1)] n^{\ell} - \gamma_{-} s_{\ell+1} n^{\ell+1}, \\ \frac{\dot{n}^{0}}{n^{0}} &= R - n^{0} - \gamma_{-} s_{1} n^{1}.\end{aligned} \tag{3.22}$$

There is another crucial difference between our model and usual neutral models in the literature. Although neutral models ignore species identity, they are stochastic. It is the *ecological drift*[10] that makes species abundances to stochastically vary. This demographic stochasticity is the ultimate reason for extinction in neutral models. On the contrary, our dynamical system is deterministic. The reason to include the (somehow arbitrary) extinction threshold n_{c} is to "mimic" this fluctuation-driven extinction of species with low abundance. The stochastic extinction of species caused by events other than predation will be accounted for with a spontaneous extinction rate in Chapter 5.

3.4.2 Structural stability

Structural stability is a fundamental property of a dynamical system referred to smooth perturbations in the set of parameters that define the system and the subsequent change in the resulting orbits. Unlike dynamical stability, which considers perturbations of initial conditions for a fixed system, structural stability deals with perturbations of the system itself.

We have chosen the constants to be uniform in our model, this making all species on each trophic level at equilibrium have equal abundance. However, according to competitive exclusion (MacArthur and Levins 1964), a tiny variation in the parameters that makes any difference among species will make the system unstable. Fortunately, for this class of models the competitive exclusion principle is not that strict. This has been discussed at length in Bastolla et al. (2005a). In this paper, authors derive upper bounds to the variability allowed for the constants that the system can tolerate without leading any species to extinction. They started by considering a one-layer system of competing species following LV equations, and the averaging of these equations led to an upper bound for the variance of the productivity distribution.[11] The more diverse the system is the narrower the productivity distribution has to be (the upper bound turns out to behave as S^{-1} for large S). The average competition load appears in the bound and competitive exclusion is recovered when the competition matrix is uniform (the same effect will show up in our model, see Section 3.6.3). Afterwards, they generalize this result to models including both predator-prey and competition interactions

[10] The stochastic changes in species abundances are commonly encompassed in the term "ecological drift" in the ecological literature.

[11] In Bastolla et al. (2005a) the term "productivity" of a species is used in reference to the r.h.s. of a dynamical system $\dot{n}_i/n_i = f(\mathbf{n})$ disregarding competition terms. In the case of our LV equations, the productivity term accounts for the growth/mortality rate and the predator-prey contributions [see Eq. (3.4)]. This terminology is rather common in ecology.

defined by general matrices, always arriving at the same conclusion: the more diverse the ecosystem is the narrower the upper bound to the variability in productivities turns out to be.

In fact, the dynamical system they discuss is the same that we have described in Section 3.1, only that it allows for variability in the interaction coefficients of different species. In any case, no matter how diverse the ecosystem is, some variation of the constants is always tolerated without this leading any species to extinction. This proves the structural stability of our system, even under the assumption of species symmetry. Modifications of our model to incorporate variability in the interaction strengths will be discussed in Chapter 7.

3.5 The assembly process as a Markov chain

At this point we can connect the assembly process with a Markov chain. Under the assumption of species symmetry, any community is determined through the set of species numbers $\{s_\ell\}_{\ell=1}^{L}$. We have proved that any interior equilibrium is globally stable. Therefore, given the set of species numbers, the corresponding community is viable and stable only if its equilibrium densities $p^\ell \geq n_c$ for all $\ell = 1, ..., L$. Thus by solving (3.16) for all choices of species numbers we can determine all viable and stable communities that are compatible with a given set of parameters.

Although in principle the population model allows for infinitely many species at each level, it turns out that the set of viable communities is finite. This is a consequence of the existence of the extinction threshold —we will prove this fact in Chapter 4, where all these technical details are compiled. There is another limitation due to the finite amount of abiotic resource that maintains our model communities. R accounts for the amount of resource that would be reached in the absence of consumers — in this sense, it represents a carrying capacity[12]. The limiting effect of the resource determines the number of trophic levels: there is a maximum number of levels allowed for a given resource saturation R. On the other hand population densities in each level decrease as s_ℓ^{-1} (see Chapter 4), so we can have populations infinitely close to (but above) zero. Therefore the existence of the extinction threshold renders the set of communities under consideration finite, and the associated Markov chain has a finite number of states. Besides this being a more realistic description of an ecosystem, it also drastically simplifies the analysis of the assembly process.

Thus for any choice of parameters there is a *finite* set of viable communities —that we denote by $\mathcal{F}$. There will be a link from community i to community j of the set $\mathcal{F}$ provided the former is transformed into the latter as a result of an invasion. Invasions are assumed to occur at a uniform rate ξ. In line with previous models, we assume that, during the assembly process, successional invasions occur and modify resident communities *at equilibrium*. This is actually what happens in natural communities: the average time between consecutive invasions (measured by ξ^{-1} in our model) is much

[12] In simple *logistic* growth models, $\dot{x} = rx\left(1 - \frac{x}{K}\right)$, the constant K coincides with the saturation value of the population. It is named "carrying capacity".

longer than the typical dynamic time scale for the community to reach the equilibrium state. In relation to the different time scales between invasion and competition, invasion events may take place at the scale of years, a time long enough for invaded communities to stabilize [for example, the rate of new invasions in islands may be one every few year (Sax et al. 2005)]. This assumption has also been made in previous papers like Kokkoris et al. (1999), where authors assume that after each invasion there is a reorganization of the community prior to a new invasion. Specifically, they solve the dynamical system describing the new community with the invader until reaching the carrying capacity. These new densities are then used as initial values for the new systems resulting from the next invasion [see details in Kokkoris et al. (1999)]. The same idea was applied in the construction of our assembly model. We also assume that the probability of a second invasion occurring before the equilibrium is restored is negligible.

We use a second hypothesis as well, namely that the population of the invader is small (it is assumed as small as possible, i.e. equal to n_c). This is what is actually observed in real situations. It is a well established fact that colonizers rarely reach a new habitat in high numbers (Roughgarden 1974; Turelli 1981). In theory, the probability of a small propagule to extend is used as the invasibility criterion. In biological control, management of invasions is based on looking for a small density of species in new areas (Liebhold and Bascompte 2003). In this case, theoretical and empirical work has taken advantage to predict conditions of eradication based on density thresholds (Allee effects[13]) and demographic stochasticity.

Therefore we can assume invaders arriving at some level ℓ of a community in equilibrium with a small abundance set equal to the extinction threshold. Under the species symmetry assumption, the dynamical system $\dot{n}_i^\ell = n_i^\ell q_i^\ell$ given by the response function (3.15) applies as well for the invaded system, with $N^\ell = \sum_{i=1}^{s_\ell} n_i^\ell + n$, n being the population density of the invader. Therefore, once the equilibrium is reached after the invasion, the density of the invader will be equal to p^ℓ (the density of the remaining species in that level), which can be obtained by solving (3.22) with an occupancy $s_\ell + 1$ in the ℓ-th level. Moreover, the global stability condition applies as well to the invaded dynamics. So we just need to check the viability of the resulting equilibria in order to determine whether the invader is accepted.

If the invasion takes place at level $L+1$, the equation for the invader is simply

$$\frac{\dot{n}}{n} = -\alpha + \gamma_+ s_L n^L - n, \tag{3.23}$$

which in fact is the last equation of the system (3.22) for a community of $L+1$ levels with occupancies $\{s_1, \ldots, s_L, 1\}$. Hence the global stability condition still remains valid and the invader will be accepted if the resulting equilibrium is viable.

This way, a simple criterium decides the acceptance of newcomers. Invasion-driven transitions between viable communities are determined as follows. Consider a community $i \in \mathcal{F}$, with L trophic levels, at its rest point. Potential invaders are species of level

[13]This effect occurs when a population exhibits a "critical density" below which the population declines on average and above which it increases on average.

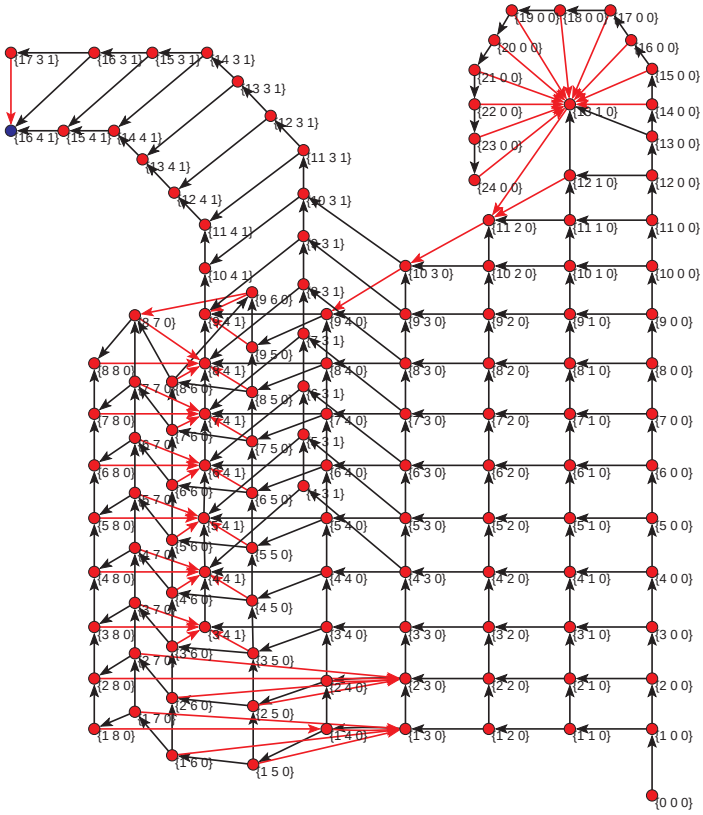

Figure 3.4: *Assembly graph* obtained for $R = 140$. It displays 130 communities with up to three trophic levels. Node labels indicate how many species are in each level $(\{s_1, s_2, s_3\})$. Black arrows represent accepted invasions; red arrows represent transitions inducing a species loss. The only absorbing node (in dark blue, corresponding to the community $\{16, 4, 1\}$) represents the end state of the assembly process. Remaining (red) nodes are transient states of the Markov chain. This graph has been computed setting $\gamma_+ = 0.5$, $\gamma_- = 5$, $\rho = 0.3$, $\alpha = 1$ and $n_c = 1$ (see Table 3.1 for their respective meaning).

$\ell = 1, \ldots, L + 1$ (species of higher levels can not feed from the existing levels). For any ℓ, we introduce a new species at level ℓ of community i, and calculate the interior equilibrium point for the extended community. If it is viable, then the invader is accepted in the resident community. The new community j will also be in $\mathcal{F}$ and a directed link will go from i to j.

If, on the contrary, the population of the species of at least one level falls below n_c, then extinctions will occur. Extinctions must be understood stochastically in our model. The stochastic effect of deleterious mutations or external variations of the environment that make species to go extinct is taken into account in our deterministic dynamics with the viability condition $n^\ell \geq n_c$. Notice however that, strictly speaking, when a species of one level falls below n_c the whole level does too. It is unrealistic that the whole level goes extinct, even though all its species have the same population. In reality, if many species are threatened, by chance one of them will be the first to become extinct. This fact may help the remaining species to survive. Accordingly we shall remove species in an inviable level as follows. As we can monitor the whole trajectory of the system, we detect the moment when the first trophic level crossed n_c. At that point we remove one species from that level and restart the evolution from that point. We keep on removing one species at a time and restarting until the new resulting equilibrium becomes viable. Two things can thus happen: either the first level to fall below n_c is the invaded one, in which case the invader is simply rejected and no transition occurs, or it is another level that falls below n_c. In the latter case the extinction sequence leads to a new community k, and a link will go from i to k. This extinction procedure will be discussed in further detail in Section 4.2 (see Figure 4.4 for an illustration of this procedure).

The assembly graph, $\mathcal{G}$, is defined as the connected component containing the empty community, $\varnothing$, of the directed graph whose nodes are elements of $\mathcal{F}$ and whose links are the transitions obtained by the invasion process just described. Obviously, the way to construct $\mathcal{G}$ is to start off from $\varnothing$, and proceed by attempting all possible invasions for every community reached along the assembly process (see Figures 3.4 and 3.5 for typical representations of two assembly graphs). From the viewpoint of statistical mechanics, $\mathcal{G}$ is the configuration space of our system. The exhaustive characterization of the set of nodes in $\mathcal{G}$ is a bit demanding (see Appendix C for details). Despite this, we have been able to analyze graphs with around 10^6 communities within.

The connection of the species assembly process with a discrete-time Markov chain on the graph $\mathcal{G}$ amounts to assigning certain transition probabilities to each link of the assembly graph. We define these probabilities in a simple way. Invaders arrive at each community at a constant rate ξ, independent of the level of invasion, and the stochastic process is updated in discrete time (each time unit is the average time elapsed between consecutive invasions). Thus, if i and j are two nodes of $\mathcal{G}$ connected by a link, we assign it the transition probability

$$p_{ij} = \delta_{ij} + \xi q_{ij}. \tag{3.24}$$

Define n_{ij} as the number of different invasions of i that lead to j. Given that $L+1$ is the number of different invasions of i, provided it has L trophic levels, the matrix elements q_{ij} are defined by

$$q_{ij} = \frac{n_{ij}}{L+1}, \quad i \neq j, \qquad q_{ii} = -\sum_{j \neq i} q_{ij}. \tag{3.25}$$

Therefore, the transition probability p_{ij} is proportional to the relative frequency of the transition among all the possible transitions starting from i, the invasion rate being the

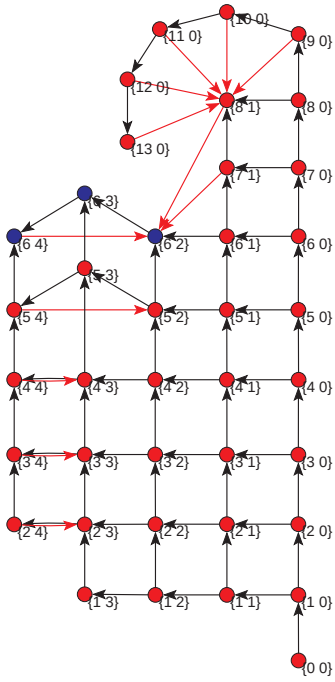

Figure 3.5: *Assembly graph.* Same as Figure 3.4 for $R = 80$. This graph is made of 16 communities, each of them with one or two trophic levels. In this case, the final end cycle of the process comprises 3 communities.

proportionality constant. The diagonal of matrix $\mathsf{Q} = (q_{ij})$ is chosen so that $\mathsf{P} = (p_{ij})$ is stochastic.

Since diagonal elements of matrix P are non-zero, the Markov chain can not be periodic (see Appendix B.1.2). As the set of viable ecosystems $\mathcal{F}$ is finite, P defines the transition matrix of a finite, aperiodic, Markov chain. The states of one such chain are either transient or recurrent (Karlin and Taylor 1975). There can be one or several subsets of recurrent states, the chain being ergodic in each of them. Every recurrent subset is a different end state of the assembly process. The end state of an ecosystem will be history-dependent only if there are at least two such recurrent subsets. Ergodicity implies that there is a stationary probability distribution over these subsets which determines the frequency with which the process visits each of them. For a brief account on Markov chains see Appendix B.1.

Parameter	*Interpretation*
$10 \leq R \leq 1700$	Saturation abundance of the resource in the absence of predation
$\alpha = 1$	Average mortality rate of consumers
$\gamma_- = 5$	Average decline rate of prey population due to feeding
$\gamma_+ = 0.5$	Average rate of increase in predators population due to feeding
$0 \leq \rho \leq 1$	Relative magnitude between intra- and interspecific competition
$n_c = 1$	Extinction threshold

Table 3.1: *Summary of model parameters* and ecological meaning of each one of them.

This concludes the definition of the Markov model for the assembly process. As we are able to compute the whole transition matrix P, we have a *complete* and *exact* characterization of the assembly process. In particular, by selecting an initial state for the Markov chain (in our case it always starts off from $\varnothing$), we can obtain the evolution of any magnitude —numerically but exactly— without resorting to taking averages over realizations of the process. This is the most important difference of this model with respect to all assembly models considered so far. In the following section we will discuss in detail the results that can be obtained from the analysis of the Markov chain.

3.6 Results

All results presented here have been obtained with parameters $\alpha = 1$, $n_c = 1$, $\gamma_+ = 0.5$, and $\gamma_- = 5$ (see Table 3.1 for a brief summary of their ecological meaning). The assumption of $\gamma_+ \ll \gamma_-$ is ecologically sound, because many prey must be consumed to produce an offspring, while loosing one prey requires a single predation event. A common choice for the energy transfer between trophic levels is about 10% (Pimm 1991), hence our choice of the ratio γ_+/γ_-. In most cases we have taken the ratio of direct inter- to intraspecific competition $\rho = 0.3$. We have checked that the model is robust against variations of the parameters within reasonable bounds. As with other parameters the model is robust against variations in direct competition (see details in Section 3.6.3).

To separate transient and recurrent states, we have applied an algorithm provided by Xie and Beerel (1998) (it is described in Appendix C). Note that the characterization of transient and recurrent states in a finite chain depends only on the graph, not on the transition probabilities. Only one subset of recurrent states was found for each set of parameters, that can be either a single (absorbing) community or a complex set formed by several recurrent communities. Let $\mathcal{R}$ denote the subgraph of $\mathcal{G}$ formed by this ergodic set. Figures 3.6 and 3.7 show two examples of these subgraphs. The particular transition probabilities assigned to each link would determine the asymptotic probability distribution within the recurrent set, but not the subset of nodes contained in it. We observe that the communities present in those sets are rather similar in their species numbers composition, and these occupancies decrease as the trophic level in-

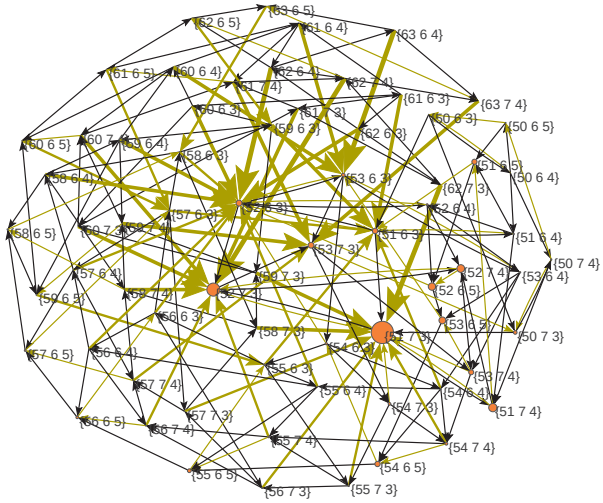

Figure 3.6: *Graph of the recurrent subset* for a resource saturation $R = 430$ (other parameters are set as in Figures 3.4 and 3.5). It contains 68 communities with 3 trophic levels. The diameter of the nodes is proportional to its asymptotic probability. Black arrows show accepted invasions and green ones those causing a reconfiguration (the thickness of each line is proportional to the relative number of extinct species). Labels indicate the number of species in each trophic level.

creases, thus conferring a pyramidal structure to each community. As a mater of fact, we observe that species in recurrent communities have populations close to the extinction threshold. The same pyramidal distribution of species is observed for absorbing end states (i.e., those formed by a single community).

3.6.1 Asymptotic distribution

In order to calculate the asymptotic probability $\boldsymbol{\pi} = (\pi_i)$ for each community $i \in \mathcal{G}$, we need to solve the linear system $\boldsymbol{\pi} = \boldsymbol{\pi}\mathsf{P}$ [see Eq. (B.21)], in other words, the row vector $\boldsymbol{\pi}$ is the (unique) left eigenvector of matrix P with eigenvalue 1. Since our graphs are rather sparse, standard numerical techniques for solving sparse systems have been applied. The eigenvector is normalized to satisfy the condition $\boldsymbol{\pi}\mathbf{1}^{\mathsf{T}} = 1$, where the row vector $\mathbf{1} = (1, \ldots, 1)$ has as many entries as the number of nodes of $\mathcal{G}$. In practice, we only need to solve this system for the subgraph $\mathcal{R}$ corresponding to the recurrent set, since by definition the asymptotic probability $\pi_i = 0$ for any transient state i. Note that our matrix of transition probabilities (3.24) reduces the condition to be satisfied by $\boldsymbol{\pi}$ to $\boldsymbol{\pi}\mathsf{Q} = \mathbf{0}$, i.e. $\boldsymbol{\pi}$ is the left eigenvector of Q with eigenvalue 0. It is

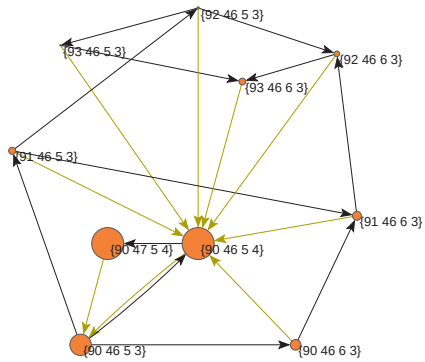

Figure 3.7: *Graph of the recurrent subset* for $R = 990$, displaying 10 communities with 4 trophic levels. In some instances, recurrent subgraphs are rather simple.

worth noticing that neither the asymptotic distribution nor the recurrent subset depend on the invasion rate.

We can thus obtain a probability distribution for each recurrent set. Having this probability distribution is therefore equivalent to defining a statistical mechanics over the set of viable communities, if we regard $\mathcal{G}$ as the phase space of our system. In Figure 3.8 we have plotted the histogram of probabilities for several values of the resource saturation R (for these values the number of communities in each set is larger than 10^3). Communities are labeled in decreasing order of probability. These distributions are found to be roughly exponential over several orders of magnitude, this meaning that only a small number of communities (in general very similar to each other in their occupancies) occur with high probability. These are the communities in which it is more likely to find the ecosystem. Nonetheless ergodicity implies that all communities in the end state are visited with non-zero probability. The ecosystem is thus in a complex state, with fluctuating species numbers in each level due to some invasions being accepted and some others causing avalanches of extinctions.

The equilibrium probability distribution $\boldsymbol{\pi}$ can be used to calculate the asymptotic average over $\mathcal{R}$ of any relevant magnitude M_i defined for every community, like for instance the average number of species, the total population, etc. We just need to evaluate $\langle M \rangle_{\mathcal{R}} = \sum_{i \in \mathcal{R}} \pi_i M_i$.

3.6.2 Dependence with the resource saturation

Assembly graphs have been obtained in a range of resource saturations that goes from $R = 10$ up to $R = 1700$ with increments $\Delta R = 5$. No viable ecosystem is found below $R = 10$. The number of communities $N_{\mathcal{G}}$ in these graphs goes from just one (for $R = 10$) up to about 10^6. We have found empirically that both this number and the

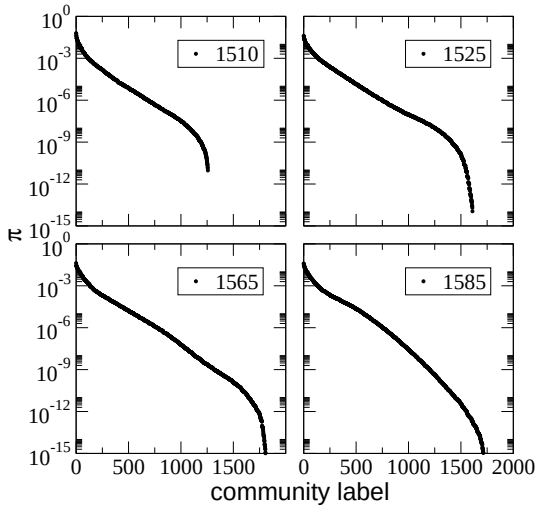

Figure 3.8: *Distribution of asymptotic probabilities* within each recurrent set, for several values of R. Communities are labeled in decreasing order of probability. The distributions are seen to be roughly exponential with a final cut-off.

total number of transitions in each graph grow roughly as $e^{\kappa\sqrt{R}}$, see Figure 3.9. The maximum number of trophic levels that are allowed up to $R = 1700$ is 5.

We have checked whether the set of communities in the assembly graph is the whole set $\mathcal{F}$. Given an estimation of the resource values that allow a maximum number of levels $L_{\max}$ (see Eq. (4.9) in Section 4.1.1), we have tested the viability of all possible combinations of species numbers $\{s_\ell\}_{\ell=1}^{L_{\max}}$ with $L_{\max}+1$ levels up to a total number of species $S_{\max}$ equal to twice the maximum number of species allowed for that value of R. Since the number of these combinations hugely increases with R, we have analyzed all values of R up to $R = 700$. Figure 3.10 shows the difference $\Delta N = N_{\mathcal{F}} - N_{\mathcal{G}}$. In nearly all cases the set of communities in the assembly graph is $\mathcal{F}$, but we have found several instances —all of them near the values of R at which a new level arise— in which $\mathcal{F}$ contains communities not reachable through the assembly process, just like in the experiment of Warren et al. (2003) (see Section 3.2.2). The largest difference is found for $R = 470$, where $N_{\mathcal{G}} = 4800$ and $\Delta N = 375$, so the highest relative difference reaches 8%.

For each R we determined the number of recurrent states of the chain (see Figure 3.11a for a plot of this number as a function of R). A comparison with Figure 3.9 shows that the number of recurrent states is a tiny fraction of the whole assembly graph. We always find a single connected graph, which implies that the end state of the assembly process does not depend on history for this model (Drake 1990). This result agrees with previous evidence found in other assembly models (Morton and Law 1997),

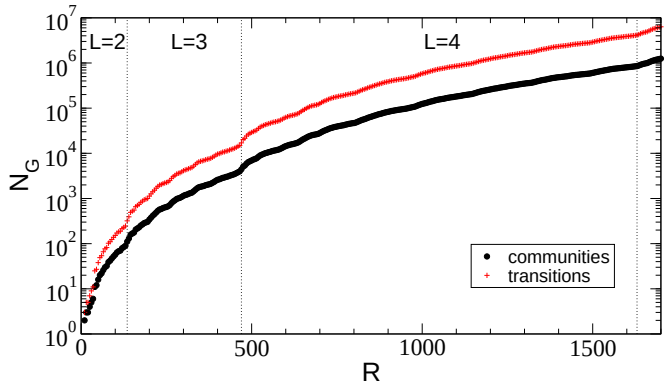

Figure 3.9: *Size of the assembly graph.* Total number of communities (black circles, below) and transitions (red crosses, above) in the Markov chain as a function of the resource saturation R.

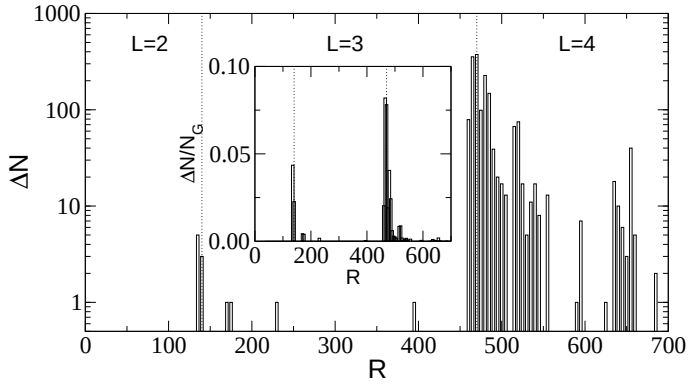

Figure 3.10: *Unreachable communities.* Number of viable states that are not reachable through invasions starting from the empty community $\varnothing$, $\Delta N = N_{\mathcal{F}} - N_{\mathcal{G}}$. Typically there is an accumulation of these communities near the onset of appearance of a new trophic level (marked with dotted lines). The inset represents the proportion $\Delta N/N_{\mathcal{G}}$ vs. R.

where the same kind of assumptions about the invasion rate are made, as well as in the experiments of Warren et al. (2003), who found empirically a final end cycle (see Figure 3.2). There are values of R for which this set consists of a unique absorbing state (or just a few, sometimes forming a cycle), but when R is reaching the values at which a new trophic level appears, the size of this set increases considerably (the largest set found contains around 1800 communities). After crossing these values the size of the

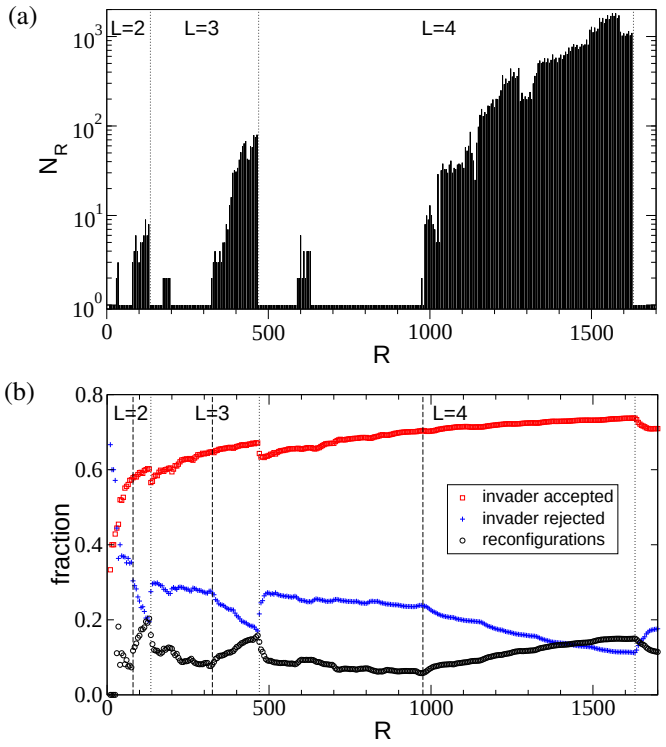

Figure 3.11: *Dependence with the resource saturation.* (a) Number of recurrent states of the Markov chain as a function of the resource saturation R. (b) Statistics of links corresponding to accepted invasions (red squares), rejected invasions (blue crosses), and invasions that lead to a reconfigured community through an avalanche of extinctions (black circles). Dotted lines correspond to the onsets of emergence of a new trophic level, and dashed lines to the beginning of the regions of complex end states.

recurrent set drops again down to just one absorbing state. Morton and Law (1997) also obtained complex end states in 6 out of the 80 pools they explored, with a number of communities ranging from 6 to 138.

In Figure 3.11b we show the fractions of links in the assembly graph corresponding to invasions that are accepted, rejected, or cause a reconfiguration in the system through a sequence of extinctions. The most frequent case is the acceptance of the invader, although there are around a 20% of rejections and reconfigurations. We can see an increasing trend to reconfigurations when R corresponds to a complex end state (c.f. Figure 3.11a). The invasibility criteria that we will obtain in Section 4.2.1 explain why we observe an increasing number of rearranged communities in these regions.

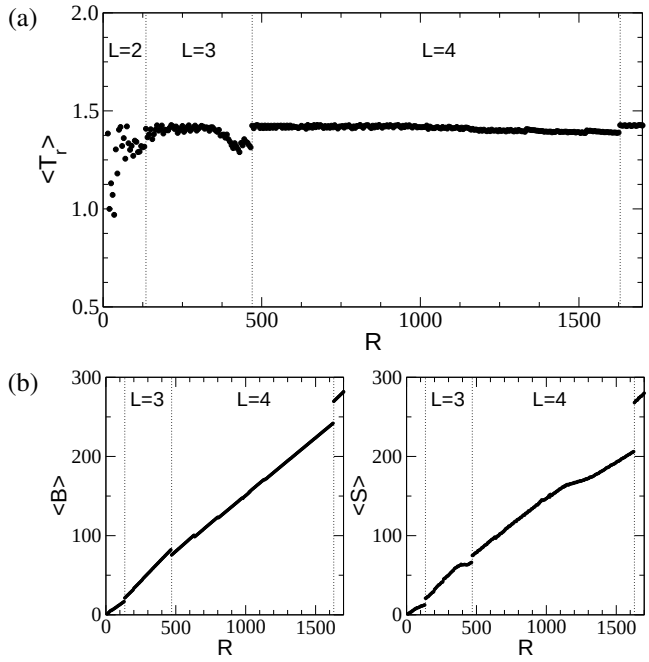

Figure 3.12: *Dependence with the resource saturation.* (a) Mean return time in the stationary state vs. resource saturation R. The behavior is approximately constant, except for the region of low resources, where the graphs contain less communities and there is more variability. (b) Mean population density of the community vs. R (left), and mean number of species (biodiversity) vs. R (right).

As for dynamic stability (resilience), we can measure the mean return time $\langle T_{\rm r}\rangle$, i.e. the mean time that a perturbed ecosystem needs to restore equilibrium (Pimm and Lawton 1977), averaged over the probability distribution of the stationary state. We observe that the time for a perturbed community to restore equilibrium is roughly independent of the end state, being approximately constant as a function of the resource saturation R (Figure 3.12a).

For each end state, regardless on whether it is an absorbing community or a recurrent set, we have calculated some other averages. In Figure 3.12b (left) we show the dependence of the total population of a community, $B = \sum_{\ell=1}^{L} s_\ell p^\ell$, averaged over the recurrent set $\mathcal{R}$, as a function of the resource saturation R. The dependence is basically linear, except for some dips near the onset of emergence of a new level. Figure 3.12b (right) shows the averaged number of species $\langle S\rangle$. Near the boundary of each level we observe a lowering of the linear behavior, followed by a discontinuous jump once the new level is established. We can explain this behavior as a *top-down* effect: the presence of a top predator controls species populations at the level immediately below,

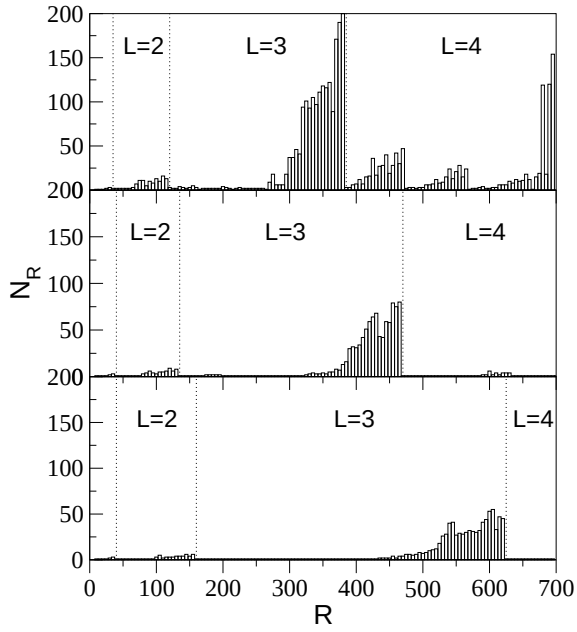

Figure 3.13: *Dependence on the parameters.* Number of communities in the recurrent sets, $N_{\mathcal{R}}$, vs. the resource saturation, R, varying direct competition (upper panel, $\rho = 0$; middle panel $= 0.3$; lower panel, $\rho = 0.7$). Observe the decrease in $N_{\mathcal{R}}$ as competition increases, and the increase of the values of R at which a new level arises.

in such a way that if the predator disappears, the population of these species grows so much that the overconsumption of their resources causes the extinction of some of them (Crooks and Soulé 1999). As a matter of fact we have checked that when a new level appears it contains a single top predator and the number of species at lower levels rises.

3.6.3 Dependence on the parameters

We have already mentioned that the model results are not qualitatively influenced by variations on its parameters. For example, we have studied the model dependence with respect to direct competition (Figure 3.13). In the absence of interspecific competition ($\rho = 0$), levels are filled up more easily, so the number of communities in the recurrent set increases with respect to the results reported so far. The effect of increasing direct competition is to reduce the number of ecosystems in these sets, and to increase the resistance to the appearance of a new level in the end state for the same values of resource saturation. Thus the global behavior of the number of communities as a function of R turns out to be similar, up to scale factors, to that obtained in Fig. 3.11a.

The particular case $\rho = 1$ (interspecific competition equal to intraspecific competition) is qualitatively different. Fixing $\rho = 1$ transforms the community into a trophic chain. All species can be grouped into a single one with population $N^\ell = s_\ell n^\ell$ (i.e. the LV equations of this system, (3.22), are closed in the variables N^ℓ). But the implications of this assumption are stronger. Even if the distinction between species becomes meaningless, one can formally keep the identities and treat them as different. But then it is easy to show that any invasion attempted at a level already occupied by at least one species will be unsuccessful because the population of the invader ends up below n_c. In fact, according to Eq. (3.15), the initial per capita growth rate of an invader at level ℓ is $-n_\mathrm{c}$ and the equations for level ℓ and for the invader coincide. Hence $\dot{N}^\ell/N^\ell = \dot{n}/n$, n being the abundance of the invader. This asymptotically yields

$$p = \frac{n_\mathrm{c}}{N^\ell(0)} P^\ell \tag{3.26}$$

since $n(0) = n_\mathrm{c}$ (p and P^ℓ are the invader and the overall ℓ-level equilibrium densities after the invasion, respectively). Now, the linear system (3.16) for the interior equilibrium point before the invasion is exactly the same after the invasion replacing $N^\ell(0)$ by $p + P^\ell$. This fact, together with (3.26), yields $p = n_\mathrm{c} N^\ell(0)/[n_\mathrm{c} + N^\ell(0)] < n_\mathrm{c}$. Since the population of the invader initially decreases, according to our extinction procedure the invader goes extinct.

Thus the assembly graph $\mathcal{G}$ becomes trivial. Using the notation $\{s_\ell\}_{\ell=1}^L$ for each community, $\mathcal{G}$ is simply

$$\varnothing \to \{1, 0, \ldots, 0\} \to \{1, 1, \ldots, 0\} \to \cdots \to \{1, 1, \ldots, 1\}. \tag{3.27}$$

This never happens if $\rho \neq 1$. Things are thus very different when this fully symmetric scenario is assumed.

It can be shown that in this purely neutral scenario the *competitive exclusion principle* applies. This principle states that there can not coexist more populations than different resources (or ecological niches) in the long term dynamics if these populations depend linearly on the resources (Hofbauer and Sigmund 1998). We can put this statement in mathematical terms. For the sake of simplicity, let us assume that there is a single trophic level with S species predating on the resource (at rates γ_{+i}, $i = 1, \ldots, S$) and let us set a non-uniform direct competition ρ_{ij} between pairs of species in that level. Let n_i be the population density of species i, α_i its death rate in the absence of consumption and n_0 the amount of resource. The LV equations for this system are

$$\frac{\dot{n}_i}{n_i} = -\alpha_i + \gamma_{+i} n_0 - \sum_{j=1}^{S} \rho_{ij} n_j. \tag{3.28}$$

If the competition matrix is singular, we can find a non-trivial solution $(c_1, \ldots, c_S)$ for the linear system $\sum_i c_i \rho_{ij} = 0$, $j = 1, \ldots, S$ (note that, in particular, the fully symmetric scenario $\rho = 1$ renders the competition matrix singular). Multiplying both

sides of Eq. (3.28) by c_i and summing over all species, we obtain

$$\sum_{i=1}^{S} c_i (\log n_i)^{\cdot} = \sum_{i=1}^{S} c_i (\gamma_{+i} n_0 - a_i) \equiv -a \tag{3.29}$$

where we can assume that a is positive (otherwise change the sign of the c_i). Integrating from 0 to t we obtain

$$\prod_{i=1}^{S} n_i(t)^{c_i} = C e^{-at}. \tag{3.30}$$

This means that one of the densities must vanish in the limit $t \to \infty$, which proves competitive exclusion.

There is a peculiarity of our model, though. If $\rho = 1$ the population of the invader at equilibrium will not be zero because in our model all constants are uniform, so the equation to solve for c_i is $\sum_i c_i = 0$. This yields $a = 0$ and spoils the argument. However, we have shown that, with our procedure of species extinction, the invader's population ends up below n_c hence not being viable. This restores competitive exclusion, albeit in a weaker sense. The result (3.27) is just a manifestation of this fact.

It is important to notice that, for a non-singular competition matrix, the competitive exclusion principle is not guaranteed to hold. In particular, if $\rho < 1$ the intra- and interspecific competition will have different magnitude, and the matrix of elements $\rho_{ii} = 1$ and $\rho_{ij} = \rho$ $(i \neq j)$ will be non-singular. The argument above does not apply anymore and, as a matter of fact, by integrating the equations for population dynamics we actually obtain more than one species coexisting with a single resource in the system.

The interesting point brought about by the above discussion is that interspecific competition induces *de facto* a niche separation for the species of the same level — which are therefore competing for the same resources— that allows them to circumvent the competitive exclusion principle [for a more thorough discussion of this point see Bastolla et al. (2005a) and Bastolla et al. (2005b)].

3.6.4 Absorption times

So far we have discussed properties of the recurrent set of the Markov chain associated to the assembly process, but we have not discussed the possibility that the process may keep trapped for a long time in transient states. In order to ascertain this point, we have calculated the mean absorption time from the empty community $\varnothing$ to the end state. See Appendix B.1.5 for details on how these time can be calculated.[14]

In Figure 3.14a we plot the mean absorption time $\tau_\varnothing$ to reach the recurrent set starting from the empty community, along with the mean number of species $\langle S \rangle$, which measures the size of the system. Both of them grow almost linearly with R, hence $\tau_\varnothing$ is roughly linear with $\langle S \rangle$ as well (see Figure 3.14b). The number of states in the Markov

[14] The linear system that has to be solved for the calculation of mean absorption times, Eq. (B.23), implies that these times are proportional to ξ^{-1}, because of the form (3.24) of our transition matrix.

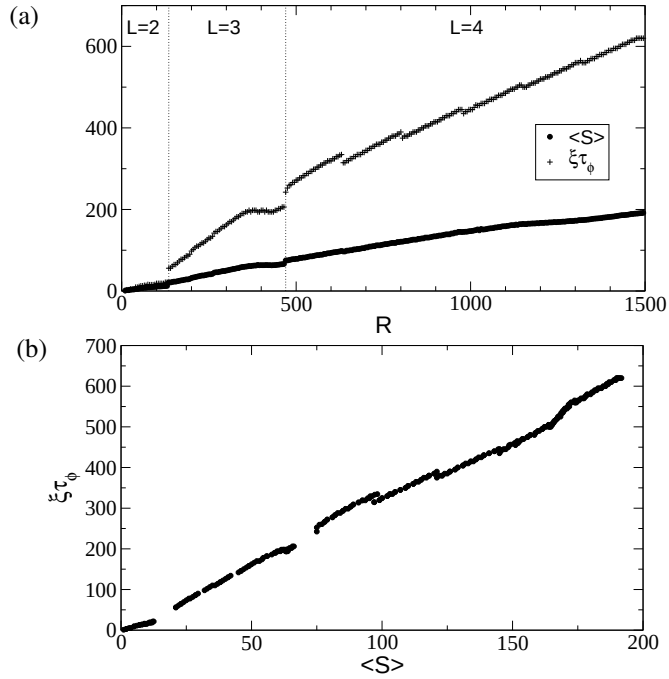

Figure 3.14: *Absorption times.* (a) Mean absorption time $\tau_\varnothing$ (in number of invasions) starting from the empty community $\varnothing$, and mean number of species $\langle S \rangle$ as a function of the resource saturation R, showing a roughly linear growth for both of them. (b) Mean absorption time $\tau_\varnothing$ vs. $\langle S \rangle$.

chain grows as $e^{\kappa\sqrt{R}}$, a very large number compared to $\xi\tau_\varnothing$. Therefore the mean time to reach the end state is small compared to the system size.

This result should be taken with a grain of salt, because it strongly relies on our assignment of probabilities to transitions. This, in turn, assumes that there is always availability of invaders, which may not be true if invaders come from a finite pool. The lack of potential invaders when the community is almost "full" would decrease the probability of a new invasion and accordingly would increase the time that the process needs to reach the end state. What the result of Figure 3.14a is actually telling us is that the assembly graph is dominated by pathways in which most invasions are accepted.

3.6.5 Extinctions distribution

As we have previously described, the assembly process can be regarded as if the ecosystem self-organizes into a state resistant to invasions. Either for transient or recurrent states, the community is continuously undergoing avalanches of extinctions caused by

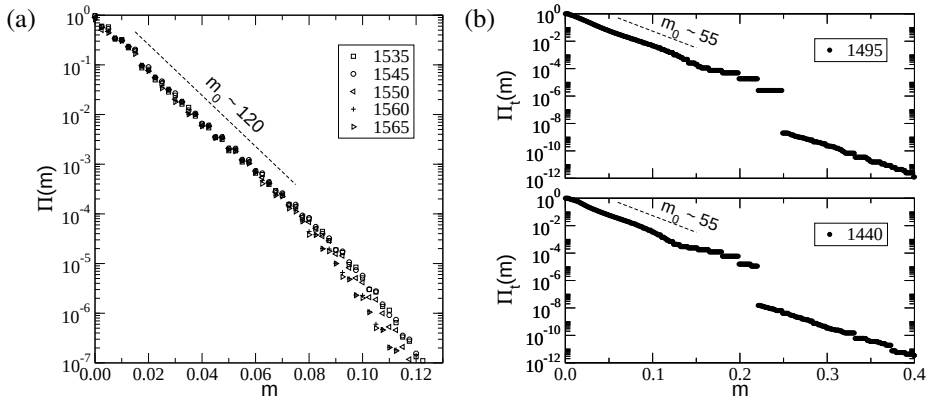

Figure 3.15: *Avalanches distribution.* (a) Probability $\Pi(m)$ that an invasion causes the extinction of at least a fraction m of the species of the invaded community, for several values of the resource saturation R. There is a characteristic magnitude m_0^{-1} around 1%. In order to have enough statistics, we have chosen values of R within the region where the number of communities in the recurrent set is above 1000 (see Figure 3.11a). Thus we have better statistics to compute the histograms than for smaller R. (b) The same probability for transient states, $\Pi_{\rm t}(m)$, is shown for two values of R. This distribution has been obtained by averaging magnitudes with the average fraction of visits to each transient state starting from the empty community $\varnothing$. The characteristic size of the avalanches here is about 2%.

new colonizations. Figure 3.15a shows a statistics of such avalanches in some recurrent sets. It represents the probability $\Pi(m)$ that an invasion causes an avalanche of magnitude greater than m (understood as the fraction of species that go extinct), averaged over the stationary state. We can see in the figure that this probability shows an exponential decay, with a typical avalanche size m_0^{-1} of about 1% of the community, m_0 being the slope of the distributions in log-linear scale. Invasions never cause big perturbations in the community.

We can calculate a similar distribution for the avalanches of extinctions in the transient states. Now we have to weight m with the average fraction of visits to each transient state. Let us denote as z_{ij} the average number of visits to state j starting from state i. The matrix $\mathsf{Z} = (z_{ij})$ is then given by

$$\mathsf{Z} = \sum_{k=0}^{\infty} \mathsf{V}^k = (\mathsf{I} - \mathsf{V})^{-1}, \tag{3.31}$$

V being the left-bottom submatrix of the reduced form (B.6) of the transition probability matrix P (i.e., V accounts for transition probabilities between transient states). Thus the number of visits to the transient j starting from $\varnothing$ is $\zeta_j = (\boldsymbol{\delta}_{\varnothing}\mathsf{Z})_j$, where the

row vector $\boldsymbol{\delta}_{\varnothing} = (\delta_{i\varnothing})$ has as many components as there are transient states. Hence we can calculate ζ by solving the linear system

$$\boldsymbol{\zeta}(\mathsf{I} - \mathsf{V}) = \boldsymbol{\delta}_{\varnothing}. \tag{3.32}$$

The resulting probability $\Pi_{\mathrm{t}}(m)$ that an invasion causes the extinction of at least a fraction m of the species of the invaded transient community is shown in Figure 3.15b. We also find an exponential behavior for the cumulative distribution, in this case with a mean characteristic fraction of species loss of 2% for transient avalanches. The species loss caused by invasions in the transient part of the graph is always small.

3.6.6 Time averages

Computing the time evolution of averages is very simple, given the transition matrix P and some initial probability distribution —which in our case is just the vector $\boldsymbol{\delta}_{\varnothing}$, since the assembly process starts from the empty community— according to Eq. (B.4). We simply need to calculate the power P^t to obtain the transition probability matrix after t time steps. Hence the probability of rejecting the invader at discrete time t is

$$p_{\mathrm{r}}(t) = \sum_j p_{jj} (\mathsf{P}^t)_{j\varnothing}, \tag{3.33}$$

and that of accepting the invader

$$p_{\mathrm{i}}(t) = \sum_j \left(\sum_{|k-j|=1} p_{jk} \right) (\mathsf{P}^t)_{j\varnothing}, \tag{3.34}$$

where the inner sum runs over transitions starting from j in which the invader is accepted. Obviously, the probability that the community undergoes a reconfiguration because of the invasion is obtained as $p_{\mathrm{a}}(t) = 1 - p_{\mathrm{r}}(t) - p_{\mathrm{i}}(t)$. Figures 3.16a and 3.16b represent the dependence in time of the probabilities p_{i} and p_{a} in two cases: one ending up in a complex recurrent set (a), and another with an absorbing community as end state (b). Notice that all curves collapse, for small ξ, when divided by ξ and plotted against ξt (mean number of invasions).

In Figure 3.16c we show the probability of invasion $p_{\mathrm{i}}(t)$ and the average species loss defined as

$$e(t) = \sum_j \left({\sum_k}' (\Delta S)_{jk} p_{jk} \right) (\mathsf{P}^t)_{j\varnothing}, \tag{3.35}$$

where $(\Delta S)_{jk}$ is the species loss in the transition from j to k and the prime denotes that we ignore in the sum transitions in which the invader is accepted. When these two magnitudes are equal there is an equilibrium between the average frequency of invasions and the average number of species loss. This is a fingerprint of the reaching of the stationary state. As expected, this time is comparable to the absorption time shown in Figure 3.14a.

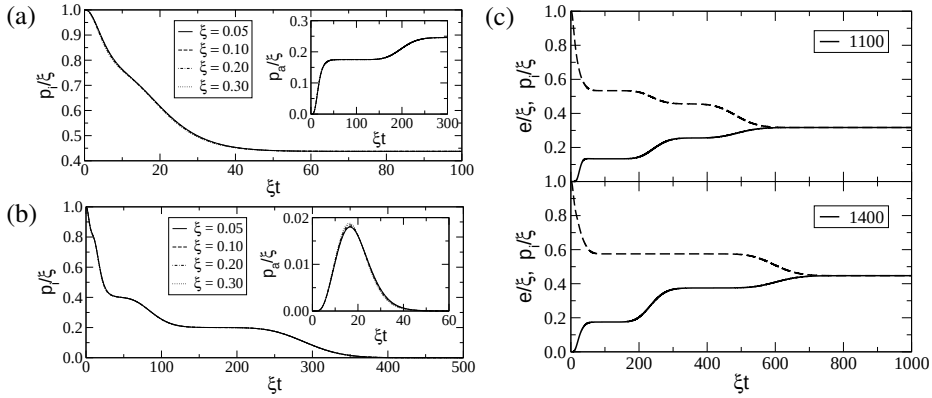

Figure 3.16: *Time averages.* (a) Probability of invasion vs. mean number of invasions (ξt) for $R = 430$ (with a complex end state). Inset: probability of reconfiguration after invasion vs. mean number of invasions. (b) The same as (a) but for $R = 540$ (the end state is a single community). (c) Probability of invasion (dashed lines) and average number of species loss (full lines) vs. mean number of invasions, for two values of R with complex end states. At the time these two magnitudes coincide, a stationary state (the recurrent set) is reached.

Another important magnitude is biodiversity. Figure 3.17a represents the evolution of the average number of species for several values of R. In all cases, it grows monotonically until reaching the stationary state, so biodiversity and resistance to invasion are positively correlated, in agreement with previous assembly models (Law and Morton 1996; Morton and Law 1997).

Figure 3.17b represents the evolution of the total population density $\langle B \rangle$ of each community. If we assume, for the sake of simplicity, the same weight per individual for all species in our model communities, then $\langle B \rangle$ can be regarded as the total biomass in the community. Although there is a clear trend for biomass to increase, it is not always at its optimum in the stationary state (see the curve for $R = 470$, a value at the onset of appearance of the fourth level). This agrees with the analysis performed by Virgo et al. (2006) on their assembly model.

We have also studied the time dependence of the average number of trophic levels during the assembly, which is shown in Figure 3.17c. At $R = 470$ the process stays a certain time trapped in three-level communities until the fourth level is finally accepted. This effect becomes smaller upon increasing R, until there is no trapping and the fourth level is reached straight away.

Figure 3.17d shows a typical time evolution of the average return time along the assembly until reaching the stationary state. Communities are less resilient (have larger return time to equilibrium) as time increases. Thus, there is a trade-off between ro-

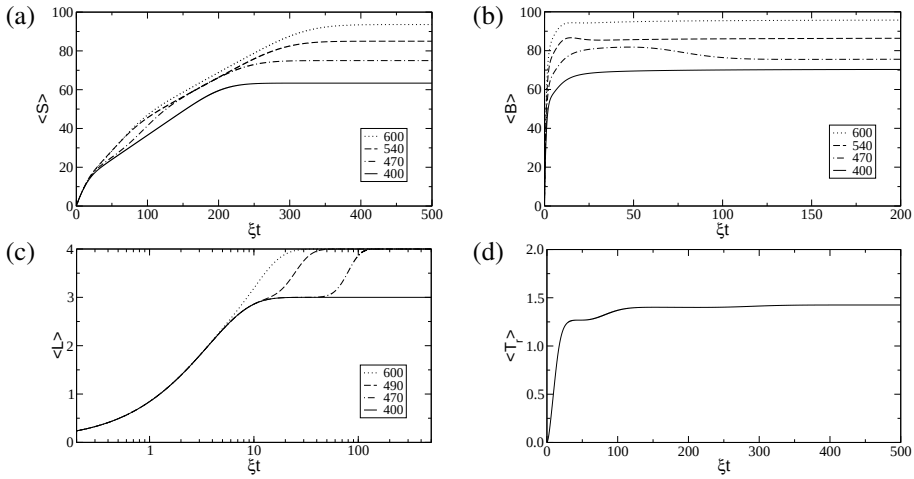

Figure 3.17: *Time averages.* Species richness (a) and total population (b) vs. mean number of invasions (ξt), for several values of the resource saturation R. At $R = 470$ (shown with dash-dotted lines) the ecosystem crosses over from 3 levels to 4 levels (this crossover corresponds to the non-monotonic behavior of the total population). (c) Mean number of levels vs. mean number of invasions. At the onset of the fourth level, the ecosystem stays some time trapped in three-level communities. (d) Typical variation of the average return time with ξt.

bustness (resistance against invasions) of the ecosystem and dynamic stability which is resolved by sacrificing the latter in favor of the former.

3.7 Discussion

Our minimalistic assembly model might be considered as a benchmark of the assembly process that builds up ecological communities. As such, we do not aim at providing a realistic description of an ecosystem but at capturing, in a very simplified model, the essential mechanisms that do occur in the construction of real ecosystems. The model rests on some oversimplistic features: communities are strictly organized in trophic levels, predation occurs only between contiguous levels, species of a given level are trophically equivalent, model parameters are chosen uniformly and the population dynamics is ruled by simple LV equations. In spite of this, our model exhibits the same behavior as those assembly models reported in the literature. This indicates that this behavior is very robust, and probably shared also by real systems and simple models alike.

Thanks to these oversimplifications the model provides important advantages on previous assembly models. The main one is a complete and exact description of both, the set of microstates and the dynamical pathways of the assembly process. Since we can trace all pathways of the assembly process, we can compute exactly all the observables of a community and characterize in a very precise manner the stationary state of the ecosystem. Our model also has a species pool, as standard assembly models, but because we allow for an arbitrary number of trophically equivalent species, the pool is infinite and the model does not suffer from the problem of exhaustion of good invaders that may trap the community in a transient state (Case 1991; Levine and D'Antonio 1999). This has permitted us to build communities with hundreds of species and explore the influence of different elements on the behavior of the assembly process.

Therefore, we are not limited, as in standard assembly models, to compute averages over a set of realizations of the process. To give a hint about what this means, we have calculated, for $R = 300$ (a case with an end state made of a single community of three trophic levels and 50 species), that there are $\sim 10^{10}$ different minimum-length pathways leading from the empty to the end state. This number is nothing that a simulation can come close to.

There is, of course, a concern about having trophically equivalent species, since they are indistinguishable regarding their feeding interactions. The grouping of trophically equivalent species is a common practice in studying food-webs, so it is tempting to do so in this model. If we do it, the model becomes equivalent to a chain, for which LV dynamics is well characterized (Hofbauer and Sigmund 1998), and the invasion process seems to become trivial. This is not true, though: if $\rho \neq 1$, i.e. if intra- and interspecific competition are different in magnitude, intraspecific competition in the equivalent chain explicitly depends on s_ℓ, so invasions modify the parameters of the chain and the invasion process becomes non trivial. Thus, it is because of the (direct) interspecific competition $\rho < 1$ that this equivalence breaks down and the model departs from triviality. We have explicitly shown that choosing $\rho = 1$ brings about the competitive exclusion principle, and indeed the model turns into a chain. But for any $\rho < 1$ this no longer holds. Interspecific competition is thus an effective way of creating new niches.

Let us now summarize the main conclusions that we can extract from the present analysis of the model.

As our model ecosystems evolve we observe three trends: biodiversity increases, resistance to invasion increases and all species decrease their populations. In the steady state biodiversity is at its maximum, all populations are close to the extinction level and either invasions are rejected or they produce transitions between a set of communities with a very similar structure. These three features are related. The increase in biodiversity is unavoidable because of the constant flux of colonizers; however, as the number of species increases, their populations necessarily decrease because all share the same resource. The invasion process guarantees that this is done in the most efficient way, because inefficient invasions cause extinctions in the community and force a more equilibrated rearrangement of the populations. This, in turn, justifies the increasing resistance to new invasions. At the end, all populations are so close to extinction

that either no new invasions are possible, or they just cause small rearrangements that leave the community in a similar state.

Final communities have typically three or four trophic levels —only ecosystems with more than ~ 200 species generate five trophic levels. On the other hand, the number of species in each level has a pyramidal structure. Both features are in qualitative agreement with what is observed in real ecosystems (Cohen et al. 1990). We will discuss at length the properties of the population dynamics that explain these features in Chapter 4.

The question as to whether the end state depends on the history of the ecosystem has a clear-cut answer in this model because we can trace all pathways of the community assembly. It turns out that this end state is always unique, and this is consistent with previous assembly models (Morton and Law 1997). Whether this is a feature that real ecosystems exhibit will, of course, depend on how well they fulfill the assumptions about the invasion rate underlying this and other assembly models. However, there is a caveat that should be made on this point related to the indistinguishability of species within the same trophic level: the end state is unique as long as we consider only the number of species at each level. Whether two communities with the same numbers have the same or different species is meaningless for this model, so the conclusion is not definitive. In fact, some relatively recent experiments on aquatic microbial communities establish that productivity-biodiversity relations depend on the history of assembly (Fukami and Morin 2003), and we can not rule out that the independence on history resulting from this model might be an artifact of the indistinguishability of species.

As for the robustness of the above results, we have tried other values of the direct competition parameter, namely $\rho = 0$ and $\rho = 0.7$, to test its influence. No qualitative difference with the behavior reported here is found. Nonetheless, there are three quantitative effects that we have observed as ρ increases: resistance to invasion increases, appearance of new trophic levels is hindered and the number of communities in complex end states decreases. Varying γ_- has similar effects; in fact, the product $\gamma_+\gamma_- = 0.1\gamma_-^2$ provides a quantitative estimate of indirect competition.

The final take-home message from this model is that we should not be afraid of oversimplifications in complex systems. Complexity normally arises as a consequence of a collective behavior of many entities, not as a result of the complexity of interactions. The key point is whether we are retaining the basic ingredients yielding the desired output. We have shown that there is no qualitative difference between the results of this oversimplified model and previous, more sophisticated assembly models. And there is a lot to gain from the wider view that this model provides of the process and the much higher control we have on the parameters. Many questions that are hard (or even impossible) to answer in previous model have a clear-cut answer here. And even if they may be too simplistic, they can still guide our intuition when dealing with real ecosystems.

4

Analysis of the invasion dynamics

Mathematicians are like Frenchmen: whatever you say to them they translate into their own language and forthwith it is something entirely different.
—Johann W. von Goethe.

In the preceding chapter we have introduced a model of ecosystem assembly and we have discussed at length the numerical results that the model produces. A detailed analysis concerning the analytical properties of the underlying LV population dynamics was provided in Chapter 3, as well as the stability properties of the interior equilibrium point. Our communities represent a mean-field version of trophic networks: the feeding relations are assumed to take place only between contiguous trophic levels and the strength of each interaction is averaged to a uniform value. This assumption of symmetry allows for simplifications in the differential equations, showing that in our model the set of species numbers at each level $\{s_\ell\}_{\ell=1}^{L}$ is enough to determine the equilibrium densities and the dynamics of a community with L trophic levels.

This chapter is devoted to study in depth some analytical findings that are essential to understand the results described in the previous discussion. Relying on these analytical results for the population dynamics, we will show how they can be combined together to describe the observables that characterize the end states with high accuracy, hence arriving at the same conclusions derived numerically. In particular, we will reproduce the dependence of the number of communities in each end state with the abundance of abiotic resources, as well as the average values of quantities like species richness. Moreover, we will show that the the existence of these complex end states is

a result of a top predator attempting to invade a community when its establishment is not allowed by the parameters of the model.

4.1 Analytical properties of the interior rest point

Invasions are assumed to occur between equilibrium communities in our model. Equilibrium abundances satisfy the linear system (3.16) depending on the set of occupancy numbers $\{s_\ell\}_{\ell=1}^{L}$ that defines the community. Accepted invasions simply change the occupancies in one unit. In order to understand the effect of invasions in equilibrium abundances, it would be interesting to cast the dependence of those abundances on $\{s_\ell\}_{\ell=1}^{L}$ in an analytical form. This section will be devoted to that issue.

4.1.1 Maximum number of species and maximum number of levels

In the numerical analysis of the model, we observed that recurrent sets were formed by pyramidal communities with populations close to the extinction threshold. Absorbing communities also share the same property. In this subsection we will obtain approximate upper bounds to the number of species that a trophic level can host among all the possible viable equilibria. We will show that the number of species decreases upwards as $s_\ell \sim (\gamma_+/\gamma_-)^\ell$ as long as the trophic level increases.

To this purpose, since populations are close to n_c, we simply set all the abundances in each level to be equal to n_c and solve the resulting linear system (3.16) for $\{s_\ell\}_{\ell=1}^{L}$ and $s_0 \equiv p^0/n_\mathrm{c}$,

$$\begin{aligned} s_0 + \gamma_- s_1 &= \frac{R}{n_\mathrm{c}}, \\ \gamma_+ s_{\ell-1} - \rho s_\ell - \gamma_- s_{\ell+1} &= 1 - \rho + \frac{\alpha}{n_\mathrm{c}}, \end{aligned} \tag{4.1}$$

for $\ell \geq 1$. Let us introduce the generating function $G(z) = \sum_{\ell=0}^{\infty} s_\ell z^\ell$ for the sequence $\{s_\ell\}_{\ell=1}^{L}$. The explicit solution will depend on two initial conditions s_0 and s_1, since we have a two-term recursion. We will leave them undetermined for the moment. The second equation of (4.1) allows us to calculate explicitly $G(z)$,

$$G(z) = \frac{(1-\rho+\alpha/n_\mathrm{c})z^2}{(1-z)(\gamma_+ z^2 - \rho z - \gamma_-)} - \frac{\gamma_- s_0 + z(\rho s_0 + \gamma_- s_1)}{\gamma_+ z^2 - \rho z - \gamma_-}. \tag{4.2}$$

We recover the general term of s_ℓ by a series expansion of the generating function. Let us first define the constants $\mu = (1-\rho+\alpha/n_\mathrm{c})/(\gamma_- - \gamma_+ + \rho)$ and $z_\pm = (\rho \pm \sqrt{\rho^2 + 4\gamma_+\gamma_-})/(2\gamma_+)$. In order to get compact expressions, we define the auxiliary sequence

$$a_\ell = \left(\frac{\gamma_+}{\gamma_-}\right)^\ell \frac{z_+^{\ell+1} - z_-^{\ell+1}}{z_+ - z_-}, \tag{4.3}$$

which satisfies the two-term recurrence relation $\gamma_- a_\ell = \rho a_{\ell-1} + \gamma_+ a_{\ell-2}$ with initial conditions $a_{-1} = 0$, $a_0 = 1$. This sequence can be fully expressed as a linear

combination of powers of ρ/γ_- and γ_+/γ_-,

$$a_\ell = \sum_{k=0}^{\lfloor \ell/2 \rfloor} \binom{\ell-k}{k} \left(\frac{\rho}{\gamma_-}\right)^{\ell-2k} \left(\frac{\gamma_+}{\gamma_-}\right)^k, \tag{4.4}$$

for all $\ell \geq 0$, $\lfloor x \rfloor$ denoting the integer part of x.

Expanding $G(z)$ we obtain s_ℓ in terms of a_ℓ,

$$s_\ell = (-1)^\ell \left[\frac{\gamma_+}{\gamma_-}(s_0+\mu)a_{\ell-2} - (s_1+\mu)a_{\ell-1}\right] - \mu, \tag{4.5}$$

for $\ell \geq 2$, where a_ℓ can be evaluated either using (4.3) or (4.4). In order to solve the system (4.1), we have to impose $s_{L+1} = 0$ for a community to have L trophic levels. This provides a linear relation between s_0 and s_1 which, together with the first equation of (4.1), forms a linear system that determines both s_0 and s_1. The result is

$$\begin{aligned} s_0 &= \frac{(R/n_\mathrm{c} + \mu\gamma_- + \mu)a_L - (-1)^L \mu\gamma_-}{a_L + \gamma_+ a_{L-1}} - \mu, \\ s_1 &= \frac{\gamma_+(R/n_\mathrm{c} + \mu\gamma_- + \mu)a_{L-1} + (-1)^L \mu\gamma_-}{\gamma_-(a_L + \gamma_+ a_{L-1})} - \mu. \end{aligned} \tag{4.6}$$

Substituting (4.6) into (4.5) and taking into account that

$$a_L a_{\ell-2} - a_{L-1}a_{\ell-1} = (-1)^\ell \left(\frac{\gamma_+}{\gamma_-}\right)^{\ell-1} a_{L-\ell} \tag{4.7}$$

is a direct consequence of the recurrence satisfied by a_ℓ, we finally get

$$s_\ell = \left(\frac{\gamma_+}{\gamma_-}\right)^\ell \left(\frac{R}{n_\mathrm{c}} + \mu\gamma_- + \mu\right) \frac{a_{L-\ell}}{a_L + \gamma_+ a_{L-1}} - \mu \left[(-1)^{L+\ell} \frac{a_{\ell-1} + \gamma_+ a_{\ell-2}}{a_L + \gamma_+ a_{L-1}} + 1\right] \tag{4.8}$$

for all $\ell \geq 1$. This is the analytical solution of the system (4.1) and gives an estimate of the maximum occupancy per level as a function of the parameters of the model. Note that, despite what (4.3) might suggest, no additional factors of the form γ_+/γ_- can be extracted from a_ℓ according to (4.4), so the lowest power of the ratio γ_+/γ_- in the expression for s_ℓ is $(\gamma_+/\gamma_-)^\ell$.

This dependence of s_ℓ on $(\gamma_+/\gamma_-)^\ell$ is remarkable. It explains why communities in end states are pyramidal. This is, in turn, a consequence of the exhaustion of the species occupancy in each trophic level. Notice also that the estimation of the maximum number of species that a community can host depends linearly on the resource saturation R. This linear dependence on R was also observed in Figure 3.12b.

Our estimation of the maximum occupancy of each trophic level also provides a condition for the maximum number of trophic levels that a set of parameters allows. Imposing $s_L \geq 1$ yields a bound for the allowance of L trophic levels,

$$\frac{R}{n_\mathrm{c}} + \mu(\gamma_- + 1) \geq \left(\frac{\gamma_-}{\gamma_+}\right)^L \left[(1+\mu)(a_L + \gamma_+ a_{L-1}) + \mu(a_{L-1} + \gamma_+ a_{L-2})\right]. \tag{4.9}$$

Therefore we have a minimum value of the resource saturation for L trophic levels to be viable in a community. This fact is reflected in the structure of Figure 3.11a, where the onsets of appearance of new trophic levels is line with this condition.

4.1.2 Approximation of the equilibrium abundances

As mentioned before, each set $\{s_\ell\}_{\ell=0}^{L}$ of species occupancies determines a set of equilibrium densities according to (3.16). Finding $p^\ell(\{s_k\})$ is difficult, but in this section we will give a rather good approximation for large enough s_ℓ. First we write the system in terms of the total population at each level, $P^\ell = s_\ell p^\ell$ ($\ell = 1, \ldots, L$) and $P^0 = p^0$,

$$\begin{aligned} &\gamma_+ P^{\ell-1} - \left(\rho + \frac{1-\rho}{s_\ell}\right) P^\ell - \gamma_- P^{\ell+1} = \alpha, \\ &P^0 + \gamma_- P^1 = R. \end{aligned} \tag{4.10}$$

Written in this way, it seems natural to expand the solution in powers of s_ℓ^{-1}. At first order in s_ℓ^{-1} we can approximate

$$P^\ell \approx \frac{T_L^\ell - (1-\rho)\sum_{k\neq\ell}^{L} Q_{L,k}^\ell / s_k}{D_L - (1-\rho)\sum_{k=1}^{L} B_{L,k}/s_k}. \tag{4.11}$$

We leave the technical details of the derivation of this formula to Appendix D, where explicit expressions for the constants T_L^ℓ, $Q_{L,k}^\ell$, D_L and $B_{L,k}$ are provided. As we can see in Figure 4.1, this first order approximation captures accurately the variation of the equilibrium densities p^ℓ with s_ℓ. Besides, we also obtain a very accurate approximation when we vary the number of species s_j in levels other than ℓ. We expect this approximation to be valid for large s_ℓ. Nevertheless, even when the occupancy of a level is small (lower panels of Figure 4.1), the approximation remains good.

In the limit $s_\ell \gg 1$ we obtain the dependence $p^\ell \sim s_\ell^{-1}$, which reflects the general trend observed in Figure 4.1. Moreover, in the biologically relevant limit $R \gg \alpha$ (the productivity of the resource is large compared to consumers average mortality rate), and taking into account the explicit expressions for T_L^ℓ and D_L given in Appendix D, populations behave like

$$p^\ell \approx \frac{R}{s_\ell}\left(\frac{\gamma_+}{\gamma_-}\right)^\ell \frac{a_{L-\ell}}{a_L + \gamma_+ a_{L-1}} \tag{4.12}$$

for $\ell \geq 0$. Several conclusions can be extracted from this dependence. First, when the number of species in the ℓ-th level is exhausted, according to Eq. (4.8), we obtain a population density $p^\ell \approx n_c$, as expected. But more importantly, it represents another reason for the extinction threshold to be explicitly included in our model. If there were no threshold, equilibrium densities would monotonically decrease with s^ℓ without ever becoming zero. Besides being unrealistic communities, the assembly graph would in this case contain infinitely many communities, thus becoming intractable.

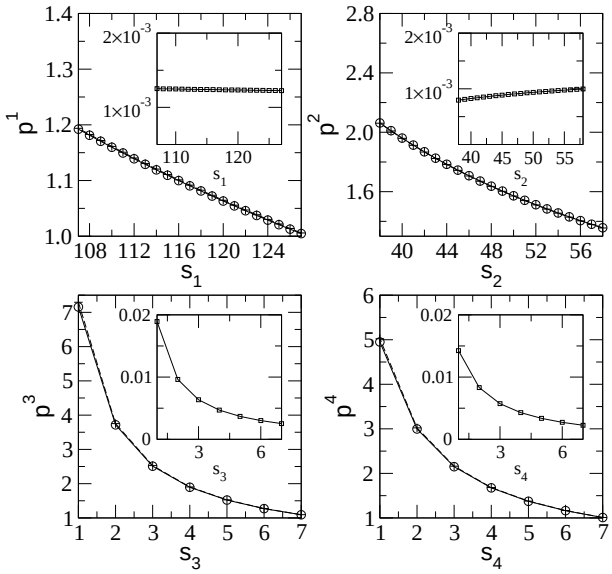

Figure 4.1: *Approximate equilibrium densities*. Starting from a community with 4 levels and occupancies $s_1 = 127$, $s_2 = 58$, $s_3 = 7$ and $s_4 = 7$, we plot p^ℓ as a function of s_ℓ, which exhibits a dependence proportional to s_ℓ^{-1}. Full lines with circles show the exact solution of (3.16), and dotted lines with crosses show our approximation (4.11). Insets contain the relative error of each approximation. Remaining parameters are $R = 1505$, $\gamma_+ = 0.5$, $\gamma_- = 5$, $\rho = 0.3$ and $\alpha = 1$.

4.2 Invaded dynamics

The complexity of the assembly dynamics comes from the cases where some level in the invaded community falls below the extinction threshold. The approach we used to determine the sequence in which species go extinct until leading to a final viable ecosystem is based on a sequential extinction procedure. For levels that fell below the extinction threshold once the equilibrium had been reached, we went back in their trajectory to the point where the population of some species crossed the extinction level n_c for the first time, we removed one species from that level and restarted the dynamics from that point. Here we will propose an alternative way to determine that sequence based on several criteria and analytical approximations that we will discuss below.

4.2.1 Invasion criteria

Consider the general dynamical system $\dot{x}_i/x_i = q_i(\mathbf{x}, x_I)$, $\dot{x}_I/x_I = q_I(\mathbf{x}, x_I)$ for an arbitrary community with S species, where $\mathbf{x}$ is the vector of species densities in the resident community and x_I is the density of the invader. The establishment of a

colonizer in systems of this kind depends crucially on the initial per-capita growth rate of the invader (Law and Morton 1996). In fact, the condition that must be satisfied for a new species to increase when rare is

$$\lim_{T\to\infty} \frac{1}{T} \int_0^T q_I(\hat{\mathbf{x}}(t), x_I = 0)dt > 0, \tag{4.13}$$

i.e., the time average of the per-capita rate of increase of the invader is positive when the species of the resident community remain under certain attractor $\hat{\mathbf{x}}(t)$ of the dynamics. In our model, the only attractor is the interior rest point, so the condition reduces to $q_I(\mathbf{p}, 0) > 0$, where $\mathbf{p}$ is the rest point of the resident community. Strictly speaking, our model has a non-zero extinction threshold, so this condition has to be replaced by $q_I(\mathbf{p}, n_c) > 0$. Since we start from a resident community initially at equilibrium and the invader initial density is n_c, this condition reduces to the initial per-capita growth rate of the invader.

The condition $q_I(\mathbf{p}, n_c) > 0$ can be used to obtain criteria for the invasibility at each level. For example, consider the initial growth rate of the invader when the invasion takes place at level $L + 1$ [Eq. (3.23)]. The condition for this rate to be positive is

$$p^L > \frac{\alpha + n_c}{\gamma_+ s_L}. \tag{4.14}$$

If this inequality does not hold, the invader is the first species to go extinct because it starts at the extinction level and with a negative initial rate. In the end states, the populations of the resident community are close to (but above) n_c, so the former condition provides the approximate bound

$$s_L \geq \frac{\alpha + n_c}{\gamma_+ n_c}. \tag{4.15}$$

Even if the initial growth rate of the invader is positive, asymptotically the level $L + 1$ may not be viable. If this happens, during the time when the population of the invader is above n_c, extinctions may occur at lower levels. This situation explains the accumulation of recurrent states that we observed in Figure 3.11a when we varied the resource saturation (see Section 4.3 for additional details).

Invasions at levels $\ell \leq L$ are subject to similar conditions. For the initial growth rate of the invader to be positive

$$p^\ell > \frac{n_c}{1 - \rho} \tag{4.16}$$

must hold. In general, an initially positive growth rate could lead to potential extinctions in the remaining levels while the equilibrium density of the invader is above n_c. But it could happen as well that the invader goes extinct at equilibrium with some initial transient time above the extinction. To estimate a condition for this to happen, let us assume that densities and occupancies are inversely proportional (see Eq. (4.11) and Figure 4.1). Then the equilibrium abundance of the invader is $s_\ell p^\ell/(s_\ell + 1)$, therefore

if

$$p^{\ell} < n_{\mathrm{c}} \left(1 + \frac{1}{s_{\ell}}\right) \tag{4.17}$$

the invader goes extinct. This condition, together with (4.16), leads to

$$s_{\ell} < \frac{1}{\rho} - 1 \tag{4.18}$$

so below this bound the invader initially grows but becomes extinct at equilibrium. We will use this condition to explain the appearance of some recurrent subsets for certain values of R (see Section 4.3).

It would be nice, however, to have a systematic way to predict the sequence of extinctions after an invasion has occurred. Based on our approximations for the equilibrium densities, we can propose a way to sequentially remove species for invasions at lower levels. Within the end states of our model, abundances are close to the extinction threshold. Then (4.8) implies that communities are pyramidal, so lower levels are highly occupied but higher levels contain a small number of species. According to the s_{ℓ}^{-1} dependence, the increase of one species in lowers level has no significant effect in the equilibrium abundances of the community. Therefore if a species goes extinct after an invasion in a low level, it has to be the invader itself.

The extinction sequence for invasions in higher levels is not so easy to predict. Nevertheless, changes in abundances upon increasing s_{ℓ} are larger the higher the level (Figure 4.1) so, in case that several levels fall below the threshold simultaneously, we can make the assumption that it is always the "highest" species the one that goes extinct first. This procedure provides a certain sequence of extinctions whose accuracy will be checked in Section 4.3.

The prediction of the sequence of extinctions can be non-trivial when a top predator invades if the resource saturation R do not allow for $L + 1$ levels. We have devised global approximations to the dynamics in this case to predict the order of extinctions without having to resort to the numerical integration of the system of differential equations.

4.2.2 Approximations to the dynamics invaded by a top predator

Our heuristic approximations to the time dynamics of the system (3.22) when an invader arrives at level $L + 1$ are somehow inspired in the matching technique used to obtain analytical approximations to perturbed differential equations [see for example Bender and Orszag (1984)]. First we calculate the equilibrium point $\{p^{\ell}\}_{\ell=0}^{L}$ by either solving (3.16) or using (4.11). Then we approximate $n^{L+1}(t)$ by the sum of its long-term dependence $n_{\mathrm{lt}}^{L+1}(t)$ (near equilibrium) plus a short-term behavior $n_{\mathrm{st}}^{L+1}(t)$. For the long term, a linear stability analysis shows that the solution exponentially decays towards the equilibrium point, so we will set

$$n_{\mathrm{lt}}^{L+1}(t) = p^{L+1} + e^{-\lambda t}[d_0 \cos(\omega t) + d_1 \sin(\omega t)] \tag{4.19}$$

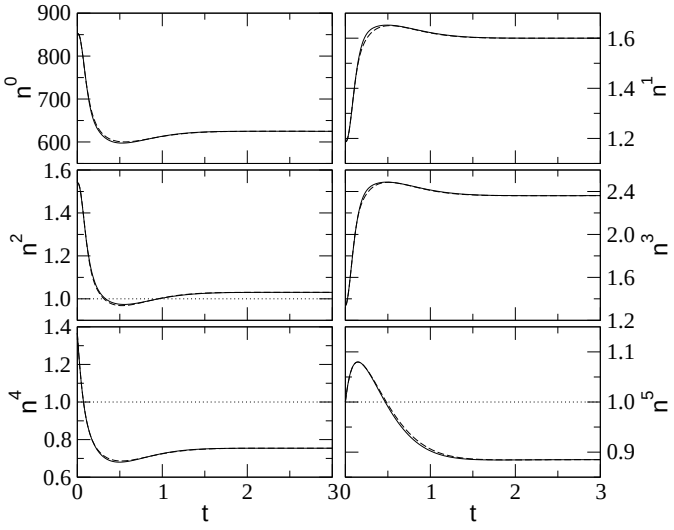

Figure 4.2: *Approximate dynamics.* Dashed lines show our approximation for the dynamics of a four-level community determined by the occupancies $s_1 = 110$, $s_2 = 50$, $s_3 = 6$ and $s_4 = 5$ when invaded by a top predator at level 5. For this case the eigenvalue of the community matrix with real part closest to zero is complex. Full lines represent the numerical integration of (3.15). Remaining parameters are the same as in Figure 4.1. The whole time evolution is accurately predicted. The extinction level $n_c = 1$ is represented with dotted lines. We can see how the first extinction in the community takes place at level 4.

where the eigenvalue of the linear stability matrix whose real part is closest to zero is $-\lambda + i\omega$ (ω may be zero). The constants d_0 and d_1 remain undetermined for the moment.

For the short-term behavior we propose

$$n_{\rm st}^{L+1}(t) = C(t)e^{-\xi t}, \tag{4.20}$$

where $C(t) = \sum_j c_j t^j$ is a polynomial whose coefficients and the exponent ξ need to be determined to capture the transient time evolution. This way to express the short-term behavior is inspired in the initial transient decay that can be observed in the initial invader's dynamics prior to getting close to the equilibrium point (see Figures 4.2 and 4.3). The polynomial has been included to properly capture the initial condition and the initial deviations to the exponential decay.

To obtain the undetermined parameters of our Ansatz we impose that the initial condition and k derivatives at $t = 0$ match the exact values which can be readily calculated. Indeed, our system has the form $\dot{x}_i = -\alpha x_i + x_i f_i(x)$, where $f_i(x) = \sum_j b_{ij} x_j$ is a linear function, therefore we can recursively calculate the $(s+1)$-th

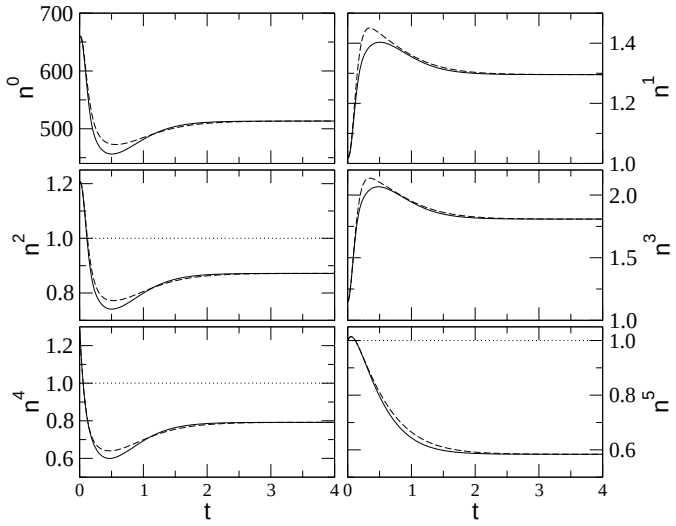

Figure 4.3: *Approximate dynamics.* Same as Figure 4.2, but with $R = 1200$ and occupancies $s_1 = 106$, $s_2 = 49$, $s_3 = 6$ and $s_4 = 4$. In this case the eigenvalue closest to zero of the community matrix is real. Although there is some discrepancy in our approximations, the global trend is captured and the extinction times after the invasion are accurately predicted.

initial derivative as

$$x_i^{(s+1)}(0) = -\alpha x_i^{(s)}(0) + \sum_{j=0}^{s} \left(\begin{array}{c} s \\ j \end{array} \right) x_i^{(s-j)}(0) f_i(x^{(j)}(0)). \tag{4.21}$$

For a real eigenvalue ($\omega = 0$), we choose $C(t)$ to be a polynomial of degree $k-2$, and for a complex one ($\omega \neq 0$) we choose degree $k-3$, in order to compensate the extra undetermined coefficient that has the long-term behavior (4.19) in this case. Equating the approximate solution to the initial condition and the first $k-1$ derivatives of our Ansatz to the exact values gives a linear system for the undetermined coefficients. The equation for the k-th derivative yields a polynomial equation to obtain ξ, namely

$$\sum_{j=0}^{k-2} \left(\begin{array}{c} k-2 \\ j \end{array} \right) H_j \xi^{k-j-2} = (\lambda^2 + \omega^2) p^{L+1}, \tag{4.22}$$

when $\omega \neq 0$, where

$$H_j = (\lambda^2 + \omega^2) n^{(j)}(0) + 2\lambda n^{(j+1)}(0) + n^{(j+2)}(0) \tag{4.23}$$

and $n^{(j)}$ stands for the j-th derivative of n^{L+1}, which can be calculated exactly using (4.21). For $\omega = 0$, Eq. (4.22) gets replaced by

$$\sum_{j=0}^{k-1} \left(\begin{array}{c} k-1 \\ j \end{array} \right) \left[\lambda n^{(j)}(0) + n^{(j+1)}(0) \right] \xi^{k-j-1} = \lambda p^{L+1}. \tag{4.24}$$

Afterwards, we just need to calculate the coefficients c_j and d_0 (and d_1, if $\omega \neq 0$) solving the linear system they satisfy.

Once we have the approximate time behavior for n^{L+1} we calculate analytically the remaining populations n^{ℓ} by direct substitution into the system (3.22), taking advantage of the recursive form of these equations once n^{L+1} is known. Notice that, since we have to calculate successive derivatives in order to get any lower population, the accuracy of n^{L+1} at short times decreases as we calculate lower level populations. Fortunately the model produces communities with a small number of trophic levels. The choice $k = 5$ seems to be enough to account for the dynamics of any community of up to $L = 4$ levels invaded by a top predator (see Figures 4.2 and 4.3). Our approximation is able to capture the global trend of the time evolution. In order to describe the time dynamics of communities with a higher number of levels we would need to choose polynomials of higher degree in our Ansatz.

To reproduce the extinction ordering we have to estimate the extinction times for each level, and these times are approximated with higher accuracy than the dynamic trajectories themselves (see Figure 4.3). In Figure 4.4 we illustrate, for a particular community, the extinction procedure compared to our analytical approximations. In this case, the first level falling below n_c is the fourth one (upper panel). Then we remove one species from that level and restart the dynamics from the point of extinction, and the fourth level falls again below n_c (second panel). After the removal of a new species, the fourth level ends up above n_c at equilibrium. Now the next level ending up below n_c is the second one. We move to the point of extinction of this second level and restart the dynamics after removing one species from $\ell = 2$. After that it is just the invader ($\ell = 5$) the only one that falls below the threshold, so we remove it and the resulting community becomes viable. Were it not, we would apply the same extinction procedure again and again until the final community is viable. The sequence of extinctions is well reproduced with our approximate solution, although slight differences that alter the order of extinctions may occur when different levels fall below n_c roughly at the same time.

A final caveat needs to be made with respect to the calculation of ξ. It has to be positive, otherwise (4.20) would be meaningless. Among all the roots of (4.22) we choose the largest, positive real solution, so that any possible initial oscillation of the polynomial $C(t)$ is damped by the exponential. In the majority of the dynamics that we have approximated (see Section 4.3), we are able to find a positive solution for ξ. However, in some cases there is no positive solution. In those cases we just minimize the difference between the exact k-th derivative and the approximate one at $t = 0$. This gives an analytical approximation adjusting up to the $(k-1)$-th derivative, which also

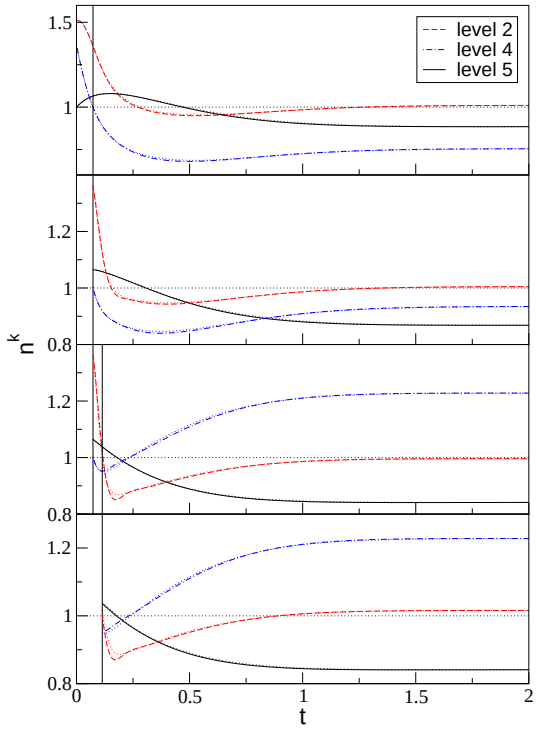

Figure 4.4: *Extinction sequence* for the community with $s_1 = 110$, $s_2 = 51$, $s_3 = 6$ and $s_4 = 5$ invaded at level 5 (parameter values are the same as in Figure 4.1, and $n_c = 1$ is depicted with a horizontal dotted line). We just show the time evolution of the levels that go extinct or are close to extinction in equilibrium. Dotted curves correspond to our analytical approximations. Vertical lines show the time for the first level to go extinct. The sequence of extinct levels is 4, 4, 2, 5 until viability is recovered.

produces an acceptable solution. In all the minimization procedures that we have run, a positive exponent ξ is always found.

4.3 Application to community assembly

Our goal in this chapter was to provide analytical support, albeit approximate, to the results obtained in Chapter 3. We want to check now whether our approximations correctly predict the recurrent sets which are end states of the assembly process. With this aim, we have varied the parameter R within the range from 10 to 1700 in steps $\Delta R = 5$. The remaining parameters of the model will be set as in Chapter 3: $\gamma_+ = 0.5$, $\gamma_- = 5$, $\rho = 0.3$, $\alpha = 1$ and $n_c = 1$.

L	$R_{\rm rec}/n_{\rm c}$	$R^*_{\rm rec}/n_{\rm c}$ (± 5)
1	25.80	30
2	75.88	80
3	323.93	325
4	973.56	975

L	$R_{\rm min}/n_{\rm c}$	$R^*_{\rm min}/n_{\rm c}$ (± 5)
2	35.80	40
3	131.88	135
4	457.53	470
5	1613.71	1630

Table 4.1: *Numerical estimations.* Estimation of the value of $R/n_{\rm c}$ for the appearance of a recurrent set with more than one community (left). Minimum values of $R/n_{\rm c}$ that allow a community with L levels, according to (4.9) (right). The interval of values of R that correspond to the recurrent sets is approximately $[R_{\rm rec}, R_{\rm min}]$. $R^*_{\rm rec}$ and $R^*_{\rm min}$ are the corresponding values found numerically mapping the whole range of R with a resolution $\Delta R = 5$.

Let us first fix the number of levels L. We can determine with (4.9) the minimum value $R_{\rm min}$ that allows for $L+1$ levels. The results are summarized in Table 4.1. Moreover, we can combine (4.8) and (4.15) to give an estimation of the initial value of $R_{\rm rec}$ for the appearance of a recurrent set with more than one community,

$$\frac{R}{n_{\rm c}} + \mu(\gamma_- + 1) \geq \left(\frac{\gamma_-}{\gamma_+}\right)^L \left[\left(\frac{\alpha + n_{\rm c}}{\gamma_+ n_{\rm c}} + \mu\right)(a_L + \gamma_+ a_{L-1}) + \mu(a_{L-1} + \gamma_+ a_{L-2})\right]. \tag{4.25}$$

The resulting values show a good agreement with those obtained numerically (see Table 4.1).

Then, for a given R, we can read off from Table 4.1 the number of levels for the communities within the recurrent set. Once we know it, we determine with (4.8) an estimation for the maximum occupancies allowed. We round off the estimates to get an integer set of values $\{s_\ell\}$ and calculate the associated interior equilibrium. It can happen that some of the p^ℓ fall below $n_{\rm c}$, so we decrease the corresponding occupancies s_ℓ eliminating species one by one until the equilibrium turns out to be viable. This way we obtain a community very close to those of the recurrent set (communities within this set are close to extinction), so we can use it as the initial community to start the assembly process. We then compute the set of viable communities connected to it, which defines an assembly graph much smaller than those obtained in Chapter 3 starting from the empty community $\varnothing$. We analyze the graph to obtain its recurrent sets using the algorithm of Xie and Beerel (1998) and we get one single set, as expected. In Figure 4.5 we plot the number of communities in each end state, showing a good agreement between the results obtained with the analytical approximations reported here and the numerical results.

For every R we can always find a community which is uninvadable at all its levels $\ell \leq L$. If R is such that (4.25) is not verified, then the invader at level $L+1$ initially decreases and goes extinct. This explains the intervals of R where only one absorbing state is found. However, if (4.15) holds (with our choice of parameters this happens

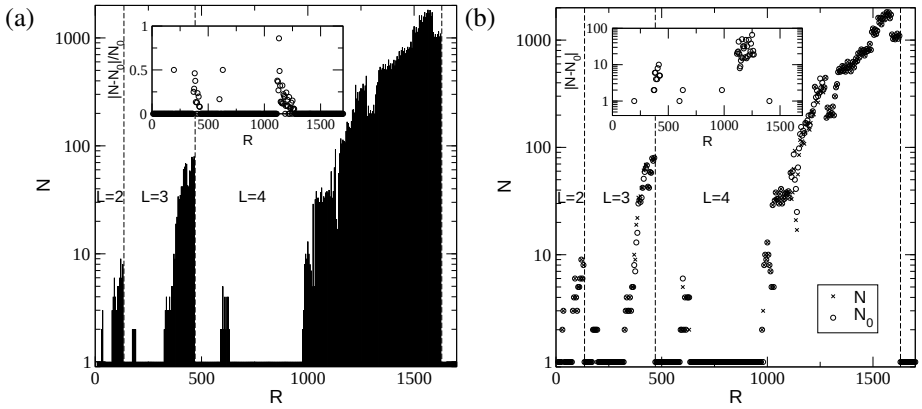

Figure 4.5: *Number of communities in the recurrent sets.* (a) These results have been obtained using our analytical approximations. There is almost no difference with numerical results (Figure 3.11a). The inset shows the relative difference in the prediction of the number of communities. Note that the discrepancies occur in a region where this number is small. This explains the relatively large error found in some cases. (b) For the sake of comparison, we represent the results provided by both the analytical approximations (N, with crosses) and the numerical values (N_0, with circles) The inset contains the absolute difference $|N - N_0|$. Differences of a few tens arise in some cases.

when $s_L \geq 4$), there is an initial time interval where the population of the invader is above the threshold. This can cause the extinction of lower level species, and generate recurrent sets with more than one community.

Our analytical approximations thus provide results very close to those obtained numerically. Besides its being more efficient (the whole assembly needs not be generated), this method also allows to predict what would happen for values of R larger than 1700, which are computationally prohibitive using the numerical method. With our bounds (4.9) and (4.25) we can estimate the next interval of R where more than one community in the end state will appear, namely $R \in [3844, 5114]$. That is out of reach of the numerical method, because the number of communities in the whole assembly graph grows as fast as $e^{\kappa\sqrt{R}}$.

From Figure 4.5 it can be observed that there are small regions where recurrent sets with more than one community are found out of the intervals predicted in Table 4.1 (around $R \approx 200$ for $L = 3$ and $R \approx 620$ for $L = 4$). For those values, a single absorbing community should be found. However, condition (4.18) for an invader at level L to initially grow and become extinct at equilibrium renders $s_L \leq 2$ for our choice of ρ. We have checked that this condition is satisfied by all these small recurrent sets, thus explaining their appearance.

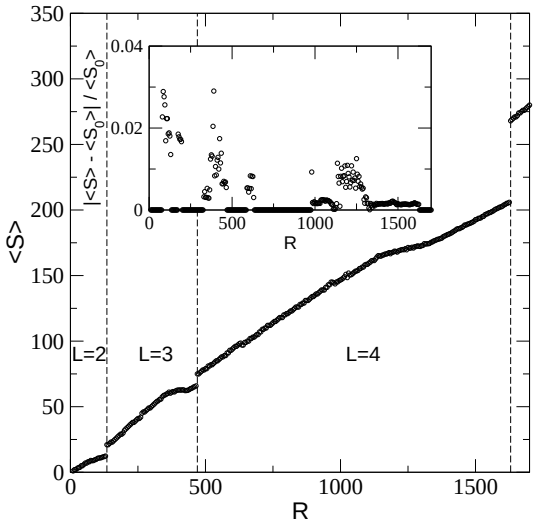

Figure 4.6: *Average number of species* $\langle S \rangle$ in the end states calculated analytically vs. R. In the inset we show the relative error between $\langle S \rangle$ and its corresponding average $\langle S_0 \rangle$ for each graph calculated numerically.

We have to assess the accuracy of the transitions predicted in the subgraph of recurrent states. Note that a slight difference in the ordering of extinctions can change the final community after the invasion. This may change the observed graph and therefore the asymptotic probability distribution of the associated Markov chain. In order to check the transition matrices we obtain, we have calculated two averages. In Figure 4.6 we show the variation of the average number of species in the recurrent sets as a function of R. The behavior is almost indistinguishable from that found in Figure 3.12b (the inset of Figure 4.6 shows that the relative error is small).

We have also checked that the number of extinctions predicted with our approximations follows the same distribution than the one calculated numerically (see Figure 3.15a). In Figure 4.7 the cumulative histogram for the distribution of these magnitudes is represented. We can see that the deviations between both distributions are small.

4.4 Discussion

We have shown in this chapter that our model of ecosystem assembly is amenable to analytical treatment. It is precisely the species symmetry assumption that has allowed us to obtain analytical results, some of them exact and some other approximate. Among them we have provided estimations for the maximum number of species allowed per level, the maximum number of levels for a given value of the resource saturation, and

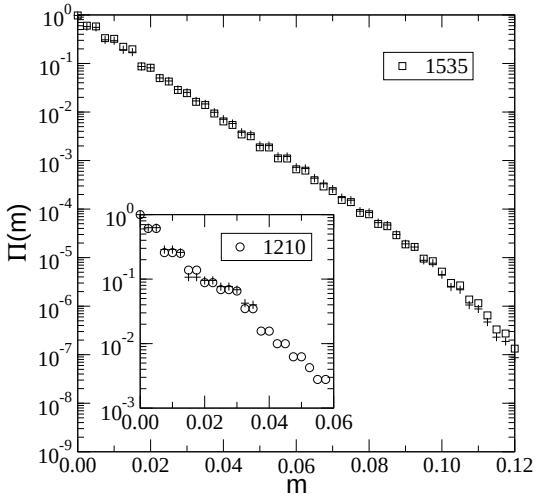

Figure 4.7: *Distribution of avalanches.* Cumulative probability function $\Pi(m)$ for the distribution of the magnitude m of extinction avalanches. Crosses represent the results for our approximated transition matrix. The number of recurrent states coincide for the analytical and numerical method. The inset shows a case where the number of communities is underestimated. This explains the absence of several points in the distribution estimated analytically. We find a rather good agreement good even in this case.

certain analytical approximations of the dependence of the equilibrium abundances on the occupancies of each level. We have combined these results with some criteria for the acceptance of an invader in our model communities, and thanks to some global approximations of the invaded dynamics we have been able to obtain, with high accuracy, the sequence of extinctions occurring after an invasion. With this procedure we have reproduced the same results obtained in Chapter 3, this time without resorting to the integration of the LV equations and without constructing the whole assembly graph. Among other things this brings the opportunity of exploring the model for resources which would otherwise be computationally prohibitive to obtain.

In Chapter 3 we have already reported that, upon increasing the resource saturation R, the number of levels L that the system is able to sustain increases discontinuously. We provide here an estimate of the values of R at which this occurs, and show that they grow essentially as $(\gamma_+/\gamma_-)^L$. Under the assumption that populations are close to the extinction level, we have shown that equilibrium communities are pyramidal — again in agreement with previous results. Close to the onset of appearance of a new level, the number of communities in the end state increases. We have identified that the requirement for this to happen is that the population of a top predator invading the community initially grows only to eventually go extinct. From this knowledge we

can estimate the value of R at which the end state starts to have more than just one community.

Our approximations have been tested by calculating some observables. Among them we report on the average species richness as a function of R, as well as the distribution of the avalanches of extinctions produced by an invasion. In both cases the agreement is very good.

We have also proposed an analytical approximation to the dynamics of a community invaded by a top predator. This approximation has been built matching the initial behavior of the solution (derived from the initial condition) and the expected asymptotic decay close to equilibrium. We have found a rather good agreement with the solutions obtained by a numerical integration of the LV equations, which has allowed us to correctly predict (in most of the cases) the order of extinctions eventually caused by the invasion of a top predator. These approximations have been applied to reproduce the assembly graphs for the recurrent sets, showing small discrepancies only for certain values of R. This provides an alternative method to analyze the system for other sets of parameter values, with a negligible computational cost compared to the construction of the whole assembly graph.

5

Phase transitions in model ecosystems

Every mathematician knows it is impossible to understand
an elementary course in thermodynamics.
—Vladimir I. Arnold.

5.1 Catastrophic regime shifts in ecological communities

Ecosystems are exposed to continuous changes in external conditions. Seasonal changes of environmental conditions, climate oscillations, variations in the amount of resources and nutrient loading, habitat fragmentation, harvest or loss of species diversity are a few examples of these gradual changes. They often change slowly, even linearly, with time (Tilman et al. 2001). It is usually assumed that the response of the system to external changes is smooth most of the times. However, occasionally sudden changes can occur. For example, the sudden loss of transparency and vegetation observed in shallow lakes due to human-induced effects (Scheffer et al. 2003); corals overgrown by macro-algae in the Caribbean reef seem to shift between two stable states rather than responding smoothly to external conditions (Done 1991; Nystrom et al. 2000); or in savannahs, sparse trees with a grass layer can switch to a dense woody state as a result of the alternation in fire and grazing regimes (Walker 1993; Ludwig et al. 1997). All these phenomena share the feature that ecosystems seem to change between two different stable states. Sudden changes between two regimes are the so-called catastrophic shifts (Scheffer et al. 2001). Hence, when subject to a slowly changing external

control variable, ecological communities may show little change until a critical point is reached. Then a sudden switch to a contrasting state can occur.

The simplest theoretical explanation to catastrophic regime shifts comes from the existence of alternative stable states in the dynamical ecosystem response to gradual changes. The shift between these two alternative states is responsible for the transition. Often their existence is associated to a nonlinear ecosystem response to smooth external variations (May 1977; Scheffer et al. 2001). The effects of nonlinearities have also been observed in natural communities. For example, it has been established that the nonlinear dynamics of overexploited marine ecosystems magnifies the variability in the abundance of exploited species (Hsieh et al. 2006; Anderson et al. 2008).

In these models, ecosystems are described from a macroscopic viewpoint. Usually a global magnitude, representative of the whole community, is used as fundamental variable (for instance, the total biomass density). Models are basically devised to describe the time evolution of this magnitude by means of nonlinear functional responses (Scheffer et al. 2001; Ludwig et al. 1978). Recently this paradigm has been applied to spatially extended interacting communities (Fernández and Fort 2009). This theoretical approach is conceptually very similar to the traditional thermodynamic explanation of phase transitions in physical systems, such as the liquid-vapor transition. The lack of convexity of theoretical thermodynamic potentials —such as free energy— leads to alternative stable states corresponding to liquid and vapor and both phases coexist below a certain critical temperature. In Ludwig et al. (1978) and Fernández and Fort (2009) the analogy is very clear. The dynamics of biomass density follows a logistic growth with carrying capacity K and a density-dependent consumption term modeled as a sigmoidal (Holling's type III) functional response.[1] It is precisely this type of functional response which allows for the existence of two separate, stable equilibrium points in the dynamics above a certain critical value of the carrying capacity.

To be more precise, the macroscopic model by Fernández and Fort (2009) involves a biomass density n, representing the community as a whole, which evolves in time according to

$$\frac{dn}{dt} = n\left(1 - \frac{n}{K}\right) - \frac{cn^2}{1+n^2}. \tag{5.1}$$

The non-trivial equilibria of this system correspond to the solutions of

$$\frac{n}{K} + \frac{cn}{1+n^2} = 1. \tag{5.2}$$

[1] A functional response in ecology accounts for the intake rate of a consumer as a function of prey density. In dynamical systems like $\dot{n}_i = f_i(\mathbf{n})$, the function $f_i(\mathbf{n})$ —where $\mathbf{n}$ is the vector of prey densities— is precisely the functional response of species i. Following Holling (1959), functional responses are generally classified into three types, which are called Holling's type I, II and III. Type I functional response assumes a linear increase in intake rate with resources densities. Type II functional response is characterized by a decelerating intake rate with saturation, which follows from the assumption that the consumer is limited by its capacity to process food (if n is the density of prey, type II functional response is often modeled by $f(n) = an/(1+bn)$, which provides saturation in abundance of resources). Type III functional response is similar to type II in that at high levels of prey density, saturation occurs. But at low prey density levels the rate of change in population density is a more than linearly increasing function. This effect is due, for instance, to the natural improvement of predator's searching efficiency as prey density increases [an example of such a functional response is the sigmoidal function, given by $f(n) = cn^2/(h^2+n^2)$].

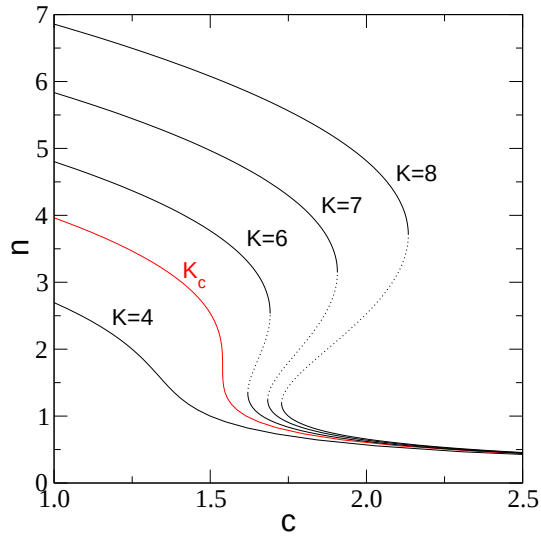

Figure 5.1: *Curves of equilibrium points* [Eq. (5.2)] for different values of the carrying capacity K [reproduced from Fernández and Fort (2009)]. The critical curve is obtained for $K_c = 3^{3/2} \approx 5.196$ and is shown in red. Unstable branches of critical points are represented with dotted lines.

There are regions where only one stable equilibrium is found for this system. In Figure 5.1 the solution curve $n(c)$ of Eq. (5.2) is depicted for different values of K. For $K \leq K_c = 3^{3/2}$ only one stable solution exists for each c. As long the increase of c is quasi-stationary, the system will exhibit a smooth response. However, for $K > K_c$, the curve of equilibrium points is folded backwards at two bifurcation points. For certain values of c the system can be found either in the upper or the lower stable branch. For increasing c, the system starts on the upper branch and changes its state smoothly until a threshold value is found, where a catastrophic transition to the lower branch occurs. Hence hysteresis phenomena emerge: if at this point c is decreased, we would not be able to recover the state of the system before the transition. Instead, the system would remain on the lower branch, until c decreases enough to reach another threshold value and "jump" to the upper branch. Such a switch between stable, alternative states of the system is related to the catastrophic regime shift. Note the similarity of Figure 5.1 with the isotherms predicted by the classical van der Waals equation in the liquid-vapor coexistence of fluids (Huang 1987).

This notwithstanding, the current understanding of phase transitions in physical systems goes beyond phenomenological, macroscopic models. The microscopic approach of statistical mechanics represents a more fundamental way of understanding phase transitions, and many elaborated theories have been developed to account for

abrupt shifts in physical systems. Our assembly model, based on a Markov chain evolving in the configuration space of viable ecosystems, can be easily modified to provide an alternative explanation to these catastrophic regime shifts in ecosystems. In the two preceding chapters we have pictured ecosystems as complex, stable entities which keep on fluctuating between different *microstates* through successional invasions of rare species. By introducing a background species extinction rate accounting for the gradual, external variations to which natural communities are subject, we will find a threshold rate above which the system undergoes a shift between a species-rich and a species-poor attractor, and the rate will play the role of control parameter.

However, our model allows us to go beyond the current theoretical analysis of catastrophic regime shifts in ecosystems. Through a spectral analysis of the transition probability matrix we will be able to show *rigorously* that the shift we observe corresponds to the "trace" of a true phase transition —according to the definition of statistical mechanics— in finite size.

Our model does not rely on nonlinearities of a global, macroscopic dynamics. In fact, we pose a linear functional response in the dynamics of individual species, but the combined effect of successional invasions and spontaneous extinctions can lead to a global shift in the ecosystem between a species-rich attractor and a state with low species richness. The early-warnings that are usually mentioned as precursors of catastrophic regimes, like the increasing fluctuations near the transition (Hsieh et al. 2006; Scheffer et al. 2009) or the appearance of trophic cascades (Daskalov et al. 2007), will be recovered within our framework. We will show that fluctuations become critical in the vicinity of the transition, and that the ultimate collapse of the ecosystem correspond to a gradual loss of species from bottom to top. It is worth remarking that trophic cascades have been recognized as signals of overexploitation in marine communities (Daskalov et al. 2007).

5.2 Background species extinction

Our assembly model pictures ecosystems evolving though successional invasions until reaching a final end state, either a single absorbent community or a complex, closed set of recurrent communities. When the process reaches a complex end state, successional invasions transform the ecosystem some community belonging to that set, so the process visits all its communities, albeit with different frequencies —given by the asymptotic probability distribution of the Markov process within this set. In terms of species this means that communities keep continuously changing and eventually, after enough time has elapsed, all the original species in the ecosystem will be replaced by new ones. Therefore the ecosystem keeps on fluctuating between the different communities comprising the closed set, which persists as a robust, stable entity.

Let us now introduce a rate of spontaneous extinctions. Species in natural communities are often subject to overexploitation. Intensive hunting in terrestrial communities or the increasing fishing pressure in marine ecosystems are good examples of this. Sometimes the species population is seriously altered due to habitat destruction,

in other cases due to exposure to epidemics or diseases. Many effects like these ones can effectively decrease to critical levels the number of individuals of a certain species or even cause its extinction. We will represent these situations by means of a probability rate, η, which accounts for the probability per unit time for a species to go extinct for reasons other than being preyed on. Actually this probability rate should depend on the species and its environment but, for the sake of simplicity, we will assume it uniform for all species.

Our model is amenable to introduce background extinctions in a simple way. Elementary processes in the original model for $\eta = 0$ were transitions between viable communities carried out by single-species invasions. Now two different processes, either invasion or extinction, can connect two communities. Thus, for a given community i with L trophic levels, we need to determine all the possible transitions carried out by invasions and spontaneous extinctions at each level (and by invasions at level $L + 1$ as well). The graph $\mathcal{G}$ will now contain both types of transitions. The links corresponding to extinction transitions can be obtained just as the invasion ones (see Section 3.5). Given a community $i \in \mathcal{G}$, we randomly remove one of its species and calculate the equilibrium population densities of the resulting community j. If the community is viable, then we establish a link between i and j. If some species go below the extinction level n_c, we apply the same sequential extinction procedure that was used to obtain the invasion graph. We repeat these sequential extinctions until the final community k is viable.

The transition probability p_{ij} for the transition from community i to community j can be written as

$$p_{ij} = \delta_{ij} + \xi q_{ij} + \eta e_{ij}, \tag{5.3}$$

where matrices $\mathsf{Q} = (q_{ij})$ and $\mathsf{E} = (e_{ij})$ account for the relative frequency of invasions and extinctions, respectively. Non-diagonal elements of matrix Q are defined according to (3.25). For $i \neq j$ we define $e_{ij} = m_{ij}/S_i$, where m_{ij} is the number of different extinctions in i that lead to j and $S_i = \sum_{\ell=1}^{L} s_\ell^{(i)}$ is the number of possible extinctions of i. We set $e_{ii} = 0$ and calculate the diagonal of Q so that $\mathsf{P} = (p_{ij})$ is stochastic, i.e.,

$$q_{ii} = -\sum_{i \neq j} \left(q_{ij} + \frac{\eta}{\xi} e_{ij} \right). \tag{5.4}$$

When $\eta = 0$ we recover the original transition matrix of our model [see Eq. (3.24)]. This is quite a singular case, though, not representative of what happens for any $\eta > 0$ —no matter how small.

In fact, there is a major difference between the cases $\eta = 0$ and $\eta > 0$, regarding the properties of the Markov chain. For any $\eta > 0$, there is a *non-zero* probability for all the S species in a community to go extinct. Let Δt be the time unit between consecutive steps of our discrete-time Markov chain. Thus the removal of all species caused by sequential spontaneous extinctions has a probability at least equal to $(\eta \Delta t)^S$. The non-vanishing probability of total extinction implies that the process can return to the initial state (the empty community $\varnothing$) and therefore the Markov chain becomes

ergodic. This has to be compared with the former model ($\eta = 0$), for which we just found a tiny fraction of recurrent states, and almost all the communities in the assembly graph were transient.

Ergodicity implies that any possible state of the ecosystem can be reached with a non-zero —albeit sometimes small— asymptotic probability. According to (5.3) we simply need to solve the linear system

$$\mathbf{0} = \boldsymbol{\pi} \left(\mathsf{Q} + \frac{\eta}{\xi} \mathsf{E} \right) \tag{5.5}$$

to obtain the (row) vector $\boldsymbol{\pi}$ of asymptotic probabilities π_i for all $i \in \mathcal{G}$. Therefore the asymptotic distribution depends on the relative strength between rates. We expect that, when this ratio is small enough, the subset of communities with the highest probability coincides with the recurrent subset found for $\eta = 0$. However, as this ratio increases, the probability of finding the process within this subset should decrease. This effect can be observed in Figure 5.2, where we plot $\mathcal{G}$ with its asymptotic distribution for $R = 120$ and 4 values of the quotient η/ξ. The remaining parameters of the model have been set as in Chapter 3: $\alpha = 1$, $\gamma_+ = 0.5$, $\gamma_- = 5$, $\rho = 0.3$ and $n_\mathrm{c} = 1$. (We will use this set of parameters throughout this chapter.) As η/ξ increases, communities that were recurrent for $\eta = 0$ are visited with decreasing asymptotic probabilities. Eventually, when the ratio is large enough, these communities are hardly visited and the process stays with high probability in communities close to the empty ecosystem, $\varnothing$.

This effect is more clearly seen in terms of the dependence of π_r —the probability of finding the process in any of the communities of the recurrent set for $\eta = 0$— and $\pi_\varnothing$ —the probability of finding the ecosystem extinct— on η/ξ. A typical behavior of these probabilities is depicted in Figure 5.3. This plot corresponds to a resource saturation $R = 1340$, for which $\mathcal{G}$ has 397698 nodes and 539 recurrent communities. In Figure 5.3 we can observe an abrupt decrease of π_r at $\eta/\xi \approx 0.33$, and $\pi_\varnothing$ increases abruptly as well when $\eta/\xi \approx 0.65$. Needless to say, these two magnitudes resemble the typical behavior of order parameters in the vicinity of a phase transition. A small increase in η causes a shift from the stable, recurrent set at $\eta = 0$ to communities close to extinction. In this sense, increasing background extinctions drive the system from a stable, species-rich attractor to a species-poor region of the phase space. The system thus undergoes a catastrophic regime shift analogous to those commonly observed in overexploited ecological communities (Scheffer et al. 2003; Done 1991; Nystrom et al. 2000; Walker 1993; Ludwig et al. 1997).

5.3 Signals of catastrophic regime shifts

From the perspective of conservation and management of ecosystems, it is very important to determine signals that may alert of the proximity of a catastrophic transition. These are the so-called early-warnings of catastrophic regime shifts (Scheffer et al. 2009), and act as flags for the approach of a critical threshold. Although our model is

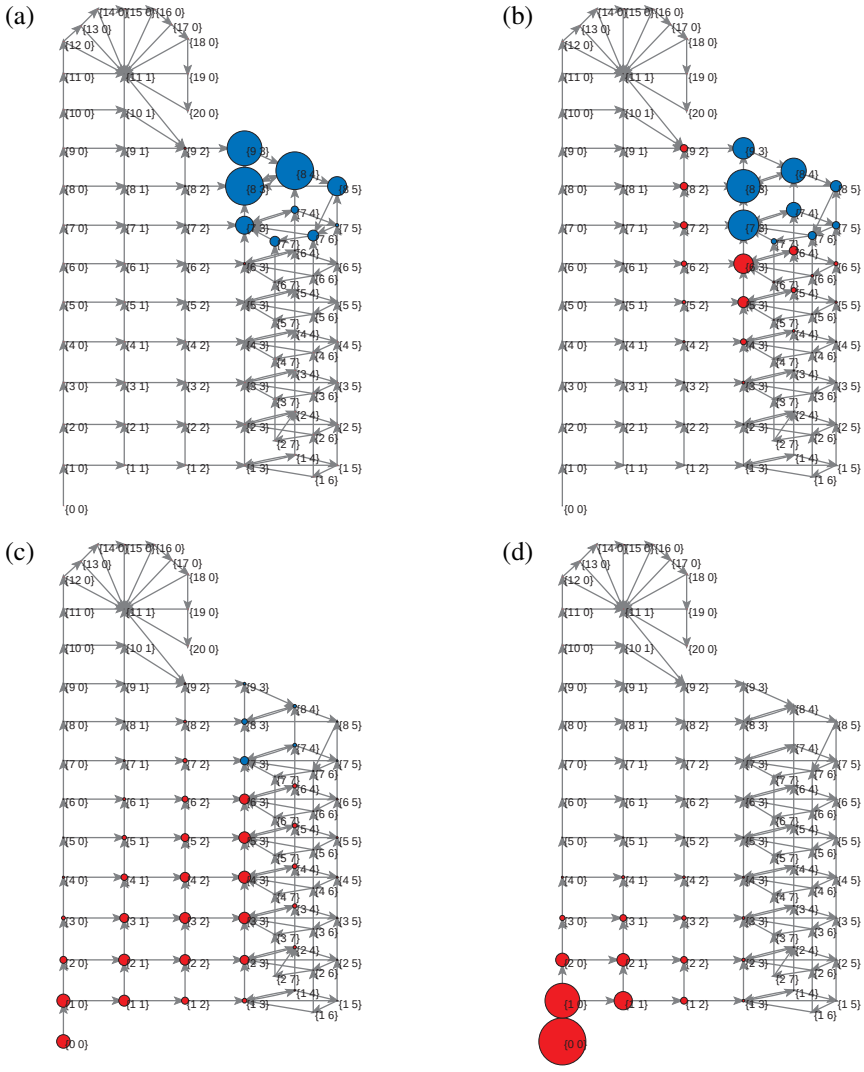

Figure 5.2: *Assembly graph* $\mathcal{G}$ obtained for $R = 120$, comprising 79 communities with up to 2 trophic levels, for 4 increasing values of η/ξ. Diameter of nodes is proportional to their asymptotic probability. Labels of nodes represent species occupancies $\{s_1, s_2\}$. For the sake of clarity, only transitions carried out through invasions are shown. For $\eta = 0$, the recurrent set contains 9 nodes (colored in blue). (a) The most probable communities are those in the recurrent set ($\eta/\xi = 0.05$). (b) Some communities, close to this set, are visited with high frequency ($\eta/\xi = 0.3$). (c) Almost none of the 9 originally recurrent communities are visited ($\eta/\xi = 0.6$). (d) The most probable community corresponds to the total extinction state ($\eta/\xi = 1$).

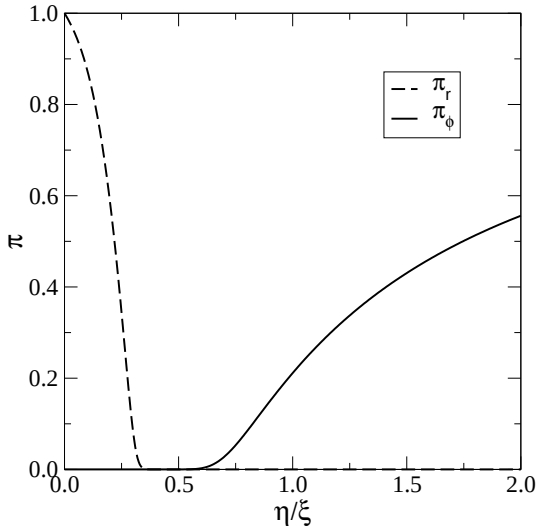

Figure 5.3: *Order parameters of the transition.* Probability π_{r} of finding the process in one of the communities of the recurrent set for $\eta = 0$ (dashed line), and probability $\pi_{\varnothing}$ of the empty community (full line), as functions of the ratio η/ξ, for $R = 1340$. For this value of R the assembly graph contains 397698 nodes and the set that was recurrent for $\eta = 0$ contains 539 communities.

minimalistic, the phenomenology of several magnitudes reveal a critical behavior near the shift described in the previous section. Now, upon gradually increasing the external "stress" —i.e., the ratio η/ξ— on our system, we will observe abrupt changes in these magnitudes close to the regime shift.

We shall begin by assuming very slow variations in η/ξ, i.e., the ecosystem undergoes very many invasions before changes in the control parameter are noticeable. In this situation we can consider the Markov process to be always at its steady state. At the end of this section we will analyze the effect of relaxing this assumption and allowing for a mixing of these two time-scales: the scale of variation of the stress and the scale of invasion.

A first precursor of the shift is the fluctuation of the mean number of species in the ecosystem. In Figure 5.4 we plot the average number of species $\langle S \rangle$. Its fluctuations are measured by the variance

$$\sigma_{\mathrm{S}}^2 = \sum_{i \in \mathcal{G}} \pi_i S_i^2 - \langle S \rangle^2. \tag{5.6}$$

The rapid growth of fluctuations provides an alert of the proximity of the catastrophic shift (Scheffer et al. 2001; Fernández and Fort 2009; Scheffer et al. 2009). Fluctuations for $R = 1340$ exhibit a double peak at $\eta_1 \approx 0.33\xi$ and $\eta_2 \approx 0.46\xi$. The first one is

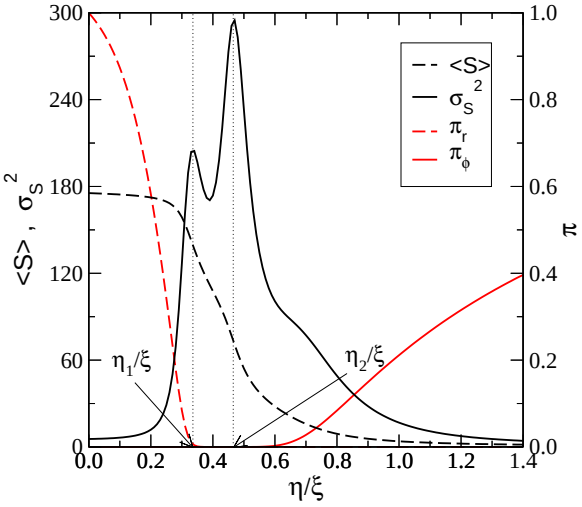

Figure 5.4: *Anomalous behavior of fluctuations.* Average number of species (black dashed line) and its variance (black full line) as functions of η/ξ, for $R = 1340$. The average number of species decreases monotonically whereas its variance exhibits a double peak at values $\eta_1/\xi \approx 0.33$ and $\eta_2/\xi \approx 0.46$. The first one coincides with the abrupt drop of $\pi_{\rm r}$ (red dashed line) but the second one precedes the increase of $\pi_\varnothing$ (red full line) announcing it.

related to the abrupt drop of the probability $\pi_{\rm r}$ that we showed in Section 5.2. In addition, these two peaks correspond to a gradual decrease in the number of species at each trophic level, as we will show below.

The second peak at η_2/ξ announces the abrupt increase of $\pi_\varnothing$, but does not coincide with it. The increase of this probability is related to the fluctuations of the time of first return to the empty community, whose mean value is given by $\tau_\varnothing = \pi_\varnothing^{-1}$ [see Eq. (B.18)]. Using the first-passage distribution of the Markov chain (Feller 1968), the relative fluctuation $\sigma_\tau^2/\tau_\varnothing^2$ can be calculated as follows.

We start from Eq. (B.11), which relates the first-passage distribution $f_{ij}^{(n)}$ (i.e. the probability that a in a process starting from i the first entry to j occurs after n steps) with the probabilities $p_{ij}^{(n)}$ of a transition from i to j in exactly n steps. Consider the case $i = j = \varnothing$. We are interested in calculating the variance of the recurrence time for the empty community. To this purpose we introduce the generating functions $V(z) = \sum_{n=0}^{\infty} p_{\varnothing\varnothing}^{(n)} z^n$ and $F(z) = \sum_{n=0}^{\infty} f_{\varnothing\varnothing}^{(n)} z^n$. Then (B.11) is equivalent (Feller 1968) to

$$F(z) = 1 - \frac{1}{V(z)} \tag{5.7}$$

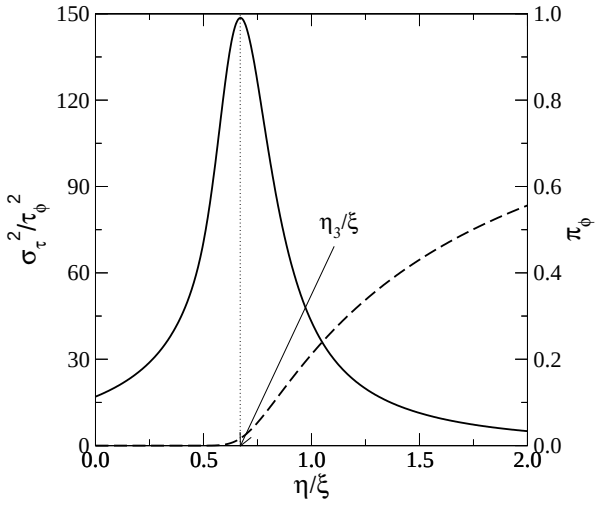

Figure 5.5: *Fluctuations in the average time of first return to the empty community.* Relative variance $\sigma_\tau^2/\tau_\varnothing^2$ of the first-return time (average $\tau_\varnothing = \pi_\varnothing^{-1}$) to the empty ecosystem (full line), compared to the probability of total extinction $\pi_\varnothing$ (dashed line), for $R = 1340$. The maximum of the relative variance roughly coincides with the point at which $\pi_\varnothing$ starts to increase. This maximum is reached at $\eta_3/\xi \approx 0.67$.

and $\tau_\varnothing = F'(1)$. It can be easily shown that the radius of convergence of $V(z)$ is equal to 1, because $V(1)$ diverges by definition. By imposing $F'(1)$ to be finite we find that, near $z = 1$, $V(z) \approx a(1-z)^{-1}$ and $a = \lim_{n\to\infty} p_{\varnothing\varnothing}^{(n)} = \pi_\varnothing$.

The variance of the recurrence time is obtained as

$$\sigma_\tau^2 = \sum_{n=0}^{\infty} n^2 f_{\varnothing\varnothing}^{(n)} - \tau_\varnothing^2 = F''(1) - F'(1)[1 - F'(1)]. \tag{5.8}$$

In order to calculate $F''(1)$, we need to obtain the next-to-leading (constant) term in the series expansion of $V(z)$ in powers of $1-z$, $V(z) = \pi_\varnothing(1-z)^{-1} + b + \mathcal{O}(1-z)$. Using (5.7) we get $F''(1) = 2b/\pi_\varnothing^2$ and

$$\frac{\sigma_\tau^2}{\tau_\varnothing^2} = 2b + \pi_\varnothing - 1. \tag{5.9}$$

The constant b can be easily computed numerically since

$$b + \mathcal{O}(1-z) = V(z) - \frac{\pi_\varnothing}{1-z} = \sum_{n=0}^{\infty} \left(p_{\varnothing\varnothing}^{(n)} - \pi_\varnothing \right) z^n. \tag{5.10}$$

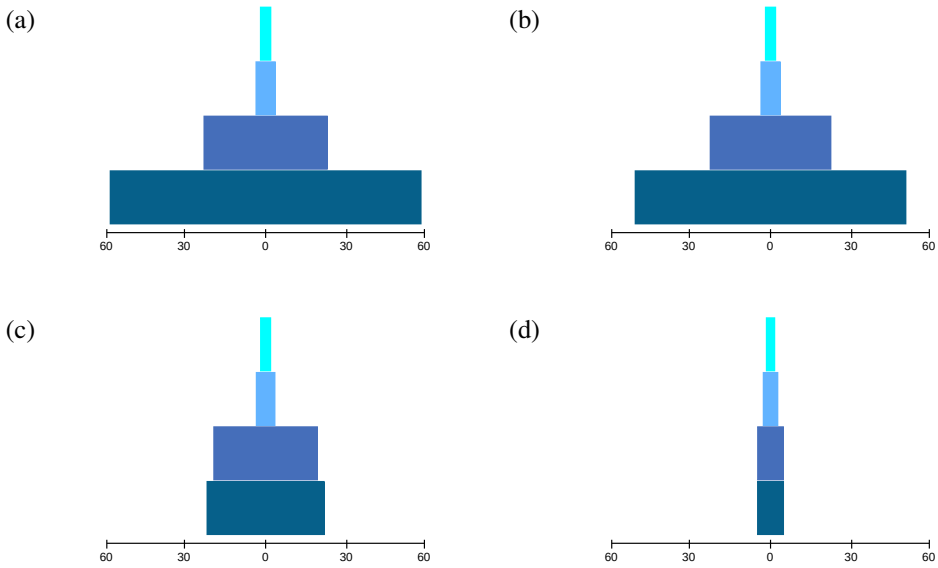

Figure 5.6: *Ecosystem profiles* (mean number of species in each trophic level) for increasing η/ξ ratios. This plot corresponds to a resource saturation $R = 1340$, for which communities have up to 4 trophic levels. Lower levels are shown with darker color. (a) The ecosystem maintain its pyramidal structure ($\eta/\xi = 0.05$). (b) The first trophic level starts to collapse ($\eta/\xi = 0.3$). (c) The second level starts to loose species ($\eta/\xi = 0.43$). (d) For large values of the ratio, the system is close to extinction ($\eta/\xi = 0.6$).

Hence, in the limit $z \to 1$,

$$b = \sum_{n=0}^{\infty} \left(p_{\varnothing\varnothing}^{(n)} - \pi_{\varnothing} \right). \tag{5.11}$$

Therefore we simply need to iterate the matrix P and truncate the series up to certain error tolerance to compute b.

Our results for the relative variance $\sigma_\tau^2/\tau_\varnothing^2$ are depicted in Figure 5.5. The maximum relative fluctuation occurs nearly at the onset of increase of $\pi_\varnothing$, $\eta_3 \approx 0.67\xi$. We thus expect that relative fluctuations in the average return time to any state i close to $\varnothing$ will be amplified close to the extinction transition. This notwithstanding, it is hard to figure out how this fluctuation could be used in practice as a signal of the catastrophe.

A second signal of the transition in this model is a gradual loss of species in trophic levels from bottom to top. This effect can be qualitatively observed in the ecosystem profile (see Figure 5.6), where the average number of species at each trophic level

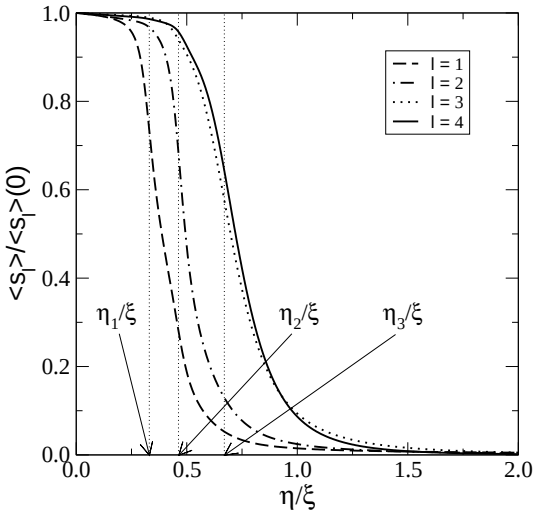

Figure 5.7: *Average number of species at each trophic level*, $\langle s_\ell \rangle = \sum_{i \in \mathcal{G}} \pi_i s_\ell^{(i)}$, for $\ell = 1, 2, 3, 4$ and $R = 1340$, normalized by the average number of species for $\eta = 0$, $\langle s_\ell \rangle(0)$. We have marked the points η_1 and η_2 corresponding to the maxima of σ_{S}^2, which roughly coincide with the points at which the first and second levels start to collapse. The species loss in the third and fourth levels starts when the probability $\pi_\varnothing$ becomes noticeable (by η_3, the maximum of $\sigma_\tau^2/\tau_\varnothing^2$).

is represented. When the quotient of rates increases from $\eta/\xi = 0.3$ [panel (b)] to $\eta/\xi = 0.43$ [panel (c)], the number of species in the first level decreases considerably, but the rest of levels remain almost unaltered. After that [panel (d)], a simultaneous loss of species in the first and second levels takes place.

Figure 5.7 shows the number of species at each level averaged over $\mathcal{G}$ versus η/ξ. We observe that the decrease of s_1 approximately coincides with the first peak of σ_{S}^2 at η_1, and the decrease of s_2 corresponds to the second peak at η_2. After that, species at lower levels are unable to sustain upper levels and a trophic cascade occurs. The third and fourth levels start to be emptied near η_3. There is a clear correspondence between the values at which trophic levels start to collapse and the location of the maxima of σ_{S}^2 and $\sigma_\tau^2/\tau_\varnothing^2$. In any case, the loss of species from bottom to top as the extinction rate increases is a clear signal of the catastrophic regime shift. Besides, trophic cascades have been recognized empirically as signals of over-fishing in marine communities (Daskalov et al. 2007).

In the remainder of the section we consider the variation of η as a non-equilibrium process. Now we shall assume that, although the variation of η is still not faster than ξ^{-1}, the two scales are comparable in the sense that the process is not able to remain in the steady state anymore. An estimate of the time scale for the convergence to the

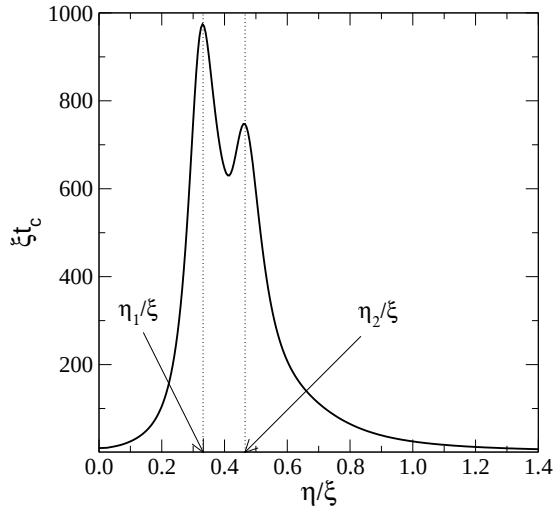

Figure 5.8: *Convergence time* $\xi t_{\rm c} = -(\log|\lambda_2|)^{-1}$ needed to reach the steady state of the Markov chain, λ_2 being the second largest eigenvalue of matrix P. Two peaks appear in $\xi t_{\rm c}$ corresponding to the two maxima of $\sigma^2_{\rm S}$.

steady state is provided by

$$\xi t_{\rm c} = -\frac{1}{\log|\lambda_2|}, \tag{5.12}$$

where λ_2 is the second largest eigenvalue (in modulus) of the stochastic matrix P (see Figure 5.8). The distance from the probability distribution after n iterations of the Markov chain to the steady state is proportional to $|\lambda_2/\lambda_1|^n$, hence the definition of $t_{\rm c}$ (note that the maximum eigenvalue $\lambda_1 = 1$ since P is stochastic). For $R = 1340$, the number of iterations needed to reach equilibrium near the shift are around 10^3.

The faster variation of η is implemented by producing a small change $\Delta\eta$ every $\Delta n < \xi t_{\rm c}$ iterations of the Markov chain. We start by increasing η in these increments until reaching an arbitrary value beyond the regime shift. Then we repeat the process by decreasing η in the same increments. This way we can track any observable along the cycle, by computing its averages after $k = 0, 1, \ldots$ increments $\Delta\eta$ using the probability distribution

$$\boldsymbol{\pi}(k\Delta\eta/\xi) = \boldsymbol{\pi}(0)\mathsf{P}^{\Delta n}(0)\mathsf{P}^{\Delta n}(\Delta\eta/\xi)\cdots\mathsf{P}^{\Delta n}(k\Delta\eta/\xi), \tag{5.13}$$

given any initial distribution $\boldsymbol{\pi}(0)$ at $\eta = 0$ (reverse order in matrix products applies for decreasing η). In Figure 5.9 the average species richness exhibits a hysteresis cycle. As Δn increases this cycle narrows, recovering the quasi-stationary process in the limit $\Delta n \to \infty$. In this limit the process is reversible and the cycle collapses to the curve of mean number of species shown in Figure 5.4. An important insight this model provides

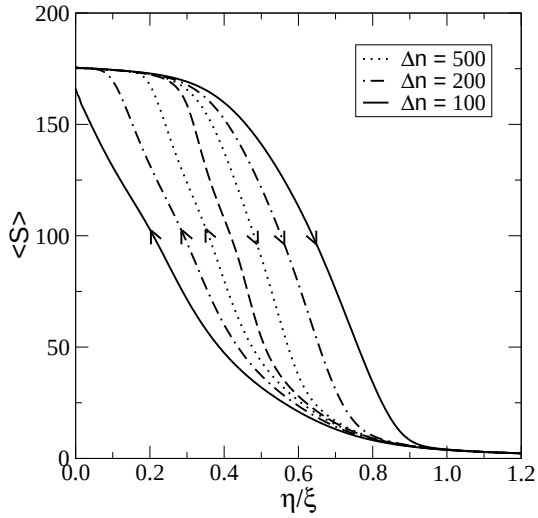

Figure 5.9: *Hysteresis cycles* for $\Delta\eta/\xi = 0.005$ and three values of Δn (see text). Dashed line represents the average number of species in the quasi-stationary process of variation of η (for $\Delta n \to \infty$). The larger Δn the closer to equilibrium the system and the narrower the cycle.

is that hysteresis can arise as a result of a time-scale mixing that keeps the system out of equilibrium rather than to nonlinearities of the underlying population model.

The existence of hysteresis loops in overexploited systems has been reported in the literature as another signal of catastrophic shifts in ecological communities (Scheffer et al. 2001; Fernández and Fort 2009; Scheffer et al. 2009). We have obtained it for the mean number of species, but a similar behavior will be observed in any other magnitude [like the total biomass density, as in Fernández and Fort (2009)]. In spite of the simplicity of our model, hysteresis cycles appear as well as other usual precursors of catastrophic regimes, such as anomalous variance. But, unlike previous models, our model allows for a deeper understanding of the transition, as we will discuss below.

5.4 Phase transition in finite size

As we have mentioned, our model provides a full description of the phase space of the system by means of a transition probability matrix. We are going to take advantage of this fact to show rigorously that the phenomenology that we have described in Section 5.3 corresponds to a phase transition —in the sense of statistical mechanics— in finite size.

In statistical mechanics, phase transitions are associated to non-analyticities of the free energy of a physical system. Whenever the system is described by a transfer

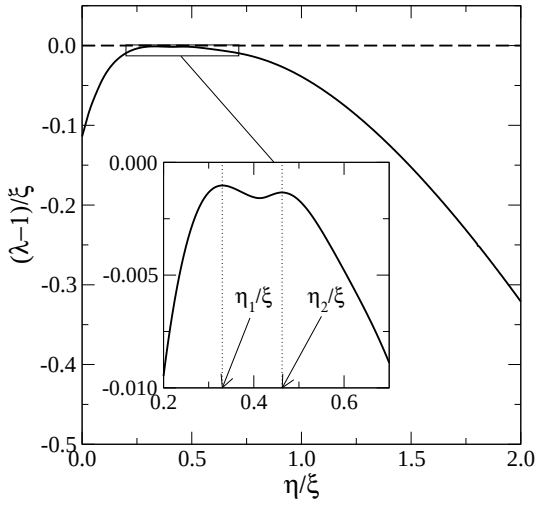

Figure 5.10: *The second eigenvalue of the transition matrix approaches to the first one in the vicinity of the transition.* First (dashed line) and second (full line) eigenvalues of P for a resource saturation $R = 1340$. Inset shows a zoom of the region for which $\lambda_1 = 1$ and λ_2 are closest, and two maxima appear at $\eta_1/\xi = 0.330520\ldots$ and $\eta_2/\xi = 0.462633\ldots$. These points coincide with the maxima observed in σ_{S}^2 and t_{c} (see Figure 5.4 and Figure 5.8).

matrix, the free energy is obtained from its largest eigenvalue. A true phase transition would then be associated to the crossing of the leading eigenvalue with the second largest (in modulus) one, because such a crossing causes a non-analytic behavior of the largest eigenvalue as a function of the control parameter (Cuesta and Sánchez 2004). The counterpart of a transfer matrix in a Markov chain is the transition probability matrix P. Thus a crossing of eigenvalues of P would *rigorously* prove that the system undergoes a phase transition.

Strictly speaking, the described shift can not be a true phase transition because of the finiteness of our system. According to the Perron-Frobenius theorem (c.f. Appendix B.1.4), an irreducible matrix with non-negative entries has a unique largest real eigenvalue and its corresponding eigenvector has strictly positive components (Meyer 2000). As summarized in Appendix B.1.3, reducible matrices are related to processes with transient states. Since the Markov chain is ergodic for $\eta > 0$, its stochastic matrix P is irreducible. Then the theorem implies that its maximum eigenvalue $\lambda_1 = 1$ is *simple* for any value of η/ξ [its corresponding *positive* left eigenvector is precisely the asymptotic probability distribution, c.f. Eq. (B.21)]. This excludes any eigenvalue crossing, therefore any phase transition. True phase transitions can only occur in infinite states Markov chains. When the limiting chain of a sequence of finite Markov

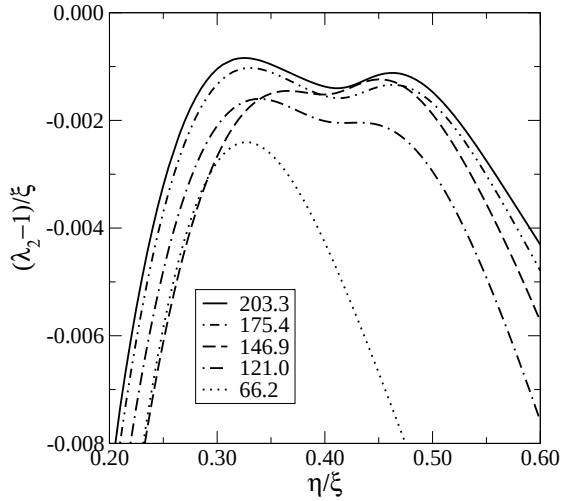

Figure 5.11: *Second eigenvalue* of P for several values of R (legend shows the average number of species for each R at $\eta = 0$). Dotted curve corresponds to $R = 465$, for which the system only allows three trophic levels and only a single maximum is observed. For higher values of R (which allow up to 4 levels), a second maximum appears, related to the trophic cascade in the second level. As the system size increases, λ_2 gets closer to 1.

chains develops an eigenvalue crossing —hence a phase transition— the second largest eigenvalue of the elements of this sequence approaches the largest one near the location of the true phase transition, the more so the larger the size (number of states) of the Markov chain. This is the fingerprint of the phase transition in finite systems. It is also associated to a qualitative change in the eigenvector associated to the leading eigenvalue.

We have computed the 10 largest eigenvalues of P (in modulus) using Arnoldi iteration (Trefethen and Bau 1997) —useful for computing a few eigenvalues of large sparse matrices. In all cases the numerical method provides a real second eigenvalue. Figure 5.10 shows the dependence of λ_2 as a function of η/ξ for $R = 1340$. Not surprisingly, we identify the transition points as those of closest approach to the first eigenvalue (i.e., the two maxima observed in λ_2). Those maxima are reached at $\eta_1/\xi = 0.330520\ldots$ and $\eta_2/\xi = 0.462633\ldots$, which coincide with the values observed for the peaks in σ_{S}^2 and t_{c} (see Section 5.3). As we have shown before, each transition yields a trophic cascade in the system, whose levels get emptied from bottom to top.

We have varied the system size (controlled by the amount of resource, R, see Figure 3.9) in order to check that the second eigenvalue gets closer to the first one as size increases. The system size is measured by the average number of species in the recurrent set for $\eta = 0$, and we do observe that the larger the system size the closer is λ_2

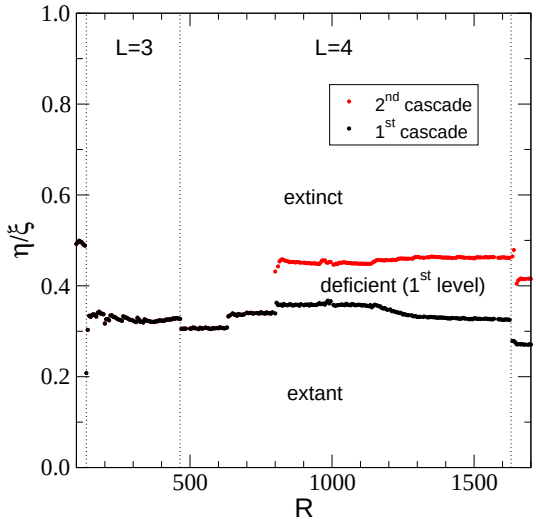

Figure 5.12: *Phase diagram of the system.* Black circles correspond to the abscissa of the first maximum of λ_2 (trophic cascade at the first level), and red ones to the second maximum (trophic cascade at the second level). Above the second transition, the process stays in communities close to the extinct ecosystem.

to 1 (see Figure 5.11). It is difficult to increase the size beyond $S \approx 300$ because the number of nodes in $\mathcal{G}$ grows exponentially (c.f. Figure 3.9). For $S \approx 300$ the number of viable communities is larger than 10^6, and the eigenvalue computation becomes very demanding.

To conclude this section, we have obtained the phase diagram of this system. In Figure 5.12 we show in a η/ξ vs. R diagram the points at which λ_2 reaches its maxima, yielding the transition lines corresponding to the different trophic cascades of the system. Basically transition lines are horizontal, and the number of undergone trophic cascades appears to be related to the number of trophic levels of the communities. We believe that, at some point in the region in which communities have 5 trophic levels, a third maximum would appear related to a separate trophic cascade at the third level. Bearing this hypothesis out is difficult, though, because it would require eigenvalue calculations with too large matrices.

All this analytical evidence allows us to claim that these model ecosystems undergo a catastrophic transition driven by the relative extinction rate. The dependence of λ_2 with η/ξ actually exhibits two maxima and so does the variance in species number. This points towards the existence of a double phase transition, each one associated to a trophic cascade that collapses the lowest and next-to-lowest trophic level in the ecosystem. Increasing the external stress over the system above these values increases the probability of driving the ecosystem to extinction. Consequently there is a threshold

in η/ξ above which the extinction of the ecosystem is the most likely event. Small variations in that region can cause the collapse of stable ecosystems.

5.5 Discussion

In this chapter we have proposed an alternative explanation to the observed catastrophic regime shifts in overexploited ecosystems (Scheffer et al. 2001; Fernández and Fort 2009). Previous models postulate nonlinearities in the dynamics of a magnitude representative of the whole ecosystem, like for instance the total biomass density, and this nonlinear behavior leads to bi-stability. The system undergoes a transition due to a change of regime that moves the system from one stable state to another. This viewpoint is almost the same used in the classical explanations of the liquid-vapor transition in thermodynamics, for which the potential of the system has two alternative stable states.

Our model, however, is inspired in a microscopic description, more related to the perspective of statistical mechanics. Our viable communities are microstates in a finite phase space and represent different states of the ecosystem. The transition between a species-rich attractor (the recurrent set at $\eta = 0$) and an attractor with low number of species (communities close to the empty ecosystem) is explained as the crossing of two eigenvalues of the transition matrix of the Markov chain. The shift is driven by an increasing external force represented by a background species extinction rate, that takes into account the overall mortality for reasons other than predation (overexploitation, habitat destruction, epidemics...).

In spite of its being minimalistic, the model reproduces qualitatively the phenomenology observed in overexploited ecosystems. We have studied for this model the behavior of several early-warnings that announce the catastrophic shift, and we have found the same behavior as that obtained both in previous models (Scheffer et al. 2001; Fernández and Fort 2009) and empirically (Scheffer et al. 2009). These features are shared by many systems under the framework of the *elementary catastrophe theory* (Thom 1975).

Catastrophes have characteristic fingerprints. Some of the standard flags of catastrophic shifts are *modality*, *anomalous variance* and *hysteresis* (Gilmore 1981). These are precisely the signals we find in our model. Our system is bimodal because it undergoes transitions between an attractor of high species richness to another stable state with low species richness. Fluctuations in the mean number of species exhibit peaks at the transition points, and take very large values compared to their values far away from the transition. We thus have anomalous behavior of variances. And the average number of species exhibits hysteresis cycles when the system is kept out of equilibrium, as we have shown in Section 5.3. This explanation of hysteresis is alternative to the existence of nonlinearities in the population model, and points towards the speed of variation of the external stress. The difference with the usual explanation is that in this case the ecosystem can recover its initial state after releasing the external stress, provided that we wait long enough and that there is availability of invaders.

The main advantage of our model is the microscopic description that it provides. The full characterization of the phase space of the system has allowed us to show rigorously that the system undergoes a true phase transition by computing the second eigenvalue of the transition matrix, which gets closest to the first eigenvalue in the vicinity of the transition. This provides a theoretical support to the critical behavior exhibited by magnitudes like the fluctuation of species richness.

We have found evidence for a double phase transition in the system, associated to the gradual loss of species from bottom to top. This effect is new to former models and could be used as early warning for the catastrophic shift by monitoring the species abundance at low trophic levels in overexploited ecosystems. Trophic cascades have been revealed as possible mechanisms of catastrophic shifts in natural communities, though (Daskalov et al. 2007). Thus, with the caveat that this is just a very simplified picture of real communities, our analysis of this model predicts that overexploited systems will begin to collapse first at lower levels.

Assuming a different extinction rate at each trophic level would be more realistic. For example, in overexploited marine ecosystems, the impact of fishing pressure is stronger in higher trophic levels. A simple model like ours could shed light in determining whether a strong extinction pressure in higher levels is more harmful than in lower levels. Refined versions of the model could allow investigating this kind of effects.

Most theoretical explanations of the catastrophic phenomena observed in ecological systems subject to high exploitation pressure rely on nonlinearities in the macroscopic dynamics of the system. On the contrary, a microscopic model like ours, based on ecologically reasonable assumptions and a simple population dynamic model, can exhibit the same phenomenology as nonlinear, macroscopic models. This way, our approach can serve as an alternative explanation of the catastrophic regime shifts observed in ecological communities.

IV

Statistical mechanics of marine size spectra

6

Scale invariance in marine population dynamics

Third Fisherman: Master, I marvel how the fishes live in the sea.
First Fisherman: Why, as men do a-land; the great ones eat up the little ones.
—William Shakespeare *(Pericles)*.

6.1 Marine size spectra

In the marine ecosystem body size is the most important species trait governing biological processes (Jennings et al. 2001). The use of size spectra (i.e., distributions of individuals according to their sizes in a given volume of the open sea) to characterize the marine ecosystem is an interesting way to reduce the complexity of marine and freshwater food-webs. The fact that species size is the relevant trait that determines the observed regular patterns in marine communities is striking and differs completely from the traditional viewpoint of food-webs as feeding networks specifying "who eats who". Alternative to the perspective of assembly models applied in the second part of this thesis, where the modeling was based on an underlying network structure for ecological communities, the approach of size-spectrum-based models leaves the network aside and uses body size as a single niche variable characterizing all individuals.

To build up the size spectrum, the number of individuals —regardless of their taxonomy— found in a given volume of the system are counted and distributed into size groups. The number of individuals in each group per unit volume (i.e. the density of individuals) is found to exhibit a power-law relationship with size (Sheldon et al.

1972). The most important parameter characterizing the density spectrum is therefore the exponent, also referred to as the spectrum slope. This exponent is negative, reflecting the well-known fact that smaller individuals are more abundant than larger ones.

Recently the marine size spectrum has been the subject of renewed attention, since changes of the exponent has been used as indicator of the behavior of the marine community. In particular it has been conjectured that fishing increases the size slope as fishing predominantly targets large individuals (Shin et al. 2005). Understanding the dynamical processes that underlie this pattern is important, since they are responsible for the transfer of mass through marine communities, which in turn determines their productivities and the levels of exploitation that they can sustain. Of its most curious applications, the size spectrum theory has been applied to calculate the number of monsters in Loch Ness! (Sheldon and Kerr 1972).

The concept of size spectrum was introduced by Sheldon et al. (1972) as a pattern of suspended particles in the ocean. During that work, the basic assumption was made that the total mass within logarithmically spaced size groups was constant over the range from micro-organisms to large vertebrates. A biological interpretation of this conjecture is that the total mass of prey is the same as the mass of its predators (Silvert and Platt 1980). Indeed, if the total population density of organisms with weight w per volume is described by the density function $\phi(w) \sim w^{-\theta}$, the total biomass within a logarithmically spaced size group is

$$\int_w^{aw} dw' w' \phi(w') \propto w^{2-\theta}. \tag{6.1}$$

Thus the conjecture of constant biomass over logarithmic bins predicts that the size spectrum exponent must be $\theta \approx 2$.

This hypothesis has been tested empirically. Such an approximate regularity, that applies over a wide range of body sizes, has been the subject of much research in ecology. Observational evidence points to the approximate validity of the size spectrum over almost ten orders of magnitude (Boudreau and Dickie 1992; Heath 1995; Kerr and Dickie 2001; Jennings and Mackinson 2003; Quinones et al. 2003; Marquet et al. 2005). Regarded as one of the most relevant regularities found in ecology, as such it should be amenable to theoretical approaches.

Commonly, the McKendrick-von Foerster equation (McKendrick 1925; von Foerster 1959) is used to model the predation and growth processes that move biomass though the ecosystem (Platt and Denman 1977; Silvert and Platt 1980; Cushing 1992; Camacho and Solé 2001; Benoît and Rochet 2004; Arino et al. 2004; Andersen and Beyer 2006; Andersen et al. 2008; Law et al. 2009). This equation is the result of performing the bookkeeping of biomass along the spectrum, and can be easily derived as follows. Let $\phi(w,t)$ be the density of individuals of a given weight w at time t, aggregated over all species, such that $\phi(w,t)dw$ represents the population per unit volume at time t in the interval of weights w and $w+dw$. Individuals loose energy due to processes like respiration. The rate $m(w)$ at which individuals loose energy is assumed to depend on weights as confirmed by allometric measurements (West et al. 1997). This

way, the number of individuals lost in the size range from w to $w + dw$ in the time interval from t to $t + dt$ is $m(w)\phi(w)dwdt$. The rate at which energy is transferred from smaller to larger individuals depends on two main processes, growth and predation.[1] We may define a continuous rate function $p(w)$, such that the energy concentrated in particles of size w at time t will appear in individuals of size $w + p(w)dt$ at some later time, $t + dt$, as a result of both growth and predation.

Due to respiration processes, the density $\phi(w, t)dw$ of individuals with size in the interval $[w, w + dw]$ at time t will decrease, at time $t + dt$, to $\phi(w', t + dt)dw'$, where $w' = w + p(w)dt$ is the size of the corresponding individuals at this later time determined by both growth and predation. Hence we can establish the following balance equation,

$$\phi(w', t + dt)dw' = [1 - m(w)dt]\phi(w, t)dw. \tag{6.2}$$

This yields

$$\phi(w + p(w)dt, t + dt)\,[1 + p'(w)dt] = [1 - m(w)dt]\phi(w, t), \tag{6.3}$$

which in the limit $dt \to 0$ reduces to the McKendrick-von Foerster equation,

$$\frac{\partial\phi(w, t)}{\partial t} + \frac{\partial}{\partial w}[p(w)\phi(w, t)] + m(w)\phi(w, t) = 0. \tag{6.4}$$

What this equation is actually telling us is that the number of individuals is conserved along the size spectrum. A power-law steady-state solution arises from this equation if some scaling with w is assumed for the respiration and feeding rates (Silvert and Platt 1978), this allometric scaling being supported by profuse empirical evidence (West et al. 1997).

Respiration processes can be interpreted as the removal of individuals due to their decrease in weight. In this sense, Eq. (6.4) couples growth at one size to death at another, because organisms grow in size spectra by eating smaller organisms. More recently, the approach of Silvert and Platt (1978) has been extended, first to allow organisms to eat those at all smaller sizes (Camacho and Solé 2001), and second, by using a feeding preference function, to allow them to eat organisms in a restricted size range (Benoît and Rochet 2004). Partial differential equations of this kind are now being used extensively to understand the dynamics of marine ecosystems (Andersen and Beyer 2006; Andersen et al. 2008). For instance, it can be shown in numerical analyses that those models provide steady states whose slopes are similar to those observed in marine ecosystems (Blanchard et al. 2009).

The McKendrick-von Foerster equation is implicitly assumed in the ecological literature to be an appropriate approximation for an underlying stochastic process in which individual organisms grow by jumps as a consequence of eating prey items. A first investigation of the very stochastic process of growth by jumps (Law et al. 2009)

[1] Strictly, predation is not a continuous process, since prey may be orders of magnitude smaller than their predators. But approximately the flow of biomass due to predation can be represented as a continuous transfer from smaller to larger individuals.

showed that the McKendrick-von Foerster equation could describe the approach of the stochastic process to a steady-state size spectrum. Later, Datta et al. (2010a) derived a mean-field population dynamics starting from the stochastic process in which individuals grow by discrete jumps due to predation events. Although this model is more realistic in describing the feeding process stochastically, there are some missing relevant biological processes like respiration, reproduction, etc. This kind of stochastic modeling will serve as a basis to our more general model of marine population dynamics, encoding processes other than predation. Besides, the additional requirement of scale invariance is key to recover the observed spectra slope in our model.

6.2 Scale invariance in the marine ecosystem

A special property of the pelagic marine ecosystem (the open sea) that has not been exploited yet from a theoretical point of view is its approximate physical scale invariance. The pelagic zone looks similar at a wide range of scales. Over many orders of magnitude there are no physical features and no strong physical principles that would single out a particular intermediate scale. We expect that this approximate scale invariance of the environment breaks down only at scales smaller than the typical size of suspended particles and at large scales at which geography affects ocean currents. This kind of scale-invariance is not present in terrestrial environments, where not only the geographical constraints set up a scale, but in addition the effects of gravity quickly become important for larger organisms.

It is not *a priori* guaranteed that the scale invariance of the physical environment will also lead to scale invariance of the ecosystem. The organisms populating the environment and their interactions could break the invariance. It can be argued that that evolution, in its drive to make use of all available ecological niches, has made optimal use of the environment by filling it with an ecosystem that roughly preserves the symmetry. It is beyond our scope to investigate the evolutionary mechanisms that would lead to the self-organization of such a scale invariant ecosystem. However, the consequences of the assumption of scale invariance for the population dynamics are empirically testable and in line with observations.

The main observational evidence for approximate scale invariance is that the stationary size distribution of organisms in the open ocean is approximately given by a power law. We have reviewed in the previous section several models that have been proposed to derive this steady-state size spectrum but, up to our knowledge, the consequences of the scale invariance of the underlying dynamical model have not been yet explored.

The principal processes that affect the abundance of organisms as a function of weight are predation, reproduction, maintenance respiration and intrinsic death. We will introduce a population model that incorporates all these processes. In general such a model will not reproduce the observed power-law size-spectrum in the steady state. This is the reason why existing work either only models predation (Silvert and Platt 1978; Silvert and Platt 1980; Benoît and Rochet 2004; Arino et al. 2004; Law

et al. 2009; Datta et al. 2010a) or makes the simplifying assumption that reproduction, maintenance respiration and death are exactly proportional to predation (Camacho and Solé 2001).

While the population dynamics leads to a power-law steady-state solution, its dynamical stability is not necessarily ensured. The conditions under which this steady state is an attractor are much less well understood. This is an important issue, because the knowledge of what makes marine ecosystems resilient or susceptible to external pressure has become extremely relevant at a time of overexploitation of marine resources. It has been observed, for example, that exploited fish stocks show more variability than unexploited ones (Hsieh et al. 2006; Anderson et al. 2008), and catastrophic shifts from one attracting state to another have been documented in marine communities through exploitation of top predators (Frank et al. 2005).

A linear stability analysis of the model by Datta et al. (2010b) showed that, for realistic choices of the parameters, the steady state in that model is unstable against small perturbations. The observed size spectrum is stable, so that model is missing some important stabilizing effect. This was the motivation for the investigations of a more general model. One of our main conclusions is that the inclusion of maintenance respiration and reproduction processes stabilizes the size spectrum.

Our starting point will be the formulation of a stochastic model encoding the basic processes of feeding, reproduction, maintenance, and death. We shall not make any assumptions about the rates for these processes but keep them as general parameters of the model. By taking the macroscopic limit of the stochastic model we derive a deterministic, mean-field equation and a linear Fokker-Planck equation for the stochastic fluctuations away from the macroscopic model (see Appendix B.2.2 for details). The requirement of scale invariance yields sufficient scaling conditions for the rate functions. This provides a power-law steady-state solution whose properties will be discussed at length along this chapter.

6.3 Size-structured population model

We start by constructing a stochastic model for the dependence of individuals abundance on weight and time, taking into account the basic processes of predation, reproduction, maintenance and intrinsic mortality.

As in previous work (Datta et al. 2010a), instead of keeping track of the weight of each individual, we aggregate individuals of similar weight into discretized weight brackets $[w_i, w_{i+1})$ for $i \in \mathbb{Z}$. Weight is the only attribute of individuals that is used in this model. Species identity and life stage are ignored. The size spectrum is observed to be valid over a weight range wide enough (Kerr and Dickie 2001) to consider an infinite interval of weights and ignore boundary effects in a first approximation. The weight distribution of individuals in a large fixed volume Ω is then described by the vector of populations $\mathbf{N} = (\dots, N_{-1}, N_0, N_1, \dots)$ whose entries give the number of organisms in each weight bracket. We will later let the size of these brackets go to zero to obtain the continuum model.

The primary events involved in the model are illustrated in Figure 6.1, which shows the various ways in which the number of organisms in bracket i can vary. The deterministic equation can be read off directly from this figure. In Appendix B.2.2 the derivation from a master equation is illustrated as well as the systematic expansion (van Kampen 2007) in powers of the inverse system volume.[2] This method is based on splitting each variable $N_i(t)$ into a deterministic, macroscopic component $\phi_i(t)$ describing the density of individuals in weight bracket i, and a fluctuation component $\psi_i(t)$ as

$$N_i(t) = \Omega\phi_i(t) + \Omega^{1/2}\psi_i(t). \tag{6.5}$$

The powers of volume are chosen so that the new variables ϕ_i and ψ_i no longer scale with the system volume. This method not only gives the macroscopic behavior for the densities $\phi_i(t)$ at leading order in the expansion, at higher orders it describes the stochastic fluctuations around the macroscopic solution as well, giving at next-to-leading order a linear Fokker-Planck equation. However, the system volume is large, so we shall concentrate on the macroscopic, deterministic equation.

From Figure 6.1 we can obtain the contributions to the time evolution of $\phi_i(t)$ from each of the considered processes: predation (P), reproduction (B for Birth), maintenance respiration (R for Respiration) and intrinsic mortality (D for Death),

$$\frac{d\phi_i}{dt} = \left(\frac{d\phi_i}{dt}\right)_{\mathrm{P}} + \left(\frac{d\phi_i}{dt}\right)_{\mathrm{B}} + \left(\frac{d\phi_i}{dt}\right)_{\mathrm{R}} + \left(\frac{d\phi_i}{dt}\right)_{\mathrm{D}}. \tag{6.6}$$

Let us describe each of them in turn below.

6.3.1 Predation

A predation event moves a predator from a weight bracket i before feeding to a higher weight bracket k after feeding and removes a prey organism from a weight bracket j. Let W^{P}_{ijk} be the rate constant for such a predation event. As illustrated in Figure 6.1a, there are three ways in which a predation event can affect the number N_i of individuals in bracket i: (i) an organism in i can eat another organism and grow; (ii) an organism belonging to i can be eaten by another organism; and (iii) an individual in a lower bracket can absorb enough prey weight and grow into bracket i. Because the rate at which a particular individual will encounter prey will be proportional to the density of prey,[3] the probability that one of the N_i individuals in bracket i preys on any of the N_j individuals of bracket j and increases its size to bracket k in the time interval from t to $t + dt$ is $W^{\mathrm{P}}_{ijk}N_iN_j\Omega^{-1}dt$. Hence the contribution of the predation events to the deterministic time evolution of the density ϕ_i of organisms in bracket i is

$$\left(\frac{d\phi_i}{dt}\right)_{\mathrm{P}} = \sum_{j,k}(-W^{\mathrm{P}}_{ijk}\phi_i\phi_j - W^{\mathrm{P}}_{jik}\phi_j\phi_i + W^{\mathrm{P}}_{jki}\phi_j\phi_k). \tag{6.7}$$

[2] The same method was used in Datta et al. (2010a).

[3] This assumption is tantamount to saying that predation processes follow a "law of mass action" similar to that of Lotka-Volterra equations.

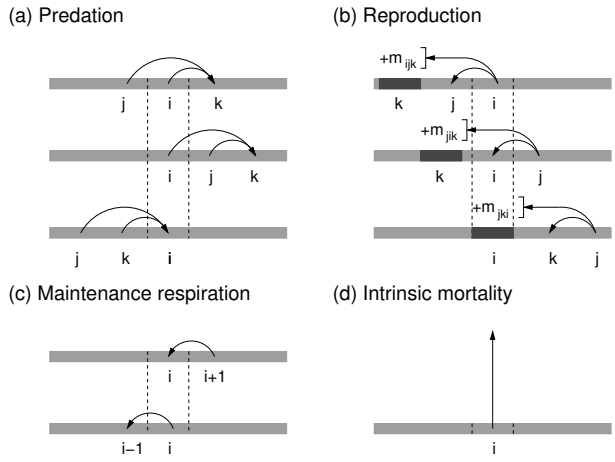

Figure 6.1: *Elementary stochastic processes involved in the model.* The figure shows all the events that affect the number of organisms in weight bracket i. Arrows indicate the movement of individuals between weight brackets. (a) Predation: There are three predation processes affecting bracket i. The first represents a predator in i preying on an individual in j and absorbing enough prey weight to end up in k. The second represents a prey in i being consumed and the third represents a predator entering i after feeding. (b) Reproduction: in the first process an individual in i produces m_{ijk} offspring in bracket k and, as a consequence, decreases its weight to j. In addition, there are two processes that increase the number of individuals in i. (c) Maintenance respiration: these processes move individuals to the next-lower bracket. There are two ways in which this affects to bracket i. (d) Intrinsic mortality: with a certain rate, a single individual in bracket i is removed from the system.

6.3.2 Reproduction

Most fishes reproduce by laying a large number of eggs that are subject to heavy predation. Only a small fraction of the eggs survives to hatch and join the consumer spectrum. However, in a size-spectrum model, in which size is the only attribute of an organism and its life stage is ignored, all organisms are assumed to be prey and predator simultaneously from the moment they are born. Therefore it is difficult to model the egg life stage and to provide an entirely realistic model of the reproductive processes. Our model is thus designed to only capture two features of reproduction that we deem essential to the size-spectrum dynamics, namely that it moves biomass down the size spectrum from large weight to small weight and that it replenishes the population numbers at smaller weight.

We assume that a reproduction event moves a parent organism from a weight bracket i to a lower weight bracket j and produces a number m_{ijk} of smaller off-

spring in weight bracket k. The number of offspring is set to $m_{ijk} = \lfloor (w_i - w_j)/w_k \rfloor$, where $\lfloor x \rfloor$ denotes the largest integer smaller than x, so that their combined weight is approximately equal to the weight lost by the parent. Let W^{B}_{ijk} be the rate constant for such an event. The probability that one of the N_i individuals in bracket i reproduces in such an event in dt is then $W^{\mathrm{B}}_{ijk} N_i dt$ (note that reproduction, unlike predation, is a density-independent process).

As depicted in Figure 6.1b, there are three ways in which reproduction changes the number of the organisms in bracket i: (i) the parent belongs to the i-th bracket, and after spawning moves to a lower bracket; (ii) a parent looses weight during spawning and moves to bracket i; and (iii) the bracket i receives m_{jki} offspring from a reproduction event. The contribution of these three possibilities to the deterministic equation is therefore given by

$$\left(\frac{d\phi_i}{dt}\right)_{\mathrm{B}} = \sum_{j,k} \left(-W^{\mathrm{B}}_{ijk}\phi_i + W^{\mathrm{B}}_{jik}\phi_j + m_{jki} W^{\mathrm{B}}_{jki}\phi_j\right). \tag{6.8}$$

6.3.3 Maintenance and mortality

In between feeding events, organisms continuously draw upon their reserves to maintain themselves. The weight loss due to respiration is modeled by events that move individuals to the next-lower weight bracket, assuming that the width of each interval is small enough (this is not a restriction, because at the end we will take the continuum limit where all these widths tend to zero). The probability that any of the N_i individuals in the bracket i undergoes a respiration process in dt is $W^{\mathrm{R}}_i N_i dt$, where W^{R}_i is the maintenance respiration rate for the bracket i. Figure 6.1c shows the two ways that these primary processes change the number of individuals in bracket i, thus leading to the deterministic equation

$$\left(\frac{d\phi_i}{dt}\right)_{\mathrm{R}} = W^{\mathrm{R}}_{i+1}\phi_{i+1} - W^{\mathrm{R}}_i \phi_i. \tag{6.9}$$

Organisms can also die for reasons other than being preyed on. This introduces a fourth process in the model that accounts for intrinsic mortality. With a probability $W^{\mathrm{D}}_i N_i dt$, a single individual in bracket i is removed from the system in dt (see Figure 6.1d). Hence

$$\left(\frac{d\phi_i}{dt}\right)_{\mathrm{D}} = -W^{\mathrm{D}}_i \phi_i. \tag{6.10}$$

Note that, like reproduction, both maintenance and background mortality are modeled as density-independent processes.

6.3.4 Continuum limit

We now take the continuum limit of each contribution to the macroscopic equation by writing $\Delta_i = w_{i+1} - w_i$ and taking the limit $\Delta_i \to 0$ uniformly for all i. The variables

$\phi_i(t)$ are combined into a density $\phi(w,t)$ of individuals per unit weight per unit volume as a function of weight and time so that $\phi(w_i,t) = \phi_i(t)/\Delta_i$. The sum over weight brackets is replaced by an integral, $\sum_i \Delta_i \to \int dw$. Continuum rate functions are introduced as

$$\begin{aligned} W^{\mathrm{P}}(w_i,w_j,w_k) &= W^{\mathrm{P}}_{ijk}/\Delta_k, \\ W^{\mathrm{B}}(w_i,w_j,w_k) &= W^{\mathrm{B}}_{ijk}/(\Delta_j\Delta_k), \\ W^{\mathrm{R}}(w_i) &= \Delta_i W^{\mathrm{R}}_i, \\ W^{\mathrm{D}}(w_i) &= W^{\mathrm{D}}_i. \end{aligned} \tag{6.11}$$

The first argument of the rate W^{P} refers to the weight of the predator before predation, the second argument is the weight of the prey and the third one is the weight of the predator after predation. Similarly, the first argument of W^{B} is the weight of a parent before a reproduction event, the second argument is the (smaller) weight after reproduction, and the third one corresponds to offspring weight.

After taking the continuum limit, the ordinary differential equation (6.6) for the densities ϕ_i assembles into a partial differential equation for $\phi(w,t)$, which will be the object of study in this chapter. This equation is made up of four terms. The contribution from predation (6.7) in this limit reduces to

$$\begin{aligned} \left(\frac{\partial\phi(w,t)}{\partial t}\right)_{\mathrm{P}} = \int dw' \int dw'' \big[& W^{\mathrm{P}}(w',w'',w)\phi(w',t)\phi(w'',t) \\ & - \{W^{\mathrm{P}}(w,w',w'') + W^{\mathrm{P}}(w',w,w'')\}\phi(w,t)\phi(w',t)\big]. \end{aligned} \tag{6.12}$$

Integrals run over all positive weights. Similarly, the continuum limit of (6.8) is

$$\begin{aligned} \left(\frac{\partial\phi(w,t)}{\partial t}\right)_{\mathrm{B}} = \int dw' \int dw'' \Bigg[& \frac{w'-w''}{w} W^{\mathrm{B}}(w',w'',w)\phi(w',t) \\ & - W^{\mathrm{B}}(w,w',w'')\phi(w,t) + W^{\mathrm{B}}(w',w,w'')\phi(w',t)\Bigg]. \end{aligned} \tag{6.13}$$

Feeding is a non-local interaction in weights. Most fishes and plankton do not feed on other individuals that are close to their own weight. Instead they prefer prey that are substantially smaller. Similarly they produce offspring at a weight far below their own. This is the reason why the population density $\phi(w,t)$ is described by a partial *integro-differential* equation involving terms that encode feeding and reproductive behavior. Note that most fishes consume organisms of smaller size, so this fact has to be made explicit in the feeding rate, which in practice will limit the range of integrals to semi-infinite intervals.

On the other hand, maintenance and intrinsic mortality are described by partial differential equations of the form

$$\left(\frac{\partial\phi(w,t)}{\partial t}\right)_{\mathrm{R}} = \frac{\partial}{\partial w}\left[W^{\mathrm{R}}(w)\phi(w,t)\right] \tag{6.14}$$

and

$$\left(\frac{\partial\phi(w,t)}{\partial t}\right)_{\mathrm{D}} = -W^{\mathrm{D}}(w)\phi(w,t), \tag{6.15}$$

respectively.

When only predation processes are considered, our model reduces to that derived in Datta et al. (2010a) when the feeding rate is chosen as

$$W^{\mathrm{P}}(w,w',w'') = k(w,w')\delta(w + Kw' - w'') \tag{6.16}$$

for some feeding preference function[4] $k(w,w')$ and a fraction K accounting for the conversion efficiency of biomass from predator to prey. This choice amounts to assume a weight after predation equal to the weight before predation plus Kw', w' being the weight of the prey. As pointed out in Datta et al. (2010a), when the typical predator:prey mass ratio is sufficiently large and the population density is sufficiently smooth the model in turn can be approximated by the McKendrick-von Foerster equation, which forms the basis of most previous theoretical studies of the size distribution. Thanks to scale invariance, our much more general model is amenable to similar investigations.

6.4 Scale invariance

Some restrictions on the feeding, reproductive, maintenance and mortality rates result from the requirement of scale invariance. We derive them in this section.

As the model describes the dependence of biomass density on two variables, namely weight and time, we could consider separate scalings in weight and in time. However, we expect invariance only under simultaneous scaling of both weight and time, because life processes run faster for smaller organisms (West et al. 1997). Hence, when the weight scale changes by a factor $c > 0$ the time scale should also change by a factor c^{φ}, where the constant φ expresses how the speed of the dynamics scales with weight. So we will consider the transformations

$$(w,t) \mapsto (cw, c^{\varphi}t). \tag{6.17}$$

Under such scale transformations the density $\phi(w,t)$ transforms as

$$\phi(w,t) \mapsto c^{\theta}\phi(cw, c^{\varphi}t) \tag{6.18}$$

with some, so far undetermined, exponent θ.

Requiring the population model (6.12)–(6.15) to remain unchanged under this transformation imposes the scalings

$$\begin{aligned} c^{\theta-\varphi-2}W^{\mathrm{P}}(w,w',w'') &= W^{\mathrm{P}}(cw,cw',cw''),\\ c^{-\varphi-2}W^{\mathrm{B}}(w,w',w'') &= W^{\mathrm{B}}(cw,cw',cw''),\\ c^{1-\varphi}W^{\mathrm{R}}(w) &= W^{\mathrm{R}}(cw),\\ c^{-\varphi}W^{\mathrm{D}}(w) &= W^{\mathrm{D}}(cw). \end{aligned} \tag{6.19}$$

[4]This function describes the feeding rate of individuals of weight w on individuals of weight w'.

We choose to factorize the feeding rate as [c.f. Eq. (6.16)]

$$W^{\mathrm{P}}(w, w', w'') = A(w, w')V(w, w', w''), \tag{6.20}$$

where $A(w, w')$ determines the rate at which a predator of weigh w feeds on a prey of weight w' and $V(w, w', w'')$ gives the probability density that such a feeding event makes the predator grow to weight w''. On average only a certain proportion K of the prey biomass will be absorbed by the predator, so that on average $w'' = w + Kw'$, but there will be some variability, due to differences in predator digestion and prey composition. This variability will be modeled by the probability density $V(w, w', w'')$ such that the mean weight after predation is

$$\int dw''\, w''V(w, w', w'') = w + Kw'. \tag{6.21}$$

Note that the model, and therefore its results, depend only on the combined rate W^{P}. We factorize it into A and V only to make the ecological origin of the rate clearer, as customary in the ecological literature (Benoît and Rochet 2004; Datta et al. 2010a), but how we choose this factorization has no influence on the results.

Hence we are free to choose the relative scaling between these factors, as long as the product scales as in (6.19). In order for V to scale as a probability density in w'', we impose that

$$\begin{aligned} V(w, w', w'') &= w''^{-1}V_0(w/w', w''/w), \\ A(w, w') &= (w/w_0)^{\theta-\varphi-1}\, A_0(w/w'). \end{aligned} \tag{6.22}$$

Here w_0 is an arbitrarily chosen reference weight. We have also introduced the functions V_0 and A_0 that are invariant under scale transformations.

Similarly, we require that the reproduction rate W^{B} scales as a density in w' and w''. Thus, according to the scaling rules (6.19),

$$W^{\mathrm{B}}(w, w', w'') = w'^{-1}w''^{-1}\,(w/w_0)^{-\varphi}\, W_0^{\mathrm{B}}(w/w', w''/w) \tag{6.23}$$

for some scaling function W_0^{B}. This behavior for the reproduction rate implies that the average weight of an offspring is proportional to $w^{1-\varphi}$, where w is the weight of its parent. This should however not be taken as a prediction of the scaling of egg sizes because, as stressed previously, our model of reproduction is not formulated at a sufficient level of detail for that purpose.

The scale transformations for maintenance and death rates allow us to express them as

$$\begin{aligned} W^{\mathrm{R}}(w) &= (w/w_0)^{1-\varphi}\, W^{\mathrm{R}}(w_0), \\ W^{\mathrm{D}}(w) &= (w/w_0)^{-\varphi}\, W^{\mathrm{D}}(w_0). \end{aligned} \tag{6.24}$$

The functions A_0, V_0 and W_0^{B}, the constants $W^{\mathrm{R}}(w_0)$ and $W^{\mathrm{D}}(w_0)$ and the exponents θ and φ are not fixed by the requirement of scale invariance and need to be determined from observations or separate theoretical arguments.

The restrictions imposed to achieve scale invariance predict the relative scaling of these rates. In particular, the scaling of all the rates contains the exponent φ. It is widely believed that the maintenance metabolic rate scales as $w^{3/4}$ (Peters 1986; Clarke and Johnston 1999; Brown et al. 2004). Then Eq. (6.24) sets the exponent $\varphi = 1/4$. This fact implies a mortality rate scaling as $w^{-1/4}$, which is in line with observations (Peters 1986; Lorenzen 1996). Moreover, the exponent θ of the scaling transformation (6.18) is determined once the scaling of the feeding preference function A and the exponent φ are known. If we assume, following Benoît and Rochet (2004), that the feeding rate is proportional to the volume searched per unit time, we can identify the scaling exponent of A as the exponent of the search volume, which is around 0.8 (Ware 1978). A value $\varphi = 1/4$ yields $\theta \approx 2$. We will see in Section 6.6 that the exponent θ coincides with the exponent of the power-law steady-state solution. Hence a power-law exponent $\theta \approx 2$ is in line with the observation of constant biomass over logarithmic bins (Blanchard et al. 2009). Therefore, it is precisely the relative scaling between density-dependent processes (feeding) and density-independent processes (reproduction, maintenance and death) that determines the spectrum slope under the requirement of scale invariance.

6.5 Change to logarithmic weight

For the upcoming analysis it is convenient to make a change of variable to $x = \log(w/w_0)$, where w_0 is the arbitrarily chosen reference weight. We refer to x as the logweight. A scale transformation $w \mapsto cw$ corresponds to a translation $x \mapsto x + \log c$.

We introduce the density $u(x)$ so that $\Omega u(x)dx$ is the number of individuals in volume Ω with a logweight between x and $x + dx$, hence $u(x) = w\phi(w)$. Under a scale transformation the function $u(x,t)$ transforms to $c^{\theta-1}u(x + \log c, c^{\varphi}t)$. We will apply this change to the various terms of the dynamical equation (6.12)–(6.15).

Let us introduce the predation rate ω_{P} such that $\omega_{\mathrm{P}}(x, x', x'') = w''W^{\mathrm{P}}(w, w', w'')$. The factorization of W^{P} into A and V in equation (6.20) together with equation (6.22) leads to

$$\omega_{\mathrm{P}}(x, x', x'') = e^{(\epsilon-\varphi)x}a(x - x')\chi_{\mathrm{P}}(x - x', x'' - x), \tag{6.25}$$

where we have defined the prey selection function $a(y) = A_0(e^y)$ and the absorption probability density $\chi_{\mathrm{P}}(y, z) = V_0(e^y, e^z)$ and we have introduced the exponent $\epsilon = \theta - 1$ for latter convenience. We now transform to logweights, substitute this form for ω_{P} into (6.12) and perform a change of variables in each of the feeding terms so that the integration variable coincides with the argument of a. The result is

$$\begin{aligned}\left(\frac{\partial u(x)}{\partial t}\right)_{\mathrm{P}} = e^{(\epsilon-\varphi)x} \int dy\, a(y) \Big[&- u(x)u(x - y) - e^{(\epsilon-\varphi)y}u(x)u(x + y) \\ &+ \int dz\, e^{-(\epsilon-\varphi)z}\chi_{\mathrm{P}}(y, z)u(x - z)u(x - y - z)\Big],\end{aligned} \tag{6.26}$$

where we have taken into account the fact that $\chi_{\mathrm{P}}(y, z)$ is a probability density and hence it is normalized to unity. The integrals all run over the whole real line. In what

follows, we will often not indicate the time-dependence of $u(x,t)$ explicitly but write just $u(x)$ instead, as in the above equation.

The same changes can be applied to the reproduction term. Using the scaling form (6.23) for W^{B} in (6.13), then transforming to logweights and defining $\chi_{\mathrm{B}}(y,z) = W_0^{\mathrm{B}}(e^y, e^z)$, we obtain

$$\begin{aligned}\left(\frac{\partial u(x)}{\partial t}\right)_{\mathrm{B}} = e^{-\varphi x}\int dy \int dz\, \chi_{\mathrm{B}}(y,z)\Big[- u(x) + e^{-\varphi y}u(x+y) \\ + e^{(\varphi-1)z}(1-e^{-y})u(x-z)\Big].\end{aligned} \tag{6.27}$$

Finally, the contribution of maintenance and intrinsic mortality can be expressed in logarithmic weights as

$$\left(\frac{\partial u(x)}{\partial t}\right)_{\mathrm{R}} = \omega_{\mathrm{R}}\frac{\partial}{\partial x}\left[e^{-\varphi x}u(x)\right] \tag{6.28}$$

and

$$\left(\frac{\partial u(x)}{\partial t}\right)_{\mathrm{D}} = -\omega_{\mathrm{D}}e^{-\varphi x}u(x), \tag{6.29}$$

respectively. Here we have introduced the constants $\omega_{\mathrm{R}} = W^{\mathrm{R}}(w_0)/w_0$ and $\omega_{\mathrm{D}} = W^{\mathrm{D}}(w_0)$. The full equation in terms of logweights is simply the sum of (6.26)–(6.29). We have chosen not to fully non-dimensionalize the equation: t still has dimension of time, $u(x)$ has the dimension of inverse volume, ω_{R}, ω_{D} and χ_{B} have dimension of inverse time, a has dimension of volume over time and χ_{P} is dimensionless.

6.6 Power-law steady-state solution

Solving the integro-differential equation given by (6.26)–(6.29) is difficult in general. However we can simplify the task by looking for solutions that are invariant under symmetry transformations.

In this section we will study a solution that is invariant under both time-translations and scale transformations —note that, besides scale invariance, our model has also time-translation invariance. Time-translation invariance means that we are looking for a steady-state solution $\hat{\phi}(x)$ that has no dependence on time. Invariance under scale transformations (6.17)–(6.18) implies

$$\hat{\phi}(w) = \hat{\phi}(w_0)\left(\frac{w_0}{w}\right)^{\theta}. \tag{6.30}$$

After transforming to logweights as in Section 6.5 the solution becomes

$$\hat{u}(x) = u_0 e^{-\epsilon x}, \tag{6.31}$$

where $u_0 = w_0\hat{\phi}(w_0)$ and $\epsilon = \theta - 1$. Substituting this form for the solution into the mean-field equation in terms of logweights gives a relation for the overall population level u_0,

$$c_{\mathrm{P}}u_0 = -\omega_{\mathrm{R}}(\epsilon+\varphi) - \omega_{\mathrm{D}} + c_{\mathrm{B}}, \tag{6.32}$$

where c_{P} and c_{B} are functions of ϵ and φ given by

$$\begin{aligned} c_{\mathrm{P}} &= \int dy\, a(y) \left[e^{\epsilon y} + e^{-\varphi y} - e^{\epsilon y} \int dz\, e^{(\epsilon+\varphi)z} \chi_{\mathrm{P}}(y,z) \right] \\ c_{\mathrm{B}} &= \int dy \int dz\, \chi_{\mathrm{B}}(y,z) \left[-1 + e^{-(\epsilon+\varphi)y} + e^{(\epsilon+\varphi-1)z}(1-e^{-y}) \right]. \end{aligned} \tag{6.33}$$

When $c_{\mathrm{P}} \neq 0$, Eq. (6.32) uniquely determines u_0 and hence the steady state solution. It can be proven that u_0 is positive under some ecologically reasonable assumptions regarding the parameter functions (we leave the details to Appendix E).

Note that scale invariance fixes the power-law form of the steady-state size spectrum and the steady-state exponent ϵ is determined entirely by the scaling behavior of the parameter functions, according to Eq. (6.19). It is not dependent on any other details of the interactions in the model.

A special situation arises in the case where maintenance, reproduction and intrinsic mortality are absent from the model. In this case only the first scaling relation in (6.19) remains and it is not enough to determine both φ and ϵ. However an equation for ϵ is obtained by noticing that in this case the right-hand side of (6.32) is zero and for $u_0 \neq 0$ this implies that $c_{\mathrm{P}} = 0$. This constraint should then be used to determine the scaling exponent ϵ given a particular choice of $a(y)$ and $\chi_{\mathrm{P}}(y,z)$. The overall population level u_0 is not determined by the model in this case. This special situation was considered in most previous work (Silvert and Platt 1978; Silvert and Platt 1980; Benoît and Rochet 2004; Datta et al. 2010a).

6.6.1 Conservation of the number of individuals

There is a continual flux of individuals from lower weight to larger weight to make up for the losses due to predation and intrinsic death. In previous models that considered only the predation process (Benoît and Rochet 2004; Datta et al. 2010a) it was necessary to impose an input source of small individuals. However, with the incorporation of reproduction processes to our model we do have a source of individuals and can impose that in the steady state this source should exactly balance the losses.

The easiest way to impose this balance is to require for each weight bracket i that the number of individuals entering the bracket from the left due to predation exactly equals the number of individuals leaving that bracket to the left, either as offspring or through weight-loss. This gives

$$\sum_{j,k} W^{\mathrm{P}}_{jki} \hat{\phi}_j \hat{\phi}_k = \sum_{j,k} (m_{ijk}+1) W^{\mathrm{B}}_{ijk} \hat{\phi}_i + W^{\mathrm{R}}_i \hat{\phi}_i. \tag{6.34}$$

Thanks to scale invariance, all these conditions for different i are equivalent. In the continuum, after substituting the steady state solution and changing to logweight notation, this condition reads

$$f_{\mathrm{P}} u_0 = f_{\mathrm{B}} + \omega_{\mathrm{R}}, \tag{6.35}$$

where we have defined

$$\begin{aligned} f_{\mathrm{P}} &= \int dy \int dz\, a(y)\, \chi_{\mathrm{P}}(y,z) e^{(\epsilon+\varphi)z+\epsilon y}, \\ f_{\mathrm{B}} &= \int dy \int dz\, \chi_{\mathrm{B}}(y,z) \left[e^{-z}(1-e^{-y})+1\right]. \end{aligned} \tag{6.36}$$

This constraint and the steady-state condition (6.32) fix the maintenance rate and the overall population level in terms of the remaining parameters of the model, as

$$\omega_{\mathrm{R}} = \frac{(c_{\mathrm{B}}-\omega_{\mathrm{D}})f_{\mathrm{P}} - c_{\mathrm{P}} f_{\mathrm{B}}}{c_{\mathrm{P}} + (\epsilon+\varphi) f_{\mathrm{P}}}, \tag{6.37}$$

and

$$u_0 = \frac{c_{\mathrm{B}} - \omega_{\mathrm{D}} + (\epsilon+\varphi) f_{\mathrm{B}}}{c_{\mathrm{P}} + (\epsilon+\varphi) f_{\mathrm{P}}}. \tag{6.38}$$

Obviously, we have to impose the restriction $\omega_{\mathrm{R}} > 0$, which it is not verified for any choice of parameters. In particular, this requirement defines a range of allowed exponents ϵ. To investigate this further, in the next section we will make specific choices for the functions that appear in the feeding and reproduction rates.

6.6.2 Choice of parameter functions

For the prey selection function $a(y)$ we choose a Gaussian which expresses that there is a preferred value e^{β} for the predator:prey mass ratio and a certain variance σ_β^2 around the mean β (Ursin 1971). Thus,

$$a(y) = a_0 g_{\sigma_\beta}(y-\beta) \tag{6.39}$$

with

$$g_\sigma(x) \equiv \frac{1}{\sqrt{2\pi}\sigma} e^{-x^2/2\sigma^2}. \tag{6.40}$$

The parameter a_0 has dimension of volume over time and sets the overall feeding rate.

For the absorption probability density χ_{P} the simplest assumption would be that a fixed proportion K of prey mass is absorbed in all feeding events, i.e., that in terms of the predator mass w and the prey mass w' the mass after feeding is always $w'' = w + Kw'$. This corresponds to a choice $\chi_{\mathrm{P}}(y,z) = \delta(z - j(y))$ where

$$j(y) = \log(1 + Ke^{-y}). \tag{6.41}$$

This choice was used in Datta et al. (2010a). However the proportion of the prey mass that is absorbed by the predator is not exactly the same in each feeding event. Variability arises for example from the difference in digestion between predator species and also from the difference in organic composition of prey organisms. In order to allow variation, the delta function is replaced by a Gaussian with variance σ_K^2,

$$\chi_{\mathrm{P}}(y,z) = g_{\sigma_K}(z - j(y)). \tag{6.42}$$

For the reproduction function $\chi_{\mathrm{B}}(y,z)$ we will use the product of Gaussians

$$\chi_{\mathrm{B}}(y,z) = b_0 g_{\sigma_\nu}(y-\nu) g_{\sigma_\mu}(z-\mu). \tag{6.43}$$

This gives a mean offspring:parent mass ratio of e^μ and a mean mass ratio between parent before reproduction and parent after reproduction of e^ν.

Finding the correct values for the parameters requires a close investigation of the data. However, we have tried to choose parameters that appear at least reasonable from a biological point of view. For example, the preferred predator:prey body mass ratio is believed to be around 10^2 or 10^3 (Jennings and Mackinson 2003), so we have chosen $\beta = 5.5$. In order to estimate ν, we need the average weight loss caused by reproduction processes. The average gonadosomatic index (i.e., the ratio between the gonadal weight and the body weight) is actually measured for fish and is rather variable. It is found to be on average around 0.1 or 0.2 (Roff 1992), thus we have chosen $\nu = 0.2$ so that the average fraction of weight loss due to reproduction is around 20%. The logweight difference between offspring and parent μ has been set to a small value around -8 or -9. For the standard deviations in the parameters we use $\sigma_\beta = 2.5$, $\sigma_\nu = 0.05$ and $\sigma_\mu = 0.5$, although a careful analysis of the available data (Fishbase 2010) will be necessary to determine them properly. We have set the absorption efficiency to $K = 0.9$ (Pandian and Marian 1985) because respiration and other metabolic processes have been modeled separately. In Datta et al. (2010b), where these processes were not separated, the net absorption efficiency was replaced by a conversion efficiency of around 0.2. In most plots we will set the variance σ_K^2 equal to zero, as well as the mortality rate.

In Figure 6.2 we have plotted the maintenance rate ω_{R} and the steady-state density coefficient u_0 as functions of ϵ for the above choices of parameters and $\varphi = 0.25$. The allowed interval for ϵ appears shaded in that figure. It is encouraging that the observed value $\epsilon \approx 1$ (Sheldon et al. 1972; Kerr and Dickie 2001; Jennings and Mackinson 2003) is contained within the interval.

6.7 Stability of the steady state

It has been observed via numerical simulations (Law et al. 2009; Datta et al. 2010a) that the power-law steady state is not always stable against small perturbations but rather that the system can undergo a bifurcation in which the steady state becomes unstable and a stable traveling wave solution emerges. This phenomenon has been investigated analytically in Datta et al. (2010b) through a linear stability analysis. We now perform a similar analysis in our generalized model.

The only other paper that we are aware of that investigates the stability of the power-law steady state is Arino et al. (2004) but it deals, for reasons of simplicity, with a model where the growth due to feeding is independent of the prey density, thus avoiding having to deal with the associated nonlinear terms.

In order to discuss stability analytically, we consider the particular case $\varphi = 0$. According to (6.24), this corresponds to a maintenance rate proportional to the weight

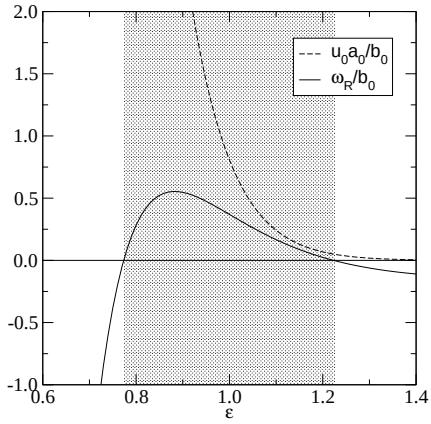

Figure 6.2: *Intervals of allowed parameters.* Plot of the curves u_0 and ω_{R} [Eqs. (6.38) and (6.37)] with the choices (6.39), (6.42) and (6.43), for $\varphi = 0.25$. Other parameters are $\beta = 5.5$, $\sigma_\beta = 2.5$, $K = 0.9$, $\sigma_K = 0$, $\mu = -10$, $\sigma_\mu = 0.5$, $\nu = 0.2$, $\sigma_\nu = 0.05$ and $\omega_{\mathrm{D}} = 0$. The region of allowed ϵ is shaded.

and a mortality rate independent of the weight. This is not quite realistic, but simplifies the analysis considerably because it leads to translational invariance in both time and logweight. This enhanced symmetry allows for the use of standard Fourier transform to solve the linearized model.

6.7.1 Perturbation in u_0

Before we consider the general, weight-dependent perturbation we focus on perturbations that affect only the overall population density u_0. So instead of (6.31) we consider the solution

$$u(x,t) = u_0(t)e^{-\epsilon x}. \tag{6.44}$$

The dynamical equation with $\varphi = 0$ turns out to be

$$\frac{du_0}{dt} = -c_{\mathrm{P}}u_0^2 + (c_{\mathrm{B}} - \omega_{\mathrm{R}}\epsilon - \omega_{\mathrm{D}})u_0. \tag{6.45}$$

The solutions to this differential equation depend crucially on the strength of reproduction relative to maintenance and mortality. If reproduction is weak, i.e. if $c_{\mathrm{B}} < \omega_{\mathrm{R}}\epsilon + \omega_{\mathrm{D}}$, then the non-zero fixed point (steady state) at $u_0 = (c_{\mathrm{B}} - \omega_{\mathrm{R}}\epsilon - \omega_{\mathrm{D}})/c_{\mathrm{P}}$ is unstable. If, however, reproduction is strong enough so that

$$c_{\mathrm{B}} > \omega_{\mathrm{R}}\epsilon + \omega_{\mathrm{D}}, \tag{6.46}$$

then the fixed point is stable. In between, the system undergoes a bifurcation at which there is a whole line of fixed points exactly when $c_{\mathrm{B}} = \omega_{\mathrm{R}}\epsilon + \omega_{\mathrm{D}}$.

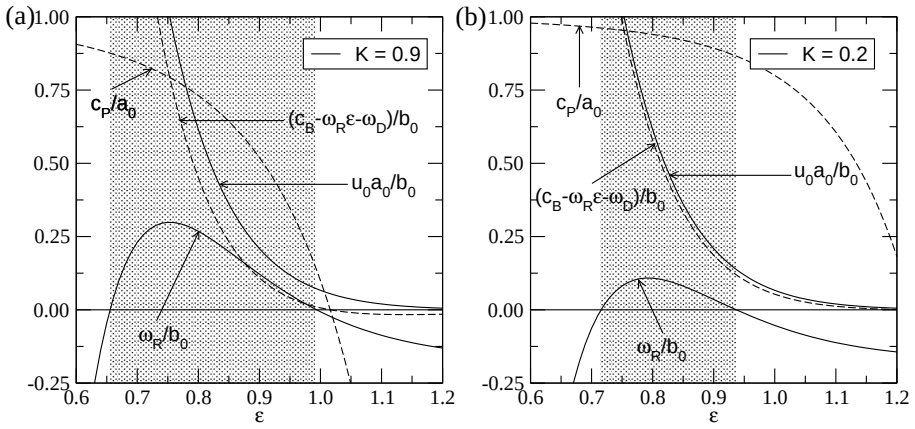

Figure 6.3: *Intervals of allowed parameters.* Same as Figure 6.2 but with $\varphi = 0$ and for two different values of K: (a) $K = 0.9$ and (b) $K = 0.2$. Other parameters remain unchanged except for $\mu = -7.5$. Shaded regions show the intervals where ω_{R} is positive, which determines regions of allowed ϵ. We find that both c_{P} and $c_{\mathrm{B}} - \omega_{\mathrm{R}}\epsilon - \omega_{\mathrm{D}}$ are positive within that interval, leading to stable values of u_0.

In particular, this observation shows that the model without reproduction can never be stable against a perturbation in the overall population density u_0. This instability was already noticed in Datta et al. (2010b), where it was argued that it could be avoided by suitable modifications of the model at the ends of the size-spectrum (plankton dynamics, senescent death). Reproduction processes can thus provide a stabilizing effect.

As we have seen, the stability against variations in u_0 requires that both c_{P} and $c_{\mathrm{B}} - \omega_{\mathrm{R}}\epsilon - \omega_{\mathrm{D}}$ are positive. In Figure 6.3 we plot these coefficients together with u_0 and ω_{R} as functions of ϵ, for two different values of K. As discussed in Section 6.6, the parameter ϵ is only allowed to lie in a certain interval where the maintenance rate is positive, which appears shaded. Within this interval, both c_{P} and $c_{\mathrm{B}} - \omega_{\mathrm{R}}\epsilon - \omega_{\mathrm{D}}$ are seen to be positive, so the steady state is stable in this case.

The region where both c_{P} and $c_{\mathrm{B}} - \omega_{\mathrm{R}}\epsilon - \omega_{\mathrm{D}}$ are negative corresponds to an unstable steady state, as shown in Figure 6.4 with the same parameters but $\mu = -10$. For the following plots we shall choose $\epsilon = 0.9$ as a suitable value leading to a stable steady state (with $\mu \approx -8$) and for the unstable solution we will choose $\epsilon = 1.1$ (for $\mu \approx -10$).

6.7.2 General perturbation

We now consider more general, weight-dependent perturbations. It is convenient to write the density u as

$$u(x,t) = u_0 e^{-\epsilon x}[1 + h(x,t)], \tag{6.47}$$

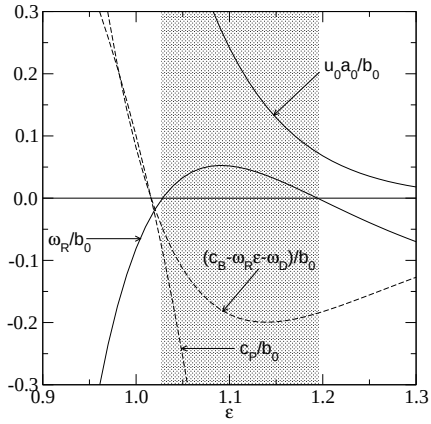

Figure 6.4: *Intervals of allowed parameters.* Same as Figure 6.3a, except that $\mu = -10$. Shaded region show the interval for allowed ϵ but unstable u_0 (note that both $c_{\rm P}$ and $c_{\rm B} - \omega_{\rm R}\epsilon - \omega_{\rm D}$ are negative within the interval).

so that we add a small perturbation $h(x,t)$ to the steady-state solution. Thanks to translational invariance, we can solve the linearized model by means of the standard Fourier transform.

Any perturbation can be expressed as a linear combination of plane waves labeled by a wavenumber k,

$$h_k(x,t) = e^{i(kx+\zeta t)}. \tag{6.48}$$

In terms of that wavenumber, substitution of the plane-wave on the linearized deterministic equation leads to a non-local dispersion relation $\zeta = \zeta(k)$.

The sign of $\lambda(k) = -{\rm Im}[\zeta(k)]$ conditions stability. If $\lambda(k)$ is positive then the amplitude of the plane wave (6.48) with wavenumber k grows exponentially with time, rendering the steady state unstable. The dispersion relation yields $\lambda(k) = \lambda_{\rm P}(k) + \lambda_{\rm B}(k)$ where

$$\begin{aligned}\lambda_{\rm P}(k) = u_0 \int dy\, a(y) \Big[& -(e^{\epsilon y}+1)\cos(ky) \\ & + \int dz e^{\epsilon(y+z)} \chi_{\rm P}(y,z)\left(\cos(kz) + \cos(k(y+z)) - 1\right)\Big]\end{aligned} \tag{6.49}$$

and

$$\lambda_{\rm B}(k) = \int dy \int dz\, \chi_{\rm B}(y,z)\left[e^{-\epsilon y}(\cos(ky)-1) + e^{(\epsilon-1)z}(1-e^{-y})(\cos(kz)-1)\right]. \tag{6.50}$$

Note that the maintenance rate parameter $\omega_{\rm R}$ and the death rate parameter $\omega_{\rm D}$ no longer appear in these expressions. Since a parent always uses weight during spawning, y is

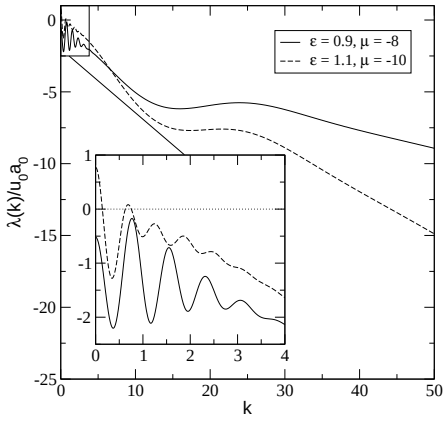

Figure 6.5: *The combined spectrum* $\lambda(k)$ for two combinations of (ϵ, μ). Remaining parameters are: $\beta = 5.5$, $\sigma_\beta = 2.5$, $K = 0.9$, $\sigma_K = 0$, $\sigma_\mu = 0.5$, $\nu = 0.2$ and $\sigma_\nu = 0.05$. Note that $\epsilon = 0.9$ lies in the region of stable u_0, whereas the fixed point for u_0 is unstable for $\epsilon = 1.1$. Inset depicts the region of small k.

positive wherever $\chi_{\mathrm{B}}(y, z)$ is nonzero, and hence we can see that $\lambda_{\mathrm{B}}(k)$ is negative for any nonzero k. This proves that reproduction always has a stabilizing effect.

In the remainder of the section we will discuss the consequences on the stability of the steady state for the choices (6.39), (6.42) and (6.43) for the reproduction and predation functions. Figure 6.5 illustrates the combined eigenvalue spectrum $\lambda(k)$ for two different values of ϵ, corresponding to both a stable ($\epsilon = 0.9$, $\mu = -8$) and unstable ($\epsilon = 1.1$, $\mu = -10$) fixed point u_0. We find that the spectrum for $\epsilon = 0.9$ is everywhere negative, corresponding to a stable steady state. The inset shows that the spectrum for $\epsilon = 1.1$ is positive for small wavenumbers, leading to an instability of the steady state against long-wavelength perturbations. At higher k the spectrum is more negative, exhibiting stronger stability against short-wavelength perturbations.

In Figure 6.6 we show the contribution from predation $\lambda_{\mathrm{P}}(k)$ for two different values of β with $K = 0.9$ and for two different values of K with $\beta = 5.5$. Increasing K from the value 0.2 used in Datta et al. (2010b) has a considerable stabilizing effect. Note that we are allowed to increase K because our model separates out the losses due to maintenance processes. On the other hand, decreasing the preferred body size ratio e^β between predator and prey has a stabilizing effect. Nevertheless, for realistic values of the parameters, the contribution from predation alone is positive at some wavenumbers k.

In order to characterize the effect of variability in K we have considered non-zero mean-square deviations in Figure 6.7. The standard deviation σ_K must be sufficiently small so that the probability that the absorption efficiency is above 100% is negligible.

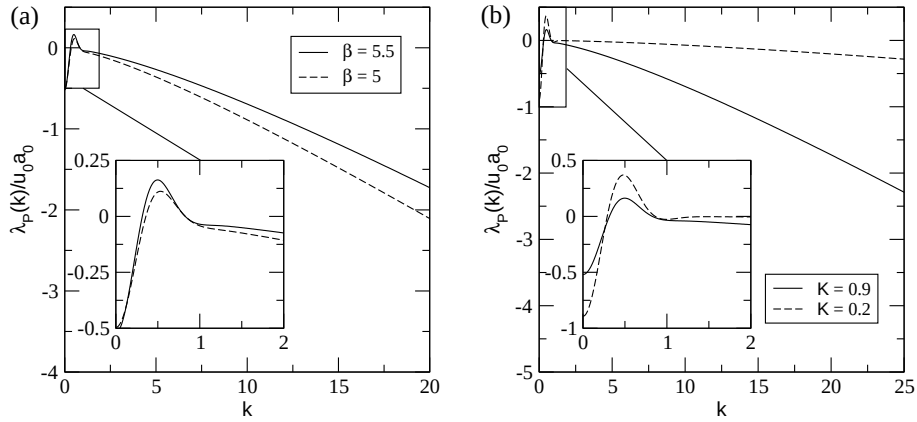

Figure 6.6: *Eigenvalue spectra* $\lambda_{\rm P}$ for two different values of β with $K = 0.9$ (a), and for two different values of K with $\beta = 5.5$ (b). Remaining parameters are: $\sigma_\beta = 2.5$, $\sigma_K = 0$ and $\epsilon = 0.9$. Insets contain zooms of the regions of small k.

This amounts to imposing that

$$\sigma_K \ll (1 - K)e^{-y} \tag{6.51}$$

for some typical value y of the logarithm of the predator:prey mass ratio. In practice, typical values are $1-K \approx 0.1$ and $y \approx 5$, so $\sigma_K \ll 6{\cdot}10^{-4}$. Therefore the fact that the predator:prey mass ratio is so large implies that σ_K has to be very small. To check its influence in stability we have chosen values around 10^{-4}. The effect is negligible for small wavenumbers, although become slightly appreciable for highly oscillating plane waves. In Figure 6.7 we plot the difference $\lambda_{\rm P} - \lambda_{\rm P}^{(0)}$, $\lambda_{\rm P}^{(0)}$ being the real part of the eigenvalue for $\sigma_K = 0$. Although the effect is very small, the variability in the feeding efficiency always enhances the stability of the steady state.

We have also studied the separate effect on stability that reproduction produces for various values for μ and ν. Results are depicted in Figure 6.8. As explained before, reproduction has a stabilizing effect. Changes in μ and ν affect the oscillatory behavior observed in the region of small k.

6.8 Discussion

The power-law size spectrum observed in the pelagic ecosystem will be predicted by any dynamic model that is invariant under scale transformations. The requirement of scale invariance has allowed us to generalize earlier models without spoiling the prediction of a power-law steady state. Where earlier models only include predation and intrinsic mortality effects, we include terms accounting for maintenance costs and

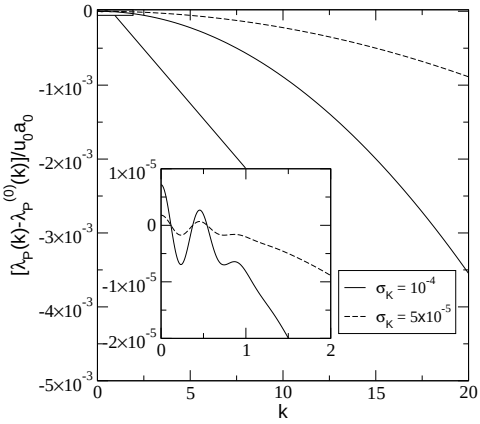

Figure 6.7: *Variability in* K. Here we plot the difference $\lambda_{\rm P}(k) - \lambda_{\rm P}^{(0)}(k)$, where $\lambda_{\rm P}^{(0)}(k)$ is the eigenvalue for $\sigma_K = 0$. The inset represents the eigenvalue spectrum for small wavenumbers. Note that the influence on stability of the variability in K is negligible. Remaining parameters are: $\beta = 5.5$, $\sigma_\beta = 2.5$, $K = 0.9$ and $\epsilon = 0.9$.

reproduction and also allow variability in the absorption efficiency. Inclusion of maintenance and reproduction has increased the stability of the steady-state solution.

By exploiting scale invariance, we can make several observations that are of ecological relevance and that were not explicit in previous work:

1. The spectrum exponent is fixed solely by the scaling properties of the parameters of the model. No detailed investigation of the model and its solutions is required to determine it. The exponent does not depend on details like the preferred predator:prey mass ratio, the feeding efficiency, the variability in feeding behavior, the absorption efficiency, the maintenance costs, the mortality rate, or the details of reproduction. This is in contrast to the results of earlier works in which only predation was considered. In that special case there are not enough scaling relations to fix the steady state exponent and it depends on the details of the model.

   It is a crucial aspect of our model that it contains both processes that are density-dependent (predation) and processes that are density-independent (maintenance respiration, intrinsic mortality, reproduction). It is the relative scaling of the rates for these processes what determines the steady-state power-law exponent.

   Camacho and Solé (2001) studied the spectrum exponent in a model with intrinsic mortality and reproduction. However they assumed that mortality and reproduction rates were proportional to predation rates. Thus, in effect, all their processes were assumed to be density-dependent and again the steady-state exponent was not determined by scaling arguments alone.

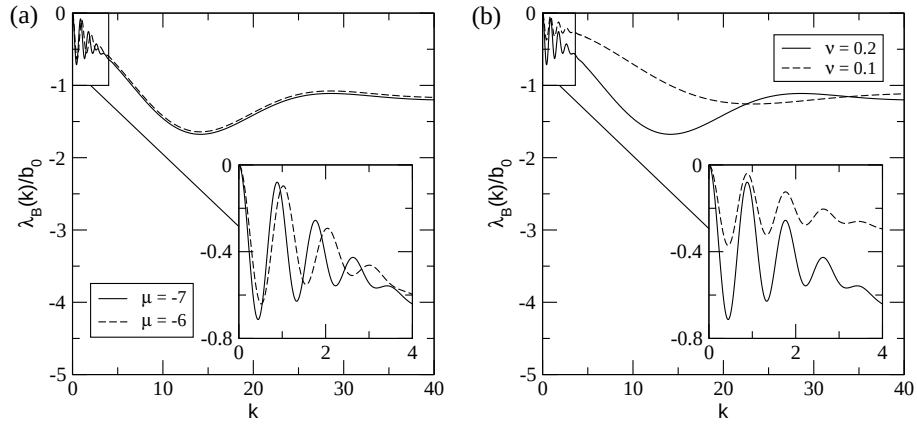

Figure 6.8: *Eigenvalue spectra* $\lambda_{\rm B}$ for two different values of μ with $\nu = 0.2$ (a), and for two different values of ν with $\mu = -7$ (b). Remaining parameters are: $\sigma_\mu = 0.5$, $\sigma_\nu = 0.05$ and $\epsilon = 0.9$. Insets contain zooms of the regions of small wavenumber.

2. The assumption of scale invariance leads to predictions about the scaling behavior (6.19) of the various parameters of the model, which can be tested through observation, as discussed in Section 6.4.

   We can also make a prediction that has not yet been tested. The prey selection function $a(x)$ can be related to data on the stomach contents of fish as follows. This stomach content reflects what prey a fish has been eating recently, which is determined by the same predation rates that we used in constructing the model. The number of individuals of a weight bracket j that are preyed on by a predator belonging to bracket i is $\tau_{\rm d} \sum_k W^{\rm P}_{ijk} N_j/\Omega$, where $\tau_{\rm d}$ is a time scale related to the speed of digestion. In the continuum limit, assuming that the fish density of prey N_j/Ω is close to the steady-state density $\hat{\phi}_i$, we get

   $$\tau_{\rm d} \sum_k W^{\rm P}_{ijk} \hat{\phi}_j \to \tau_{\rm d} \int dw'' W^{\rm P}(w, w', w'') \hat{\phi}(w') dw'. \tag{6.52}$$

   Let $l(x, x')dx'$ be the observed average number of prey with logweight between weight x' and $x' + dx'$ in the stomach of a fish of logweight x. Changing to logweights and using Eqs. (6.25), (6.26) and (6.31) we obtain

   $$l(x, x') = u_0 e^{-\varphi x} a(x - x') \tau_{\rm d} \tag{6.53}$$

   from (6.52). Therefore this model provides a precise prediction for the scaling of the density of prey observed in fish stomachs. There is a lot of data available (Barnes et al. 2008) and it should be possible, via a careful analysis, to determine the scaling exponent φ. We predict that this will confirm that $\varphi \approx 1/4$.

3. From the condition that in the steady state the number of individuals must be conserved we have deduced a relation between the parameters of the model which in particular restricts the exponent ϵ to an interval. For biologically reasonable values of the parameters this interval is around $\epsilon \approx 1$, which is in agreement with observations.

4. The steady state in the model without reproduction and with $\varphi = 0$ is unstable against perturbations in the overall population density u_0. In fact this was our motivation for including a reproduction term in the model. The stability against this perturbation is ensured if the condition (6.46) for the magnitude of the reproduction rate with respect to the magnitude of the maintenance and mortality rates holds.

5. We have studied the stability of the steady state against all small perturbations in the case $\varphi = 0$. The stability is determined by the eigenvalue spectrum $\lambda(k)$, which has two contributions: $\lambda_{\mathrm{P}}(k)$ from predation and $\lambda_{\mathrm{B}}(k)$ from reproduction. Maintenance and mortality do not enter these expressions. The contribution $\lambda_{\mathrm{P}}(k)$ coincides with that calculated in Datta et al. (2010b) in the case of fixed absorption efficiency, however with a conversion efficiency of around 20% replaced by the much larger absorption efficiency K, which turns out to be an important stabilizing effect. The contribution $\lambda_{\mathrm{B}}(k)$ from reproduction is always negative, thus enhancing stability.

6. We have generalized previous models for the predation process to allow for variability in the absorption efficiency and have found that this does not have a big impact on the stability of the steady state.

The power-law size spectrum has been observed over many orders of magnitude and covers not only fish but also all types of plankton and even inanimate particles. Our model is appropriate only for organisms that feed by swallowing smaller organisms and that reproduces by spawning a large number of smaller organisms. It is not appropriate for phytoplankton or inanimate particles. Other models are needed for these and it will be interesting to see how these models can be coupled together.

There is a limit to the amount of detail that can be incorporated into a community size spectrum model. In particular, because only the size of individuals is taken into account, their different behavior in different life stages can not be modeled. A first step in the direction of refining the model was taken in Andersen and Beyer (2006) where an individual is described not only by its size but also by one species-specific trait, namely its size at maturity. That allowed individuals to follow more realistic ontogenetic growth curves. An interesting observation of Andersen and Beyer (2006) was how the size spectra of different species, each of which singles out a particular scale in the form of the maturity size, combine into a power-law community spectrum described by a scale-invariant McKendrick-von Foerster equation.

In Andersen and Beyer (2006) the size of offspring was encoded through a boundary condition on the species' size spectrum but when combining these spectra into a

community size spectrum the boundary condition had to be ignored in order to achieve a power-law steady-state size spectrum. It would be interesting to see if that work could be extended to include a realistic model of the reproduction process and still produce a power-law community spectrum.

In a pure size spectrum model like ours, that does not take life stages into account, a realistic modeling of reproduction is not possible. For example, the offspring of many marine species start their life in an egg stage during which they are not part of the consumer spectrum but are already preyed on. In our model we had to neglect this fact. The scaling relation (6.23) implies that the typical size of offspring is proportional to the size of the parent. However, because we can not model the egg life stage, we can not claim that this gives a reliable prediction for the relation between egg size and parent size. Indeed, while such a relation may hold for copepods (Huntley and Lopez 1992), it certainly does not hold for fish (Fishbase 2010), where most species lay eggs of a similar size.

One might be tempted to simply replace the reproduction function (6.23) by one that represents the fact that most fishes lay eggs of a similar size. However this would immediately lead to a steady state solution that is not a power law. The steady state spectrum would exhibit a peak at the preferred egg size which is not observed in the size-spectrum data. The correct approach is not to break the scale invariance of the community spectrum model, but instead to study how more detailed models at the species level can combine into a scale-invariant model at the community level, in the spirit of Andersen and Beyer (2006), Hartvig et al. (2010). Models at the level of species would have to take into account effects like the duration of the egg stage, the separation between spawning grounds and feeding grounds, the various spawning strategies, like for example the laying of eggs in clusters, and many more. How and why the combination of many such details at the species-level can lead to a power-law spectrum at the community level is an intriguing problem and it is to be hoped that the emergence of scale invariance can be used as guiding principle for further theoretical studies.

V

Conclusions

7

Conclusions and open problems

Science may be described as the art of systematic over-simplification:
the art of discerning what we may with advantage omit.
—Karl R. Popper.

The original work presented in this thesis has been focused on three different complex systems of doubtless biological relevance. The self-organization of these systems is a consequence of the microscopic interactions involved, and a very rich phenomenology arises as a result. The three models studied clearly demonstrate how the techniques commonly used in statistical physics can be rigorously applied to biological systems, and serve as powerful tools to analyze the emergence of patterns in complex systems. All models have been formulated as Markov processes, so we have exploited the theory of stochastic processes all over this work. The fact that the results obtained are of application to other systems in physics and biology highlights the universality of the mechanisms described by these models. We will summarize in this concluding chapter the main results obtained in each part of this thesis and we will discuss some open questions left out for future work.

Viral infection propagation

In the second part of this thesis we have presented a simple epidemiological model of viral infection propagation in a two-dimensional lattice, whose sites are interpreted as susceptible cells. The motivation of our study relies on empirical observations of how

viral infections propagate in environments with different geometrical properties, which is an issue of interest in virology. We have how the competition for cells conditions the spreading of the infection. This struggle for space constitutes a new mechanism leading to the extinction of a heterogeneous ensemble of viral types beyond the error threshold predicted by the classical theory of quasispecies. Our model describes the phenotypic evolution of the quasispecies subject to beneficial, deleterious, and lethal mutations. Hosts can develop defenses to face the pathogen. Viral extinction supervenes when both mutagenesis or host defenses increase beyond a critical threshold. This results in a transition line in the phase space of the system. We have characterized the criticality of this transition as belonging to the universality class of directed percolation. Our main conclusion relies on the limitation of the advantage that viral types can obtain from increasing their progeny caused by spatial constraints. Hence the propagation of viral infections shows a completely different phenomenology when individuals get their mobility reduced (e.g., propagation in tissues or plant leaves). But more importantly, the geometry of the environment is critical when it comes to infection clearance. Quasispecies models have motivated the development of specific experiments aimed at testing theoretical predictions (as the error threshold) and have even led to the design of control therapies. Therefore, the implications of a new extinction mechanism and the current knowledge on percolation processes might be key to devising new control strategies leading to the clearance of viral infections.

One should bear in mind that our model, described by the probabilistic rules (2.17)–(2.18), defines a multicomponent generalization of the DK cellular automaton. Our model only explores a limited region of its parameters in which an active-inactive transition ($q > 0$) or several ($q = 0$) occur with the criticality of directed percolation. Exploring in depth the whole phase space of this multicomponent DK automaton in search for deviations of this behavior is an interesting open question left out by the present study. Besides, it is worth remarking the importance of knowing the universality class of the infection propagation. Current knowledge of models of different nature belonging to the same universality class can help to a better understanding of the propagation of infections constrained by spatial limitations.

The effect of genetic complementation has not been included in the model. We consider that the replicative ability of a viral type is entirely determined by each phenotypic class, and that there are no trans-interactions between phenotypes affecting their replicative ability. Therefore the inclusion of cross interactions between phenotypes of different replicative abilities, resulting in an "effective" replicative ability, could change the results reported in Chapter 2. The inclusion of genetic complementation in the model would be an interesting pathway for future investigations.

At present, this model constitutes a minimal approach to the actual propagation of viral infections in two dimensions. As such, further effects can be introduced in the model to study new mechanisms leading to viral clearance or to tackle different, more realistic situations. As pointed out in Chapter 2, different individuals often develop different abilities to fight the infection. In reality, the cell resistance parameter π is a host-dependent variable, hence the propagation in crops —for example— can be modeled by just including quenched spatial disorder. The randomness in the spatial config-

uration occurs as a consequence of having a heterogeneous distribution of individuals occupying fixed positions in space. It is well known that percolation in the presence of spatially quenched disorder leads to universality classes different from DP (Hinrichsen 2000). Age-dependence of host susceptibility to infection can be explicitly considered in the model by introducing temporally quenched disorder. Further effects like host superinfection or the increase on viral mobility (i.e., increasing the number of neighbors available to the pathogen) remain as pending tasks for future studies.

Ecosystem assembly

In the third part of this thesis we have modeled ecological communities as trophic networks. We have introduced a simple model of ecosystem assembly for which the whole phase space is displayed as a directed graph whose nodes are communities and whose links are transitions between them induced by invasion events. The model exhibits a unique set of communities —i.e., the end state of the process— which is resistant to subsequent invasions. In spite of its simplicity, the model shares most of the features with standard assembly models reported in the literature. We have discussed at length the results provided by the model in Chapter 3 as well as some analytical calculations in Chapter 4 that explain the observed phenomenology. In Chapter 5 we have introduced a background extinction rate in our model, which leads to the observation in finite size of a phase transition between a species-rich and a species-poor attractor. This simple modification introduced in the model serves as an illustration of the spirit of this thesis: in a minimalistic model like ours, the addition of a new effect is easy to deal with, and as a result the model can reveal an entirely new phenomenology.

The model has several limitations, though. Perhaps the most important one is the choice of the Lotka-Volterra equations. Different choices of population dynamics have been reported to influence strongly in the final shape of ecological communities (Drossel et al. 2004; Lewis and Law 2007). Introducing nonlinear equations leads to more complex stability patterns than simply rest points. How to account for them is not yet clear to us, but neither is whether this will really affect the qualitative behavior of the assembly process. Thus, this remains an important open question that deserves further analysis.

On the other hand, it can be argued that parameters should depend on the trophic level rather than being uniform for all species. This refinement does not change the dynamic stability patterns, because Eq. (3.11) provides a Lyapunov function even for this general case. We have not attempted any test in this direction, but it is hard to believe that such a variant of the model will produce any qualitative difference. The assembly graphs are expected to be similar to the ones found for the present model. Something more can be said about the invasion rate. We have presently assumed that the invasion probability is the same for all trophic levels, but notice that the assembly graph is utterly independent on this choice (as long as invasion probabilities are nonzero), so certainly choosing a different invasion probability will change the numerical value of the nonzero entries of the transition matrix P [Eq. (3.24)], but only them. The

graph, as well as the structure of transient and recurrent states of any finite Markov chain, only depends on which elements of P are zero (Karlin and Taylor 1975), so not just the graph but the set of communities in the end state will be exactly the same as those reported here (the probability distribution in the steady state will, of course, be different).

Our assembly model is based on several assumptions regarding the invasion process. Two of the most important ones are that newcomers invade at low population and the average time between invasions is large compared to the time for the communities to reach the equilibrium. If the invasion rate is too high (Fukami 2004; Bastolla et al. 2005b) or if the invasion is not produced by rare species (Hewitt and Huxel 2002), the assembly process —and hence the resulting end states— can be drastically altered. The reason is that communities non-accessible from the equilibrium state may be so from a transient or if there is a massive invasion. This changes the assembly graph in ways that we can neither predict nor even check, because these processes are out of reach of our model. For instance, considering invading transients, one of the strong simplifications we make use of is that of starting always from a well-defined initial condition, namely the equilibrium state. If the system can be invaded at any moment during a transient there are infinitely many initial conditions to start off from, something we cannot implement. So what happens if any of those two hypotheses is violated remains an open question.

Let us discuss now on further extensions of the model. We are currently working on some of them, and can provide some preliminary results.

Species diversification

One of the most drastic simplifications of our model is the species symmetry assumption. The neutrality of the model, i.e., the indistinguishability of species regarding both their feeding relations and the interaction strengths involved, is something that could affect the results. It is not clear to what extent the simplified food-web topology that we are assuming conditions the results arising from the model. In order to elucidate this issue we can introduce a variant of the model which, without loosing its features, allows for a larger species diversification.

So far the trophic level is the only niche variable that characterizes species in our model. However, we can increase the number of species traits without causing a combinatorial blow-up in the number of viable communities. Species traits will modify species feeding abilities —hence their interaction strengths. We can assume that this modification assigns a finite set of values to those strengths. Consider, for instance, body size as a specific species trait. According to body size, species would be roughly classified either as “large” or “small”. Let us assume that both types of species can occupy every trophic level. The transferred energy from prey to predators will therefore depend on their respective sizes: if both predator and prey have the same size, the biomass transfer rate from prey to predator is still given by γ_+. If a large predator feeds on a small prey this transfer rate is reduced by a factor $r < 1$. Finally, a small predator can not feed on large prey in a level below because body size acts as a defensive mech-

anism. As for the mean damage caused by predation (i.e., the interactions involving γ_-), it will be constant and equal to γ_- —because each predation event always causes the removal of a prey— except for the case of small predators and large prey, which do not the interact.

Another example of trait that tunes predation is species speed. We could classify species either as "fast" or "slow". Fast predators can feed on any prey, but obtain a larger energetic benefit if the hunting process is fast (we can assume again that a factor $r < 1$ reduces the benefit when a fast species tries to feed on another fast species). Slow predators can not feed on fast prey. Similarly, the mean damage caused by predation is uniform except for the latter case, for which it is zero. These two traits —size and speed— can be combined together and the corresponding rates can be obtained as products of the relative rate of each trait separately, maybe neglecting factors $\mathcal{O}(r^2)$ —this would preclude, for example, the feeding of a small, fast prey by a large, fast predator. All these considerations would make our model to depart from the assumption of species symmetry within trophic levels.

Similarly, direct competition would depend on the set of traits that define each species. As we mentioned in Chapter 3, direct competition can be accounted for as the number of shared prey between species i and j relative to the total number of prey of both species. Hence a possible way of writing the competition factor would be

$$\rho_{ij} = \frac{|\pi_i \cap \pi_j|}{|\pi_i \cup \pi_j|}, \tag{7.1}$$

where π_i stands for the set of prey of species i (and $|A|$ denotes the cardinal of set A).

The most important fact that this variant of the model should address is whether the uniqueness of the end state persists, or on the contrary there are different end states of the process. An appropriate choice of traits could make different combinations of them equally beneficial for species. Then, depending on the assembly history, the end state might induce the selection of a particular sets of traits. Were this the case, it would be a relevant finding. The reason is two-fold: first, a damaged community with some extinct species might not be eventually restored to its initial state for purely contingent reasons, depending on whether the restoring invasion sequence is contained in the assembly graph or not. On the other hand, the sequence of invasions might induce *epistasis*[1] in the genes that determine those traits, and these epistatic effects would not be caused by molecular factors. This effect of gene selection would constitute a manifestation of the evolutionary influence of the highest level (the ecosystem) on the lowest level (genes).

Stochasticity and structural stability

We have mentioned that our model is neutral in the sense that it does not make any explicit distinction between species interactions (except for the different relative strength

[1] Epistasis is the phenomenon by which the phenotypic effects of one gene are modified by molecular interactions with one or several other genes. The gene whose phenotype is expressed is said to be epistatic, while the phenotype altered or suppressed is said to be hypostatic.

between intra- and interspecific competition). Species extinction supervenes in neutral models due to demographic stochasticity. The role that our extinction level n_c plays in the model is to mimic such stochasticity in populations close to extinction. Therefore, including stochastic effects in our model would be interesting *per se*.

Related to the neutrality assumption the concept of structural stability arises. The problem of species coexistence and its relation with the competitive exclusion principle was discussed in Chapter 3. Regarding species coexistence, the main result obtained by Bastolla et al. (2005a) is that mean-field dynamics like ours allow for a relative variance in the interaction strengths limited by certain upper bounds. Those bounds depend on the number of species that the community can hold as S^{-1}, so the higher the biodiversity the more restrictive the bound is and the less the system tolerates variability in the parameters. In this sense diversity and structural stability oppose each other.

Although the structural stability of our communities is granted by the aforementioned bounds, we have not studied whether they are fragile or not for fixed relative variances in the interaction strengths. It could happen that the variability imposed on a diverse community would render it unstable according to those bounds. In order to ascertain this, we have extended our population dynamics in order for the model to depart from neutrality. Now the requirement of structural stability replaces the former viability condition.

Our discussion will be centered on species coexistence at dynamical equilibrium. The interior equilibrium point for the mean-field system, $\mathbf{p}$, can be obtained by solving the linear system (3.16), i.e., it has the form

$$\mathsf{M}\mathbf{p} = \mathbf{a} \tag{7.2}$$

where matrix $\mathsf{M} = (M_{ij}^{\ell_1\ell_2})$ is block-tridiagonal with entries

$$M_{ij}^{\ell_1\ell_2} = \gamma_+^{\ell_2}\delta_{\ell_1-1,\ell_2} - [(1-\rho^{\ell_2})\delta_{ij} + \rho^{\ell_2}]\delta_{\ell_1,\ell_2} - \gamma_-^{\ell_2}\delta_{\ell_1+1,\ell_2}. \tag{7.3}$$

$M_{ij}^{\ell_1\ell_2}$ stands for the interaction strength between species i at level ℓ_1 (for all $i = 1,\ldots,s_{\ell_1}$) and species j at level ℓ_2 ($j = 1,\ldots,s_{\ell_2}$). All constants in (7.3) are uniform across species of the same level. Matrix elements are defined for $1 \leq \ell_1, \ell_2 \leq L$, L being the total number of trophic levels of the community. The elements of vector $\mathbf{a}$ are the growth rates α^ℓ. The 0-th row of M —related to the resource— is

$$M_{ij}^{0\ell} = -\delta_{ij}\delta_{0\ell} - \gamma_-^{\ell}\delta_{1\ell}, \tag{7.4}$$

and $a_0^0 = -R$. We have shown in Section 3.4 that the equilibrium point that results from this system has uniform population densities within each level (provided that all interaction strengths are independent of the trophic level).

A general, trophic-level structured food-web will have different interaction strengths between species. Equilibrium densities will vary from one species to another, even within the same level. We now introduce a stochastic component in each interaction strength. For a given set of species, interaction strengths will be distributed around the average strength with some variability. Then the stochasticity in strengths arises

from their variation from one species to another. For a particular species, its interaction strength remains fixed (i.e., the stochastic component is not associated to noise or any other source of fluctuation). We can therefore assume that different strengths are different trials of a given stochastic distribution. In this sense, we are introducing "quenched" fluctuations in the set of parameters due to variations in the constants for different species. This stochasticity will induce a probability for a given community to be viable. Let us calculate now this probability under certain assumptions.

The system for the interior equilibrium point transforms into

$$(\mathsf{M}+\Delta\mathsf{M})(\mathbf{p}+\Delta\mathbf{p})=\mathbf{a}+\Delta\mathbf{a}, \tag{7.5}$$

where matrix $\Delta\mathsf{M}=(\Delta\mathsf{M}_{ij}^{\ell_1\ell_2})$ is defined by

$$\begin{aligned}\Delta\mathsf{M}_{ij}^{\ell_1\ell_2}&=\Delta A_{ij}^{\ell_2}\delta_{\ell_1-1,\ell_2}-\Delta B_{ij}^{\ell_2}\delta_{\ell_1,\ell_2}-\Delta C_{ij}^{\ell_2}\delta_{\ell_1+1,\ell_2},\\ \Delta\mathsf{M}_{ij}^{0\ell}&=-\Delta B^0\delta_{0\ell}-\Delta C_{ij}^{\ell}\delta_{1\ell}.\end{aligned} \tag{7.6}$$

Each fluctuation is simply the difference between the actual value of the interaction strength and the corresponding averaged value. To be precise, we have the following definitions:

$$\begin{aligned}\Delta A_{ij}^{\ell}&=A_{ij}^{\ell}-\gamma_{+}^{\ell}, && \ell=0,\dots,L-1,\\ \Delta B_{ij}^{\ell}&=B_{ij}^{\ell}-(1-\rho^{\ell})\delta_{ij}-\rho^{\ell}, && \ell=0,\dots,L,\\ \Delta C_{ij}^{\ell}&=C_{ij}^{\ell}-\gamma_{-}^{\ell}, && \ell=1,\dots,L,\end{aligned} \tag{7.7}$$

where A_{ij}^{ℓ}, B_{ij}^{ℓ} and C_{ij}^{ℓ} are the actual interaction strengths observed in the food-web. The vector on the r.h.s. of Eq. (7.2) has a fluctuation component defined by $\Delta a_i^{\ell}=a_i^{\ell}-\alpha^{\ell}$ ($\ell=1,\dots,L$) and $\Delta a_0^0=-a_0^0+R$ (once again, a_i^{ℓ} stand for the stochastic growth rates).

We assume that all the fluctuations $\Delta\mathsf{M}$ and $\Delta\mathbf{a}$ are independent, Gaussian stochastic variables with zero mean and a given (uniform) variance. Under this assumption, the probability distribution of the fluctuation vector $\Delta\mathbf{p}$ remains undetermined. However, the solution to (7.5) can help to determine this unknown distribution. The formal solution of this system is

$$\Delta\mathbf{p}=\mathsf{M}^{-1}\Delta\mathbf{a}+\sum_{k=1}^{\infty}(-\mathsf{M}^{-1}\Delta\mathsf{M})^k\mathsf{M}^{-1}(\mathbf{a}+\Delta\mathbf{a}). \tag{7.8}$$

The simplest case is obtained neglecting next-to-leading order corrections in fluctuations. This yields

$$\Delta\mathbf{p}=\mathsf{M}^{-1}\left(\Delta\mathbf{a}-\Delta\mathsf{M}\mathsf{M}^{-1}\mathbf{a}\right). \tag{7.9}$$

Therefore, in the limit of small fluctuations $\Delta\mathbf{p}$ is a linear combination of Gaussian stochastic variables, hence the fluctuations in population densities are Gaussian in this limit. The particular dependence of $\Delta\mathbf{p}$ given by Eq. (7.9) will introduce correlations

between each Δp_i and we have to calculate the covariance matrix in order to obtain the multivariate distribution of the vector $\Delta\mathbf{p}$ of stochastic variables.

The probability density function of a vector $\mathbf{x}$ of q Gaussian stochastic variables is the so-called multivariate normal distribution,

$$f(\mathbf{x}) = \frac{1}{(2\pi)^{q/2}|\mathsf{\Lambda}|^{1/2}} \exp\left\{-\frac{1}{2}(\mathbf{x}-\boldsymbol{\zeta})^{\mathsf{T}}\mathsf{\Lambda}^{-1}(\mathbf{x}-\boldsymbol{\zeta})\right\}, \tag{7.10}$$

where $\boldsymbol{\zeta}$ is the vector of mean values and the symmetric, positive-definite matrix $\mathsf{\Lambda} = \langle \mathbf{x}\mathbf{x}^{\mathsf{T}}\rangle$ is known as covariance matrix. Our vector of $S+1$ stochastic variables satisfy $\boldsymbol{\zeta} = \langle\Delta\mathbf{p}\rangle = \mathbf{0}$ and their covariance matrix $\langle\Delta\mathbf{p}\Delta\mathbf{p}^{\mathsf{T}}\rangle$ follows from (7.9) and the variances of each parameter. We find that the covariance matrix satisfies the equation

$$\mathsf{M}\langle\Delta\mathbf{p}\Delta\mathbf{p}^{\mathsf{T}}\rangle\mathsf{M}^{\mathsf{T}} = \langle\Delta\mathbf{a}\Delta\mathbf{a}^{\mathsf{T}}\rangle + \langle\Delta\mathsf{M}\mathbf{p}\mathbf{p}^{\mathsf{T}}\Delta\mathsf{M}^{\mathsf{T}}\rangle. \tag{7.11}$$

Assuming that the variances of the stochastic variables ΔA_{ij}^{ℓ} are uniform and independent of both the species index and the level index means that $\langle\left(\Delta A_{ij}^{\ell}\right)^2\rangle = \sigma_{\mathrm{A}}^2$ for all i, j and ℓ in their respective ranges. Similar formulae hold for the variances σ_{B}^2, σ_{C}^2 and σ_{a}^2. We will assume that the coefficient of variation of any parameter X, $\mu \equiv \sigma_{\mathrm{X}}/\langle X\rangle$, is constant and small, so that the limit of small fluctuations holds.[2]

Obviously $\langle\Delta\mathbf{a}\Delta\mathbf{a}^{\mathsf{T}}\rangle_{ij}^{\ell_1\ell_2} = \sigma_{\mathrm{a}}^2\delta_{ij}\delta_{\ell_1\ell_2}$ is a diagonal matrix, due to stochastic independence. In order to determine the covariance matrix we have to calculate the average $\langle\Delta\mathsf{M}\mathbf{p}\mathbf{p}^{\mathsf{T}}\Delta\mathsf{M}^{\mathsf{T}}\rangle$. It turns out to be diagonal as well. The matrix element to average is

$$(\Delta\mathsf{M}\mathbf{p}\mathbf{p}^{\mathsf{T}}\Delta\mathsf{M}^{\mathsf{T}})_{ij}^{\ell_1\ell_2} = \sum_{\ell_3\ell_4} p^{\ell_3}p^{\ell_4}\Delta\mathsf{M}_{i\cdot}^{\ell_1\ell_3}\Delta\mathsf{M}_{j\cdot}^{\ell_2\ell_4}, \tag{7.12}$$

where $X_{i\cdot} \equiv \sum_j X_{ij}$. Taking (7.6) into account, and omitting cross terms (which do not give any contribution to averages due to stochastic independence), we obtain

$$\begin{aligned}(\Delta\mathsf{M}\mathbf{p}\mathbf{p}^{\mathrm{T}}\Delta\mathsf{M}^{\mathrm{T}})_{ij}^{\ell_1\ell_2} = {} & p^{\ell_1-1}p^{\ell_2-1}\Delta A_{i\cdot}^{\ell_1-1}\Delta A_{j\cdot}^{\ell_2-1} + p^{\ell_1}p^{\ell_2}\Delta B_{i\cdot}^{\ell_1}\Delta B_{j\cdot}^{\ell_2} \\ & + p^{\ell_1+1}p^{\ell_2+1}\Delta C_{i\cdot}^{\ell_1+1}\Delta C_{j\cdot}^{\ell_2+1} + \ldots.\end{aligned} \tag{7.13}$$

Now we take averages on this expression. We have, for example,

$$\langle\Delta A_{i\cdot}^{\ell_1-1}\Delta A_{j\cdot}^{\ell_2-1}\rangle = \left\langle \sum_{p=1}^{s_{\ell_1-1}} \Delta A_{ip}^{\ell_1-1} \sum_{q=1}^{s_{\ell_2-1}} \Delta A_{jq}^{\ell_2-1} \right\rangle = s_{\ell_1-1}\delta_{\ell_1\ell_2}\delta_{ij}\sigma_{\mathrm{A}}^2, \tag{7.14}$$

since all matrix elements are independent and there is no correlation between blocks of different levels. Analogous formulae hold for matrices B^{ℓ} and C^{ℓ}. Hence we get

$$\langle\Delta\mathsf{M}\mathbf{p}\mathbf{p}^{\mathrm{T}}\Delta\mathsf{M}^{\mathrm{T}}\rangle_{ij}^{\ell_1\ell_2} = \delta_{ij}\delta_{\ell_1\ell_2}\left[s_{\ell_1-1}(p^{\ell_1-1}\sigma_{\mathrm{A}})^2 + s_{\ell}(p^{\ell_1}\sigma_{\mathrm{B}})^2 + s_{\ell_1+1}(p^{\ell_1+1}\sigma_{\mathrm{C}})^2\right]. \tag{7.15}$$

[2]There is a peculiarity with the variances $\langle(\Delta a_0^0)^2\rangle$ and $\langle(\Delta B^0)^2\rangle$, though. These variances refer to resource parameters (i.e., the growth rate of the resource, R, and its carrying capacity R/B^0). They can fluctuate in time, but such a fluctuation should be modeled as an external noise. The kind of fluctuations that we are considering arise from the variability of interaction strengths for different species. Since the resource is unique, its corresponding variances are equal to zero, i.e., $\langle(\Delta B^0)^2\rangle = 0$ and $\langle(\Delta a_0^0)^2\rangle = 0$.

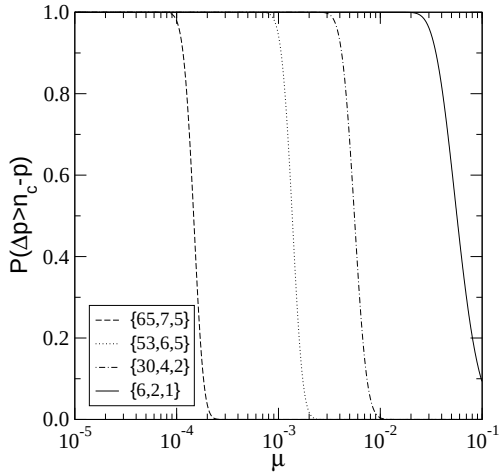

Figure 7.1: *Structural instability due to stochastic fluctuations of parameters.* The probability of coexistence of all species is plotted as a function of μ. Remaining parameters are: $R = 450$ (which allows up to 3 trophic levels when $\mu = 0$), $\alpha = 1$, $\rho = 0.3$, $\gamma_+ = 0.5$, $\gamma_- = 5$, $n_\mathrm{c} = 1$. The legend shows the number of species in each level in the mean-field communities (i.e., for $\mu = 0$). Communities close to (but above) the extinction threshold for $\mu = 0$, such as $\{65, 7, 5\}$, now become unstable for tiny deviations. Communities less biodiverse, such as $\{6, 2, 1\}$, tolerate larger fluctuations.

When $\ell_1 = 0$ we obtain

$$\langle \Delta \mathsf{M} \mathbf{p}\mathbf{p}^\mathrm{T} \Delta \mathsf{M}^\mathrm{T} \rangle_{ij}^{0\ell} = \delta_{ij}\delta_{0\ell} s_{\ell+1} (p^{\ell_1+1}\sigma_\mathrm{C})^2. \tag{7.16}$$

In practice, to determine whether the species forming a community are likely to coexist, we have to calculate the probability that $p_i + \Delta p_i \geq n_\mathrm{c}$ for all i, i.e.,

$$P(\Delta \mathbf{p} \geq n_\mathrm{c}\mathbf{1} - \mathbf{p}, \Delta p^0 \geq -p^0), \tag{7.17}$$

where $P(\mathbf{x})$ is the multivariate normal cumulative distribution. In order to compute it we apply the algorithm provided by Genz (1992), which uses the Cholesky factorization of the correlation matrix [i.e., the matrix whose elements are the normalized covariances $\sigma_{ij}/(\sigma_i\sigma_j)$] as well as a reordering of the integrals involved. This method works for multivariate normal distributions of up to 500 variables. It is based on Monte-Carlo integration, which turns out to be surprisingly efficient for this computation.

Varying μ we get the probability of coexistence shown in Figure 7.1. The main effect that fluctuations in the parameters cause to mean-field communities is to render communities close to the extinction threshold unstable. The reason is obvious: those communities tolerate small relative fluctuations in the parameters. As long as the community is less biodiverse (hence far away from the threshold), there is a wider range of tolerated fluctuations.

We intend to use this kind of calculations to construct an assembly graph by obtaining the probability that a particular species population is lower than n_c. This probability weights the link from the former community to the community with that species removed. Species can be accommodated by invasions, as in the current model, but this time we will not use the (deterministic) dynamics to obtain the sequence of species removed after a destructive invasion has occurred. In order for the Markov chain to be finite, we can set a (small) threshold probability so that the community persists over time only if the probability of coexistence [i.e., Eq. (7.17)] is above that threshold.

The upper bounds in productivities that Bastolla et al. (2005a) find limit the number of species that can coexist in a community, thus providing a (structural) stability criterium. However, under our approach, any community has certain probability to be stable, hence leading to species coexistence. Thanks to the connection between the assembly process and a Markov chain there will be a subset of communities highly visited (i.e., those structurally stable) but less-stable communities can be visited as well. We expect to find the same shape of ecological networks found by Lässig et al. (2001), since we have two opposite effects: the assembly dynamics tends to fill trophic levels up to their maximum occupancies, but when spontaneous extinctions come into play the first level to collapse is the basal level. Hence we expect that the requirement of structural stability, under this stochastic interpretation, will favor communities for which the second trophic level is the most occupied one. In any case, we do not expect the exhaustion of trophic levels, as our current model predicts, since communities close to the extinction level will tolerate small fluctuations.

This variant of our model will render the Markov chain ergodic, hence the dependence on history can not be addressed by the determination of recurrent states. However, we could eventually obtain separate regions in the configuration space with high probability. If several disjoint subsets of highly-visited communities were found, we would have the counterpart of our end states of recurrent communities provided that the time to move from one subset to another is long enough. This way the effect of history dependence could be interpreted under this stochastic formulation of the model.

Metacommunities

There are further open questions such as the application of this model to metacommunities. The resulting ecosystems can be readily altered when migration takes place among spatially distributed patches. With a simple model like ours, it might be possible to build up an assembly graph between different communities in different patches. The interplay between communities in different patches could lead to an outcome different from the one we obtain for a single patch. On the other hand, a simple model like this can provide us with basic understanding of complex processes such as, for instance, the rebuilding of a natural community after its degradation. Very little is known about the processes that help to reconstruct damaged communities, and a simple framework like ours could provide some hints about how to tackle this problem from a theoretical point of view.

Quasispecies	*Metacommunity*
Genotypes	Communities in each patch
Mutation rate	Invasion rate
Fitness	Structural stability
Adaptive landscape	Assembly graph
Mutation probabilities	Transition probabilities

Table 7.1: *Analogy between quasispecies and metacommunities.*

The extended version of the model to metacommunities allows for establishing an analogy with quasispecies models (see Table 7.1). In a quasispecies, an ensemble of coexisting genotypes evolves as a result of high mutation rates.[3] A metacommunity is an ensemble of communities, distributed spatially, which interact with each other as a result of migrations between patches. Hence each particular community in a patch can be interpreted as the counterpart of a genotype in a quasispecies. Communities change "pointwise" their composition due to colonizations of species from different patches. Thus the invasion rate would correspond to the mutation rate under this viewpoint.

Whether an invasion is accepted or not in each community will depend on the structural stability of the extended community. It is precisely this type of stability what determines the transition probabilities according to the stochastic version of our model presented in the previous subsection. Hence the structural stability of each community can be regarded as a "fitness", and selection acts on communities according to their structural stability. The metacommunity will evolve in its configuration space (i.e., the assembly graph), which in turn corresponds to the adaptive landscape of the quasispecies, and the transition probabilities in the graph would be the counterpart of the mutation probabilities in the quasispecies.

The similarity between these two models goes beyond a formal analogy and could be further exploited. For example, it could happen that the Markov chain associated to the metacommunity would lead to a stationary probability distribution such that a single set of communities has a high structural stability compared to the remaining communities in the configuration space. Were this the case, the metacommunity model would reproduce a single-peak landscape similar to that of Eigen's theory. Hence the error catastrophe of the quasispecies could be translated into an "extinction catastrophe" in the metacommunity, in which the most stable community disappears as long as migrations take place at a very large rate.

[3]There are two limits in evolutionary models depending on the mutation rate: population genetics models in the limit of low mutation rates, and quasispecies models in the limit of high mutation rates. Therefore the current version of our assembly model would correspond to the limit of population genetics. In contrast, a metacommunity would play the role of a quasispecies in this analogy.

Marine size spectra

In the fourth part of this thesis we have introduced and discussed a model for population dynamics in size-structured food-webs. We have applied scale invariance in the construction and analysis of a size-structured dynamical population model. The model accounts for the basic processes of predation, reproduction, maintenance respiration and intrinsic mortality, and constitutes an extension of earlier models based on the McKendrick-von Foerster equation (Silvert and Platt 1978). The exponent of the power-law steady-state solution is determined by the relative scaling between the rates of the density-dependent processes (predation) and the rates of the density-independent processes (reproduction, maintenance, mortality). A linear stability analysis of the power-law steady-state solution has shown that inclusion of maintenance respiration and reproduction in the model stabilizes the size spectrum.

In the future we intend to extract further interesting information from the model by taking more detailed ecological information into account. In particular, some theoretical results from metabolic theories regarding energy budgets (Kooijman 2000; Nisbet et al. 2000; Brown et al. 2004) can help to determine the relative strength of the various processes in our model. Observational data will also provide appropriate choices of the parameters.

Our stability analysis was restricted to the case $\varphi = 0$. In this case the symmetry generated by time-translations and scale transformations simplifies to the symmetry group of translations in time and logweight. This allowed us to perform the stability analysis in terms of plane waves. It would be nice if the technique could be extended to the general symmetry of time-translations and scale transformations, which will allow for the stability analysis of the observed mortality rate exponent $\varphi = 1/4$. However, the symmetry group when $\varphi \neq 0$ is non-commutative, so techniques from non-commutative harmonic analysis (Kirillov 1994) would have to be applied.

When age dependence is included in size-structured population models, at the species level a maximum size arises —the so-called size at maturation—, which constitutes a species trait. Individuals can not be larger that their maximum size. This introduces a cut-off in the species size spectra, which precludes any attempt to exploit scale invariance to the size spectra at the species level. However, although species do not exhibit power-law spectra, the community spectrum (i.e., the integral of all species spectra over those asymptotic sizes) has to match the observational power-law-shaped spectrum. The work by Andersen and Beyer (2006) is a first attempt in this direction, based on the assumption that the steady-state at the species level follows the McKendrick-von Foerster equation. They recover the community spectrum as a power law, although at the species level the solution exhibits a cut-off at every species asymptotic size. These authors limit themselves to the study of the steady state. It would be interesting, though, to check whether the steady state is stable against small perturbations.

Another important issue that should be addressed is to reconcile the two ways of modeling ecosystems: the more traditional food-web viewpoint and the recent modeling based on body size, ignoring species taxonomy. In this sense, Hartvig et al. (2010)

present for the first time a generic food-web framework suitable for modeling systems where the populations have a large difference between size as offspring and size at maturation. In such systems individuals encounter predators and prey from different trophic levels as they grow (life history omnivory) —an ecological fact that traditional unstructured food-web models ignore. Any progress along this line of research will stand as a breakthrough in the theoretical understanding of ecological communities.

VI

Appendices

A

The Domany-Kinzel cellular automaton

Cellular automata (CA) are discrete, spatially extended dynamic systems. These systems are composed of adjacent cells or sites arranged as a regular d-dimensional lattice, which evolve in discrete time steps. Each cell is characterized by an internal state whose value belongs to a finite set. The update is performed simultaneously according to a common local transition rule involving only a neighborhood of each cell.

Depending on the type of updates, we distinguish between deterministic and stochastic cellular automata. We shall limit ourselves to stochastic automata [which are known as *probabilistic* cellular automata (PCA)]. A general classification of PCA can be found in Wolfram (1983).

A.1 Markov processes and probabilistic cellular automata

PCA are formulated as discrete-time *Markov processes*. A stochastic process is Markovian if all sites are updated simultaneously and the probability of any particular future behavior, when its current state is known exactly, is not changed by additional knowledge of its past behavior. Conceptually, a Markov process is the probabilistic analogue of the processes treated by classical mechanics, where the future development is completely determined by the present state and is independent of the way in which the present state has evolved.

Formally, the process $\{X_t\}$ is said to be Markovian if

$$\Pr\{X_{t_n} = x_n | X_{t_0} = x_0, \ldots, X_{t_{n-1}} = x_{n-1}\} = \Pr\{X_{t_n} = x_n | X_{t_{n-1}} = x_{n-1}\} \tag{A.1}$$

whenever successive times satisfy $t_0 < t_1 < \cdots < t_n$ (x_n stands for the value of X_{t_n} at time t_n and is termed "realization" or "state" of the process; the set $\{x_n\}$ of all possible states is called the configuration space of the process). The process is fully determined once the conditional probabilities

$$\omega(x_n|x_{n-1}) \equiv \Pr\{X_{t_n} = x_n | X_{t_{n-1}} = x_{n-1}\} \tag{A.2}$$

and the initial probability distribution $\Pr\{X_{t_0} = x_0\} = p_{x_0}$ are specified. We shall now prove this fact, restricting ourselves —without loss of generality— to the case of discrete time ($t_n = n$). Thus X_{t_n} will be denoted as X_n.

It is enough to show how to compute the quantities

$$\Pr\{X_0 = x_0, X_1 = x_1, \ldots, X_n = x_n\}, \tag{A.3}$$

as any probability may be obtained by summing terms of this form. By definition of conditional probabilities,

$$\begin{aligned}\Pr\{X_0 = x_0, \ldots, X_n = x_n\} = \Pr\{X_n = x_n | X_0 = x_0, \ldots, X_{n-1} = x_{n-1}\} \\ \times \Pr\{X_0 = x_0, \ldots, X_{n-1} = x_{n-1}\}.\end{aligned} \tag{A.4}$$

Now by the Markov property (A.1)

$$\Pr\{X_n = x_n | X_0 = x_0, \ldots, X_{n-1} = x_{n-1}\} = \omega(x_n|x_{n-1}). \tag{A.5}$$

If we proceed by induction (A.3) becomes

$$\Pr\{X_0 = x_0, X_1 = x_1, \ldots, X_n = x_n\} = p_{x_0}\omega(x_1|x_0)\cdots\omega(x_n|x_{n-1}). \tag{A.6}$$

This way, once the transition probabilities $\omega(x_n|x_{n-1})$ are known, we can obtain the probability at time t of any configuration of the state space by summing probabilities at time $t-1$ according to the theorem of total probability.

A.2 The Domany-Kinzel cellular automaton

The mapping of some special cases of the PCA introduced in Chapter 2 for viral infection propagation with the *Domany-Kinzel* cellular automaton (DKCA) (Domany and Kinzel 1984) deserves a brief summary of its properties. It is defined as follows. Consider a finite one-dimensional array of L_a cells. The configuration the DKCA is determined by a set of stochastic variables $\boldsymbol{\sigma} = \{\sigma_i\}_{i=1}^{L_\mathrm{a}}$ defined at each lattice site at discrete times $t \geq 0$. Site i may be in one of the 2 states $\sigma_i \in \{0, 1\}$, describing active or empty cells, respectively. The vector of replicative abilities $\mathbf{r}$ of our model is the counterpart of $\boldsymbol{\sigma}$.

Now consider an ensemble of such states where each state $\boldsymbol{\sigma}$ occurs with probability distribution $p_t(\boldsymbol{\sigma})$ at time t. According to the Markovian property of PCA and

$\sigma_i \backslash \sigma_i, \sigma_{i+1}$	$1,1$	$1,0$	$0,1$	$0,0$
0	p_2	p_1	p_1	1
1	$1-p_2$	$1-p_1$	$1-p_1$	0

Table A.1: *Microscopic transition rules of the DK cellular automaton.*

Transition point	$p_{1,\mathrm{c}}$	$p_{2,\mathrm{c}}$
site DP	$0.705489(4)$	$0.705489(4)$
bond DP	$0.6447001(1)$	$0.8737620(2)$
Wolfram rule 18	$0.801(2)$	0

Table A.2: *Special transition points in the DK cellular automaton* (see Figure A.1).

the theorem of total probability, the time evolution of $p_t(\boldsymbol{\sigma})$ is determined once the (conditional) transition probabilities $\omega(\boldsymbol{\sigma}|\boldsymbol{\sigma}')$ are specified. This yields

$$p_{t+1}(\boldsymbol{\sigma}) = \sum_{\boldsymbol{\sigma}'} \omega(\boldsymbol{\sigma}|\boldsymbol{\sigma}') p_t(\boldsymbol{\sigma}'). \tag{A.7}$$

The probability of the transition $\boldsymbol{\sigma}' \to \boldsymbol{\sigma}$ satisfies the conditions $\omega(\boldsymbol{\sigma}|\boldsymbol{\sigma}') \geq 0$ and $\sum_{\boldsymbol{\sigma}} \omega(\boldsymbol{\sigma}|\boldsymbol{\sigma}') = 1$. In particular, the transition probability for the DKCA is a product of factors associated with each site:

$$\omega(\boldsymbol{\sigma}|\boldsymbol{\sigma}') = \prod_{i=1}^{L_\mathrm{a}} w_i(\sigma_i|\boldsymbol{\sigma}'), \tag{A.8}$$

where $w_i(\sigma_i|\boldsymbol{\sigma}')$ is the conditional probability for site i to be in state σ_i at time $t+1$, given the configuration $\boldsymbol{\sigma}'$ at time t. The probabilities $w_i(\sigma_i|\boldsymbol{\sigma}')$ are translation-invariant and *local*. In fact, they are assumed to depend only on the variables σ_i and σ_{i+1} at the previous time step,

$$w_i(\sigma_i|\boldsymbol{\sigma}') = w_{\mathrm{DK}}(\sigma_i|\sigma_i, \sigma_{i+1}). \tag{A.9}$$

The above relations, with the elementary rules $w_{\mathrm{DK}}(\sigma_i|\sigma_i, \sigma_{i+1})$ given in Table A.1, define the DKCA. All the transition probabilities are expressed in terms of two parameters p_1 and p_2. Note that the transition $(0,0) \to (1)$ is forbidden, hence the configuration $\sigma_i = 0$ for all i is *absorbing* (see Appendix B.1.1).

In Figure A.1 the corresponding p_1 vs. p_2 diagram of the DK model has been reproduced from Hinrichsen (2000). It comprises an active and an inactive phases, separated by a transition line. In the active phase a fluctuating state persists, whereas in the inactive phase the model always reaches the absorbing state in finite time.

The DKCA phase diagram includes three special cases. The choice $p_2 = p_1(2-p_1)$ corresponds to the so-called *directed bond percolation* (Broadbent and Hammersley

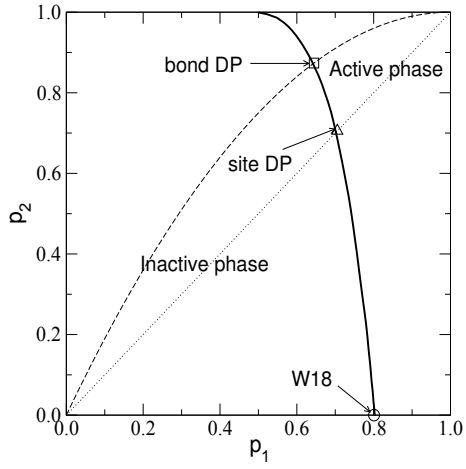

Figure A.1: *Phase diagram of the DK model* [reproduced from Hinrichsen (2000)].

1957). Another special case is *directed site percolation* (Kinzel 1983), corresponding to the choice $p_1 = p_2$. The third special case $p_2 = 0$ is equivalent to the rule 'W18' of Wolfram's classification scheme (Wolfram 1983). Numerical estimates for the corresponding critical points of these particular cases are summarized in Table A.2.

There is strong numerical evidence that the critical behavior along the whole phase transition line (except for its upper terminal point) is that of directed percolation. This means that all the critical points in the transition line exhibit the same type of long-range correlations. Short-range correlations, however, are non-universal and may be different when moving along the critical line.

One of the most striking properties of DP models is their robustness with respect to variations in the microscopic dynamic rules. In fact, the DP class covers a wide range of models. The variety and robustness of DP models led Janssen (1981) and Grassberger (1982) to the *conjecture* that a model should belong to the DP universality class if the following conditions hold:

1. The model exhibits a continuous phase transition from a fluctuating phase to a *unique* absorbing state.

2. The order parameter that characterizes the transition is *scalar*.

3. Dynamics involves *short-range* elementary rules.

4. The system has neither special symmetries nor quenched disorder.

Although this conjecture has not yet been rigorously proven, it is highly supported by numerical evidence. In particular, the DKCA verifies the conjecture, which is consistent with the numerical evidence for its belonging to the DP universality class.

A.3 Approximations to the critical line

The critical behavior of the DKCA can be approximated through a "mean-field" description at one-, two- and three-site levels (Tomé 1994). We start with the m-site marginal probabilities. The evolution of the one-site distribution,

$$p_t(\sigma_i) \equiv \sum_{\sigma_j, j\neq i} p_t(\boldsymbol{\sigma}), \tag{A.10}$$

is given by [see Eq. (A.7)]

$$p_{t+1}(\sigma_i) = \sum_{\sigma'_i, \sigma'_{i+1}} w_{\mathrm{DK}}(\sigma_i|\sigma'_i, \sigma'_{i+1}) p_t(\sigma'_i, \sigma'_{i+1}) \tag{A.11}$$

where $p_t(\sigma'_i, \sigma'_{i+1})$ is the marginal distribution for a pair of nearest-neighbor sites. The evolution of the latter is coupled to the three-site probability, so

$$p_{t+1}(\sigma_i, \sigma_{i+1}) = \sum_{\sigma'_i, \sigma'_{i+1}, \sigma'_{i+2}} w_{\mathrm{DK}}(\sigma_i|\sigma'_i, \sigma'_{i+1}) \times w_{\mathrm{DK}}(\sigma_{i+1}|\sigma'_{i+1}, \sigma'_{i+2}) p_t(\sigma'_i, \sigma'_{i+1}, \sigma'_{i+2}). \tag{A.12}$$

Evidently we have an infinite hierarchy of equations. In the m-site approximation the hierarchy is truncated by estimating the $(m+1)$-site probabilities on the basis of those for m sites.

The simplest case is the one-site approximation (also known as "mean-field" approximation), in which $p_t(\sigma_i, \sigma_{i+1})$ is factored into a product of one-site probabilities (assuming statistical independence) as

$$p_t(\sigma_i, \sigma_{i+1}) \approx p_t(\sigma_i) p_t(\sigma_{i+1}). \tag{A.13}$$

This relation provides a closure of the hierarchy and (A.11) transforms into the recurrence relation

$$\rho_{t+1} = \rho_t[2p_1 - (2p_1 - p_2)\rho_t], \tag{A.14}$$

where $\rho_t \equiv p_t(1)$ is the density of active sites (the order parameter for the DKCA). This equation admits two stationary solutions, corresponding to the two possible DKCA phases: absorbing [$\rho \equiv \lim_{t\to\infty} p_t(1) = 0$], and active, in which, for $p_1 > 1/2$,

$$\rho = \frac{2p_1 - 1}{2p_1 - p_2}. \tag{A.15}$$

Thus the critical line at the site level is $p_1 = 1/2$.

In the pair approximation the three-site probability is written in terms of two-site quantities, using conditional probabilities:

$$p_t(\sigma_i, \sigma_{i+1}, \sigma_{i+2}) \approx \frac{p_t(\sigma_i, \sigma_{i+1}) p_t(\sigma_{i+1}, \sigma_{i+2})}{p_t(\sigma_{i+1})}. \tag{A.16}$$

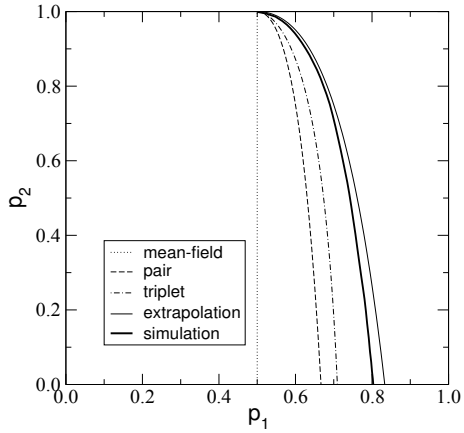

Figure A.2: *Transition line* for the DKCA in the mean-field (one-site, dotted line), pair (two-site, dashed line) and triplet (three-site, dash-dotted line) approximation regimes. The simulated transition line is shown for comparison (thick, full line). The extrapolation (A.23) is represented with a thin, full line.

[The one-site probabilities are given by $p_t(\sigma_i) = \sum_{\sigma_{i+1}} p_t(\sigma_i, \sigma_{i+1})$.] If we define the correlations $x_{ij} \equiv \lim_{t\to\infty} p_t(i,j)$, where $i,j \in \{0,1\}$, the hierarchy closed by (A.16) reduces, in the asymptotic limit $t \to \infty$, to the nonlinear system

$$\begin{aligned} \rho &= x_{01} + x_{11}, \\ \rho &= 2p_1 x_{01} + p_2 x_{11}, \\ x_{11} &= \frac{1}{\rho}[p_1 x_{01} + p_2 x_{11}]^2 + \frac{p_1^2 x_{01}^2}{1-\rho}. \end{aligned} \tag{A.17}$$

In the active stationary state, these relations lead to the density

$$\rho = \frac{p_2(p_1-1)^2 + p_1(3p_1-2)}{(2p_1-p_2)(2p_2-1)}. \tag{A.18}$$

Therefore, under this approximation, the critical line in the (p_1, p_2) plane is simply

$$p_2 = \frac{p_1(2-3p_1)}{(1-p_1)^2}. \tag{A.19}$$

We can go further and obtain a *triplet approximation* assuming that

$$p_t(\sigma_i, \sigma_{i+1}, \sigma_{i+2}, \sigma_{i+3}) \approx \frac{p_t(\sigma_i, \sigma_{i+1}, \sigma_{i+2}) p_t(\sigma_{i+1}, \sigma_{i+2}, \sigma_{i+3})}{p_t(\sigma_{i+1}, \sigma_{i+2})}. \tag{A.20}$$

Let $x_{ijk} \equiv \lim_{t\to\infty} p_t(i,j,k)$ be the asymptotic three-site correlations in the active phase, $i,j,k \in \{0,1\}$. Since these correlations are coupled to the four-site marginal distribution,

$$p_{t+1}(\sigma_i,\sigma_{i+1},\sigma_{i+2}) = \sum_{\sigma'} w_{\mathrm{DK}}(\sigma_i|\sigma'_i,\sigma'_{i+1}) w_{\mathrm{DK}}(\sigma_{i+1}|\sigma'_{i+1},\sigma'_{i+2}) \\ \times w_{\mathrm{DK}}(\sigma_{i+2}|\sigma'_{i+2},\sigma'_{i+3}) p_t(\sigma'_i,\sigma'_{i+1},\sigma'_{i+2},\sigma'_{i+3}), \quad \text{(A.21)}$$

the linear system to solve turns out to be

$$\begin{aligned}
\rho &= 2p_1(\rho - x_{11}) + p_2 x_{11},\\
x_{11} &= p_1^2 x_{101} + 2p_1p_2(x_{11} - x_{111}) + p_1^2(\rho - 2x_{11} + x_{111}) + p_2^2 x_{111},\\
x_{111} &= \frac{p_2}{x_{11}}[p_1(x_{11} - x_{111}) + p_2 x_{111}]^2\\
&\quad + \frac{2p_1^2}{\rho - x_{11}} x_{101}[p_1(\rho - 2x_{11} + x_{111}) + p_2(x_{11} - x_{111})],\\
x_{101} &= \frac{1-p_2}{x_{11}}[p_1(x_{11} - x_{111}) + p_2 x_{111}]^2 + p_1^2 \frac{(\rho - x_{11} - x_{101})^2}{1 - 2\rho + x_{11}}\\
&\quad + \frac{2p_1(1-p_1)}{\rho - x_{11}} x_{101}[p_1(\rho - 2x_{11} + x_{111}) + p_2(x_{11} - x_{111})].
\end{aligned} \quad \text{(A.22)}$$

These equations can be analytically solved but the solution is too cumbersome to be reproduced here. However, the critical line at this level can be written implicitly as $\sum_{k=0}^{12} p_1^k \Lambda_k(p_2) = 0$, where $\Lambda_k(x)$ are polynomials up to sixth degree:

$$\begin{aligned}
\Lambda_0(x) &= x^3(x+1),\\
\Lambda_1(x) &= -2x(x^4 + 5x^3 + 7x^2 + 4x - 1),\\
\Lambda_2(x) &= x^6 + 16x^5 + 57x^4 + 92x^3 + 69x^2 + 4x - 3,\\
\Lambda_3(x) &= -2(3x^6 + 32x^5 + 108x^4 + 185x^3 + 156x^2 + 48x - 4),\\
\Lambda_4(x) &= 17x^6 + 160x^5 + 560x^4 + 1014x^3 + 962x^2 + 435x + 34,\\
\Lambda_5(x) &= -2(14x^6 + 133x^5 + 506x^4 + 995x^3 + 1065x^2 + 576x + 107),\\
\Lambda_6(x) &= 28x^6 + 296x^5 + 1277x^4 + 2832x^3 + 3434x^2 + 2134x + 535,\\
\Lambda_7(x) &= -4(4x^6 + 53x^5 + 276x^4 + 719x^3 + 1010x^2 + 724x + 212),\\
\Lambda_8(x) &= 4(x^6 + 22x^5 + 154x^4 + 502x^3 + 849x^2 + 721x + 242),\\
\Lambda_9(x) &= -4(x+1)(4x^4 + 44x^3 + 179x^2 + 306x + 205),\\
\Lambda_{10}(x) &= 8(3x^4 + 26x^3 + 85x^2 + 120x + 62),\\
\Lambda_{11}(x) &= -16(x+2)^2(x+3),\\
\Lambda_{12}(x) &= 4(x+3)^2.
\end{aligned}$$

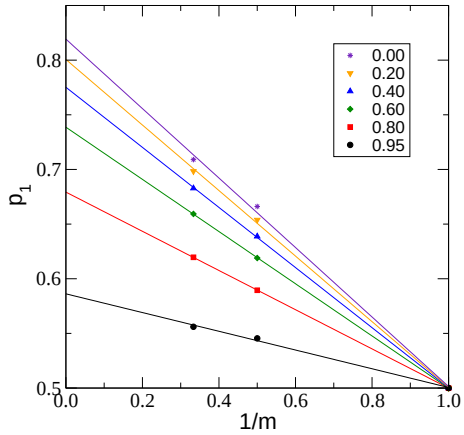

Figure A.3: *Extrapolation of the one-, two- and three-site approximation levels.* At fixed p_2 (for values given in the legend), we prove that these approximations depend linearly on $1/m$, m being the number of sites involved in the approximation. Lines are fittings to the corresponding points.

In Figure A.2 we observe that the triplet transition line, compared to the pair approximation result, gets closer to the simulated critical line. This notwithstanding, the approximate description at the triplet level is still far from being correct.

These three approximations, however, can be improved using an extrapolation technique. We consider, at fixed p_2, the dependence of p_1 with the approximation order (see Figure A.3). Since the three levels of approximation behave linearly with m^{-1}, i.e. the reciprocal of the number of sites involved in each approximation level, the extrapolated values at $m \to \infty$ provide more accurate approximations to the critical line. This extrapolation procedure is simply a convergence acceleration technique that we are able to use since the linear dependence of successive approximations is easy to predict with just three points. Moreover, an analytical estimate of the DKCA transition line can be obtained if we simply extrapolate the approximants for one and two sites, yielding the expression

$$p_2 = \frac{5 + 4p_1 - 12p_1^2}{(3 - 2p_1)^2}. \tag{A.23}$$

For the sake of comparison, this approximation to the critical line has been represented in the phase diagram (Figure A.2). The line extrapolated with the one- and two-site approximants yields a reasonably good analytical prediction to the simulation line.

B

A quick tour through Markov processes

This appendix is based on the books by Feller (1968) and van Kampen (2007).

B.1 Discrete-time finite Markov chains

A *discrete-time Markov chain* $\{X_n\}$ is a Markov process (see Section A.1) whose state space is a countable set, and which evolves according to discrete units of time ($n \in \{0, 1, \dots\}$). It is frequent to label the state space of the process by nonnegative integers, and it is customary to speak of X_n being in state i if $X_n = i$.

The probability of X_{n+1} being in state j, given that X_n is in state i (called one-step transition probability), is denoted by $p_{ij}^{n,n+1}$, i.e.

$$p_{ij}^{n,n+1} = \Pr\{X_{n+1} = j | X_n = i\}. \tag{B.1}$$

The notation emphasizes that in principle the transition probabilities are functions not only of the initial and final state, but also of the transition time as well. When one-step transition probabilities are independent of the time variable n, we say that the Markov chain has stationary transition probabilities. We will limit our discussion to such cases, so $p_{ij}^{n,n+1} = p_{ij}$ and represents the probability that the state value undergoes a transition from i to j in one trial. The matrix $\mathsf{P} = (p_{ij})$ is the so-called transition probability matrix of the process. If the cardinal of the state space is finite (let this number be $N_\mathrm{s} + 1$) then P is a finite square matrix whose dimension is equal to the number of

states. Clearly, these probabilities satisfy

$$p_{ij} \geq 0, \qquad i,j = 0,1,\ldots, \tag{B.2}$$

$$\sum_{j=0}^{N_\mathrm{s}} p_{ij} = 1, \qquad i = 0,1,\ldots. \tag{B.3}$$

Any matrix that satisfies the second relation is said to be *stochastic*.

The analysis of a Markov chain concerns mainly the calculation of probabilities of the possible realizations of the process. Central in these calculations are n-step transition probability matrices $\mathsf{P}^{(n)} = (p_{ij}^{(n)})$. Here $p_{ij}^{(n)}$ denotes the probability that the process goes from state i to j after n transitions,

$$p_{ij}^{(n)} = \Pr\{X_{n+m} = j | X_m = i\}. \tag{B.4}$$

The Markovian property (A.1) allows us to express these matrices in terms of powers of P. This is due to the following

Theorem B.1. *If the one-step transition probability matrix of an $(N_\mathrm{s}+1)$-state Markov chain is $\mathsf{P} = (p_{ij})$, then*

$$p_{ij}^{(n)} = \sum_{k=0}^{N_\mathrm{s}} p_{ik}^{(r)} p_{kj}^{(s)} \tag{B.5}$$

for any fixed pair of nonnegative integers r and s satisfying $r+s=n$, where we define $p_{ij}^{(0)} = \delta_{ij}$.

We immediately recognize Eq. (B.5) as the formula for matrix multiplication, so that the numbers $p_{ij}^{(n)}$ are simply the entries of the n-th power of P, P^n. Equation (B.5) is known as the Chapman-Kolmogorov equation.

B.1.1 Closed sets

State j is said to be *accessible* from state i if for some integer $n \geq 0$, $p_{ij}^{(n)} > 0$, i.e., if there is non-zero probability that in a finite number of trials state j can be hit starting from i. If two states are not accessible to each other, then either $p_{ij}^{(n)} = 0$ or $p_{ji}^{(n)} = 0$. We say that the Markov chain is *irreducible* if all states are accessible from each other.

A set $\mathcal{C}$ of states forms a *closed* set if no state outside $\mathcal{C}$ can be reached from any state $i \in \mathcal{C}$. A single state forming a closed set will be called *absorbing*. Clearly $\mathcal{C}$ is closed if and only if $p_{ij} = 0$ whenever $i \in \mathcal{C}$ and $j \notin \mathcal{C}$, since in this case we can see from (B.5) that $p_{ij}^{(n)} = 0$ for every n. Any state will be absorbing if and only if $p_{ii} = 1$. For an arbitrary set $\mathcal{A}$ of states, the smallest closed set containing $\mathcal{A}$ is called the *closure* of $\mathcal{A}$.

Consider a $(N_\mathrm{s}+1)$-state chain such that the subset of states $\{0,1,2,\ldots,k\}$ forms a closed set ($k < N_\mathrm{s}+1$). From the discussion above we deduce that the $k+1$ by $k+1$

submatrix of P appearing on the left upper corner is stochastic, and we can partition P in the form

$$\mathsf{P} = \begin{pmatrix} \mathsf{U} & \mathsf{0} \\ \mathsf{W} & \mathsf{V} \end{pmatrix} \tag{B.6}$$

where U and V are square matrices. From (B.5) it is obvious that higher-order transition matrices admit a similar partitioning,

$$\mathsf{P}^n = \begin{pmatrix} \mathsf{U}^n & \mathsf{0} \\ \mathsf{W}_n & \mathsf{V}^n \end{pmatrix}. \tag{B.7}$$

This structure allows to studying Markov chains by considering separately the states in the closed set $\mathcal{C}$ and those of its complement. Moreover, if $\mathcal{C}$ is reducible it shall decompose into additional closed subsets. Hence U may admit further partitioning.

B.1.2 Classification of states of a Markov chain

The first classification concerns *periodicity*. The *period* of state i, $d(i)$, is defined as the greatest common divisor of all integers $n \geq 1$ for which $p_{ii}^{(n)} > 0$ [If $p_{ii}^{(n)} = 0$ for all $n \geq 1$ it is defined $d(i) = 0$.] A Markov chain in which each state has period one is called *aperiodic*. In particular, any chain with all diagonal elements positive will be aperiodic because it satisfies $p_{ii}^{(1)} > 0$ for all i. The vast majority of Markov chains we deal with are aperiodic.[1]

In order to describe a periodic state i it suffices to consider the chain at the trials number $0, d(i), 2d(i), \ldots$. This way we obtain a new Markov chain where i is aperiodic. Therefore the results concerning aperiodic states can be transferred to periodic ones.

More interestingly, states can be classified into *transient* and *recurrent*. Let $f_{ij}^{(n)}$ be the probability that in a process starting from i the first entry to j occurs at the n-th step,

$$f_{ij}^{(n)} = \Pr\{X_n = j | X_m \neq j, m = 1, \ldots, n-1, X_0 = i\}, \tag{B.8}$$

and define

$$f_{ij} = \sum_{n=1}^{\infty} f_{ij}^{(n)}, \tag{B.9}$$

$$\mu_i = \sum_{n=1}^{\infty} n f_{ii}^{(n)}. \tag{B.10}$$

Obviously f_{ij} is the probability that, starting from i, the system will ever pass through j. Thus $f_{ij} \leq 1$. When $f_{ij} = 1$, $\{f_{ij}^{(n)}\}$ is a proper probability distribution and we shall refer to it as the *first-passage* distribution for state j. In particular, $\{f_{ii}^{(n)}\}$ represents the distribution of *recurrence times* for i. The definition (B.10) is meaningful only

[1] An important exception is the random walk on a square lattice.

when $f_{ii} = 1$, i.e., when the return to i is certain. In this case μ_i is obviously the *mean recurrence time* for i.

The probabilities $f_{ij}^{(n)}$ are related to the probabilities $p_{ij}^{(n)}$ of a transition from i to j in exactly n steps according to

$$p_{ij}^{(n)} = \sum_{m=0}^{n} f_{ij}^{(m)} p_{jj}^{(n-m)}, \qquad n \geq 1, \tag{B.11}$$

where we define $f_{ij}^{(0)} = 0$. This equation allows us to calculate of the distribution $f_{ij}^{(n)}$.

A state i is said recurrent if and only if $f_{ii} = 1$ and transient if $f_{ii} < 1$. Hence recurrence implies that the probability of returning to i after a finite number of steps is one. An aperiodic recurrent state i with mean recurrence time $\mu_i < \infty$ is called *ergodic*. In finite Markov chains all recurrent states are ergodic.

The recurrence of any state is related to the behavior of the n-step transition probabilities $p_{ii}^{(n)}$ according to

Theorem B.2. *(i) State i is transient if and only if $\sum_{n=1}^{\infty} p_{ii}^{(n)} < \infty$. (ii) For any ergodic state i, as $n \to \infty$*

$$p_{ij}^{(n)} \to f_{ij}\mu_j^{-1}. \tag{B.12}$$

The average number of returns to state i, given that $X_0 = i$, is $\sum_{n=1}^{\infty} p_{ii}^{(n)}$. Thus, the previous theorem states that any state is recurrent if and only if the expected number of returns is infinite. For a transient state, the probability of returning infinitely often to itself vanishes.

B.1.3 Irreducible chains. Decompositions

As an immediate consequence of Theorem B.2 it can be shown that all states of an irreducible chain are recurrent. This means that recurrence, like periodicity, is a class property. The importance of this results becomes apparent in conjunction with

Theorem B.3. *For a recurrent state i there exist a unique irreducible closed set $\mathcal{C}$ containing i and such that for every pair j, k of states in $\mathcal{C}$*

$$f_{jk} = 1 \qquad \textit{and} \qquad f_{kj} = 1. \tag{B.13}$$

In other words, starting from any arbitrary state i, in $\mathcal{C}$ the system is certain to pass through every other state of that set. This implies that the closure of a recurrent state is an irreducible set. This is not necessarily true for transient states (in particular, no transient state can be reached from a recurrent one). If the chain contains both types of states, P can be partitioned (after a convenient index permutation) as in (B.6) where U corresponds to recurrent states. Needless to say, U may be further decomposable, but every recurrent state belongs to a unique irreducible subset, and no transition between

subsets is possible. Hence there is a unique decomposition in non-overlapping sets, rendering a block-diagonal structure for matrix U,

$$\mathsf{U} = \begin{pmatrix} \mathsf{U}_0 & \mathsf{0} & \cdots & \mathsf{0} \\ \mathsf{0} & \mathsf{U}_1 & \cdots & \mathsf{0} \\ \vdots & \vdots & \ddots & \vdots \\ \mathsf{0} & \mathsf{0} & \cdots & \mathsf{U}_s \end{pmatrix}, \tag{B.14}$$

corresponding to s closed, recurrent subsets.

The concept of irreducibility can be also applied to matrices. A matrix P is reducible if there exists a permutation matrix Y such that

$$\mathsf{Y}^{\mathsf{T}}\mathsf{P}\mathsf{Y} = \begin{pmatrix} \mathsf{U} & \mathsf{0} \\ \mathsf{W} & \mathsf{V} \end{pmatrix}, \tag{B.15}$$

i.e., the permutation transforms the matrix into the form (B.6). Hence the Markov chain associated to a reducible, stochastic matrix is also reducible and contains transient states.

B.1.4 Invariant distributions

Since every recurrent state belongs to an irreducible set whose asymptotic behavior can be studied independently of the remaining states, we shall now concentrate on irreducible chains. We will focus in chains whose states are aperiodic and recurrent with finite mean recurrence times. Such chains are called *ergodic*.

Theorem B.4. *In an irreducible ergodic Markov chain the limits*

$$\pi_i = \lim_{n\to\infty} p_{ji}^{(n)} \tag{B.16}$$

exist and are independent of the initial state j. Furthermore,

$$\pi_i = \sum_{j=0}^{N_\mathrm{s}} \pi_j p_{ji}, \qquad \sum_{i=0}^{N_\mathrm{s}} \pi_i = 1, \tag{B.17}$$

and $\pi_i > 0$.

Conversely, suppose that the chain is irreducible and aperiodic, and that there exists numbers $\pi_i \geq 0$ satisfying (B.17)*. Then the chain is ergodic and π_i verify both* (B.16) *and*

$$\pi_i = 1/\mu_i. \tag{B.18}$$

To appreciate the meaning of Theorem B.4 consider the development of the process starting from an initial distribution $\{p_i\}$. The probability of the state i at the n-th trial is

$$p_i^{(n)} = \sum_j p_j p_{ji}^{(n)}. \tag{B.19}$$

In view of (B.16), as $n \to \infty$

$$p_i^{(n)} \to \pi_i. \tag{B.20}$$

In other words, irrespective of the initial distribution, the asymptotic probability tends to the vector $\boldsymbol{\pi} = (\pi_i)$. Thus sometimes it is referred to as the *asymptotic* distribution. On the other hand, when $\boldsymbol{\pi}$ is the initial distribution, the probabilities at each step verify $p_i^{(n)} = \pi_i$. Hence this distribution perpetuates itself along time (for this reason it is called *invariant*).

The existence of the asymptotic probability distribution for an irreducible, ergodic chain is related to the Perron-Frobenius theorem (Meyer 2000):

Theorem B.5. (Perron-Frobenius) *Any irreducible matrix with non-negative entries has a unique largest real eigenvalue and its corresponding eigenvector has strictly positive components.*

In particular, if the (stochastic) transition matrix P is irreducible, then the theorem applies and exists a unique largest real eigenvalue whose eigenvector has positive entries. But the first equation of (B.17) simply reads as

$$\boldsymbol{\pi} = \boldsymbol{\pi}\mathsf{P}, \tag{B.21}$$

i.e., $\boldsymbol{\pi}$ is the left-eigenvector of P with eigenvalue 1 (which is the largest eigenvalue in modulus since the matrix is stochastic). Accordingly, the asymptotic distribution has strictly positive entries in an irreducible chain, as expected for a vector of probabilities.

B.1.5 Mean absorption times

In this section we will illustrate how we can calculate the distribution of mean times to absorption (i.e., to get to touch a recurrent state). This can be done given the partition (B.6) that separates recurrent and transient states in the transition matrix P, where matrix U contains the transition probabilities within the recurrent set, and V contains transition probabilities between transient states. Let $\mathcal{G}$ be the set of states of the Markov chain, and $\mathcal{R}$ the subset of recurrent states of the chain.

The average time that it takes to go from the transient state i to state j of the recurrent set is the element t_{ij} of matrix T, where

$$\mathsf{T} = \sum_{k=1}^{\infty} k\mathsf{V}^{k-1}\mathsf{W} = (\mathsf{I} - \mathsf{V})^{-2}\mathsf{W}, \tag{B.22}$$

I being the identity matrix. This expression counts as k the absorption time when the process remains $k-1$ time steps within the transient subset and jumps to a recurrent state in the k-th step. The mean absorption time for a process starting from the transient state i will thus be $\tau_i = \sum_{j\in\mathcal{R}} t_{ij} = (\mathsf{T}\mathbf{1}^{\mathsf{T}})_i$, where $\mathbf{1} = (1, \ldots, 1)$. Since P is stochastic, $\sum_j (V_{ij} + W_{ij}) = (\mathsf{V}\mathbf{1}^{\mathsf{T}})_i + (\mathsf{W}\mathbf{1}^{\mathsf{T}})_i = 1$ for all $i \in \mathcal{G} - \mathcal{R}$, so $\mathsf{W}\mathbf{1}^{\mathsf{T}} = (\mathsf{I} - \mathsf{V})\mathbf{1}^{\mathsf{T}}$ or, equivalently, $(\mathsf{I} - \mathsf{V})^{-1}\mathsf{W}\mathbf{1}^{\mathsf{T}} = \mathbf{1}^{\mathsf{T}}$. Together with (B.22) this implies

$$(\mathsf{I} - \mathsf{V})\boldsymbol{\tau}^{\mathsf{T}} = \mathbf{1}^{\mathsf{T}}, \tag{B.23}$$

where $\boldsymbol{\tau} = (\tau_i)$. Hence the calculation of mean times to absorption for any transient state amounts to solve the linear system (B.23).

B.2 Continuous-time Markov processes

B.2.1 From the Chapman-Kolmogorov equation to the master equation

In this section we will describe *continuous-time* Markov processes. They are Markov processes for which the time variable can take a continuous set of values $t \in [0, \infty)$. As such, they satisfy the Markov property [Eq. (A.1)] and are fully determined by the initial condition $\Pr\{X(0) = x_0\}$ and the set of transition probabilities

$$\Pr\{X(t_n) = x_n | X(t_{n-1}) = x_{n-1}\} \tag{B.24}$$

where $t_{n-1} < t_n$.

An immediate relation verified by continuous-time Markov processes is the so-called *Chapman-Kolmogorov* equation. This is simply a generalization of Eq. (B.5) to continuous time. According to (A.6), and denoting the transition probabilities as

$$\omega_{t_2,t_1}(x_2|x_1) \equiv \Pr\{X(t_2) = x_2 | X(t_1) = x_1\}, \tag{B.25}$$

for $t_1 < t_2 < t_3$ we can write

$$\begin{aligned}\Pr\{X(t_1) = x_1, X(t_2) = x_2, X(t_3) = x_3\} = \omega_{t_3,t_2}(x_3|x_2) \\ \times \omega_{t_2,t_1}(x_2|x_1)\Pr\{X(t_1) = x_1\}.\end{aligned} \tag{B.26}$$

Integrating this identity over x_2 and dividing both sides by $\Pr\{X(t_1) = x_1\}$ we get

$$\omega_{t_3,t_1}(x_3|x_1) = \int dx_2 \omega_{t_3,t_2}(x_3|x_2)\omega_{t_2,t_1}(x_2|x_1). \tag{B.27}$$

This identity (Chapman-Kolmogorov) must be obeyed by the transition probability of any continuous-time Markov process. The time ordering is essential: t_2 lies between t_1 and t_3.

As noted before, the Markov process is fully determined by the initial condition $\Pr\{X(0) = x_0\}$ and the transition probability functions. These functions cannot be chosen arbitrarily, however, since they obey two identities: the Chapman-Kolmogorov equation and the obvious relation

$$\Pr\{X(t_2) = x_2\} = \int dx_1 \omega_{t_2,t_1}(x_2|x_1)\Pr\{X(t_1) = x_1\}. \tag{B.28}$$

And conversely: any non-negative function that satisfies these two consistency conditions defines uniquely a Markov process.

Processes for which the transition probability does not depend on t_1 and t_2 but only on the time interval $\tau = t_2 - t_1$ (named generically as *stationary*) are of special

interest, in particular for describing equilibrium fluctuations. For stationary processes, the Chapman-Kolmogorov equation becomes (τ, $\tau' > 0$)

$$\omega_{\tau+\tau'}(x_3|x_1) = \int dx_2 \omega_{\tau'}(x_3|x_2)\omega_\tau(x_2|x_1). \tag{B.29}$$

If one reads the integral as a product of two matrices, or integral kernels, this equation may be written as $\omega_{\tau+\tau'} = \omega_{\tau'}\omega_\tau$, and the analogy with (A.6) is apparent.

The master equation, however, is a more convenient version of the Chapman-Kolmogorov equation, because it is a differential equation obtained by going to the limit of vanishing time difference τ. For this purpose it is necessary first to ascertain how ω_τ behaves as τ tends to zero. We will assume that

$$\omega_\tau(x_2|x_1) = [1 - a(x_1)\tau]\delta(x_2 - x_1) + \tau W(x_2|x_1) + \mathcal{O}(\tau^2). \tag{B.30}$$

$W(x_2|x_1)$ is referred to as the *transition probability per unit time* from x_1 to x_2 and of course $W(x_2|x_1) \geq 0$. This Ansatz assumes that within the interval $\tau \ll 1$ a single transition event is likely to occur and it does so with probability $a(x_1)\tau$. Once a transition occurs, the probability that the new state is x_2 is $\tau W(x_2|x_1)$ (van Kampen 2007). Consistency requires that

$$a(x_1) = \int dx_2 W(x_2|x_1). \tag{B.31}$$

Now in the Chapman-Kolmogorov equation (B.29) we insert expression (B.30) for $\omega_{\tau'}$, which yields

$$\omega_{\tau+\tau'}(x_3|x_1) = [1 - a(x_3)\tau']\omega_\tau(x_3|x_1) + \tau' \int dx_2 W(x_3|x_2)\omega_\tau(x_2|x_1) + \mathcal{O}(\tau'^2). \tag{B.32}$$

Dividing by τ', taking the limit $\tau \to 0$ and using (B.31) we get

$$\frac{\partial}{\partial\tau}\omega_\tau(x_3|x_1) = \int dx_2 \left\{W(x_3|x_2)\omega_\tau(x_2|x_1) - W(x_2|x_3)\omega_\tau(x_3|x_1)\right\}. \tag{B.33}$$

This differential version of the Chapman-Kolmogorov equation, valid for the transition probability of any stationary Markov process obeying (B.30), is called the *master equation*.

It is useful to cast the equation in a more intuitive form. First note that $\omega_\tau(x_2|x_1)$ corresponds to the probability distribution $P(x_2)$ of the ensemble $\{x_2\}$ of states determined starting by the initial condition x_1. Hence we may write

$$\frac{\partial P(x,t)}{\partial t} = \int dx' \left\{W(x|x')P(x',t) - W(x'|x)P(x,t)\right\}. \tag{B.34}$$

This is the customary form of the master equation. If the range of X is a discrete set of states with labels i (i.e., we are dealing with a continuous-time Markov chain), the

equation reduces to

$$\frac{dp_i(t)}{dt} = \sum_j \{W_{ij}p_j(t) - W_{ji}p_i(t)\}\,. \tag{B.35}$$

In this form the meaning becomes particularly clear: the master equation is a *gain-loss equation* for the probability of state i, since the first term is the gain due to transitions from other states j, and the second term is the loss due to transitions into other states.

B.2.2 Systematic expansion of the master equation

To conclude this Appendix we will illustrate the method of systematic expansion of the master equation in powers of the inverse system volume Ω^{-1} (van Kampen 2007). This expansion separates the macroscopic behavior from fluctuations, and gives a linear Fokker-Planck equation describing fluctuations. We will use the model of size-structured population dynamics introduced in Chapter 6 to illustrate this method.

That model is based on the continuous-time Markov process described in Section 6.3, which accounts for four different elementary events: predation, reproduction, maintenance and mortality. Hence the model may be described by a master equation that gives the time evolution of the probability $P(\mathbf{N}, t)$ that the system hits the state $\mathbf{N} = (N_i)$ at time t (recall that N_i is the number of individuals in a given bracket i of body sizes). There will be a contribution from each of the processes involved,

$$\frac{\partial P}{\partial t} = \left(\frac{\partial P}{\partial t}\right)_{\mathrm{P}} + \left(\frac{\partial P}{\partial t}\right)_{\mathrm{B}} + \left(\frac{\partial P}{\partial t}\right)_{\mathrm{R}} + \left(\frac{\partial P}{\partial t}\right)_{\mathrm{D}}. \tag{B.36}$$

Since the procedure is quite similar for the four processes we are dealing with, we will only give the details for the predation process and will write the contributions of the other processes thereafter.

A concise way of writing the contribution of predation events to the master equation uses the step operator notation (van Kampen 2007). Since the probability to undergo a predation event in dt is $W^{\mathrm{P}}_{ijk}N_iN_j\Omega^{-1}$, we have

$$\left(\frac{\partial P(\mathbf{N}, t)}{\partial t}\right)_{\mathrm{P}} = \sum_{i,j,k} \frac{W^{\mathrm{P}}_{ijk}}{\Omega}(\mathbb{E}_i\mathbb{E}_j\mathbb{E}_k^{-1} - \mathbb{I})[N_iN_jP(\mathbf{N}, t)], \tag{B.37}$$

where the step operators $\mathbb{E}_i$ and $\mathbb{E}_i^{-1}$ act on any function $f(\mathbf{N})$ as $\mathbb{E}_i f(\mathbf{N}) = f(\dots, N_i + 1, \dots)$ and $\mathbb{E}_i^{-1} f(\mathbf{N}) = f(\dots, N_i - 1, \dots)$, respectively.

In Section 6.3 we already introduced the split of each variable $N_i(t)$ into a deterministic, macroscopic component $\phi_i(t)$ describing the density of individuals in weight bracket i, and a fluctuation component $\psi_i(t)$ as

$$N_i(t) = \Omega\phi_i(t) + \Omega^{1/2}\psi_i(t). \tag{B.38}$$

The new stochastic variables ψ_i have a probability distribution

$$\Pi(\boldsymbol{\psi}, t) = \Omega^{1/2}P(\mathbf{N}, t) \tag{B.39}$$

for which we can write

$$\left(\frac{\partial P(\mathbf{N},t)}{\partial t}\right)_{\mathrm{P}} = \Omega^{-1/2}\left(\frac{\partial \Pi(\boldsymbol{\psi},t)}{\partial t}\right)_{\mathrm{P}} - \sum_i \left(\frac{\partial \Pi(\boldsymbol{\psi},t)}{\partial \psi_i}\right)_{\mathrm{P}}\left(\frac{d\phi_i}{dt}\right)_{\mathrm{P}}, \quad \text{(B.40)}$$

where we have used that $\Omega^{-1/2}d\psi_i/dt = -d\phi_i/dt$ (this follows from (6.5) taking the time derivative for fixed N_i; we fix N_i because we are interested in the *partial* derivative of $P(\mathbf{N},t)$ with respect to t). The step operator $\mathbb{E}_i$ now transforms ψ_i into $\psi_i + \Omega^{-1/2}$, and can be expanded as

$$\mathbb{E}_i = \mathbb{I} + \Omega^{-1/2}\frac{\partial}{\partial \psi_i} + \frac{1}{2}\Omega^{-1}\frac{\partial^2}{\partial \psi_i^2} + \cdots \quad \text{(B.41)}$$

Substituting this expansion into the master equation (B.37) we arrive at an equation containing different powers of the system volume Ω. The highest order (Ω^0) terms in the expansion contain only macroscopic variables ϕ_i and vanish if these satisfy the macroscopic equation (6.7).

Terms at next order ($\Omega^{-1/2}$) give a linear Fokker-Planck equation for the probability distribution $\Pi(\boldsymbol{\psi},t)$ of the fluctuations,

$$\left(\frac{\partial \Pi(\boldsymbol{\psi},t)}{\partial t}\right)_{\mathrm{P}} = -\sum_{ij} L_{ij}^{\mathrm{P}}\frac{\partial}{\partial \psi_i}\left(\psi_j \Pi\right) + \frac{1}{2}\sum_{ij} D_{ij}^{\mathrm{P}}\frac{\partial^2 \Pi}{\partial \psi_i \partial \psi_j}. \quad \text{(B.42)}$$

By introducing the symmetric combination

$$f_{ijk} = \frac{1}{2}(W_{ijk}^{\mathrm{P}} + W_{jik}^{\mathrm{P}}), \quad \text{(B.43)}$$

and using the macroscopic equations, we can give concise expressions for the coefficients in the Fokker-Planck equation,

$$\begin{aligned}
L_{ii}^{\mathrm{P}} &= -2\sum_{jl} f_{ijl}\phi_j, \\
L_{ij}^{\mathrm{P}} &= -2\sum_{l}\left(f_{ijl}\phi_i - f_{ljl}\phi_l\right), \\
D_{ii}^{\mathrm{P}} &= \sum_{jl}\left(2f_{ijl}\phi_i\phi_j + f_{jli}\phi_j\phi_l\right), \\
D_{ij}^{\mathrm{P}} &= 2\sum_{l}\left(f_{ijl}\phi_i\phi_j - f_{ilj}\phi_i\phi_l - f_{ljl}\phi_l\phi_j\right).
\end{aligned} \quad \text{(B.44)}$$

Terms at higher order in Ω^{-1} specify how the fluctuations deviate from being Gaussian. Fluctuations are seen to be damped by a factor $\Omega^{-1/2}$, and the volume occupied by marine communities is very large. This justifies that we concentrated ourselves on the study of the macroscopic equation in Chapter 6.

The remaining processes involved in the model can be treated in a similar fashion. The master equation for reproduction can be written as

$$\left(\frac{\partial P(\mathbf{N},t)}{\partial t}\right)_{\mathrm{B}} = \sum_{i,j,k} W^{\mathrm{B}}_{ijk}(\mathbb{E}_i\mathbb{E}_j^{-1}\mathbb{E}_k^{-m_{ijk}} - \mathbb{I})[N_i P(\mathbf{N},t)]. \tag{B.45}$$

At leading order the expansion in powers of Ω gives the deterministic contribution (6.8). At next-to-leading order the fluctuations are governed by a Fokker-Planck equation similar to (B.42), with coefficients given by

$$\begin{aligned}
L^{\mathrm{B}}_{ii} &= -\sum_{jl} W^{\mathrm{B}}_{ijl}, \\
L^{\mathrm{B}}_{ij} &= \sum_{l} \left(W^{\mathrm{B}}_{ijl} + W^{\mathrm{B}}_{jli} m_{jli}\right), \\
D^{\mathrm{B}}_{ii} &= \sum_{jl} \left(W^{\mathrm{B}}_{ijl}\phi_i + W^{\mathrm{B}}_{jil}\phi_j + W^{\mathrm{B}}_{jli} m^2_{jli}\phi_l\right), \\
D^{\mathrm{B}}_{ij} &= \sum_{l} \left(-W^{\mathrm{B}}_{ijl}\phi_i - W^{\mathrm{B}}_{ilj}\phi_i + W^{\mathrm{B}}_{lji} m_{lji}\phi_l\right).
\end{aligned} \tag{B.46}$$

The effect of maintenance on the time evolution of the probability $P(\mathbf{N},t)$ is given by

$$\left(\frac{\partial P(\mathbf{N},t)}{\partial t}\right)_{\mathrm{R}} = \sum_{i} W^{\mathrm{R}}_{i}(\mathbb{E}_{i-1}^{-1}\mathbb{E}_i - \mathbb{I})[N_i P(\mathbf{N},t)], \tag{B.47}$$

which leads to (6.9) at leading order and to the following contributions to the coefficients of the Fokker-Planck equation,

$$\begin{aligned}
L^{\mathrm{R}}_{ii} &= -W^{\mathrm{R}}_{i}, \\
L^{\mathrm{R}}_{ij} &= \delta_{i+1,j} W^{\mathrm{R}}_{j}, \\
D^{\mathrm{R}}_{ii} &= W^{\mathrm{R}}_{i}\phi_i + W^{\mathrm{R}}_{i+1}\phi_{i+1}, \\
D^{\mathrm{R}}_{ij} &= -\delta_{i+1,j} W^{\mathrm{R}}_{j}\phi_j - \delta_{i,j+1} W^{\mathrm{R}}_{i}\phi_i.
\end{aligned} \tag{B.48}$$

Finally, the contribution of intrinsic mortality to the master equation is

$$\left(\frac{\partial P(\mathbf{N},t)}{\partial t}\right)_{\mathrm{D}} = \sum_{i} W^{\mathrm{D}}_{i}(\mathbb{E}_i - \mathbb{I})[N_i P(\mathbf{N},t)], \tag{B.49}$$

whose deterministic component leads to (6.10). For the fluctuations we get non-zero contributions to the diagonal coefficients in the Fokker-Planck equation,

$$\begin{aligned}
L^{\mathrm{D}}_{ii} &= -W^{\mathrm{D}}_{i}, \\
D^{\mathrm{D}}_{ii} &= W^{\mathrm{D}}_{i}\phi_i,
\end{aligned} \tag{B.50}$$

whereas off-diagonal coefficients are equal to zero. Note that the master equation for the complete model (B.36) is simply the sum of all the contributions, so the combined effect of all the processes in the macroscopic and Fokker-Planck equations is just the sum of all terms.

C

Computational methods

This appendix is devoted to provide some details regarding the computational methods applied in Chapter 3 for the computation of the assembly graph and its subsequent analysis.

A schematic flowchart of the program that we have developed for this purpose is depicted in Figure C.1. Our program is based in three main modules: (i) the routine `BUILD-CHAIN`, which calculates a *ternary tree* containing the assembly graph for a given set of parameters; (ii) the routine `READ-TREE`, responsible for generating the adjacency matrix of the assembly graph; and (iii) the routine `XIE-BEEREL`, which applies the algorithm by Xie and Beerel (1998) to classify the nodes of the graph as either transient or recurrent. Let us describe each module in turn.

Among all the routines conforming the program, `BUILD-CHAIN` is undoubtedly the main one. Figure C.2 shows the pseudocode of this module. All the communities generated along the assembly process are stored in a *stack* $\mathcal{S}$. The subroutine `STACK` adds a new set of species occupancies $\{s_\ell\}_{\ell=1}^{L}$ to $\mathcal{S}$. The process starts with the empty community, $\varnothing$.

For each iteration of the process, we initially extract the last (upper) element of the stack using the subroutine `LAST-ELEM`, that returns the target community $\{s_\ell\}$ for that iteration as well as its number of trophic levels L. We then perform all the possible invasions at levels $\ell_i = 1, \ldots, L+1$. The routine that determines the resulting community after the invasion has been named `DYNAMICS`, and we will describe it separately below.

Once the new community —$\{s'_\ell\}$, comprising L' levels— has been obtained, we need to store it. The storage of all the communities appearing along the process has

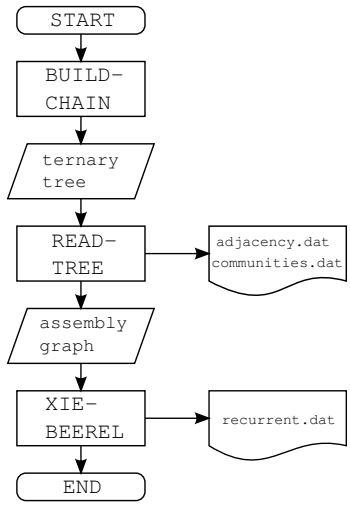

Figure C.1: *Schematic flowchart* for the program which builds up the assembly graph and classify its states as transient or recurrent. Rectangular boxes represent program modules and rhomboidal boxes stand for internal data. Three data files are generated as output: one for the nodes of the graph ('communities.dat'), a second one for links ('adjacency.dat') and another file containing the recurrent subsets ('recurrent.dat').

been carried out by using a ternary tree $\mathcal{T}$ (Knuth 1997). We have exploited the mapping between any integer s_ℓ and a binary number, it suffices to concatenate the binary representations of each species number s_ℓ to form a branch of the ternary tree. Each node of our tree has three possible links: `zero`, `one` and `sep`, the last one representing a "separator" in between the occupancies of each level. Thus it is easy to form a branch for each configuration. For example, the community defined by the set of occupancies $\{26, 7, 2\}$ is mapped to the branch

```
one one zero one zero sep one one one sep one zero
```

since $26 = 11010_{(2}$, $7 = 111_{(2}$ and $2 = 10_{(2}$. Subroutine `TREE` adds communities to $\mathcal{T}$. At each "leave" of the tree (i.e. the node at each terminating link, corresponding to a particular community; in the example above the terminating link would be `zero`) we store an integer as a "label" for that community and an array of integers containing the labels of all the different communities resulting from all the possible invasions of the original community. Hence, we can store both nodes (i.e. the branches of the ternary tree) and directed links (i.e. the arrays stored at each leave corresponding to a node) of our assembly graph in a single computational structure (see Figure C.3 for a pictorial example of the mapping of the assembly graph to a ternary tree).

Sometimes it will happen that the outcome of an invasion will not be a new community. We use the ternary tree to check so, and if the community is not new (boolean

```
BUILD-CHAIN ( )
   S ← STACK ( ∅, 0 );
   do
      ( {s_ℓ}, L ) ← LAST-ELEM ( S );
      for ( ℓ_i = 1 : L+1 )
         ( {s'_ℓ}, L' ) ← DYNAMICS ( {s_ℓ}, ℓ_i );
         ( new, T ) ← TREE ( {s'_ℓ}, L' );
         if ( new > 0 )
            S ← STACK ( {s'_ℓ}, L' );
         end;
      next ℓ_i;
   while ( IS-EMPTY ( S ) > 0 );
   return ( T );
```

Figure C.2: *Pseudocode* for the routine BUILD-CHAIN.

variable new $= 0$), we do not store the final community in the stack to avoid repetitions. Otherwise, the final community $\{s'_\ell\}$ is stored in $\mathcal{S}$. The process keeps going on until the stack is emptied (i.e. when the function IS-EMPTY returns 0).

Subroutine DYNAMICS, which allows for obtaining the resulting community after an invasion, is more involved, though. Figure C.4 shows the pseudocode for this subroutine. Its input variables are the occupancies $\{s^0_\ell\}$ of the resident community before the invasion, and the invasion level ℓ_i. All the communities being globally stable, they stay at equilibrium before the invasion takes place, since the time scale of invasion is assumed to be large compared to the return time to equilibrium. Therefore, we first compute the equilibrium abundances $\{p^0_\ell\}$ corresponding to $\{s^0_\ell\}$ according to (3.16). This task is performed by subroutine THOMAS, which applies the so-called *Thomas algorithm* to solve a tridiagonal system. The solution of (3.16) is obtained recursively as

$$p_\ell = m_{\ell+1} p_{\ell+1} + c_{\ell+1} \tag{C.1}$$

for $\ell = 0, \ldots, L$. Substitution on (3.16) yields the following recurrences for m_ℓ and c_ℓ,

$$\begin{aligned} m_{\ell+1} &= \frac{\gamma_- s_{\ell+1}}{\gamma_+ s_{\ell-1} m_\ell - (1 - \rho + \rho s_\ell)}, \\ c_{\ell+1} &= \frac{\alpha - \gamma_+ s_{\ell-1} c_\ell}{\gamma_+ s_{\ell-1} m_\ell - (1 - \rho + \rho s_\ell)}, \end{aligned} \tag{C.2}$$

supplemented with the initial conditions $m_1 = -\gamma_- s_1$, $c_1 = R$. We can therefore calculate $\{m_\ell\}_{\ell=1}^{L+1}$ and $\{c_\ell\}_{\ell=1}^{L+1}$. The requirement $p_{L+1} = 0$ for a community to have exactly L trophic levels yields $p_L = c_{L+1}$. Using (C.1) we backsubstitute to obtain p_ℓ for $\ell = L-1, \ldots, 0$.

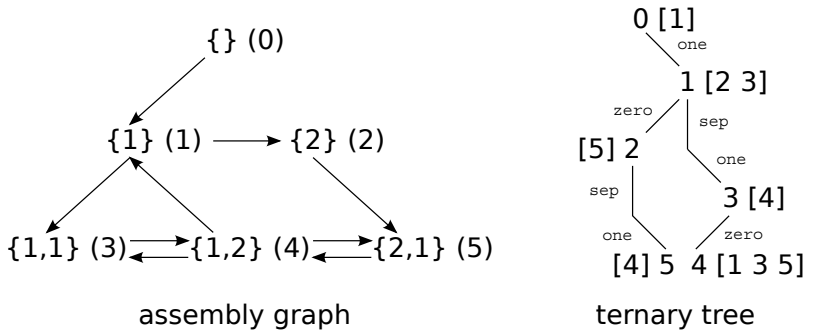

Figure C.3: *An example of assembly graph and its associated ternary tree.* The set $\{s_\ell\}$ of species occupancies of each node in the assembly graph are shown. Nodes are labeled —quite arbitrarily— with numbers in parentheses. The tree shows these labels as nodes. Three types of links can connect two nodes: `zero` (left-pointing link), `one` (right-pointing link) and `sep` (separator of trophic levels; vertical link). In the leave associated to community i an array (shown in brackets) is stored containing the community labels accessible from i in one step.

The process of invasion at level ℓ_i amounts to increasing s_{ℓ_i} in one unit. Subroutine `CHECK-VIABILITY` checks whether the new interior equilibrium $\{p_\ell\}$ is viable —in this case it returns a boolean equal to 0— or not. If the equilibrium is viable, we recover the final number of levels of the community using the routine `GET-LEVELS` and `DYNAMICS` terminates by returning the extended community and the resulting number of levels. Otherwise, if the extended equilibrium is not viable, we apply the sequential procedure of species extinction. The algorithm for this process goes as follows. Firstly we set the populations at time step $i = 0$ equal to $\{p_\ell^0\}$ —the abundances before the invasion— and the initial population of the invader $n_i(0) = n_c$. Subroutine `RUNGE-KUTTA` computes a single time step for the dynamical system (3.22) using a fourth-order, fixed-step Runge-Kutta (RK) method. The RK method is iterated until a level crosses the extinction threshold, provided that the level becomes actually extinct at equilibrium.

Routine `FIRST-EXTINCT` determines the first trophic level to cross the extinction threshold among those that asymptotically become extinct. If no level goes extinct, or the first level to cross the threshold does not go extinct asymptotically, an integer $\ell_j = 0$ is returned. Otherwise, the extinct level ℓ_j is returned, and evolution is restarted from the extinction point $\{n_\ell(i)\}$.

Finally, one species is removed from level ℓ_j (see Figure C.4), and we use subroutine `CHECK-LEVELS` to check whether a whole level has become eventually unpopulated: in that case, the levels immediately above go extinct as well, and the number of levels is updated. The process of sequential removal of species one by one is repeated until the asymptotic viability of the resulting community is restored.

```
DYNAMICS ( {s_ℓ^0}, ℓ_i )
   {p_ℓ^0} ← THOMAS ( {s_ℓ^0} );
   s_{ℓ_i} ← s_{ℓ_i}^0 + 1;
   {p_ℓ} ← THOMAS ( {s_ℓ} );
   L ← GET-LEVELS ( {s_ℓ} );
   if ( CHECK-VIABILITY ( {p_ℓ} ) > 0 )
      {n_ℓ(0)} ← {p_ℓ^0};
      n_i(0) ← n_c;
      do
         extinct ← 1;
         i ← 0;
         while ( extinct = 1 )
            {n_ℓ(i+1)} ← RUNGE-KUTTA ( {n_ℓ(i)} );
            ℓ_j ← FIRST-EXTINCT( {n_ℓ(i+1)}, {p_ℓ} );
            if ( ℓ_j > 0 )
               extinct ← 0;
               {n_ℓ(0)} ← {n_ℓ(i)};
            else
               i ← i + 1;
            end;
         end;
         s_{ℓ_j} ← s_{ℓ_j} − 1;
         ( {s_ℓ}, L ) ← CHECK-LEVELS ( {s_ℓ} );
         {p_ℓ} ← THOMAS ( {s_ℓ} );
      while ( CHECK-VIABILITY ( {p_ℓ} ) > 0 );
   end;
   return ( {s_ℓ}, L );
```

Figure C.4: *Pseudocode* for the subroutine DYNAMICS, which is used in the module BUILD-CHAIN.

This concludes the description of the module BUILD-CHAIN that generates a ternary tree containing the nodes and links of our assembly graph. A simple reading routine, READ-TREE, generates two output files containing both the set of occupancies associated with each node ('communities.dat') and the adjacency matrix of the graph ('adjacency.dat'). The only remaining task is to classify the set of nodes of the assembly graph, for which we use the algorithm provided by Xie and Beerel (1998) (module XIE-BEEREL).

The algorithm is based on a theorem that characterizes both transient and recurrent sets of a directed graph $\mathcal{G} = \{\mathcal{N}, \mathcal{L}\}$. First we define the *forward* and *backward* sets of a given node i of the chain. The forward set of i, denoted by $\mathcal{F}(i)$, is the set of nodes accessible from i (recall the notion of accessibility given in Appendix B.1.1), that is,

```
XIE-BEEREL ( 𝒩, ℒ )
  𝒩′ ← 𝒩;
  ℒ_i ← INVERSE-GRAPH ( ℒ );
  while ( 𝒩′ ≠ ∅ )
    s ← INITIAL-TAKE ( 𝒩′ ) ;
    ℱ(s) ← FORWARD-SET( s, ℒ );
    ℬ(s) ← FORWARD-SET( s, ℒ_i );
    if ( ℱ(s) ∩ ℬ(s)‾ = ∅ )
      report ℱ(s) as a recurrence class;
      report ℬ(s) ∩ ℱ(s)‾ all transient;
      𝒩′ ← 𝒩′ ∩ ℬ(s)‾;
    else
      report s ∪ ℬ(s) all transient;
      𝒩′ ← 𝒩′ ∩ s ∪ ℬ(s)‾;
    end;
  end;
```

Figure C.5: *Pseudocode* for the subroutine XIE-BEEREL.

$\mathcal{F}(i) = \{j \in \mathcal{N} | i \to j\}$. Similarly, the backward set of i, $\mathcal{B}(i)$, is the set of nodes which i can be accessed from, i.e., $\mathcal{B}(i) = \{j \in \mathcal{N} | j \to i\}$. The algorithm is thus based on the following

Theorem C.1. *Let $i, j \in \mathcal{N}$.*

(i) If $j \in \mathcal{F}(i)$, then $\mathcal{F}(j) \subseteq \mathcal{F}(i)$. Similarly, if $j \in \mathcal{B}(i)$, then $\mathcal{B}(j) \subseteq \mathcal{B}(i)$.

(ii) A node $i \in \mathcal{G}$ is recurrent if and only if $\mathcal{F}(i) \subseteq \mathcal{B}(i)$. In other words, i is transient if and only if $\mathcal{F}(i) \not\subseteq \mathcal{B}(i)$.

(iii) If node $i \in \mathcal{N}$ is transient, then nodes in $\mathcal{B}(i)$ are all transient. If node i is recurrent, on the other hand, nodes in $\mathcal{F}(i)$ are all recurrent. In the latter case, $\mathcal{F}(i)$ is a recurrent class, and the set $\mathcal{B}(i) - \mathcal{F}(i)$, if not empty, contains only transient nodes.

The pseudocode given in Figure C.5 for the module XIE-BEEREL exploits item (iii). For a given node i, FORWARD-SET computes $\mathcal{F}(i)$ by following the directed graph $\{\mathcal{N}, \mathcal{L}\}$. This subroutine uses a stack to store the set of nodes accessible from i in one step. After that, we recover the last element of the stack and repeat the process until the stack is emptied.

In order to obtain the backward set, at the beginning of XIE-BEEREL we compute the inverse graph containing, for each node, links to the set of nodes which can be accessed from it in one step (subroutine INVERSE-GRAPH). Hence the computation of $\mathcal{B}(i)$ is reduced to applying FORWARD-SET to the set of links $\mathcal{L}_i$ of the inverse graph.

Given a node i, if $\mathcal{F}(i) \subseteq \mathcal{B}(i)$ then Theorem C.1(iii) ensures that the subset $\mathcal{F}(i)$ is a recurrent class. We classify it as such and include it in the output file 'recurrent.dat'. We remove those nodes from $\mathcal{N}$, leading to the new set $\mathcal{N}'$ of unclassified nodes. For any loop of the `XIE-BEEREL` routine, the set $\mathcal{N}' \cap \overline{\mathcal{F}(i)}$ remains unclassified. Moreover, if $\mathcal{B}(i) \cap \overline{\mathcal{F}(i)} \neq \varnothing$, all its nodes can be classified as transient. In this case, the set $\mathcal{N}' \cap (\overline{\mathcal{B}(i)} \cup \mathcal{F}(i))$ still remains unclassified. Therefore the new set of nodes to classify is $\mathcal{N}' \cap (\overline{\mathcal{B}(i)} \cup \mathcal{F}(i)) = \mathcal{N}' \cap \overline{\mathcal{B}(i)}$.

On the other hand, if $\mathcal{F}(i) \not\subseteq \mathcal{B}(i)$, Theorem C.1(ii)–(iii) implies that all nodes in $i \cup \mathcal{B}(i)$ are transient, so these nodes are classified as such. A single iteration of the algorithm provides a complete characterization of a set of nodes connected with i either by the direct or the inverse graph. The set of nodes $\mathcal{N}'$ not yet classified is updated and the process is repeated until the classification is complete. Therefore, the computation of the sets $\mathcal{F}(i)$ and $\mathcal{B}(i)$ for a given node allows not only for the classification of a single node i, but also for a set of nodes connected to i. Hence the remaining nodes to be classified can be reduced considerably.

The only difference that we have incorporated to the algorithm by Xie and Beerel (1998) is an improved search of the initial node to start off the procedure. The choice of the initial node is performed in routine `INITIAL-TAKE`. We randomly choose a node i and calculate its backward and forward sets. If $\mathcal{F}(i) \subseteq \mathcal{B}(i)$, i is recurrent and is chosen as starting point of the algorithm. If $\mathcal{F}(i) \not\subseteq \mathcal{B}(i)$ —i.e. i is transient—, we calculate the set $\mathcal{F}(i) \cap \overline{\mathcal{B}(i)}$, which contains all nodes j for which i is unreachable but are reachable starting from i. In this sense, it is likely that some element of $\mathcal{F}(i) \cap \overline{\mathcal{B}(i)}$ is recurrent. We randomly choose one of the elements of this set as initial node, which is returned as output of `INITIAL-TAKE`.

This concludes the description of the module that classifies states as either transient or recurrent. Once this classification has been done, the communities in the assembly graph have been analyzed and our program terminates.

D

Technical details of the explicit formulae for equilibrium abundances

The mathematical details of the derivation of Eq. (4.11) will be discussed at length in this appendix. The solution of the system (4.10) can be obtained through Cramer's rule as

$$s_\ell p^\ell = \frac{\Xi_{L,\ell}}{\Delta_L} \tag{D.1}$$

for certain determinants $\Xi_{L,\ell}$ and Δ_L. Our approximation is based in some recurrence equations that can be derived for these determinants.

Let us start with the $(L+1)\times(L+1)$ determinant

$$\Delta_L = \begin{vmatrix} -1 & -\gamma_- & 0 & \cdots & 0 \\ \gamma_+ & -d_1 & -\gamma_- & \cdots & 0 \\ 0 & \gamma_+ & -d_2 & \cdots & 0 \\ \vdots & \vdots & \vdots & & \vdots \\ 0 & 0 & 0 & \cdots & -d_L \end{vmatrix}, \tag{D.2}$$

where $d_\ell \equiv \rho + \frac{1-\rho}{s_\ell}$. Hence the densities depend on $\{s_\ell\}_{\ell=1}^L$ only through the inverse of all the possible products $s_{i_1}s_{i_2}\cdots s_{i_k}$, for some combination $(i_1, i_2, \ldots, i_k)$ of k elements of the set $\{1, 2, \ldots, L\}$. In the recurrent sets we get the largest species occupancies in each level allowed by the resource according to (4.6)–(4.8), so we expect that a rather good approximation for the equilibrium densities amounts to neglecting

orders higher than s_ℓ^{-1}. Hence

$$\Delta_L = D_L - (1-\rho)\sum_{\ell=1}^{L}\frac{B_{L,\ell}}{s_\ell} + \mathcal{O}\left(s^{-2}\right), \tag{D.3}$$

where

$$D_L = \begin{vmatrix} -1 & -\gamma_- & 0 & \cdots & 0 \\ \gamma_+ & -\rho & -\gamma_- & \cdots & 0 \\ 0 & \gamma_+ & -\rho & \cdots & 0 \\ \vdots & \vdots & \vdots & & \vdots \\ 0 & 0 & 0 & \cdots & -\rho \end{vmatrix} \tag{D.4}$$

has dimension $(L+1)\times(L+1)$ and $B_{L,\ell}$ is the determinant obtained by substituting the ℓ-th column of D_L by the column vector $\boldsymbol{\delta}_\ell = (\delta_{\ell,i})$, $i = 0, 1, \ldots L$.

The determinant D_ℓ satisfies the recursion

$$D_\ell = -\rho D_{\ell-1} + \gamma_+\gamma_- D_{\ell-2}, \tag{D.5}$$

for $\ell = 1, 2, \ldots L$, $D_0 = -1$ and $D_1 = \rho + \gamma_+\gamma_-$. This relation can be solved using a generating function. On the other hand, it is easy to see that $B_{L,\ell} = D_{\ell-1}E_{L-\ell-1}$, with E_ℓ the $(\ell+1)\times(\ell+1)$ determinant

$$E_\ell = \begin{vmatrix} -\rho & -\gamma_- & 0 & \cdots & 0 \\ \gamma_+ & -\rho & -\gamma_- & \cdots & 0 \\ 0 & \gamma_+ & -\rho & \cdots & 0 \\ \vdots & \vdots & \vdots & & \vdots \\ 0 & 0 & 0 & \cdots & -\rho \end{vmatrix}, \tag{D.6}$$

which also satisfies Eq. (D.5) with $E_0 = -\rho$ and $E_1 = \rho^2 + \gamma_+\gamma_-$.

The generating function that results from (D.5) is

$$G(z) = \sum_{\ell=0}^{\infty} D_\ell z^\ell = \frac{D_0 + (D_1 + \rho D_0)z}{\gamma_+\gamma_- z^2 - \rho z - 1}, \tag{D.7}$$

and after the series expansion we get

$$D_\ell = (-\gamma_-)^{\ell-1}\left[(D_1 + \rho D_0)a_{\ell-1} - \gamma_- E_0 a_\ell\right], \tag{D.8}$$

with a_ℓ given by (4.3). Hence the following compact expressions result:

$$D_\ell = (-1)^{\ell+1}\gamma_-^\ell\left[a_\ell + \gamma_+ a_{\ell-1}\right], \tag{D.9}$$

$$E_\ell = (-1)^{\ell+1}\gamma_-^{\ell+1} a_{\ell+1}. \tag{D.10}$$

The explicit expression for $\Xi_{L,\ell}$ is obtained from Δ_L by substituting its ℓ-th column by the $(L+1)\times 1$ column vector $(-R,\alpha,\ldots,\alpha)^{\mathsf{T}}$. We can expand it up to leading order in powers of s_ℓ^{-1} to get

$$\Xi_{L,\ell} = T_L^\ell - (1-\rho)\sum_{\substack{j=1\\ j\neq\ell}}^{L} \frac{Q_{L,j}^\ell}{s_j} + \mathcal{O}\left(s^{-2}\right). \tag{D.11}$$

where

$$T_L^\ell = \begin{vmatrix} -1 & -\gamma_- & 0 & \cdots & -R & \cdots & 0 \\ \gamma_+ & -\rho & -\gamma_- & \cdots & \alpha & \cdots & 0 \\ 0 & \gamma_+ & -\rho & \cdots & \alpha & \cdots & 0 \\ \vdots & \vdots & \vdots & & \vdots & & \vdots \\ 0 & 0 & 0 & \cdots & \alpha & \cdots & -\rho \\ (0) & & & & (\ell) & & (L) \end{vmatrix} \tag{D.12}$$

and $Q_{L,j}^\ell$ is the determinant that results when we substitute the j-th column of T_L^ℓ by $\boldsymbol{\delta}_j$ ($j\neq\ell$).

Expanding T_L^ℓ along its first row we get

$$T_L^\ell = -\alpha A_{L,\ell} + \alpha\gamma_+\gamma_- A_{L-1,\ell-1} + (-1)^{\ell+1} R\gamma_+^\ell E_{L-\ell-1}, \tag{D.13}$$

where we define the new $i\times i$ determinants $A_{i,j}$ as

$$A_{i,j} = \begin{vmatrix} -\rho & -\gamma_- & 0 & \cdots & 1 & \cdots & 0 \\ \gamma_+ & -\rho & -\gamma_- & \cdots & 1 & \cdots & 0 \\ 0 & \gamma_+ & -\rho & \cdots & 1 & \cdots & 0 \\ \vdots & \vdots & \vdots & & \vdots & & \vdots \\ 0 & 0 & 0 & \cdots & 1 & \cdots & -\rho \\ (1) & & & & (j) & & (i) \end{vmatrix} \tag{D.14}$$

that satisfy the recurrence equation

$$A_{n,j} = -\rho A_{n-1,j} + \gamma_+\gamma_- A_{n-2,j} + \gamma_-^{n-j} E_{j-2}, \tag{D.15}$$

for $j = 1,2,\ldots,n-1$ (with the boundary conditions $A_{j,j+1}=0$ and $A_{j,0}=0$), and

$$A_{n,n} = -\gamma_+ A_{n-1,n-1} + E_{n-2}. \tag{D.16}$$

These relations can be explicitly solved. On the one hand, by definition $A_{1,1}=1$, which amounts to choosing $E_{-1}\equiv 1$ for this to be compatible with (D.16). Moreover, making use again of a generating function, the solution of (D.16) is

$$A_{j,j} = \frac{(-1)^{j-1}\gamma_-^j}{\gamma_- - \gamma_+ + \rho}\left[\frac{\rho}{\gamma_-}a_{j-1} + \frac{\gamma_+ + \rho}{\gamma_-}a_{j-2} + \frac{\gamma_+}{\gamma_-}a_{j-3} - \left(\frac{\gamma_+}{\gamma_-}\right)^j\right], \tag{D.17}$$

for $j \geq 2$. On the other hand, the explicit solution of (D.15) is

$$A_{j+k,j} = (-1)^k \gamma_-^{k+1} a_{k+1} A_{j,j} + \frac{\gamma_-^k E_{j-2}}{\gamma_- - \gamma_+ + \rho} \left[(-1)^{k+1} (\gamma_- a_k - \gamma_+ a_{k-1}) + \gamma_- \right], \tag{D.18}$$

for $k \geq 1$. Therefore equations (D.17) and (D.18), together with (D.13), provide an explicit expression for the determinant T_L^ℓ.

Fortunately, $Q_{L,j}^\ell$ can be written in terms of previous determinants since $Q_{L,j}^\ell$ is a block-diagonal determinant that satisfies

$$Q_{L,j}^\ell = D_{j-1} A_{L-\ell,\ell-j}, \quad \text{for} \quad k < j, \tag{D.19}$$

$$Q_{L,j}^\ell = E_{L-j-1} T_{j-1,\ell}, \quad \text{for} \quad k > j. \tag{D.20}$$

This completes the analytical approximation of the equilibrium densities of our dynamical model. We have derived explicit expressions for all the terms involved in (D.1), (D.3) and (D.11) up to leading order in s_ℓ^{-1}. Note that the same technique applied in this approximation can be extended to obtain the exact dependence on $\{s_\ell\}_{\ell=1}^L$. Higher-order terms in powers of s_ℓ^{-1} introduce in the corresponding determinants several column vectors of the type of $\boldsymbol{\delta}_\ell$ making each determinant to be block-diagonal involving D_ℓ, E_ℓ, $A_{i,j}$ or $T_{\ell,k}^j$, so that the general solution contains in each term a product of a certain combination of these determinants. This expression can be explicitly written, but it is too cumbersome. The approximations here obtained are both sufficiently simple and accurate enough to capture the behavior of population densities in the communities belonging to recurrent sets.

E

Proof of the positivity of the overall population level

This appendix is devoted to proving that the overall population level u_0 [Eq. (6.38)] is positive under ecologically sound assumptions. This result is stated in the following

Theorem E.1. *The overall population level u_0 given by Eq.* (6.38) *is positive if*

$$\epsilon > 1/e - \varphi, \tag{E.1}$$

$$\omega_{\mathrm{D}} < c_{\mathrm{B}}|_{\epsilon=1/e-\varphi} + \frac{1}{e} f_{\mathrm{B}}|_{\epsilon=1/e-\varphi}, \tag{E.2}$$

c_{B} and f_{B} being defined by Eqs. (6.33) *and* (6.36) *respectively, and the following (natural) assumptions hold:*

(i) Predators only eat prey that are smaller than themselves. This means that $a(y) \neq 0$ only if $y > 0$.

(ii) Predators always gain weight during feeding, i.e., $\chi_{\mathrm{P}}(y, z) \neq 0$ only if $z > y$.

(iii) Offspring are always smaller than their parent, which always looses weight during spawning, i.e., $\chi_{\mathrm{B}}(y, z) \neq 0$ only if both $y > 0$ and $z < 0$.

(iv) All the functions a, χ_{P} and χ_{B} are non-negative and have non-vanishing integrals.

Let us now prove the theorem.

We define the functions $q_1(\epsilon) = c_{\rm P} + (\epsilon+\varphi) f_{\rm P}$ and $q_2(\epsilon) = c_{\rm B} - \omega_{\rm D} + (\epsilon+\varphi) f_{\rm B}$. These are the denominator and numerator in the expression (6.38) for u_0. We will show that these two functions are both positive under the above assumptions.

The partial derivative of q_1 with respect to ϵ is

$$\frac{\partial q_1}{\partial \epsilon} = \int dy a(y) e^{\epsilon y} \left[y + (\epsilon+\varphi-1) \int dz (y+z) e^{(\epsilon+\varphi)z} \chi_{\rm P}(y,z) \right] + f_{\rm P}. \quad \text{(E.3)}$$

Assumptions (i) and (ii) imply that, wherever the integrand is nonzero, we have $z > y > 0$, hence $e^{(\epsilon+\varphi)z} > 1$ and

$$\int dz (y+z) e^{(\epsilon+\varphi)z} \chi_{\rm P}(y,z) > y, \quad \text{(E.4)}$$

since $\chi_{\rm P}$ is normalized to unity. Substituting back into (E.3) and using assumption (iv) shows that $\partial q_1/\partial\epsilon > 0$ for all ϵ. Moreover, at the particular point $\epsilon = -\varphi$ we can calculate

$$q_1(-\varphi) = \int dy\, a(y) e^{-\varphi y} > 0. \quad \text{(E.5)}$$

Therefore the monotonicity of q_1 implies that $q_1(\epsilon) > 0$ for all $\epsilon > -\varphi$ (in particular, this argument proves that $q_1(\epsilon) > 0$ for $\epsilon > 1/e - \varphi$).

Similarly we calculate

$$\frac{\partial q_2}{\partial \epsilon} = \int dy \int dz\, \chi_{\rm B}(y,z) \left[1 - y e^{-(\epsilon+\varphi)y} + e^{-z}(1-e^{-y})(z e^{(\epsilon+\varphi)z} + 1) \right]. \quad \text{(E.6)}$$

According to assumption (iii), $y > 0$ and $z < 0$ wherever the integrand is nonzero, therefore $1 - e^{-y} > 0$. For $\epsilon > 1/e - \varphi$ we also have $y e^{-(\epsilon+\varphi)y} < 1$ and $z e^{(\epsilon+\varphi)z} > -1$ wherever the integrand is nonzero.[1] Hence assumption (iv) implies that $\partial q_2/\partial\epsilon > 0$ and q_2 is strictly increasing with ϵ. This implies the positivity of q_2 for all $\epsilon > 1/e - \varphi$ if q_2 is nonnegative at $\epsilon = 1/e - \varphi$, i.e., if Eq. (E.2) holds. Such a condition represents a positive upper bound on the mortality rate $\omega_{\rm D}$ because $f_{\rm B}$ is always positive and $c_{\rm B} > 0$ at $\epsilon + \varphi = 1/e$. In particular, in the absence of intrinsic mortality ($\omega_{\rm D} = 0$) the upper bound (E.2) is automatically verified. Therefore, if $\epsilon > 1/e - \varphi$ and the bound (E.2) holds then the overall population level is positive and the theorem is proven.

This theorem shows that, under ecologically natural assumptions, the overall population level is positive when the mortality rate is "not too large" and the steady-state exponent satisfies $\epsilon > 1/e - \varphi$. Note that this inequality holds for exponents contained in the region of observed values, since $\theta \approx 2$ ($\epsilon \approx 1$) and $\varphi \approx 1/4$.

[1] The bound $y e^{-(\epsilon+\varphi)y} < 1$ for $\epsilon + \varphi > 1/e$ is a consequence of the fact that the maximum value of the function $y e^{-(\epsilon+\varphi)y}$ is reached at $y = (\epsilon+\varphi)^{-1}$. At that point, the maximum value $[(\epsilon+\varphi)e]^{-1} < 1$ if $\epsilon + \varphi > 1/e$.

Publications

The original content of this thesis appears in the following papers:

- Chapter 2:
  - *The struggle for space: Viral extinction through competition for cells*, J. A. Cuesta, J. Aguirre, J. A. Capitán and S. C. Manrubia, submitted to *Phys. Rev. Lett.* (2010).
- Chapters 3 and 4:
  - *Statistical mechanics of ecosystem assembly*, J. A. Capitán, J. A. Cuesta and J. Bascompte, *Phys. Rev. Lett.* **103**, 168101-4 (2009).
  - *Species assembly in model ecosystems, I: Analysis of the population model and the invasion dynamics*, J. A. Capitán and J. A. Cuesta, *J. Theor. Biol.* DOI:10.1016/j.jtbi.2010.09.032 (2010).
  - *Species assembly in model ecosystems, II: Results of the assembly process*, J. A. Capitán, J. A. Cuesta and J. Bascompte, *J. Theor. Biol.* DOI:10.1016/j.jtbi.2010.10.031 (2010).
- Chapter 5:
  - *Catastrophic regime shifts in model ecological communities are true phase transitions*, J. A. Capitán and J. A. Cuesta, *J. Stat. Mech.* **10**, P10003 (2010).
- Chapter 6:
  - *Scale-invariant model of marine population dynamics*, J. A. Capitán and G. W. Delius, *Phys. Rev.* E, **81**, 061901-15 (2010).

Resumen

En esta tesis hemos aplicado las técnicas y herramientas de la mecánica estadística y la teoría de procesos estocásticos al estudio y análisis de tres modelos representativos de sistemas biológicos de interés. Estos modelos se han introducido siguiendo el espíritu de la mecánica estadística, es decir, tratando de desarrollar modelos simplificados que predigan, al menos cualitativamente, los fenómenos bioógicos que se intentan describir. En particular, nos hemos centrado en dos tipos de sistemas: (i) conjuntos heterogéneos de virus y (ii) ecosistemas, los cuales han sido descritos desde dos puntos de vista distintos pero complementarios: como redes de interacciones tróficas, por un lado, y como distribuciones de tamaño, por otro, olvidándonos de la taxonomía y describiendo las especies exclusivamente según su tamaño corporal. Como sistemas complejos, todos muestran los fenómenos de auto-organización y transiciones de fase, y se pueden describir adecuadamente, desde un punto de vista teórico, en el marco de la mecánica estadística.

Esta tesis tiene una clara división en tres partes. En la primera (Capítulo 2) se introduce y analiza un modelo espacial de propagación de infecciones virales. La replicación a altas tasas de mutación y la producción de un gran número de réplicas es una estrategia usual que los virus han desarrollado para sobrevivir, y que les permite una rápida adaptación a ambientes variables. Esto fuerza a las células susceptibles de infección a desarrollar mecanismos de lucha contra el virus. Es de vital importancia entender los mecanismos que producen la extinción de cepas virales, para el diseño de terapias y protocolos que anulen la propagación. La explicación tradicional proviene de la teoría de cuasiespecies (Eigen 1971), según la cual la mutación a ritmos altos puede provocar la extinción del fenotipo más adaptado. Sin embargo, la evidencia experimental acumulada desde entonces ha dado lugar a modelos más realistas.

Nuestro modelo de infección viral (Cuesta et al. 2010) se basa en un nuevo mecanismo de extinción debido a la competición espacial para infectar células susceptibles. El modelo describe la dinámica de un conjunto fenotípicamente heterogéneo de virus sujeto a mutaciones beneficiosas, deletéreas y letales. Además, la célula es capaz de desarrollar defensas contra la infección. Cuando el número de células accesibles es ilimitado, la población viral puede crecer ilimitadamente para evitar la extinción. Por el contrario, cuando la restricción espacial se hace explícita en el modelo, la ventaja

que el virus puede obtener queda limitada por la accesibilidad a células vecinas, y la extinción resulta cuando las defensas celulares aumentan por encima de un umbral crítico. Nuestros resultados pueden ser relevantes para enterder la propagación de infecciones en cosechas o tejidos que limiten la movilidad viral, como las hojas de plantas. Este modelo es, por tanto, relevante en cuanto a las implicaciones que diferentes geometrías tienen en el diseño de terapias de control efectivas.

En la segunda parte (Capítulos 3–5) nos centramos en el modelado matemático de ecosistemas como redes tróficas. El proceso histórico por el cual los ecosistemas van formándose es un claro ejemplo de auto-organización. Aunque el estado de cada comunidad ecológica es consecuencia directa de su historia, hay patrones globales que se pueden extraer de ellas. Nuestro trabajo (Capitán et al. 2009; Capitán y Cuesta 2010b; Capitán et al. 2010) es una manifestación de este hecho. En estos trabajos introducimos un modelo sencillo de "ensamblado" de ecosistemas para el que podemos analizar todos los posibles caminos generados por invasiones sucesivas de especies. Así, el modelo caracteriza de forma completa el espacio de fases del sistema como un grafo dirigido, cuyos nodos son las comunidades modelo y cuyos enlaces son transiciones entre ellas inducidas por invasiones. Esto nos permite describir el proceso de ensambado como una cadena de Markov, de la que demostramos que tiene un único conjunto de estados recurrentes, que resulta ser el estado final del proceso dado que sucesivas invasiones no sacan al proceso fuera de este conjunto. A pesar de su simplicidad, nuestro modelo recupera la mayoría de los resultados de modelos previos similares, como el aumento de la biodivdersidad creciente conforme tienen lugar las invasiones, o la tendencia a aumentar en media la población total. Todo ello con la ventaja de que todas las magnitudes pueden calcularse de forma exacta.

En el Capítulo 3 realizamos un análisis exhaustivo del modelo. El estudio del grafo nos permite clasificar las comunidades como transitorias o recurrentes, pudiendo ser estas últimas o bien una sola comunidad o bien un conjunto cerrado de ellas conectadas mediante invasiones. Esto prueba que los estados finales del proceso son independientes de la secuencia de invasiones. La cadena de Markov permite hallar una distribución asintótica de probabilidades para los estados recurrentes, que sirve para promediar cuaquier observable así como la variación temporal de las magnitudes en el tiempo. Como los tiempos de absorción al estado recurrente resultan ser pequeños comparados con el tamaño del sistema, el estado final se alcanza rápidamente (en unidades del tiempo medio entre invasiones) y las comunidades pueden verse como un sistema complejo fluctuando en el que las especies se van reemplazando continuamente sin salir del conjunto de patrones recurrentes.

En el Capítulo 4 se obtienen algunos resultados analíticos y, mediante ciertas aproximaciones, se reconstruyen los resultados obtenidos mediante simulación. En particular, probamos que las comunidades de los estados finales son piramidales y las densidades de población en equilibrio dependen inversamente del número de especies en cada nivel trófico. Además, resulta que la tasa de crecimiento per cápita de un invasor en el nivel $L + 1$ (en una comunidad de L niveles tróficos) es clave para explicar la aparición de conjuntos recurrentes complejos. El signo de esa tasa permite separar regiones donde hay un único estado absorbente y regiones con conjuntos recurrentes

con más de una comunidad. Hemos obtenido también aproximaciones a la dinámica global de las poblaciones, lo que nos ayuda a determinar con buena aproximación qué comunidades están presentes en los estados finales. La comparación con los resultados obtenidos integrando las ecuaciones numéricamente es excelente.

El modelo es "minimalista" y, como tal, permite introducir modificaciones que revelen una fenomelogía completamente nueva. En el Capítulo 5 se discute el efecto que las extinciones espontáneas de especies tienen en nuestro modelo, dando lugar a una transición de fase entre dos estados, uno con comunidades diversas y otro con comunidades de pocas especies. Este fenómeno no es nuevo. En la naturaleza se observa que los ecosistemas pueden sufrir cambios abruptos como respuesta a variaciones ambientales graduales. Tales cambios se explican teóricamente como transiciones entre dos estados estables alternativos. Los modelos al uso introducen términos no lineales en la dinámica que dan lugar a atractores estables diferentes entre los que tiene lugar la transición. Por el contrario, con nuestro modelo damos una expliación alternativa a estos cambios catastróficos de régimen. Las comunidades en nuestro modelo son diferentes micro-estados en el espacio configuracional de la cadena de Markov. La tasa se extinción espontánea, que engloba genéricamente los cambios en las condiciones externas, sirve de parámetro de control. Al aumentar la tasa de extinción se produce un cambio de régimen. Este punto de vista microscópico permite recuperar los principales resultados de los trabajos previos empíricos y teóricos como varianzas anómalas, ciclos de histéresis, cascadas tróficas, etc. Y lo que es más importante, un análisis espectral de la matriz de transiciones de la cadena de Markov nos permite establecer rigurosamente que estamos observando la traza, en un sistema de tamaño finito, de una verdadera transición de fase provocada por extinciones espontáneas (Capitán y Cuesta 2010a).

Finalmente, en la tercera parte (Capítulo 6) se introduce y discute un modelo de dinámica de poblaciones para ecosistemas basados en el tamaño. Los ecosistemas marinos se describen bien ignorando las relaciones exactas de depredación entre especies. Bajo esta suposición se observa una regularidad sorprendente en estos escosistemas: la abundancia de organismos en función de su tamaño sigue aproximadamente una ley de potencias válida en varios órdenes de magnitud. Este resultado lo interpretamos como evidencia de que la dinámica de poblaciones en el océano es aproximadamente invariante de escala. Mediante un proceso de Markov definido por los procesos elementales de depredación, reproducción, respiración y mortalidad, derivamos una ecuación en derivadas parciales que describe la dependencia en tiempo y tamaño de las abundancias de especies. Este modelo representa una extensión de modelos previos basados en la ecuación de McKendrick-von Foerster (Silvert y Platt 1978). El exponente de la ley de escala obtenida como estado estacionario viene determinado por el escalado relativo de las tasas de procesos dependientes de la densidad (depredación) y las tasas de procesos independientes de la densidad (reproducción, respiración y mortalidad). La estabilidad del estado estacionario frente a pequeñas perturbaciones es analizada y encontramos que los procesos respiratorios y reproductivos tienen un fuerte efecto estabilizador (Capitán y Delius, 2010).

References

Numbers in brackets show the page numbers in which references are cited.

Aguirre J., and Manrubia S. C. (2008). Effects of spatial competition on the diversity of a quasispecies. *Phys. Rev. Lett.* **100**, 38106–4. [10, 25, 28, 33, 42]

Alonso D., Ostling A., and Etienne R. S. (2008). The implicit assumption of symmetry and the species abundance distribution. *Ecol. Lett.* **11**, 93–105. [61]

Altmeyer S., and McCaskill J. S. (2001). Error threshold for spatially resolved evolution in the quasispecies model. *Phys. Rev. Lett.* **86**, 5819–5822. [25]

Andersen K. H., and Beyer J. E. (2006). Asymptotic size determines species abundance in the marine size spectrum. *Am. Nat.* **168**, 54–61. [126, 127, 148, 149, 164]

Andersen K. H., Beyer J. E., and Lundberg P. (2008). Trophic and individual efficiencies of size-structured communities. *Proc. R. Soc. B* **276**, 109–114. [126, 127]

Anderson C. N. K., Hsieh C.-H., Sandin S. A., Hewitt R., Hollowed A., Beddington J., May R. M., and Sugihara G. (2008). Why fishing magnifies fluctuations in fish abundance. *Nature* **452**, 835–839. [104, 129]

Anderson P. W. (1973). More is different. *Science* **177**, 393–396. [3, 4]

Arino O., Shin Y.-J., and Mullon C. (2004). A mathematical derivation of size spectra in fish populations. *C. R. Biol.* **327**, 245–254. [126, 129, 140]

Atman A. P. F., and Dickman R. (2002). Quasistationary distributions for the Domany-Kinzel stochastic cellular automaton. *Phys. Rev. E* **66**, 046135–9. [35]

Baker G. L., and Gollub J. P. (1990). *Chaotic dynamics: An introduction*. Cambridge: Cambridge University Press. [4]

Barnes C., Bethea D. M., Brodeur R. D., Spitz J., Ridoux V., Pusineri C., Chase B. C., Hunsicker M. E., Juanes F., Kellermann A., Lancaster J., Ménard F., Bard F.-X., Munk P., Pinnegar J. K., Scharf F. S., Rountree R. A., Stergiou K. I., Sassa

C., Sabates A., and Jennings S. (2008). Predator and prey body sizes in marine food webs. *Ecology* **89**, 881–881. [147]

Barrat A., Barthélemy M., and Vespignani A. (2008). *Dynamical processes on complex networks*. Cambridge: Cambridge University Press. [24]

Bascompte J., and Melián C. J. (2005). Simple trophic modules for complex food webs. *Ecology* **86**, 2868–2873. [56]

Bastolla U., Lässig M., Manrubia S. C., and Valleriani A. (2005a). Biodiversity in model ecosystems, I: Coexistence conditions for competing species. *J. Theor. Biol.* **235**, 521–530. [57, 58, 63, 78, 158, 162]

Bastolla U., Lässig M., Manrubia S. C., and Valleriani A. (2005b). Biodiversity in model ecosystems, II: Species assembly and food web structure. *J. Theor. Biol.* **235**, 531–539. [57, 58, 78, 156]

Bender C. M., and Orszag S. A. (1984). *Advanced mathematical methods for scientists and engineers*. Singapore: McGraw–Hill. [93]

Benoît E., and Rochet M.-J. (2004). A continuous model of biomass size spectra governed by predation and the effects of fishing on them. *J. Theor. Biol.* **226**, 9–21. [126, 127, 129, 135, 136, 138]

Blanchard J. L., Jennings S., Law R., Castle M. D., McCloghrie P., Rochet M.-J., and Benoît E. (2009). How does abundance scale with body size in coupled size-structured food webs? *J. Anim. Ecol.* **78**, 270–280. [127, 136]

Borrvall C., Ebenman B., and Jonsson T. (2000). Biodiversity lessens the risk of cascading extinction in model food webs. *Ecol. Lett.* **3**, 131–136. [59]

Boudreau P. R., and Dickie L. M. (1992). Biomass spectra of aquatic ecosystems in relation to fisheries yield. *Can. J. Fish. Aquat. Sci.* **49**, 1528–1538. [126]

Broadbent S. R., and Hammersley J. M. (1957). Percolation processes. Crystals and mazes. *Proc. Camb. Phil. Soc.* **53**, 629–641. [172]

Brown J. H., Gillooly J. F., Allen A. P., Savage V. M., and West G. B. (2004). Toward a metabolic theory of ecology. *Ecology* **85**, 1771–1789. [136, 164]

Bull J. J., Meyers L. A., and Lachmann M. (2005). Quasispecies made simple. *PLoS Comput. Biol.* **1**, 450–460. [23, 24]

Camacho J., and Solé R. V. (2001). Scaling in ecological size spectra. *Europhys. Lett.* **55**, 774–780. [126, 127, 129, 146]

Capitán J. A., and Cuesta J. A. (2010a). Catastrophic regime shifts in model ecological communities are true phase transitions. *J. Stat. Mech.* **10**, P10003. [13]

Capitán J. A., and Cuesta J. A. (2010b). Species assembly in model ecosystems, I: Analysis of the population model and the invasion dynamics. *J. Theor. Biol.* DOI:10.1016/j.jtbi.2010.09.032. [12]

Capitán J. A., Cuesta J. A., and Bascompte J. (2009). Statistical mechanics of ecosystem assembly. *Phys. Rev. Lett.* **103**, 168101–4. [12]

Capitán J. A., Cuesta J. A., and Bascompte J. (2010). Species assembly in model ecosystems, II: Results of the assembly process. *J. Theor. Biol.* DOI:10.1016/j.jtbi.2010.10.031. [12]

Capitán J. A., and Delius G. W. (2010). Scale-invariant model of marine population dynamics. *Phys. Rev. E* **81**, 061901–15. [13]

Case T. J. (1990). Invasion resistance arises in strongly interacting species-rich model competition communities. *Proc. Natl. Acad. Sci. USA* **87**, 9610–9614. [50, 51]

Case T. J. (1991). Invasion resistance, species build-up and community collapse in metapopulation models with interspecies competition. *Biol. J. Linn. Soc.* **42**, 239–266. [55, 84]

Cases-González C., Arribas M., Domingo E., and Lázaro E. (2008). Beneficial effects of population bottlenecks in an RNA virus evolving at increased error rate. *J. Mol. Biol.* **384**, 1120–1129. [25]

Clarke A., and Johnston N. M. (1999). Scaling of metabolic rate with body mass and temperature in teleost fish. *J. Anim. Ecol.* **68**, 893–905. [136]

Cohen J. E., Briand F., and Newman C. M. (1990). *Community food webs*. Berlin: Springer-Verlag. [85]

Cohen J. E., Pimm S. L., Yozdis P., and Saldaña J. (1993). Body sizes of animal predators and animal prey in food webs. *J. Anim. Ecol.* **62**, 67–78. [51]

Coutts B. A., Thomas-Carroll M. L., and Jones R. A. C. (2004). Analysing spatial patterns of spread of Lettuce necrotic yellows virus and lettuce big-vein disease in lettuce field plantings. *Ann. Appl. Biol.* **145**, 339–343. [25]

Crooks K. R., and Soulé M. E. (1999). Mesopredator release and avifaunal extinctions in a fragmented system. *Nature* **400**, 563–566. [76]

Cuesta J. A. (2010). Huge progeny production during the transient of a quasi-species model of viral infection, reproduction and mutation. *Math. Comp. Mod.*, submitted. [26, 27]

Cuesta J. A., Aguirre J., Capitán J. A., and Manrubia S. C. (2010). The struggle for space: Viral extinction through competition for cells. *Phys. Rev. Lett.*, submitted. [11, 205]

Cuesta J. A., and Sánchez A. (2004). General non-existence theorem for phase transitions in one-dimensional systems with short range interactions, and physical examples of such transitions. *J. Stat. Phys.* **115**, 869–893. [117]

Cushing J. M. (1992). A size-structured model for cannibalism. *Theor. Popul. Biol.* **42**, 347–361. [126]

Daskalov G. M., Grishin A. N., Rodionov S., and Mihneva V. (2007). Trophic cascades triggered by overfishing reveal possible mechanisms of ecosystem regime shifts. *Proc. Natl. Acad. Sci. USA* **104**, 10518–10523. [106, 114, 121]

Datta S., Delius G. W., and Law R. (2010a). A jump-growth model for predator-prey dynamics: derivation and application to marine ecosystems. *Bulletin of Mathematical Biology* **72**, 1361–1382. [128–130, 134, 135, 138–140]

Datta S., Delius G. W., Law R., and Plank M. J. (2010b). A stability analysis of the power-law steady state of marine size spectra. *arXiv:1001.3826v1*. [129, 140, 142, 144, 148]

Domany E., and Kinzel W. (1984). Equivalence of cellular automata to Ising models and directed percolation. *Phys. Rev. Lett.* **53**, 311–314. [170]

Done T. J. (1991). Phase shifts in coral reef communities and their ecological significance. *Hydrobiologia* **247**, 121–132. [103, 108]

Drake J. A. (1990). The mechanics of community assembly and succession. *J. Theor. Biol.* **147**, 213–233. [50, 51, 72]

Drake J. A. (1991). Community-assembly mechanics and the structure of an experimental species ensemble. *Am. Nat.* **137**, 1–26. [50]

Drossel B., McKane A. J., and Quince C. (2004). The impact of nonlinear functional responses on the long-term evolution of food-web structure. *J. Theor. Biol.* **229**, 539–548. [155]

Dunne J. A. (2006). The network structure of food webs. In Pascual M., and Dunne J. A. (Eds.), *Ecological Networks*, pp. 27–86. Oxford: Oxford University Press. [49, 50, 56]

Durrant W. E., and Dong X. (2004). Systemic acquired resistance. *Annu. Rev. Phytopathol.* **42**, 185–209. [43]

Eigen M. (1971). Self-organization of matter and evolution of biological macromolecules. *Naturwissenschaften* **58**, 465–523. [11, 18, 30, 205]

Eigen M. (2002). Error catastrophe and antiviral strategy. *Proc. Natl. Acad. Sci. USA* **99**, 13374–13376. [24]

Eigen M., and Schuster P. (1977). The hypercycle, a principle of natural self-organization. Part A: Emergence of the hypercycle. *Naturwissenschaften* **64**, 541–565. [9]

Eklöf A., and Ebenman B. (2006). Species loss and secondary extinctions in simple and complex model communities. *J. Anim. Ecol.* **75**, 239–246. [59]

Elton C. S. (1958). *Ecology of invasions by animals and plants*. London: Chapman & Hall. [47]

Etienne R. S., and Alonso D. (2007). Neutral community theory: How stochasticity and dispersal-limitation can explain species coexistence. *J. Stat. Phys.* **128**, 485–510. [61]

Feller W. (1968). *An introduction to probability theory and its applications*, Volume I. New York: Wiley. [111, 177]

Fernández A., and Fort H. (2009). Catastrophic phase transitions and early warnings in a spatial ecological model. *J. Stat. Mech.* **9**, 09014–21. [104, 105, 110, 116, 120]

Fernández P., and Solé R. V. (2005). Graphs as models of large-scale biochemical organizarion. In Bonachev D., and Rouvrai D. H. (Eds.), *Complexity in chemistry, biology and ecology*, pp. 155–190. New York: Springer. [9]

Fishbase (2010). World Wide Web electronic publication. Edited by R. Froese and D. Pauly. `http://www.fishbase.org` (version 01/2010). [140, 149]

Fontana W. (2002). Modelling 'evo-devo' with RNA. *BioEssays* **24**, 1164–1177. [22]

Frank K. T., Petrie B., Choi J. S., and Leggett W. C. (2005). Trophic cascades in a formerly cod-dominated ecosystem. *Science* **308**, 1621–1623. [129]

Fukami T. (2004). Community assembly along a species pool gradient: Implications for multiple-scale patterns of species diversity. *Popul. Ecol.* **46**, 137–147. [156]

Fukami T., and Morin P. J. (2003). Productivity-biodiversity relationships depend on the history of community assembly. *Science* **424**, 423–426. [85]

Gabriel W., Lynch M., and Burger R. (1993). Muller's ratchet and mutational meltdowns. *Evolution* **47**, 1744–1757. [24]

García-Arenal F., Fraile A., and Malpica J. M. (2001). Variability and genetic structure of plant virus populations. *Annu. Rev. Phytopathol.* **39**, 157–186. [24]

Gavrilets S. (2004). *Fitness landscapes and the origin of species*. Princeton: Princeton University Press. [17, 18, 22]

Genz A. (1992). Numerical Computation of Multivariate Normal Probabilities. *J. Comp. Graph. Stat.* **1**, 141–150. [161]

Gilmore R. (1981). *Catastrophe theory for scientists and engineers*. New York: Dover. [120]

Grande-Pérez A., Lázaro E., Lowenstein P., Domingo E., and Manrubia S. C. (2005). Suppression of viral infectivity through lethal defection. *Proc. Natl. Acad. Sci. USA* **102**, 4448–4452. [24]

Grassberger P. (1982). On phase transitions in Schögl's second model. *Z. Phys. B* **47**, 365–374. [172]

Grassberger P. (1983). On the critical-behavior of the general epidemic process and dynamical percolation. *Math. Biosc.* **63**, 157–172. [42]

Grassberger P., and de la Torre A. (1979). Reggeon field theory (Schögl's first model) on a lattice: Monte Carlo calculation of critical behaviour. *Ann. Phys. (New York)* **122**, 373–396. [34]

Hartvig M., Andersen K. H., and Beyer J. E. (2010). Food web framework for size-structured populations. *arXiv:1004.4138v1*. [149, 164]

Heath M. R. (1995). Size spectrum dynamics and the planktonic ecosystem of Loch Linnhe. *ICES J. Mar. Sci.* **52**, 627–642. [126]

Hewitt C. L., and Huxel G. R. (2002). Invasion success and community resistance in single and multiple species invasion models: Do the models support the conclusions? *Biol. Inv.* **4**, 263–271. [156]

Hinrichsen H. (2000). Non-equilibrium critical phenomena and phase transitions into absorbing states. *Adv. Phys.* **49**, 815–958. [30, 34, 42, 155, 171, 172]

Hofbauer J., and Sigmund K. (1998). *Evolutionary games and population dynamics*. Cambridge: Cambridge University Press. [52, 56, 58, 60, 61, 77, 84]

Holling C. S. (1959). The components of predation as revealed by a study of small-mammal predation of the European pine sawfly. *Can. Entomol.* **91**, 293–320. [104]

Hsieh C.-H., Reiss C. S., Hunter J. R., Beddington J. R., May R. M., and Sugihara G. (2006). Fishing elevates variability in the abundance of exploited species. *Nature* **443**, 859–862. [104, 106, 129]

Huang K. (1987). *Statistical mechanics*. New York: Wiley. [4, 50, 105]

Hubbell S. P. (2001). *The unified theory of biodiversity and biogeography*. Princeton: Princeton University Press. [61]

Huntley M. E., and Lopez M. D. G. (1992). Temperature-dependent production of marine copepods: A global synthesis. *Am. Nat.* **140**, 201–242. [149]

Huynen M. A., Stadler P. F., and Fontana W. (1996). Smoothness within ruggedness: The role of neutrality in adaptation. *Proc. Natl. Acad. Sci. USA* **93**, 397–401. [22]

Iranzo J., and Manrubia S. C. (2009). Stochastic extinction of viral infectivity through the action of defectors. *Europhys. Lett.* **85**, 18001. [10, 24]

Janssen H. K. (1981). On the non-equilibrium phase-transition in reaction-diffusion systems with an absorbing stationary state. *Z. Phys. B: Cond. Mat.* **42**, 151–154. [172]

Jennings S., and Mackinson S. (2003). Abundance and body mass relationships in size-structured food webs. *Ecol. Lett.* **6**, 971–974. [126, 140]

Jennings S., Pinnegar J. K., Polunin N. V. C., and Boon T. W. (2001). Weak cross-species relationships between body size and trophic level belie powerful size-based trophic structuring in fish communities. *J. Anim. Ecol.* **70**, 934–944. [125]

Kang B.-C., Yeam I., and Jahn M. M. (2005). Genetics of plant virus resistance. *Annu. Rev. Phytopathol.* **43**, 581–621. [42]

Karlin S., and Taylor H. M. (1975). *A first course in stochastic processes*. New York: Academic Press. [55, 68, 156]

Kauffman S. A. (1969). Metabolic stability and epigenesis in randomly constructed genetic nets. *J. Theor. Biol.* **22**, 437–467. [9]

Kauffman S. A. (1993). *The origins of order*. Oxford: Oxford University Press. [10]

Kauffman S. A. (1995). *At home in the universe. The search for laws of self-organization and complexity*. Oxford: Oxford University Press. [6]

Kerr S. R., and Dickie L. M. (2001). *The biomass spectrum: A predator-prey theory of aquatic production*. New York: Columbia University Press. [126, 129, 140]

Kimmel M., and Axelrod D. E. (2002). *Random processes in biology*. New York: Springer-Verlag. [19]

Kimura M. (1968). Evolutionary rate at the molecular level. *Nature* **217**, 624–626. [21]

Kinzel W. (1983). Directed percolation. In Deutscher G., Zallen R., and Adler J. (Eds.), *Percolation structures and processes: Annals of the Israel physical society*, Volume V, pp. 143–171. Bristol: Adam Hilger. [172]

Kirillov A. A. (1994). *Representation theory and noncommutative harmonic analysis*, Volume I. New York: Springer. [164]

Knipe D. M., and Howley P. M. (2007). *Fields Virology*, Volume I. Philadelphia, USA: Lippincott, William & Wilkins. [26, 43]

Knuth D. (1997). *The art of computer programming*, Volume I. Fundamental algorithms. Reading, Massachusetts: Addison-Wesley. [190]

Kokkoris G. D., Troumbis A. Y., and Lawton J. H. (1999). Patterns of species interaction strength in assembled theoretical competition communities. *Ecol. Lett.* **2**, 70–74. [59, 65]

Kooijman S. A. L. M. (2000). *Dynamic energy and mass budgets in biological systems*. Cambridge: Cambridge University Press. [164]

Koonin E. V., Senkevich T. G., and Dolja V. V. (2006). The ancient Virus World and evolution of cells. *Biol. Direct* **1**, 29. [24]

Kraus M., Wintz W., Seifert U., and Lipowsky R. (1996). Fluid vesicles in shear flow. *Phys. Rev. Lett.* **77**, 3685–3688. [9]

Kun A., Santos M., and Szathmáry E. (2005). Real ribozymes suggest a relaxed error threshold. *Nat. Gen.* **37**, 1008–1011. [22]

Lässig M., Bastolla U., Manrubia S. C., and Valleriani A. (2001). Shape of ecological networks. *Phys. Rev. Lett.* **86**, 4418–4421. [57–59, 162]

Law R. (1999). Theoretical aspects of community assembly. In McGlade J. (Ed.), *Advanced ecological theory: Principles and applications*, pp. 143–171. Oxford: Blackwell Science. [50–52]

Law R., and Blackford J. C. (1992). Self-assembling food webs: A global viewpoint of coexistence of species in Lotka-Volterra communities. *Ecology* **73**, 567–579. [50]

Law R., and Morton R. D. (1993). Alternative permanent states of ecological communities. *Ecology* **74**, 1347–1361. [50]

Law R., and Morton R. D. (1996). Permanence and the assembly of ecological communities. *Ecology* **77**, 762–775. [50, 51, 82, 92]

Law R., Plank M. J., James A., and Blanchard J. L. (2009). Size-spectra dynamics from stochastic predation and growth of individuals. *Ecology* **90**, 802–811. [126, 127, 129, 140]

Lee Y., and Yin J. (1996). Detection of evolving viruses. *Nat. Biotech.* **14**, 491–493. [25]

Levine J. M., and D'Antonio C. M. (1999). Elton revisited: A review of evidence linking diversity and invasibility. *Oikos* **87**, 15–26. [55, 84]

Lewis H. M., and Law R. (2007). Effects of dynamics on ecological networks. *J. Theor. Biol.* **247**, 64–76. [50, 155]

Liebhold A. M., and Bascompte J. (2003). The Allee effect, stochastic dynamics and the eradication of alien species. *Ecol. Lett.* **6**, 133–140. [65]

Lorenz E. N. (1963). Deterministic nonperiodic flow. *J. Atmos. Sci.* **20**, 130–141. [3]

Lorenzen K. (1996). The relationship between body weight and natural mortality in juvenile and adult fish: A comparison of natural ecosystems and aquaculture. *J. Fish Biol.* **49**, 627–647. [136]

Lotka A. J. (1920). Undamped oscillations derived from the law of mass action. *J. Amer. Chem. Soc.* **42**, 1595–1598. [48]

Ludwig D., Jones D. D., and Holling C. S. (1978). Qualitative analysis of insect outbreak systems: The spruce budworm and forest. *J. Anim. Ecol.* **47**, 315–332. [104]

Ludwig D., Walker B., and Holling C. S. (1997). Sustainability, stability, and resilience. *Conserv. Ecol.* **1**, [online] (`http://www.consecol.org/vol1/iss1/art7`). [103, 108]

MacArthur R. H. (1955). Fluctuations of animals populations and a measure of community stability. *Ecology* **36**, 533–536. [47]

MacArthur R. H., and Levins R. (1964). Competition, habitat selection, and character displacement in a patchy environment. *Proc. Natl. Acad. Sci. USA* **51**, 1207–1210. [63]

MacArthur R. H., and Wilson E. O. (1967). *The theory of island biogeography*. Princeton: Princeton University Press. [51]

Maynard Smith J. (1970). Natural selection and the concept of protein space. *Nature* **225**, 563–564. [22]

Manrubia S. C., Domingo E., and Lázaro E. (2010). Pathways to extinction - Beyond the error threshold. *Phil. Trans. R. Soc.* **365**, 1943–1952. [22, 24]

Manrubia S. C., and Lázaro E. (2006). Viral evolution. *Phys. Life Revs.* **3**, 65–92. [24, 27]

Marquet P. A., Quinones R. A., Abades S., Labra F., Tognelli M., Arim M., and Rivadeneira M. (2005). Scaling and power-laws in ecological systems. *J. Exp. Biol.* **208**, 1749–1769. [126]

Martinez N. D. (1991). Artifacts or attributes? Effects of resolution on the Litte Rock Lake food web. *Ecol. Monogr.* **61**, 367–392. [49]

Martinez N. D. (1992). Constant connectance in community food webs. *Am. Nat.* **139**, 1208–1218. [49]

Martinez N. D., Williams R. J., and Dunne J. A. (2006). Diversity, complexity and persistence in large model ecosystems. In Pascual M., and Dunne J. A. (Eds.), *Ecological Networks*, pp. 163–186. Oxford: Oxford University Press. [56]

May R. M. (1972). Will a large complex system be stable? *Nature* **238**, 413–414. [48, 49]

May R. M. (1973). *Stability and complexity in model ecosystems*. Princeton: Princeton University Press. [49]

May R. M. (1977). Thresholds and breakpoints in ecosystems with a multiplicity of stable states. *Nature* **269**, 471–477. [104]

McCann K. S. (2000). The diversity-stability debate. *Nature* **405**, 228–233. [50]

McKendrick A. G. (1925). Applications of mathematics to medical problems. *Proc. Edinb. Math. Soc.* **44**, 98–130. [126]

Mendes J. F. F., Dickman R., Henkel M., and Marques M. C. (1994). Generalized scaling for models with multiple absorbing states. *J. Phys. A* **27**, 3019–3023. [34]

Meyer C. D. (2000). *Matrix analysis and applied linear algebra*. Philadelphia: SIAM. [117, 182]

Morton R. D., and Law R. (1997). Regional species pools and the assembly of local ecological communities. *J. Theor. Biol.* **187**, 321–331. [50, 51, 55, 72, 74, 82, 85]

Newman S. A., and Forgacs G. (2005). Complexity and self-organization in biological development and evolution. In Bonachev D., and Rouvrai D. H. (Eds.), *Complexity in chemistry, biology and ecology*, pp. 49–96. New York: Springer. [8]

Nicolis G., and Prigogine I. (1989). *Exploring complexity: An introduction*. New York: W. H. Freeman. [3]

Nisbet R. M., Muller E. B., Lika K., and Kooijman S. A. L. M. (2000). From molecules to ecosystems through dynamic energy budget models. *J. Anim. Ecol.* **69**, 913–926. [164]

Nollert P., Kiefer H., and Jähnig F. (1995). Lipid vesicle adsorption versus formation of planar bilayers on solid surfaces. *Byophys. J.* **69**, 1447–1455. [9]

Nowak M. A. (2006). *Evolutionary dynamics: Exploring the equations of life*. Cambridge, Massachusetts: Belknap Press. [19, 21]

Nystrom M., Folke C., and Moberg F. (2000). Coral reef disturbance and resilience in a human-dominated environment. *Trends Ecol. Evol.* **15**, 413–417. [103, 108]

Odum E. P. (1953). *Fundamentals of ecology*. Philadelphia: Saunders. [47]

Pandian T. J., and Marian M. P. (1985). Nitrogen content of food as an index of absorption efficiency in fishes. *Mar. Biol. (Berlin)* **85**, 301–311. [140]

Pastor-Satorras R., and Solé R. V. (2001). Field theory for a reaction-diffusion model of quasispecies dynamics. *Phys. Rev. E* **64**, 51909. [25]

Perales C., Agudo R., Tejero M., Manrubia S. C., and Domingo E. (2009). Benefits of sequential inhibitor-mutagen lethal mutagenesis treatments. *PLoS Pathog.* **5**, e1000658. [24]

Petermann T., and de los Ríos P. (2004). Cluster approximations for epidemic processes: A systematic description of correlations beyond the pair level. *J. Theor. Biol.* **229**, 1–11. [24]

Peters R. H. (1986). *The ecological implications of body size*. Cambridge: Cambridge University Press. [136]

Pimm S. L. (1982). *Food webs*. London: Chapman & Hall. [50]

Pimm S. L. (1991). *The balance of nature: Ecological issues in the conservation of species and communities*. Chicago: University of Chicago Press. [59, 69]

Pimm S. L., and Lawton J. H. (1977). The number of trophic levels in ecological communities. *Nature* **268**, 329–331. [75]

Platt T., and Denman K. (1977). Organisation in the pelagic ecosystem. *Helgol. Mar. Res.* **30**, 575–581. [126]

Post W. M., and Pimm S. L. (1983). Community assembly and food web stability. *Math. Biosci.* **64**, 169–192. [50, 51, 56]

Quinones R. A., Platt T., and Rodríguez J. (2003). Patterns of biomass-size spectra from oligotrophic waters of the Northwest Atlantic. *Prog. Oceanogr.* **57**, 405–427. [126]

Rand D. A., Keeling M., and Wilson H. B. (1995). Invasion, stability and evolution to criticality in spatially extended, artificial host-pathogen ecologies. *Proc. R. Soc. Lond. B* **259**, 55–63. [25]

Rezende E., Lavabre J., aes P. G., Jordano P., and Bascompte J. (2007). Non-random coextinctions in phylogenetically structured mutualistic networks. *Nature* **448**, 925–929. [58]

Roff D. A. (1992). *The evolution of life histories: Theory and analysis*. London: Chapman & Hall. [140]

Roughgarden J. (1974). Species packing and the competition function with illustrations form coral reef fish. *Theor. Popul. Biol.* **5**, 163–186. [65]

Sax D. F., Stachowicz J. J., and Gaines S. D. (Eds.) (2005). *Species invasions: Insights into ecology, evolution, and biogeography*, Sunderland, Massachusetts. Sinauer Associates Inc. [65]

Scheffer M., Bascompte J., Brock W. A., Brovkin V., Carpenter S. R., Dakos V., Held H., van Nes E. H., Rietkerk M., and Sugihara G. (2009). Early-warning signals for critical transitions. *Nature* **461**, 53–59. [106, 108, 110, 116, 120]

Scheffer M., Carpenter S., Foley J. A., Folke C., and Walker B. (2001). Catastrophic shifts in ecosystems. *Nature* **413**, 591–596. [7, 103, 104, 110, 116, 120]

Scheffer M., Szabó S., Gragnani A., van Nes E. H., Rinaldi S., Kautsky N., Norberg J., Roijackers R. M. M., and Franken R. J. M. (2003). Floating plant dominance as a stable state. *Proc. Natl. Acad. Sci. USA* **100**, 4040–4045. [103, 108]

Schelling T. C. (1971). Dynamic models of segregation. *J. Math. Sociol.* **1**, 143–186. [6]

Schuster P., Fontana W., Stadler P. F., and Hofacker I. L. (1994). Fron sequences to shapes and back: A case study in RNA seondary structures. *Proc. R. Soc. Lond. B* **255**, 279–284. [22]

Seneta E. (2006). *Non-negative matrices and Markov chains*. New York: Springer. [20]

Sheldon R. W., and Kerr S. (1972). The population density of monsters in Loch Ness. *Limnol. Oceanogr.* **17**, 796–798. [126]

Sheldon R. W., Prakash A., and Sutcliffe W. H. (1972). The size distribution of particles in the ocean. *Limnol. Oceanogr.* **17**, 327–340. [126, 140]

Shin T.-J., Rochet J.-M., Jennings S., Field J., and Gislason H. (2005). Using size-based indicators to evaluate the ecosystem effects of fishing. *ICES J. Mar. Sci.* **62**, 384–396. [126]

Silvert W., and Platt T. (1978). Energy flux in the pelagic ecosystem: A time-dependent equation. *Limnol. Oceanogr.* **23**, 813–816. [13, 127, 129, 138, 164]

Silvert W., and Platt T. (1980). Dynamic energy-flow model of the particle size distribution in pelagic ecosystems. In Kerfoot W. C. (Ed.), *Evolution and ecology of zooplankton communities*, pp. 754–763. Hanover, New Hampshire: New England University Press. [126, 129, 138]

Solé R. V., and Goodwin B. (2001). *Signs of life: How complexity pervades biology*. New York: Basic Books. [10]

Stanley H. E. (1971). *Introduction to phase transitions and critical phenomena*. Oxford: Oxford University Press. [6]

Stanley H. E. (2000). Exotic statistical physics: Applications to biology, medicine and economics. *Physica A* **285**, 1–17. [6]

Stich M., Briones C., and Manrubia S. C. (2007). Collective properties of evolving molecular quasispecies. *BMC Evol. Biol.* **7**, 110–13. [10]

Stich M., Lazaro E., and Manrubia S. C. (2010). Phenotypic effect of mutations in evolving populations of RNA molecules. *BMC Evol. Biol.* **10**, 46–17. [26]

Takahashi T., Sugawara T., Yamatsuta T., Isogai M., Natsuaki T., and Yoshikawa N. (2007). Analysis of the spatial distribution of identical and two distinct virus populations differently labeled with cyan and yellow fluorescent proteins in coinfected plants. *Phytopathol.* **97**, 1200–1206. [29]

Takeuchi N., and Hogeweg P. (2007). Error-threshold exists in landscapes with lethal mutants. *BMC Evol. Biol.* **7**, 15. [24]

Tarazona P. (1992). Error thresholds for molecular quasispecies as phase transitions: From simple landscapes to spin-glass models. *Phys. Rev. A* **45**, 6038–6050. [10]

Thom R. (1975). *Structural Stability and Morphogenesis*. Reading, Massachusetts: Benjamin. [120]

Tilman D., Fargione J., Wolff B., D'Antonio C., Dobson A., Howarth R., Schindler D., Schlesinger W. H., Simberloff D., and Swackhamer D. (2001). Forecasting agriculturally driven global environmental change. *Science* **292**, 281–284. [103]

Tomé T. (1994). Spreading of damage in the Domany-Kinzel cellular automaton: A mean-field approach. *Physica A* **212**, 99–109. [35, 173]

Toyabe S., and Sano M. (2005). Spatial suppression of error catastrophe in a growing pattern. *Physica D* **203**, 1–8. [25]

Trefethen L. N., and Bau D. (1997). *Numerical linear algebra*. Philadelphia: SIAM. [118]

Turelli M. (1981). Niche overlap and invasion of competitors in random environments, I: Models without demographic stochasticity. *Theor. Popul. Biol.* **20**, 1–56. [65]

Ursin E. (1971). On the prey size preferences of cod and dab. *Meddr Danm. Fisk.-og Havunders* **7**, 85–98. [139]

van Kampen N. G. (2007). *Stochastic processes in physics and chemistry*. Amsterdam: North Holland. [130, 177, 184, 185]

Virgo N., Law R., and Emmerson M. (2006). Sequentially assembled food webs and extremum principles in ecosystem ecology. *J. Anim. Ecol.* **75**, 377–386. [82]

Volterra V. (1931). *Leçons sur la theorie mathematique de la lutte pour la vie*. Paris: Gauthiers-Villars. [48]

von Foerster H. (1959). Some remarks on changing populations. In Stohlman J. F. (Ed.), *The kinetics of cellular proliferation*. New York: Grune and Stratton. [126]

Waldrop M. M. (1993). *Complexity: The emerging science at the edge of order and chaos*. New York: Simon & Schuster. [3, 7]

Walker B. H. (1993). Rangeland ecology: Understanding and managing change. *Ambio* **22**, 80–87. [103, 108]

Ware D. M. (1978). Bioenergetics of pelagic fish: Theoretical change in swimming speed and ration with body size. *J. Fish. Res. Board Can.* **35**, 220–228. [136]

Warren P. H. (1989). Spatial and temporal variation in the structure of a fresh-water food web. *Oikos* **55**, 299–311. [49]

Warren P. H., Law R., and Weatherby A. J. (2003). Mapping the assembly of protist communities in microcosms. *Ecology* **84**, 1001–1011. [52–55, 72, 73]

Watts D., and Strogatz S. H. (1998). Collective dynamics of 'small-world' networks. *Nature* **393**, 440–442. [9]

Watts D. J. (2003). *Six degrees: The science of a connected age*. New York: W. W. Norton & Company, Inc. [7]

West G. B., Brown J. H., and Enquist B. J. (1997). A general model for the origin of allometric scaling laws in biology. *Science* **276**, 122–126. [126, 127, 134]

Wilke C. O. (2005). Quasispecies theory in the context of population genetics. *BMC Evol. Biol.* **5**, 44. [24]

Wolfram S. (1983). Statistical mechanics of cellular automata. *Rev. Mod. Phys.* **55**, 601–644. [169, 172]

Xie A., and Beerel P. A. (1998). Efficient state classification of finite-state Markov chains. *IEEE Trans. Comput. Aided Des.* **17**, 1334–1339. [69, 98, 189, 193, 195]